Characterization and modeling of the thermomechanical behavior of polypropylene-based composites : effect of recycling and filler content

Kui Wang

UNIVERSITÉ DE STRASBOURG

ÉCOLE DOCTORALE MATHEMATIQUES, SCIENCES DE L'INFORMATION ET DE L'INGENIEUR

ICube, Département Mécaniques

THÈSE

présentée par :

Kui WANG

soutenue le : **06 Juin 2013**

pour obtenir le grade de : **Docteur de l'université de Strasbourg**

Discipline/ Spécialité : **Mécanique des matériaux**

Characterization and modeling of the thermomechanical behavior of polypropylene-based composites: effect of recycling and filler content

THÈSE dirigée par :

Nadia Bahlouli	Professeur, Université de Strasbourg
Said AHZI	Professeur, Université de Strasbourg

RAPPORTEURS :

A. Dahoun	Professeur, Ecole des Mines de Nancy
F. Lauro	Professeur, Université de Valenciennes

AUTRES MEMBRES DU JURY :

V. Toniazzo	Docteur, CRP-HT, Luxembourg
K. Jacob	Professeur, Georgia Tech.,USA

Acknowledgments

The work presented in this thesis was performed at the ICube (previously Institute of fluid and solid mechanics (IMFS)), and at the Public Research Centre Henri Tudor (CRP-HT). It was funded by the Fond National de la Recherche (FNR) of Luxembourg (reference PhD-09-069-RE). During my Ph.D thesis from November 2009 to April 2013, I got lots of helps, supports and advises from my supervisors, advisors, and other people. I would like to express my gratitude to all of them and to acknowledge the Fond National de la Recherche (FNR) of Luxembourg and the Alsace region for their financial support.

I also thank the previous director of the IMFS (actually the director of the graduate school MSII), Prof. Yves Rémond, for giving me the opportunity to work in his laboratory. I am also thankful to Prof. Saïd Ahzi, the director of the multiscale materials and biomechanics group. As my Ph.D co-supervisor, he has contributed with excellent scientific support, ideas and suggestions. I wish also to express my gratitude to my Ph.D supervisor, Prof. Nadia Bahlouli, who supported me with worthful suggestions and discussions.

I am indebted to Dr. David Ruch, the director of the Advanced Materials and Structures (AMS) Department of CRP-HT, and Dr. Valérie Toniazzo, head of the Material Unit of AMS, for providing me the chance to achieve my Ph.D thesis in their research center. I am grateful to my Ph.D scientific advisor, Dr. Frédéric Addiego, for his advises and suggestions, particularly in the domain of polymer processing and characterization.

I am thankful Prof. René Muller and Mr. Badi Triki from the Laboratoire d'Ingénierie des Polymères pour les Hautes Technologies (LIPHT) for their helps regarding polymer processing. I wish to thank Mr. Régis Vaudemont, Mr. Benoît Marcolini, Dr. Jérôme Bour, Ms. Christèle Vergne, Mr. Jean-Luc Biagi and Dr. Claire Arnoult from the CRP-HT for their help concerning material characterization. I would like to thank Dr. Rodrigue Matadi for his valuable discussion in the field of polymer mechanical behavior modeling.

I am extremely grateful to my wife, my daughter, my parents and grandparents for their understanding, supports and encouragements.

Special thanks are reserved for all my friends and colleagues from the ICube and the CRP-HT for their helps to achieve my thesis and shearing this precious period.

This experience of Ph.D study will be the most precious memory of all my life. Even after a long time, I will have the same sincere appreciation to all of them who give me the important helps and supports.

Abstract

The use of thermoplastic olefins (TPOs) like polypropylene (PP) is currently growing in the automotive industry, and in particular for both exterior and interior parts of cars. However, the increasing use of TPOs causes an increase of wastes from end of life vehicles (ELV), and hence, represents a threat to our environment. In this context, the European Union wishes that 85 wt. % of the materials used for a vehicle per year must be re-used or recycled in 2015 (Directive 2000/53/EC). Although different recycling methods exist for plastics, the most acceptable and ecological one is the mechanical recycling. The reprocessing of plastics, conducted under important shear conditions at high temperature, and with the presence of oxygen and impurities, could lead to marked thermo-oxidative and thermomechanical degradations of the materials and consequently to a loss of properties. It is of fundamental importance to identify these degradation mechanisms and to study their impact on the material properties, to know either recycled materials could be re-used for the same application or for applications requiring less drastic properties.

The first objective of this thesis was to identify the degradation mechanisms of lab-made PP-based composites resulting from mechanical recycling procedures by grinding and reprocessing. These materials were generally used to produce automotive bumpers. Degradation mechanisms were identified in terms of oxidation by Fourier Transformation Infrared spectroscopy (FTIR) and in terms of chain scission by Gel Permeation Chromatography (GPC). In particular, attention was focused on the impact of the filler content on these degradation mechanisms. The second objective of this work was to study the impact of these degradation mechanisms on the rheological, thermal, physical and mechanical properties of the PP-based composites. Concerning mechanical properties, a detailed investigation of

quasi-static tensile behavior of the materials and a detailed investigation of dynamic compressive behaviors were done. The dynamic behavior was assessed in a wide range of strain rates and temperatures, to fit at best the end-use conditions of automotive bumpers. The third objective of the present work was to predict the yield and the elastic behaviors of non-recycled and recycled materials with temperature and strain rate dependences. For the recycled materials, we took into account the reprocessing effect by incorporating the reprocessing sensitive coefficient into the models.

Within our investigated recycling number (6 recycling procedures), it is found that thermomechnical degradation induces chains scission mechanisms in PP matrix without significant oxidation. The recycled materials have a good thermal stability despite the re-extrusion-induced thermo-mechanical degradation. The recycled neat PP and PP-based composites can be used in the same temperature range than the non-recycled ones. We found that the ethylene octene copolymer (EOC) inclusions stabilized the tensile elongation at break up to 3 recycling cycles due to a decrease of their size and a homogenization of their shape during the reprocessing. Otherwise, the talc fillers increased the stiffness and the strength of composite with the number of recycling cycle due to a decrease of their geometry and an increase of their aspect ratio.

Our proposed models for the stiffness and the yield behaviors yield fair predictions of the experimental data (obtained by the dynamic tests) for the considered PP-based composites by taking the filler content and recycling effects.

Résumé

L'utilisation des oléfines thermoplastiques (TPO) comme le polypropylène (PP) est actuellement de plus en plus utilisé dans l'industrie automobile, particulièrement pour les parties extérieures et intérieures des véhicules. Ce phénomène est dû au fait que les matériaux à base de PP sont choisis pour remplacer d'autres matériaux tels que le polycarbonate (PC), acrylonitrile butadiène styrène (ABS) et le polychlorure de vinyle (PVC) composites en raison de leur faible poids, de leur bonne résistance au vieillissement et de leur coût modéré. Pour fabriquer les pare-chocs de la voiture, des élastomères tels que l'éthylène-propylène élastomères (EPR) et l'éthylène propylène diène monomère (EPDM) sont souvent synthétisés avec le PP pour améliorer la ténacité du PP à basse température. Cependant, l'addition des particules élastomères diminue la rigidité des composites. Dans ce cas-là, des renforts organiques telles que des fibres naturelles ou des renforts minéraux comme le carbonate de calcium, l'argile et le talc sont souvent ajoutés dans les composites PP/élastomère. Les particules rigides limitent les pertes de rigidité des matériaux. Parmi ces agents de renforcement, le talc est l'une des charges minérales les plus utilisées et permettent donc d'améliorer les propriétés thermiques et mécaniques du PP. Cette charge facilite également la mise en forme du PP en réduisant et en homogénéisant le retrait au moulage. Cette propriété est idéale pour les connexions sans joint et les zéro écarts pièces comme les pare-chocs.

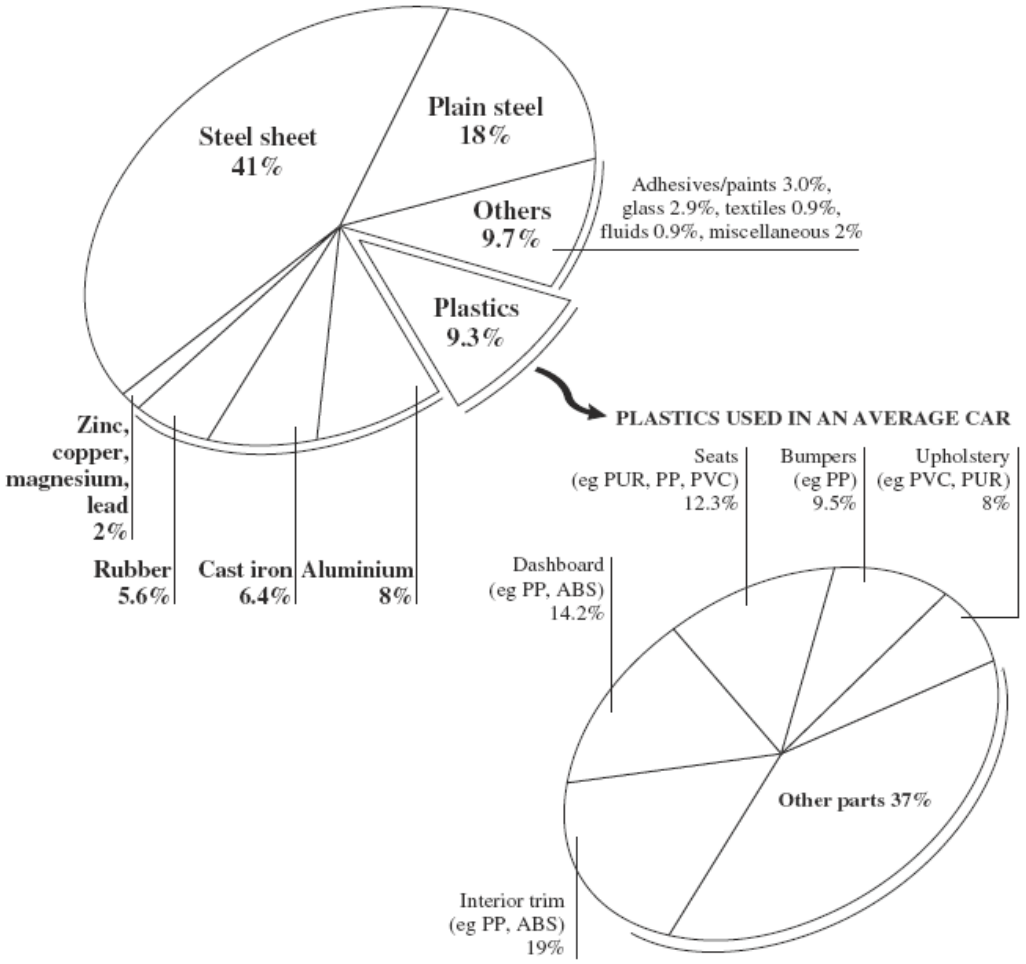

Figure R1 : Les matériaux utilisés dans la production des voitures dans l'Union européenne [Kanari et al., JOM, 2003].

Toutefois, l'utilisation croissante des TPOs entraîne une augmentation des déchets provenant des véhicules hors d'usage (VHU) et, par conséquent, représente une menace pour notre environnement. En effet, ces matériaux ne sont pas produits à partir de sources renouvelables, mais à partir de sources polluantes. En pratique, les matières plastiques utilisées sont rarement recyclées ce qui génèrent des déchets importants. Afin de protéger l'environnement et de limiter la gestion des déchets, les gouvernements légifèrent en introduisant le concept de recyclage iso-fonctions. En effet, le taux de valorisation des véhicules hors d'usage (VHU) avoisine aujourd'hui les 85 % et concerne essentiellement la réutilisation et le recyclage des pièces

métalliques. A l'horizon 2015, l'objectif fixé par la Directive européenne 2000/53/CE est d'atteindre un taux de réutilisation et de valorisation de 95 % en masse, dont 85 % de réutilisation et de recyclage.

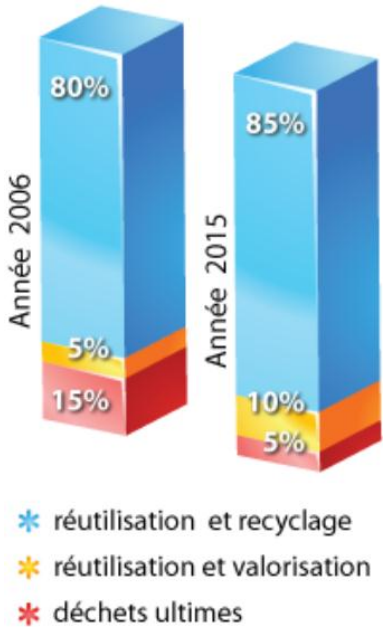

Figure R2: Objectif réglementaire d'atteindre les taux de recyclage et de valorisation [http://www.indra.fr/environnement_reglementaire.html].

Différentes méthodes de recyclage existent, mais la plus acceptable d'un point de vue écologique est le recyclage mécanique. En fin de vie, les pièces plastiques sont mécaniquement broyées et réinjectées afin d'obtenir de nouvelles pièces structurelles. Mais le retraitement des matières plastiques, induit un fort taux de cisaillement à haute température. De plus, la présence d'oxygène et d'impuretés, pourraient conduire à des dégradations importantes thermo-oxydatives et thermomécaniques des matériaux et par conséquent à une perte de propriétés. Pour tenter de prolonger la vie des TPOs au cours des procédures de recyclage multipliés, il est important d'identifier les mécanismes de dégradation. La connaissance des caractéristiques moléculaires ainsi que les propriétés rhéologiques et mécaniques des polymères recyclés peuvent

donner une bonne indication sur le nombre de recyclage maximum possibles préservant le niveau de qualité requis pour une application spécifique.

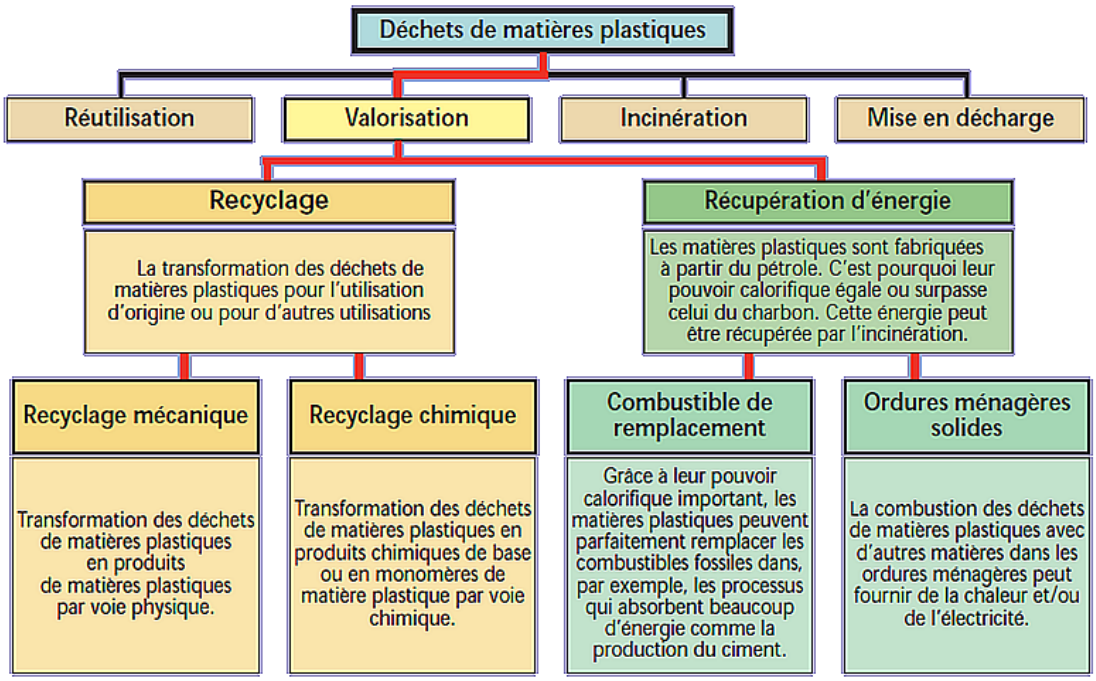

Figure R3 : Les diverses options pour la gestion des déchets de matières plastiques [Kang et al. Resources, Conservation and Recycling, 2005]

Récemment, un nouveau grade de copolymères d'éthylène et d'octène (EOC) tend à remplacer les élastomères conventionnels pour le renforcement de la matrice de polypropylène. L'EOC est un copolymère non polaire. Il présente une meilleure compatibilité avec le polypropylène par rapport aux copolymères d'éthylène polaires. En outre, l'EOC présente une meilleure facilité de traitement grâce à leur faible poids moléculaire par rapport à l'EPR ou à l'EPDM. Le PP/EOC composite est caractérisé par une rigidité et une élasticité exceptionnelle par rapport à d'autres oléfines thermoplastiques (TPOs). Enfin, il doit être mentionné que les composites PP/EOC présentent une excellente résistance aux intempéries et une aptitude à la peinture élevée. Toutes ces raisons impliquent que l'EOC est la prochaine génération

modificateur de TPO. Cependant, actuellement, il n'existe aucune étude sur l'effet du recyclage sur les propriétés physiques et mécaniques des PP/EOC composites et plus particulièrement sur l'effet des charges sur le recyclage.

Les objectifs de cette étude sont les suivants:

(1) Identifier les mécanismes de dégradation thermomécanique de composites à base de polypropylène, en fonction du contenu des charges.

(2) Etudier l'impact de la dégradation sur les propriétés rhéologiques, thermiques, physiques et mécaniques des matériaux. Concernant ces derniers, une caractérisation détaillée sur le comportement de traction quasi-statique des matériaux et une étude détaillée des comportements de compression dynamiques ont été réalisées.

(3) Modéliser le module d'élasticité et la contrainte seuil des matériaux recyclés par des approches basée sur des modèles micromécaniques avec prise en compte du taux de charge, de la vitesse, de la température et de l'effet de recyclage.

Pour atteindre les objectifs ci-dessus, la présente thèse est divisée en quatre parties. Le premier chapitre se compose de d'une synthèse bibliographique. Dans cette partie, nous présentons brièvement les propriétés des matériaux. Les matériaux étudiés sont non seulement le polymère pur, mais aussi leurs composites. Ensuite, les effets de la température et de la vitesse de la déformation sur le comportement mécanique des matériaux est décrit. Différents procédés de recyclage sont présentés et comparés. Ensuite, nous présentons différent aspects de dégradations des polymères. Pour le recyclage mécanique, les effets de retraitement sur différentes propriétés du polypropylène sont résumés. À la fin de chapitre 1, nous nous concentrons sur la

modélisation de la contrainte seuil et du module d'élasticité des matériaux. Pour modéliser la contrainte seuil des polymères, nous introduisons le modèle coopératif. Pour modéliser le module d'élasticité des matériaux, nous présentons un modèle statistique.

Le deuxième chapitre de cette thèse est concentré autour de l'identification de l'influence des charges et des mécanismes de dégradations thermomécaniques de composites à base de polypropylène. Pour préparer des composites, des copolymères d'éthylène et d'octène (formation nodules d'élastomère dans la matrice PP, 0 wt. %, 10 wt. %, and 20 wt. %) et des particules de talc (0 wt. %, 10 wt. %, and 20 wt. %) sont mélangés avec le polypropylène dans un malaxeur BUSS extrudeuse à 200 °C et à 50 tours par minute. L'extrusion a été réalisée avec une mono-vis sous condition atmosphérique. Les filaments fondus obtenus de composites ont été trempés dans un bain d'eau froide. Un granulateur rapide a été utilisé pour couper les filaments réfrigérés. Les granulés obtenus sont séchés dans un four à circulation d'air pendant 60 min pour éliminer l'eau et, par conséquent, pour réduire l'humidité pour l'étape suivante. Pour simuler les procédés de recyclage, le PP pur, PP/EOC, PP/talc et PP/EOC/talc composites ont été soumis à des procédures d'extrusion multiples en utilisant la même extrudeuse et les mêmes conditions de procédé, et ceci 6 fois de suite. Nous notons que 6 étapes de recyclages successifs sont suffisantes pour identifier les mécanismes de dégradation. Enfin, les échantillons de traction pour tous les matériaux sont injectés grâce a une machine de moulage avec une température autour 200 ° C et une vitesse de rotation de vis à 180 tours par minute.

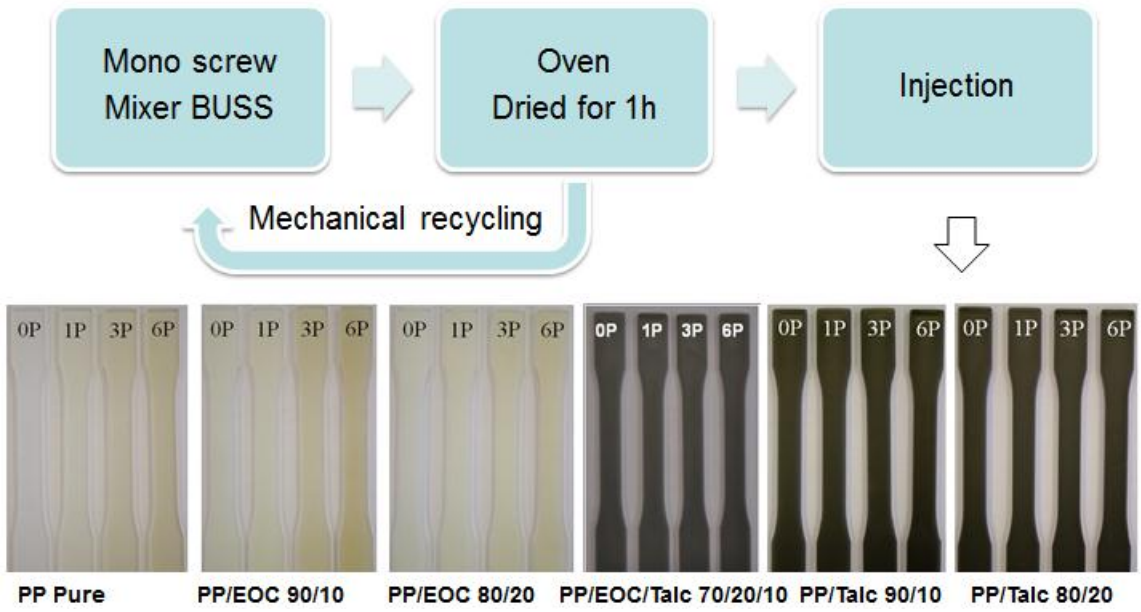

Figure R4 : La procédure de recyclage mécanique.

Pour étudier les propriétés des composites recyclés à base de PP, une approche multi-physique est proposée. Les déterminations de masses moléculaires ont été réalisées par chromatographie sur gel perméable (GPC). L'indice de fluidité (MFI) a été mesuré par un indexeur de fluidité. La stabilité thermique des matériaux a été étudiée par analyse thermogravimétrique (TGA). La spectroscopie infrarouge à Transformée de Fourier a utilisée pour caractériser l'état d'oxydation des composites pendant le recyclage. Il est également supposé que la dégradation thermomécanique a un impact sur les propriétés physiques des matériaux. Dans ce cas, la calorimétrie différentielle à balayage (DSC), la diffusion des rayons X aux grands angles (WAXS) et la microscopie électronique à balayage (MEB) sont utilisés. Enfin, l'influence du recyclage sur les propriétés mécaniques de composites est déterminée par l'analyse mécanique dynamique (DMA) et l'essai de traction quasi-statique.

Nous avons trouvé que la masse moléculaire des matériaux recyclés sont légèrement diminuées après six recyclages successifs. La diminution de la masse

moléculaire des matériaux peut être attribuée au mécanisme de coupures des chaînes de polymère. Ceci peut être dû aux températures élevées et à l'état de cisaillement intensif subi par les matériaux pendant le process de recyclage. Cette diminution de masse moléculaire a entraîné une diminution de la viscosité des matériaux. Par conséquent, une augmentation continue de la MFI avec le cycle de recyclage a été mesurée pour toutes les matières. La réduction de la longueur des chaînes du PP peut accroître leur mobilité et donc faciliter leur réarrangement au cours de la cristallisation. Cette augmentation de mobilité des chaînes du PP accrue a entraîné une légère augmentation de la cristallinité avec le nombre de recyclage. Pour les propriétés thermiques, l'addition d'EOC et le talc ont augmenté la température de décomposition du PP. Concernant le recyclage, bien que le processus ait induit la dégradation des matériaux, le changement de la température de décomposition resté limité. Il est indiqué que les matériaux recyclés peuvent être utilisés dans la même gamme de la température que les matériaux non-recyclés. En outre, en raison de la présence de l'antioxydant, aucune oxydation significative n'a été observée.

Pour les comportements mécaniques de PP pur et PP/EOC à faible vitesse de déformation, la contrainte seuil et le modules d'Young de PP pur et PP/EOC composites ont augmenté après un premier recyclage car le taux de cristallinité a augmenté. Mais les deux comportements (la contrainte seuil et le modules d'Young) ont diminué pour les nombres de recyclage élevés car la dégradation des matériaux était plus importante que l'augmentation de la cristallinité. Nous avons aussi montré que les nodules d'élastomères ont stabilisé l'allongement en traction à la rupture jusqu'à 3 recyclages successifs. Ceci est dû à la diminution de leur taille et à une homogénéisation de leur forme. Pour les comportements mécaniques du PP/talc à la faible vitesse, les charges de talc ont augmenté le module d'Young mais la contrainte

seuil des matériaux n'est pas modifiée en raison d'une diminution des tailles des particules de talc et une augmentation de leur facteur de forme.

Ces matériaux à base de PP sont généralement utilisés dans la fabrication de pare-chocs où les taux de chargement sont élevés et sont appliqués sur une large gamme de températures et de vitesses. Dans ce cas, une étude détaillée de la sensibilité des matériaux recyclés à grande vitesse de déformation et à température différente est réalisée dans le chapitre 3. Dans nos études, on a réalisé des essais dynamiques en compression sur un système de barres d'Hopkinson pour des températures variant de -30°C à 85°C (-30°C, 0°C, 25°C, 50°C et 85°C) et pour des vitesses de déformation allant de 592 s^{-1} à 3346 s^{-1} (592 s^{-1}, 1276 s^{-1}, 2221 s^{-1} et 3346 s^{-1}). Dans ce chapitre, on a étudié le nombre de recyclage 0 (non-recyclage), 3 et 6.

Les résultats de comportement dynamique de matériaux ont montré que les composites à base de PP sont sensible à la vitesse de déformation et à la température. Le PP pur et PP/talc composites ont un comportement fragile à -30°C et 0°C. Mais le PP/EOC et PP/EOC/talc composites ont montré une ténacité aux mêmes températures car la présence d'EOC nodules augmente la ductilité du matériau. L'addition d'EOC a diminué la contrainte seuil et le module d'élasticité des matériaux tandis que la présence de talc a augmenté le module d'élasticité du PP. Toutefois, la contrainte seuil pour PP/talc 80/20 (20 wt.% talc) était inférieure à celle de PP/talc 90/10 (10 wt.% talc) en raison des endommagements plus importants et par le décollement de matrice/charge dans PP/talc 80/20 lors du test de traction. Avec l'augmentation du nombre de recyclage, les comportements dynamiques du PP pur et PP/EOC composites ont diminué en raison du mécanisme de scission des chaînes. Les réponses dynamiques du PP/talc ont augmenté avec l'augmentation du cycle de recyclage en

raison d'un mécanisme d'auto-renforcement plus important en réduisant des dimensions des particules de talc. Pour les PP/EOC/talc composites, les réponses dynamiques étaient moins notifiées par les cycles de recyclage. Ceci est dû au mécanisme de scission des chaînes mentionné et au mécanisme d'auto-renforcement qui ont été impliqués ensembles pour de PP/EOC/talc composites. L'équilibre a été trouvé entre ces deux mécanismes.

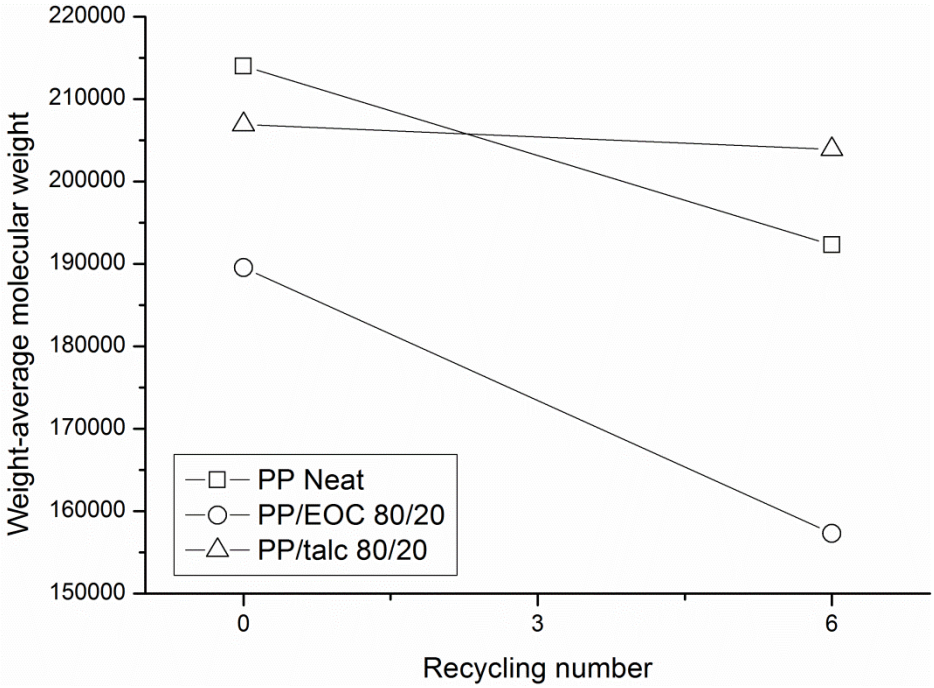

Figure R5 : Poids moléculaire des matériaux en fonction du nombre de recyclage.

Les comportements dynamiques des matériaux considérés sont corrélés avec leur morphologie en utilisant la microscopie optique (OM). A basse température (-30 °C), le PP pur et les PP/talc composites ont montrés des faciès de rupture explosif où d'autres matériaux ont présentés des faciès de rupture partiel par les fragmentations périphériques ou les fragmentations internes. Ces défaillances sont attribuées à des mécanismes de fissuration et à l'apparition des bandes de cisaillement. A température ambiante (25 °C), ces défaillances étaient moins marquées pour le PP pur et les

PP/talc composites où les fragmentations partielles ont été observées. A haute température (85 °C), les matériaux sont déformés de façon plus homogène, sans fissure importante. Les défaillances observées des matériaux par l'OM sont en accord avec les réponses dynamiques de nos matériaux étudiés.

Tous les essais dynamiques réalisés ont permis d'établir une base de données pour alimenter des codes de calculs. Le but recherché est de tenir compte des effets du recyclage lors des designs des pièces en matière recyclée. C'est la raison pour laquelle ce dernier chapitre de la thèse est consacré à l'utilisation des modèles micromécaniques dans lesquels nous avons intégré les paramètres permettant de décrire l'effet du recyclage et du pourcentage de charge sur la contrainte seuil et le module d'élasticité. Les effets de vitesse et de température sont aussi décrits dans ces modèles. Un bon accord entre les prédictions du modèle et les données expérimentales ont été obtenus pour tous les composites à base de PP non-recyclés et recyclés.

.

Table of Content

General Introduction

General introduction

Context

Polymers are essential and ubiquitous materials that can be produce from non-renewable resource (oil) or renewable resource (vegetal), in this latter case they are called biopolymers. The development of polymers was very quick from 1970. Today, though polymer annual world production by weight didn't exceed steels, its production in terms of volume achieved 122 million m^3 comparing with 96 million m^3 for steels [1]. This was due to the extraordinary range of properties of polymers including low density, high flexibility, high resistance to corrosion, low cost, fast and easy shaping, that enabled to replace conventional materials such as glass, textile and wood, and create new applications. The reduction of the carbon dioxide footprint is currently one of the main concerns of the society. The use of biopolymers enables to reduce CO_2 footprint but due to their limited performance, they cannot be used in structural applications requiring drastic properties. In this context, the main utilized polymers are thermoplastic olefins (TPOs) produced from non-renewable resources. To reduce the CO_2 footprint for these applications, the re-use of TPOs after a mechanical recycling procedure can be a solution. However, only about 4% of these polymers are currently re-used [2].

Automotive industry started to use plastics in 1946 [3]. The main reason for using polymer materials in car manufacturing is decreasing the total weight of the vehicle, which saves fuel. Currently, polymers and their composites are used to manufacture both automotive exterior parts as bumpers, trims, spoilers and interior parts as steering wheels, battery casings, covers, ducts. Because polymeric materials

have a wide range of performance characteristics, the use of plastic materials for automobile application shares 8 wt.%-13 wt.% of whole plastic market [1]. The use of polymer in cars steadily increased from 1978 to 2000 as shown in Figure 0-1.

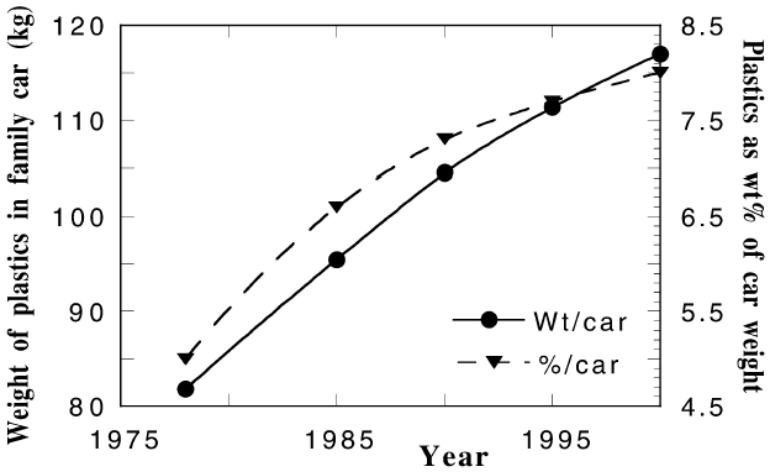

Figure 0-1 : Increase of polymeric content in North American family car [3].

Among the different polymeric materials, the use of thermoplastic olefins (TPOs) as polypropylene (PP) is currently growing in the automotive industry. This phenomenon is due to the fact that PP-based materials are selected to replace other materials such as polycarbonate (PC), acrylonitrile butadiene styrene (ABS) and polyvinyl chloride (PVC) compounds due to their lower weight, higher resistance to aging and lower cost. For manufacturing car bumpers, elastomers such as ethylene propylene rubber (EPR) and ethylene propylene diene monomer (EPDM) are frequently blended with PP to increase the inherent low toughness of PP at low temperature. To balance the decrease of stiffness and strength of materials induced by the addition of rubber particles, mineral rigid reinforcements such as talc are usually blended into the binary composite of PP/elastomer [4]. Talc can improve both the thermal and mechanical properties of PP. This filler also facilitates the shaping of PP

by reducing and homogenizing the molding shrinkage. This property is suitable for jointless connections and zero-gap parts [5, 6].

Recently, a new grade of ethylene alpha-olefin copolymer (ethylene octene copolymer (EOC)) tends to replace conventional elastomers for the reinforcement of the polypropylene matrix. EOC, which is a non-polar ethylene alpha-olefin copolymer, exhibiting a higher compatibility with polypropylene compared to polar ethylene copolymers. Furthermore, EOC has a higher processability than EPR or EPDM due to its lower molecular weight [7]. The PP/EOC compounds are characterized by outstanding strength, stiffness and toughness compared to other TPOs containing the same rubber concentration [7]. Moreover, PP/EOC blends exhibit an excellent weatherability and paintability. All these reasons lead EOC to become the next generation modifier for TPOs [8].

Problematic

The increasing use of TPOs causes an increase of wastes from end-of-life vehicles (ELV), and hence, represents a threat to our environment. For both environmental protection and waste management considerations, the European directive 2000/53/UE has been legislated to increase the re-use and recovery rate of the plastic wastes to a minimum of 95% by an average weight per vehicle in 2015. Unlike metallic materials that have mature recovery and recycling techniques, the knowledge about recycling of plastic materials is quite limited to date. Although different recycling methods exist, the most acceptable and ecological one is the mechanical recycling where the end-of-life plastics were mechanically re-crushed and re-processed to obtain new structural parts. However, the reprocessing of plastics, conducted under important shear conditions at high temperature, and with the

presence of oxygen and impurities, could lead to marked thermo-oxidative and thermo-mechanical degradations of the materials and consequently to a loss of properties [9-14]. It is of fundamental importance to identify these degradation mechanisms and to investigate their effect on the material properties, to know either recycled materials could be re-used for the same application or for applications requiring less important properties. The knowledge of the molar characteristics as well as the rheological and mechanical properties of reprocessed polymers can give a good indication on the maximum number of reprocessing which are possible to accomplish while keeping the level of quality required for a specific application [15].

Aim of the thesis

In this thesis, lab-made PP/EOC, PP/talc and PP/EOC/talc systems will be compounded by extrusion and shaped by injection. Recycling procedures consisted of a mechanical grinding of the extrudates and re-extrusion. The objectives of this thesis are:

- To identify the degradation mechanisms of polypropylene based composites resulting from the recycling procedures, with attention focused on the impact of the fillers' content (EOC and talc) on these degradation mechanisms.

- To study the impact of the degradation mechanisms on the rheological, thermal, physical, and mechanical properties of the materials, concerning the latters, a detailed investigation of quasi-static tensile behavior of the materials and a detailed investigation of dynamic compressive behaviors were conducted.

- To predict the elastic modulus and the yield stress of dynamic behavior of the recycled materials by implementing the effect of recycling in the micromechanical models.

In order to achieve the above objectives, the present thesis is divided into four parts. The first chapter consists of literature review where we briefly present the materials' characteristics of interest for this research project. In this part, the studied materials are introduced not only in the case of neat polymer but also in the case of their composites. Then, the temperature and strain rate effects on the mechanical behavior of materials are described. Different recycling processes are presented and compared. The recycling effects on the properties of PP-based composites are introduced. At the end of this chapter, we focus on the review of the modeling of the materials' mechanical responses.

The second chapter is dedicated to the characterization of the degradation mechanisms of the materials induced by recycling in terms of oxidation by Fourier Transform Infrared Spectroscopy (FTIR), and chain scission by Gel Permeation Chromatography (GPC). To fully assess the impact of recycling on the materials' properties, the rheological properties of the materials are studied by melt flow index (MFI) measurements, the thermal properties of the materials are studied by differential scanning calorimetry (DSC) and thermogravimetric measurements (TGA), the physical properties are investigated by scanning electron microscopy (SEM) and X-ray diffraction (XRD). The viscoelastic properties obtained by dynamic mechanical analysis (DMA) and the tensile behavior of the materials were also assessed. Attention is focused on the impact of the inclusions content (EOC and talc) on the degradation mechanisms of re-extruded polypropylene-based composites.

The dynamic mechanical behavior of non-recycled and recycled materials is investigated in the third chapter. The dynamic tests were conducted in a wide range of temperatures and strain rates using a lab-made split Hopkinson pressure bar. In order to understand the macromechanical results of materials, a morphological analysis was carried out.

In the fourth chapter, the laboratory developed micromechanical modeling was used to predict the yield and the elastic behaviors of non-recycled and recycled materials with temperature and strain rate dependences. For the recycled materials, we took into account the reprocessing effect by incorporating the reprocessing sensitive coefficient into the models.

Finally, general conclusions and the perspectives for the continuity of this thesis are reported. The appendix for the estimation of the applied shear stress in the extruder to break the talc particles, and the appendix for the modeling equations are added at the end as complementary.

References

[1] Biron M. Thermoplastics and Thermoplastic Composites. Thermoplastics and Thermoplastic Composites. 2007.

[2] Charles E, Carraher J. Giant Molecules: Essential Materials for Everyday Living and Problem Solving. Journal of Chemical Education. 1990;67.

[3] Utracki LA. Polymer Blends Handbook: Kluwer Academic Publishers; 2002.

[4] Öksüz M, Eroglu M, Yıldırım H. Effect of talc on the properties of polypropylene/ethylene/propylene/diene terpolymer blends. Journal of Applied Polymer Science. 2006;101:3033-3039.

[5] Jahani Y. Comparison of the effect of mica and talc and chemical coupling on the rheology, morphology, and mechanical properties of polypropylene composites. Polymers for Advanced Technologies. 2011;22:942-950.

[6] Branciforti MC, Oliveira CA, de Sousa JA. Molecular orientation, crystallinity, and flexural modulus correlations in injection molded polypropylene/talc composites. Polymers for Advanced Technologies. 2010;21:322-330.

[7] Chum PS, Swogger KW. Olefin polymer technologies--History and recent progress at The Dow Chemical Company. Progress in Polymer Science. 2008;33:797-819.

[8] C. Yu T. Mentallocane plastomer modification of polypropylenes. Polymer Engineering and Science. 2001;41:656-671.

[9] Navarro R, Torre L, Kenny JM, Jiménez A. Thermal degradation of recycled polypropylene toughened with elastomers. Polymer Degradation and Stability. 2003;82:279-290.

[10] Hinsken H, Moss S, Pauquet JR, Zweifel H. Degradation of polyolefins during melt processing. Polymer Degradation and Stability. 1991;34:279-293.

[11] Aurrekoetxea J, Sarrionandia MA, Urrutibeascoa I, Maspoch ML. Effects of recycling on the microstructure and the mechanical properties of isotactic polypropylene. Journal of Materials Science. 2001;36:2607-2613.

[12] Valenza A, La Mantia FP. Recycling of polymer waste: Part II - Stress degraded polypropylene. Polymer Degradation and Stability. 1988;20:63-73.

[13] Hamskog M, Klügel M, Forsström D, Terselius B, Gijsman P. The effect of base stabilization on the recyclability of polypropylene as studied by multi-cell imaging chemiluminescence and microcalorimetry. Polymer Degradation and Stability. 2004;86:557-566.

[14] González-González VA, Neira-Velázquez G, Angulo-Sánchez JL. Polypropylene chain scissions and molecular weight changes in multiple extrusion. Polymer Degradation and Stability. 1998;60:33-42.

[15] Bahlouli N, Pessey D, Raveyre C, Guillet J, Ahzi S, Dahoun A, Hiver JM. Recycling effects on the rheological and thermomechanical properties of polypropylene-based composites. Materials and Design. 2012;33:451-458.

Chapter 1:
State of the art

1. State of the art

In this chapter, we will present the literature review for this research project. At the beginning of each followed chapter, we will give a briefly introduction.

1.1. Material properties

1.1.1. Classification of polymers

There are different ways of classifying polymers in which the oldest one is based on their response to heat. By this way, we have two type polymers, thermoplastics and thermosets.

As an intuitive Figure 1-1, it shows the different between thermoplastics and thermosets.

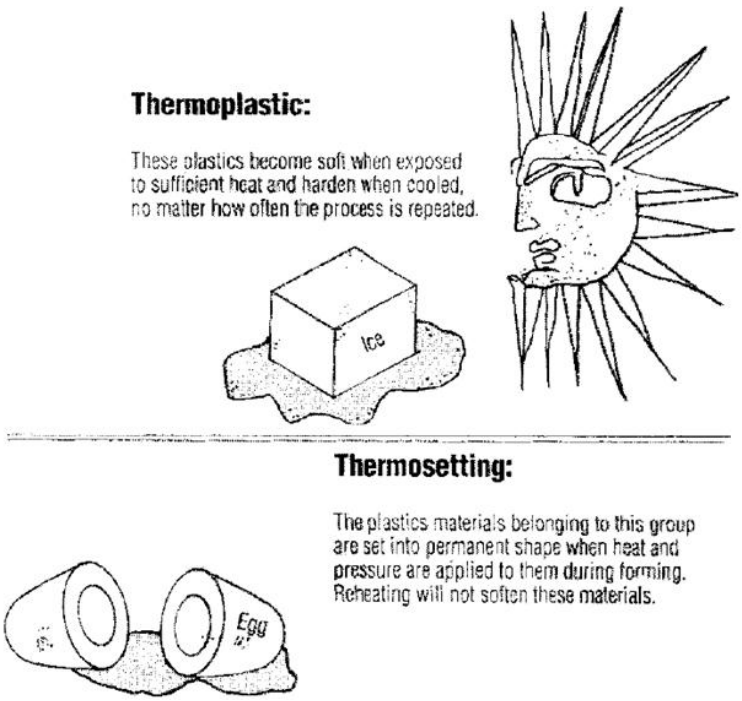

Figure 1-1 : thermoplastic and thermoset [1].

Thermoplastics (TPs) are predominantly used nearly 85% of all plastics processed [2]. As its name, they become plastic by heating/melting and return to the original state by cooling/solidification and this cycle can be repeated. So we can conclude that TPs are sensitive to temperature. Note that TPs are soluble in specific solvant. They consist of more or less linear chains linked together by van der Waals forces or dipole.

Different from TPs, thermosets (TSs) become permanently insoluble and infusible under the influence of heat or light so that they are not recyclable. During heating, they undergo chemical changes or crosslinking whose rate is 10 to 100 times higher than elastomers [3]. By consequence, they are usually used in composite materials as matrix for long fibers.

Beside classification ways by heating, one of the most well-known ways to classify polymers is according their structures, which can be 100% amorphous or partially crystalline

Amorphous polymers: amorphous refers to the random arrangement of the polymer chains showing no structural order [4]. This amorphous structure is represented by Figure 1-2. An important aspect of amorphous region is the density of entanglement, and the mass between entanglement that dictate the viscosity, the elastic properties and the toughness of the material [5].

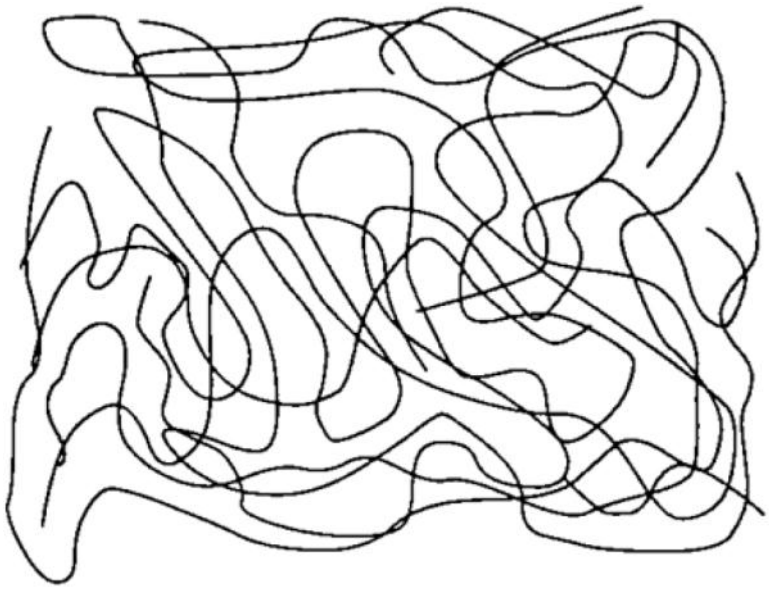

Figure 1-2 : Schema of an amorphous structure [6].

Semi-crystalline polymers: they consist of a part of amorphous regions and a part of crystalline regions (the crystals). A crystal is an ordered spatial arrangement of atoms or molecules over a long distance. In a crystalline polymer, molecules are squeezed against each other and perfectly arranged in crystalline lamellae. The representation of a crystalline lamella containing folded chains is shown in Figure 1-3. Its height is about 10 nm with the length and width about 10 to 20 μm. The semi-crystalline morphology is respresented in Figure 1-4. An important aspect of crystalline lamella is their thickness that is generally proportional to the yield point of the material [7]. It is also to be noted that some polymer chain belongs to at least two crystalline lamellae and have an important rule on mechanical properties: the tie molecules. They enable to transmit stress from the amorphous regions to crystalline regions, and are responsible for the tensile strength.

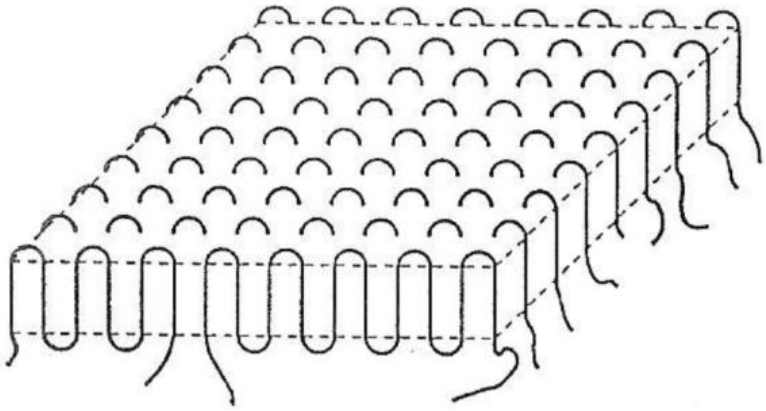

Figure 1-3: Representation of a crystalline lamella containing folded chains [3].

Most of industrial polymers are semi-crystalline. That is to say, semi-crystalline polymers are most commonly used.

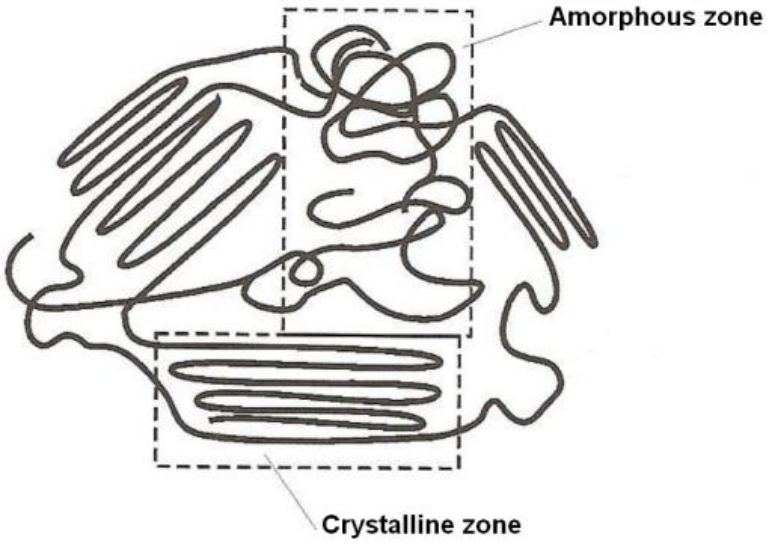

Figure 1-4: Schema of a semi-crystalline polymer [6].

1.1.2. Polypropylene

Polypropylene (PP) is one of the most used semi-crystalline thermoplastic materials. Figure 1-5 indicate the market shares by weight of the main thermoplastics versus total thermoplastics in the main industrialized countries [8].

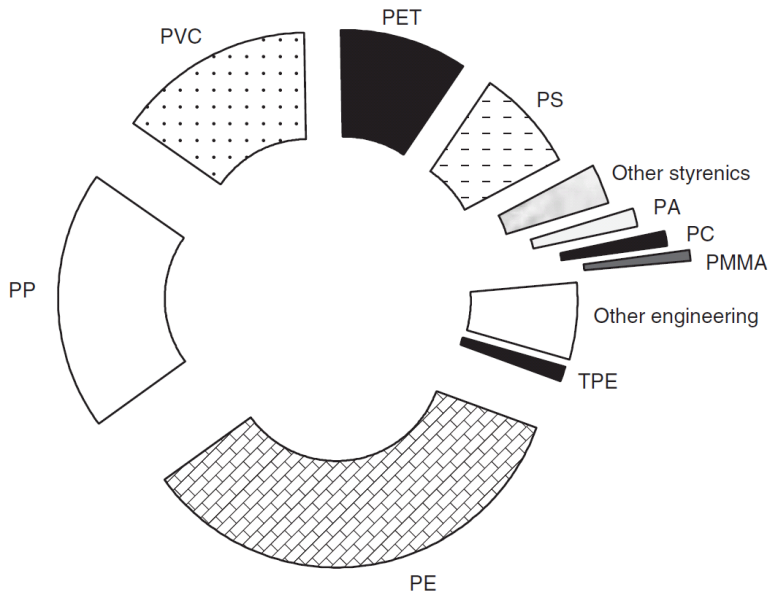

Figure 1-5: Market shares based on total thermoplastic consumption [8].

Many chemists used the Nobel laureate K.Ziegler catalyst to product PP in the early 1950s [9]. PP is compatible with many processing techniques so that it used in many different commercial applications.

The low cost (about 0.5 euro per kilo [10]) and high thermal and mechanical properties of PP compared to other TPs as polyethylene contribute to its strong growth rate. It is one of the lightest of all thermoplastics. In particular, due to its high strength to weight ratio, it is more rigid than other polyolefins. It has the highest melting temperature of all commodity thermoplastics and higher heat resistance than other low cost thermoplastics.

PP is prepared by polymerizing propylenes (monomer) that are joined together to form one macromolecule of PP. Its chemical structure consists of a linear carbon chain in which the bonds are covalent. Links between chains are Van der Waals physical interactions. The molecular structure of PP is shown in Table 1-1:

Table 1-1: Structure of polypropylene.

Monomer	Polymer	Abbreviation
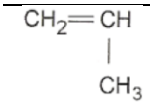	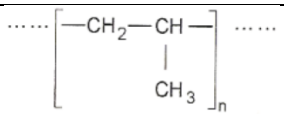	PP

Because of different structures and standardized methods, the properties of PP are not the same. Table 1-2 summarizes the main characteristics of PP.

Table 1-2: Characteristics of polypropylene [11].

Physical properties	
Density ($kg \cdot m^{-3}$)	890 to 910
Thermal properties	
Melting temperature (℃)	130 to 170
Glass transition temperature (℃)	-25 to -15
Thermal conductivity ($W \cdot m^{-1} \cdot K^{-1}$)	0.22
Heat capacity ($J \cdot kg^{-1} \cdot K^{-1}$)	1700
Mechanical Properties	
Young's modulus in tension (MPa)	900 to 1700
Yield stress in tension (MPa)	17 to 38
Poisson's ratio	0.4052 to 0.4269

1.1.3. Elastomer

Elastomers are polymers whose glass transition temperature is below the using temperature. They have an important capability for reversible deformation, which can reach several hundred percent [12]. This strain capability just exists in a certain range of temperature. In other words, their properties are very sensitive to temperature. To achieve the rubber state, the three basic conditions are necessary for their behaviors [10]:

- Long and flexible chains.

- Low energy barriers for the change of conformation.

- Existence of anchor points between molecules.

Two elastomers are made based on statistical copolymers of ethylene and propylene. One is ethylene propylene diene monomer rubber (EPDM), in which the diene portion, D, serves as a cross-linking site. Another is its non-cross-linking counterpart, EPM or called EPR (Ethylene Propylene Rubber) [13, 14]. Because they have excellent resistance to oxygen, ozone, light, high and low temperatures, acids, alkalies, and oils [14], they are used in a wide range of applications, such as gaskets, hoses and belts. The ethylene content in EPDM is about 45 wt. % to 75 wt. %, higher ethylene content, higher loading capacity of the polymer, better mixing and extrusion.

Different from traditional elastomers, plastomers are ethylene-alpha-olefin (such as 1-butene, 1-hexene, and 1-octene) copolymers with compositions and properties spanning between those of plastics and those of elastomers [15]. Their densities are ranging from 0.910 to 0.865 g/cm^3 (see Figure 1-6). The plastomers were produced with a metallocene catalyse which inserted comonomers uniformly along

the ethylene backbone, such that at relatively low comonomer incorporation level [16].

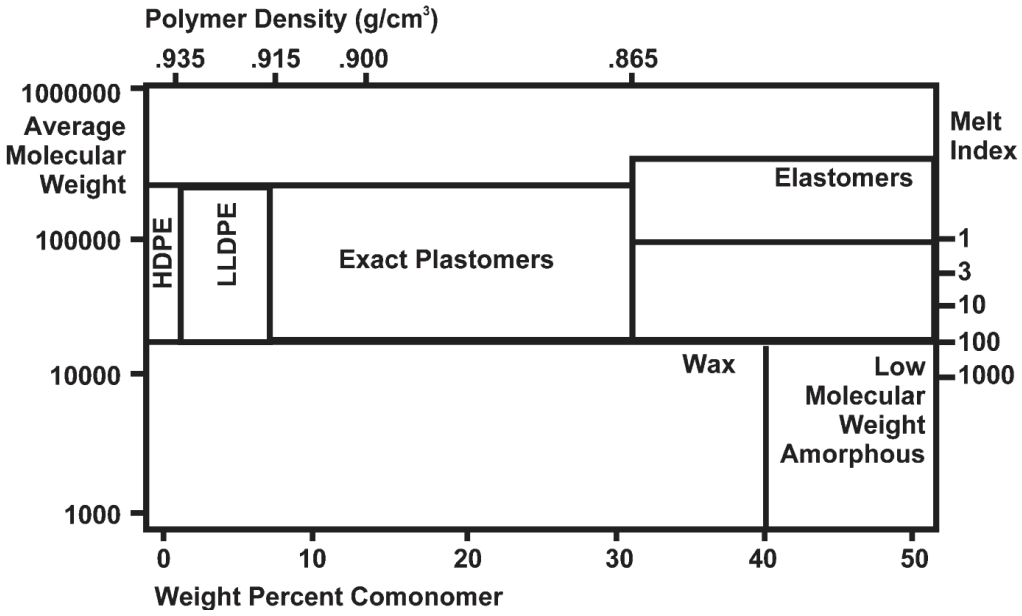

Figure 1-6: Ethylene-based polymers product regions [17].

The stress–strain curves of ethylene octene copolymers (EOCs) with different densities measured at a strain rate of 0.04 s^{-1} and at room temperature are shown in Figure 1-7. The yield region of copolymers is enlarged at the right side of the figure. The density of polymer profoundly affected the response to deformation, as shown by the broad spectrum of tensile properties. In the case of high densities, the deformation had characteristics common to semi-crystalline thermoplastics with localized yielding and cold drawing. For copolymers having medium densities, significant strain hardening was observed. For copolymers having low densities, the moduli were low and the deformation was essentially uniform and elastomeric [18].

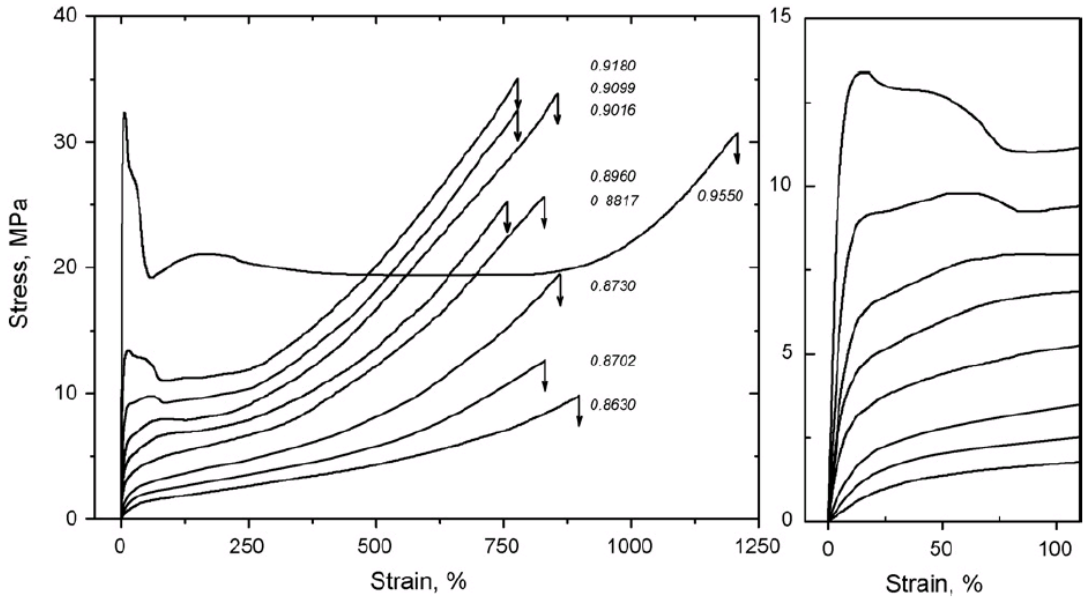

Figure 1-7: Engineering stress strain properties of ethylene octene copolymers at a strain rate of 0.04 s^{-1} and at room temperature [18].

1.1.4. Talc

Talc is one of the natural mineral fillers found worldwide. It is the major constituent of rocks known as soapstone and steatite. The color of talc is not only white but also gray, green, blue, pink and black [2].

Pure talc is a hydrated magnesium silicate with the chemical formula $Mg_3Si_4O_{10}(OH)_2$. The central brucite plane is chemically bonded by bridging oxygen atoms to two tetrahedral silica planes as show in Figure 1-8:

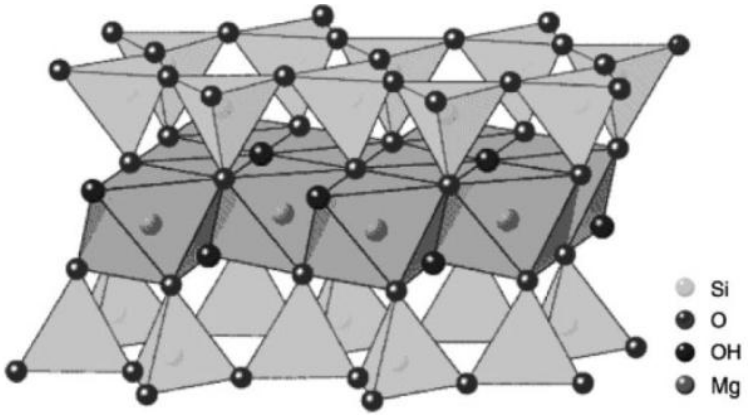

Figure 1-8: Molecular structure of talc [2].

Below 800°C, talc has a plate-like structure (Figure 1-9). The planar surfaces of the individual platelets are held together by weak van der Waals force, which means that talc can be delaminated at low shearing forces. This makes the mineral easily dispersible and accounts for its slippery feel. This property leads to use talc as a lubricant. Talc is the softest mineral with the Mohs hardness scale equivalent to 1 [19].

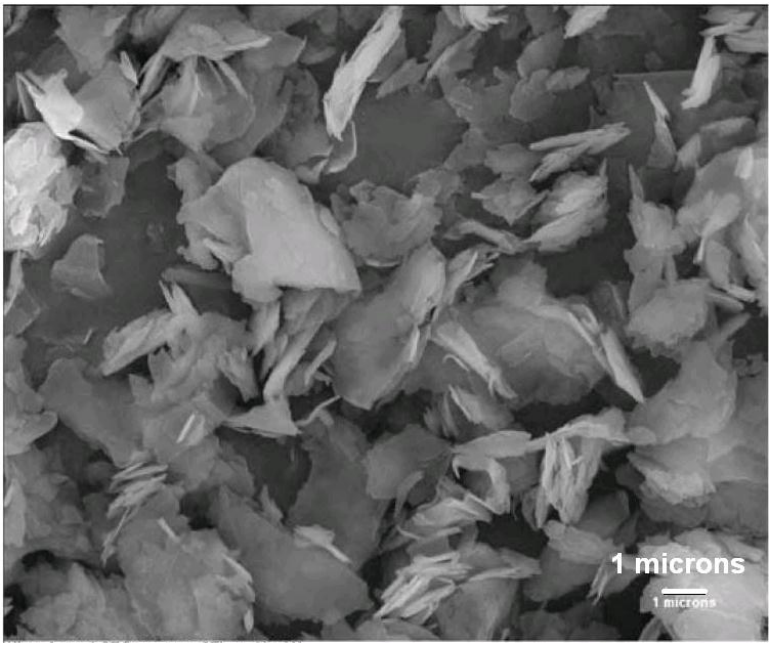

Figure 1-9: micrograph of talc [2].

1.2. Reinforced polypropylene

The worldwide plastic consumption consists two parts, unreinforced plastic and reinforced plastic (also called plastic composites or polymer composites). The latter case represents about 36% of total plastics consumption [20]. In most of the cases, the pure plastics, in other words the polymers, have numerous shortcomings. They are generally soft and have a low resistance to temperature. The reinforced plastics were first used for structural and semi-structural products, but now appear in different markets particularly since the 1940s [21]. These materials have been developed to produce exceptionally strong materials that can be used in different environments (Figure 1-10).

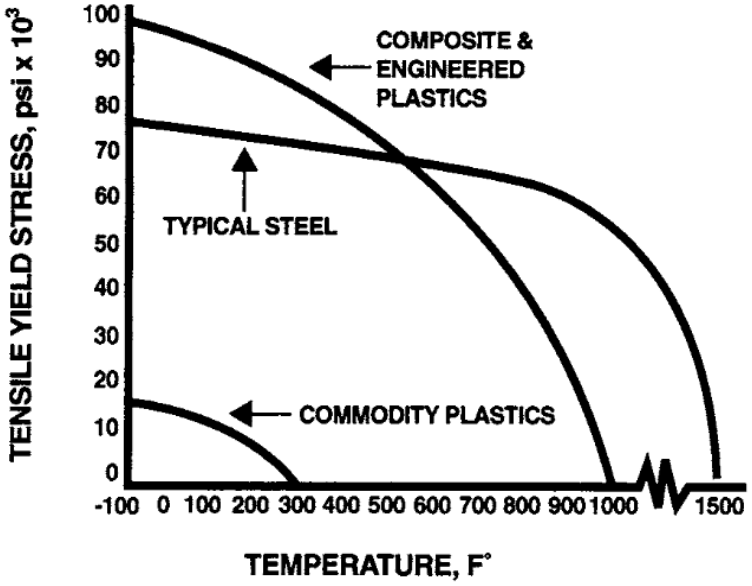

Figure 1-10: Strength vs. temperature of plastics and typical steel [21].

There exist lots of benefits when using polymer composites.

- Achieving desired properties or modifying shortcoming properties at very low price.

- Extending the engineering resins' performance.

- Performing a good engineered flexibility to design, fabricate.

These aspects can be obtained by mixing the polymer and fillers according the laws of physics, chemistry, and mechanics. The fillers like glass, aramid, carbon, graphite, metal, elastomer and mineral are usually used for the required properties of polymer (improve the mechanical properties, the conductivity properties, the impact properties…). There are several factors of reinforcement that can influence the composites properties.

- Interface cohesion.

- Fillers geometry.

- Particles nature and distribution.

- Volume fraction of reinforcements.

Approximately 31% of composite matrices are thermoplastics, and 69% are thermosets (Figure 1-11). The unsaturated polyester resins (thermosets) are the most used, followed by polypropylene (thermoplastic) [8]. It is widely used in almost all sectors. But its application as an engineering thermoplastic is somewhat limited due to its low impact strength, especially at low temperature. To improve its impact toughness and expand its application, numerous studies and extensively deep research on reinforced PPs have been done during the past 20 years.

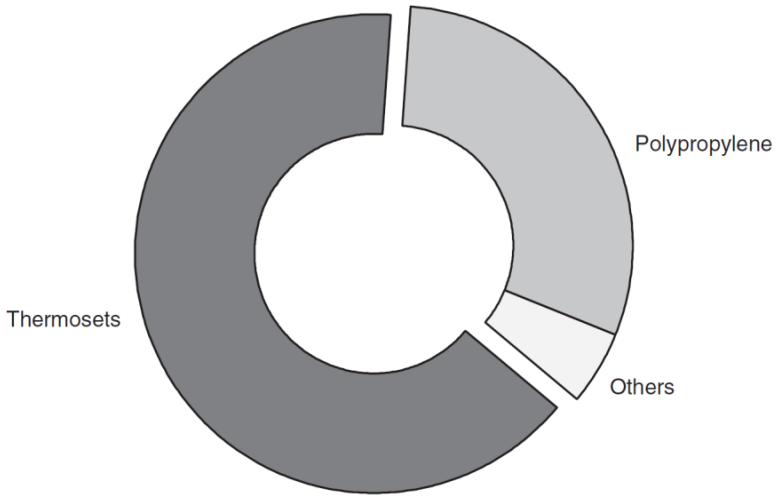

Figure 1-11: Market shares for the two main composite matrices [8].

After using traditional fillers in polypropylene, there is a significant growth in the use of nanoclay composites in the automotive industry. Besides that, a few of new application areas for composites containing nanosilicates, carbon nanotubes, ultrafine TiO_2, ultrafine talc and synthetic hydroxyapatite show a superiorly modification of matrix properties which are described below:

- Improvement of mechanical properties, barrier properties, electrical conductivity, and flame retardancy.

- Improvement of UV absorption and scratch resistance.

- Reduction of oxygen degradation.

1.2.1. Polypropylene/Elastomer

As mentioned above, polypropylene has several disadvantages that are corrected by blending with specific additives. Pure polypropylene is brittle , especially at temperature below glass transition temperature [22]. In order to improve its low temperature impact behavior, polypropylene is usually blended with EPDM or EPM

by using a coupling agent as dimethylol-phenolic curative or peroxide/coagents which provide the means of modifying the crystallinity of the rigid component, thus adjusting the properties, as well as the economy [22]. PP/elastomer composites show very high toughness, particularly at low temperature, excellent processability, high softening temperature and low shrinkage. They are known as thermoplastic olefins in the market. They are used since the early 1990's as bumper shaped by injection [20].

Arruda et al. [23] tested thermoplastic olefins which included PP, high density polyethylene (HDPE) and EPDM. Zebarjad et al. performed comparison of mechanical properties between neat polypropylene and polypropylene with different weight percentages of EPM [24, 25]. The results show that the impact strength increases with increasing of EPM content and test temperatures (Figure 1-12). In particular, the increase of EPM content shifts the brittle-ductile transition temperature (BDTT) to lower positions.

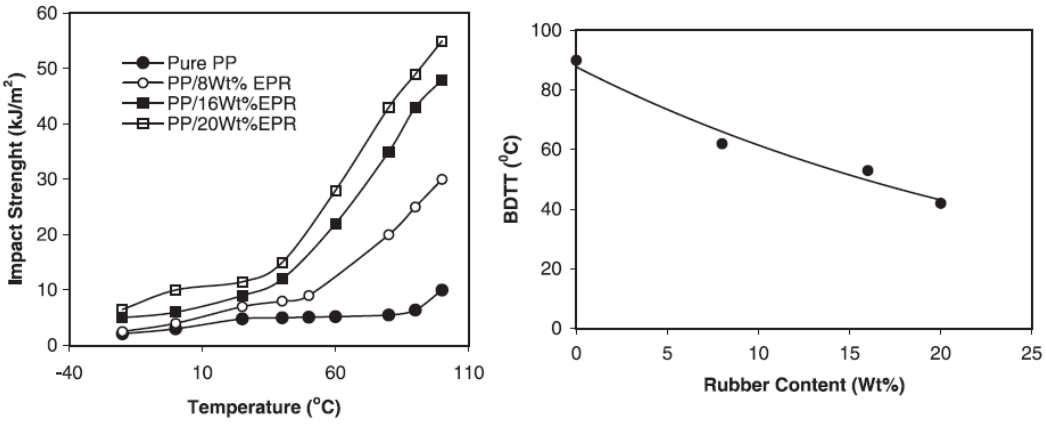

Figure 1-12: Variation of impact resistance against temperature according to the content of EPM (right) and variation of the brittle-ductile transition temperature (BDTT) against the content of EPM (Left) [25].

In quasi static tensile tests, we can observe that the increase of rubber content in polypropylene matrix reduces the yield stress and Young's modulus of materials. However, the increase of rubber content increases the fracture toughness of materials. Figure 1-13 shows the effects of EPM content on the mechanical properties of PP/EPM composites.

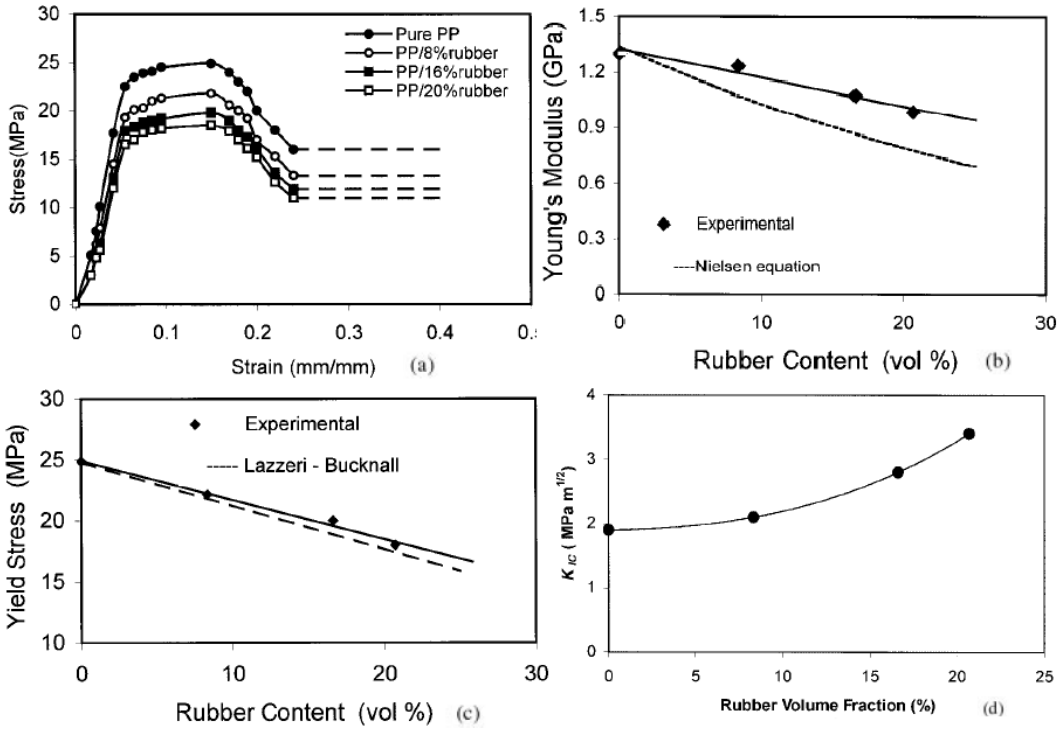

Figure 1-13: Influence of EPM content (a) quasi static tensile stress-strain curves (b) Young's modulus (c) Yield stress (d) fracture toughness (strain rate 0.03 s^{-1}) [24].

Figure 1-14 shows micrograph of the tensile fracture surface of PP/EPM obtained by scanning electron microscope (SEM). On this surface, many rubber nodules are present. We can find the debonding between the matrix and the rubber particles.

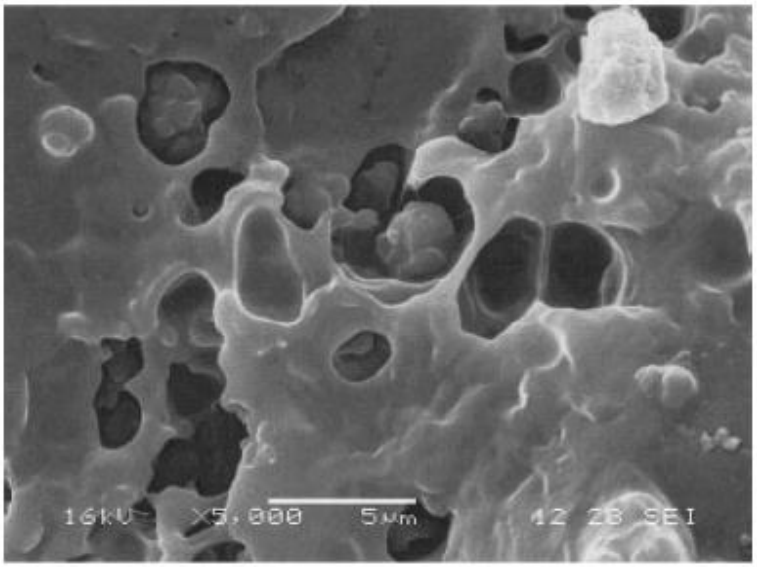

Figure 1-14: SEM micrograph of tensile fracture surface of PP/EPM [24].

Compared to EPM and EPDM, the non-polar plastomers are significantly more compatible with polypropylene and other polyolefins [15]. They can be blended with polypropylene without additives. Plastomers offer several advantages in comparison with EPM and EPDM and are considered as the next generation modifier for TPO. In addition to lower cost, plastomers are supplied in free flowing pellets, which allows for both batch and continuous TPO production. Similar molecular weight and compatibility between plastomer and polypropylene results in sub-micron dispersions of plastomer even in high flow polypropylene [15].

1.2.2. Polypropylene/Talc

Polypropylene filled with talc is shaped by both injection moulding and is generally used for structural applications. The addition of talc can improve stiffness and heat deformation resistance of PP. Generally, the typical loading of talc in PP matrix is in the range of 10 wt. % to 40 wt. %. Increasing talc content has a direct effect on the stiffness of materials as shown in Table 1-3. Compared with neat PP, PP

mixed with 40 wt.% of talc exhibits a decrease of tensile strength and impact strength but exhibits an increase of flexural modulus.

Table 1-3: Typical properties of talc-filled polypropylene [2].

properties	unfilled	40 wt.%
Density, 10^3 kg·m^{-3}	0.903	1.22
Flexural modulus, MPa	1655	3275
Tensile strength, MPa	35.5	31.4
Notched Izod impact strength J·m^{-1} (22°C)	45.7	20.9

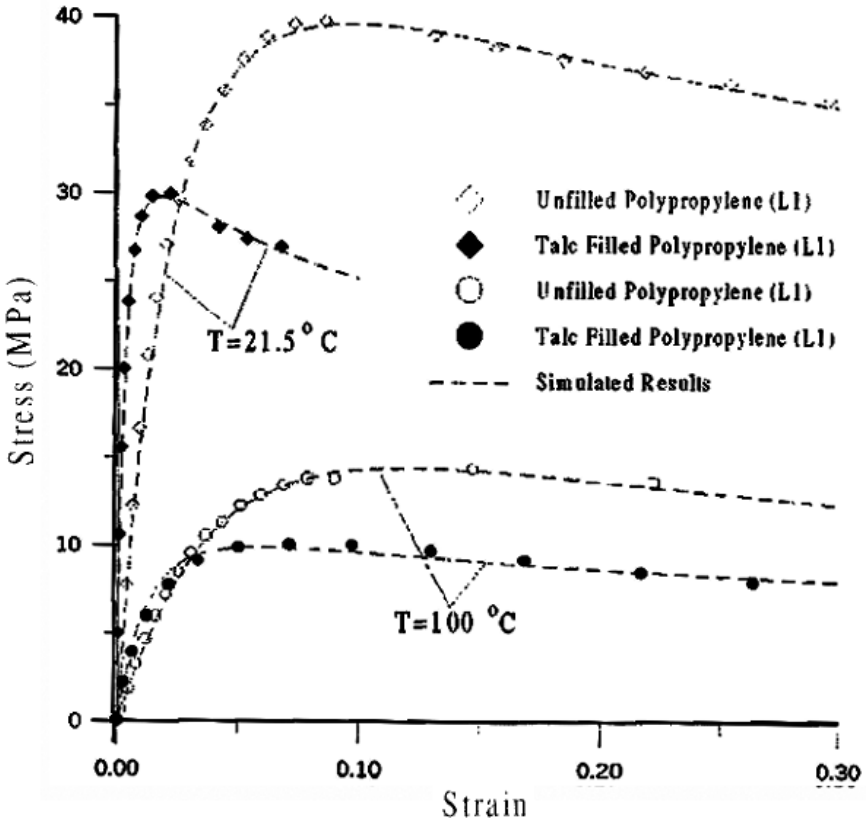

Figure 1-15: Comparison of the stress strain curves of unreinforced and reinforced polypropylene with 40 wt.% talc at 21.5 °C and 100 °C under strain rate 5 min^{-1} [26].

The uniaxial tensile behaviors of neat and reinforced polypropylene with 40 wt. % of talc were for example obtained by Zhou et al. [26, 27]. In Figure 1-15, we can compare the curves of unreinforced and reinforced polypropylene at 21.5 °C and 100 °C. For each temperature, the addition of talc increases the Young's modulus, but decreases the yield stress.

The surface of talc is hydrophobic and talc has a low surface energy. It is quite difficult to directly mix talc with a polymer matrix and getting an optimal dispersion of talc, so surface treatment of talc is necessary. One of the most used surface treatments of talc is using titanate coupling agent. This agent is well known to increase talc dispersion and composite' impact strength and to decrease melt viscosity and glass transition temperature of materials [2].

1.2.3. Polypropylene/Elastomer/Talc

The reinforcement of elastomers effectively improves the impact toughness of polypropylene. However, these rubber particles lead to a decrease of the materials stiffness . In order to balance the decrease induced by the addition of rubber particles, mineral rigid reinforcements such as talc are usually blended within the binary composite of PP/elastomer [28-32].

Öksüz et al. [33] carried out tensile tests (crosshead speed of 50 mm/min and at room temperature) with isotactic polypropylene (iPP) blended with EPDM and different weight percent of talc. They concluded that the talc content affects the tensile strength, Young's modulus and elongation at break of the composites. Figure 1-16 shows that the increase of talc content until 6 wt. % improves the yield strength, elastic modulus, tensile and impact strength of materials. For higher talc content, all

these parameters decrease. This is due to the dispersion of talc that becomes poor in the case of high talc contents, while it is good for low talc contents.

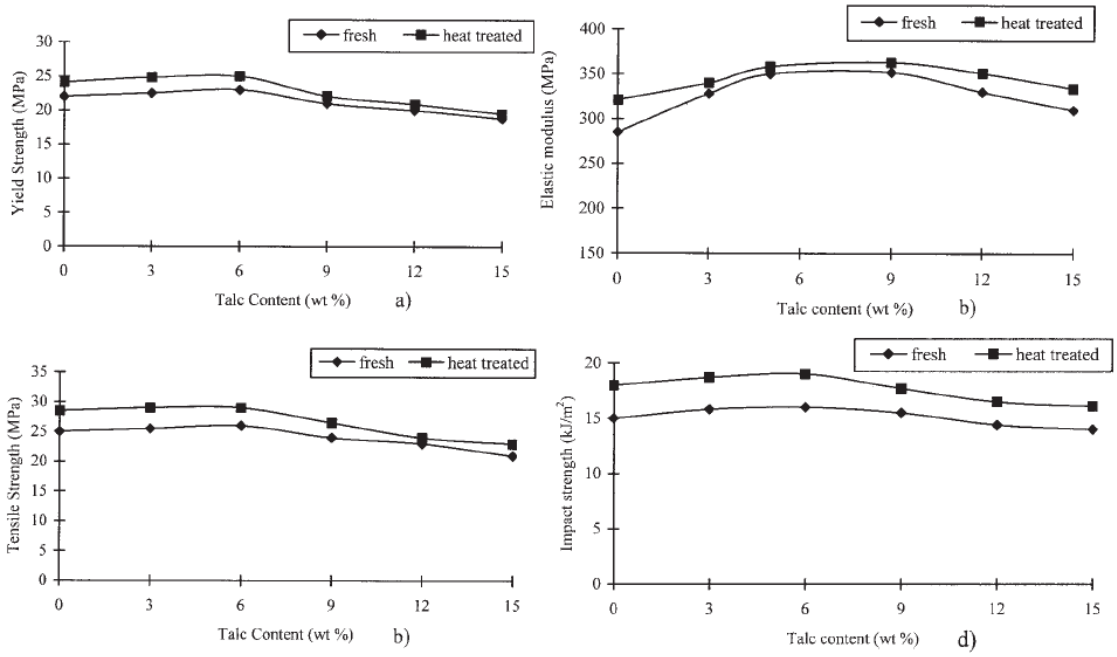

Figure 1-16: Effect of talc content on (a) yield strength (b) elastic modulus (c) tensile strength (d) impact strength, of iPP/EPDM/talc composite [33].

1.3. Temperature and strain rate sensitivities of polymer mechanical behavior

1.3.1. Temperature effect

The effect of temperature on the physical and mechanical behaviors of polymers is multifaceted. In the case of semi-crystalline polymers, the low and high temperatures lead two main transitions of polymer, glass transition and melt transition, respectively. Here we discuss the temperature effects on the mechanical properties of polymers.

The mechanical behaviors of most polymers are sensitive to temperature. For amorphous polymers, tests performed at high temperature decrease the yield stress and the Young's modulus of the materials [34-37]. Similar temperature sensitivity of semi-crystalline polymers is also reported [23, 38-42]. Figure 1-17 exhibits stress - strain curves of semi-crystalline polymers and amorphous polymers at different temperatures. On the left side of this figure, high density polyethylene (HDPE) samples are tested at 8 different temperatures from -75 °C to 100 °C under compressive strain rate of 10^{-2} s^{-1}. On the right side of figure 1-17, polyamide-imide (PAI) samples are tested at 6 different temperatures from -55 °C to 200 °C under compressive strain rate of about 2500 s^{-1}. It can be noted that increasing the test temperature in the case of quasi static and dynamic tests decreases the Young's modulus, yield stress and the tensile strength of the two materials.

When the temperature rises, the distance between the structural units increases due to the thermal agitation. Consequently, interaction forces decrease which implies an increase of chain mobility and hence, a lower resistance of the molecular network

toward deformation in the elastic stage (decrease of the elastic modulus) and in the viscoplastic stage (decrease of tensile strength). Concerning yield stage, the activation of plasticity, dictated to the shear slip mechanisms of crystalline lamellae, is activated by temperature, explaining the decrease if yield stress with increasing temperature.

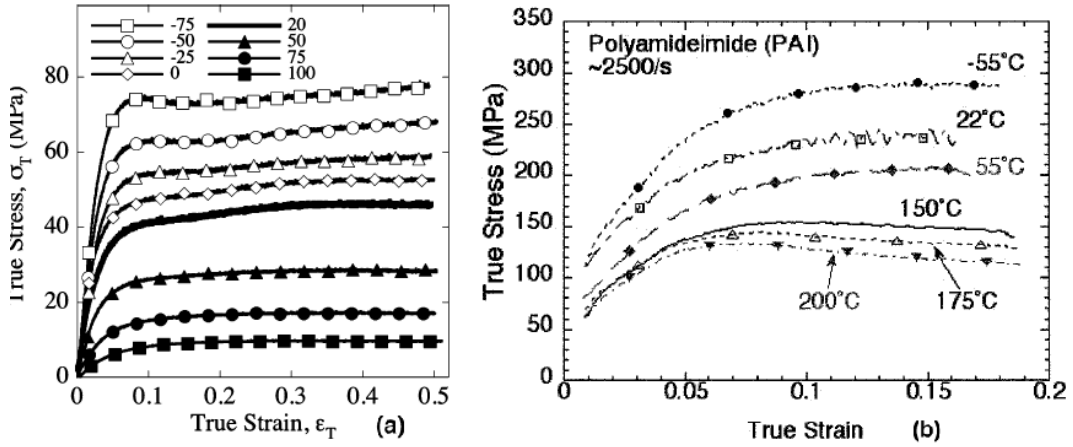

Figure 1-17: Mechanical response of (a) HDPE and (b) PAI as a function of temperature under strain rate 10^{-2} s^{-1}, 2500 s^{-1}, respectively [40].

Furthermore, for dynamic tests, plastic deformation of the materials is accompagnied with an increase of temperature because of the inner friction of materials. At low strain rate, due to the long test duration, heat was easily dissipated by the polymeric network. We suppose that is an isothermal process, although some maximum temperature rise of 5 °C was reported [43]. Generally, a high strain rate leads to a marked elevation of Young's modulus and yield stress of the materials. However, it generates a rise in temperature that cannot be ignored. For dynamic test, test duration is very short. There is no heat dissipation which means an adiabatic process. In this case, the rise in temperature has an opposite action. Because a high temperature leads to a decrease of Young's modulus and yield stress of the materials.

Thus, it is important to determine the elevation of temperature during the dynamic test.

Few researchers studied the energy converted into heat during plastic deformation of polymers. The main problem is the ratio β which represents the plastic deformation work converted into heat. Farren and Taylor [44], Taylor and Quinney [45] found that about 90-95% of the energy transformed into heat in the metallic samples. Mason et al. [46], Hodowany et al. [47] found that the ratio of energy transformed into heat depended on the type of metal, the deformation and the strain rate. They found a variation of the ratio β from 60% to 90%.

For polymeric materials, Chou et al. [43] measured the increase of temperature in the case of four polymers (Polymethylmethacrylate, cellulose acetate butyrate, polypropylene and nylon 6-6) by using thermocouples at different strain rates (10^{-4} s^{-1} to 10^{3} s^{-1}). One of their conclusions indicated that at high strain rate (about 50 s^{-1}), the mechanical work has been completely transformed into heat after a certain level of deformation. Boyce et al. [48] have studied the increase of temperature in two polymers (polycarbonate and epoxy EPON 862/W) under low and high strain rates by using an infrared camera. They found that the temperature elevation during the dynamic test may cause a softening temperature (an increase of temperature about 32 °C for polycarbonate at 3400 s^{-1} and about 35°C for epoxy EPON 862/W at 2500 s^{-1}), so the dynamic responses of these two materials show post-yield softening. Values of ratio β varying from 0.4 to 1 were recorded by using a thermocouple by Rittel [49] under strain rates from 5000 s^{-1} to 8500 s^{-1} for polycarbonate. This author had similar conclusions than Hodowany who found that the quantity of energy transformed into heat depended on the deformation level and strain rate. However, Li et al. [50] found

a ratio β of polycarbonate (PC) ranging from 0.5 to 0.6 (400 s^{-1} to 2500 s^{-1}) by using an infrared camera. They concluded that the ratio β did not depend on strain rate in their test strain rate range.

In the literature, different conclusions were reported about the temperature elevation of polymers subjected to high strain rates, even in the case of the same polymer. Figure 1-18 shows the comparison of experimental data among three researchers for the increase of temperature of PC during dynamic compression tests.

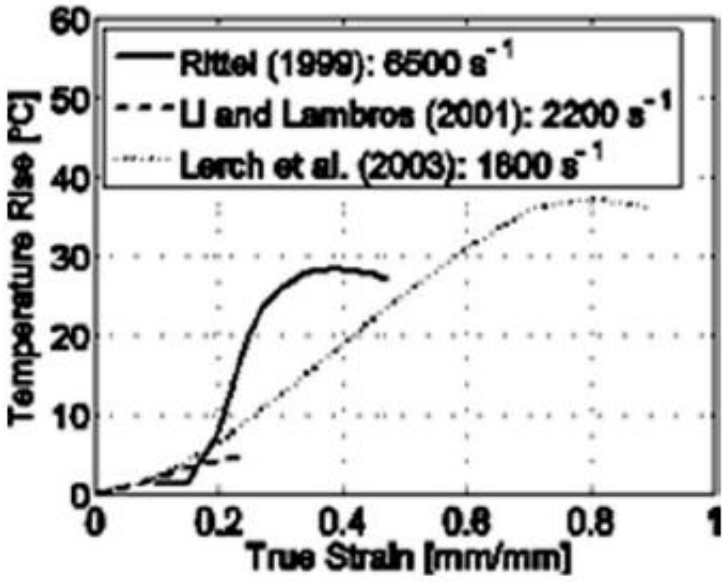

Figure 1-18: Temperature change during dynamic compression test for PC [48].

Garg et al. [48] calculated the ratio β by true stress-strain curve. The temperature was measured by an infrared camera. They defined three types of energy as indicated below:

W_{py} : Plastic deformation work per unit volume N/m^2

U_{py} : Stored energy per unit volume N/m^2

Q_{py} : Dissipated energy per unit volume N/m^2.

The relationship of these three energies is given by Equation 1-1:

$$W_{py} = Q_{py} + U_{py} \tag{1.1}$$

True stress-strain curves and the increase of temperature for PC under uniaxial compression are plotted in Figure 1-19 (a) (b). Plastic deformation work, W_{py}, is calculated by using the curve (a) and Equation 1-2: where σ is the true stress and ε is the true strain.

$$W_{py} = \sigma \cdot \varepsilon \tag{1-2}$$

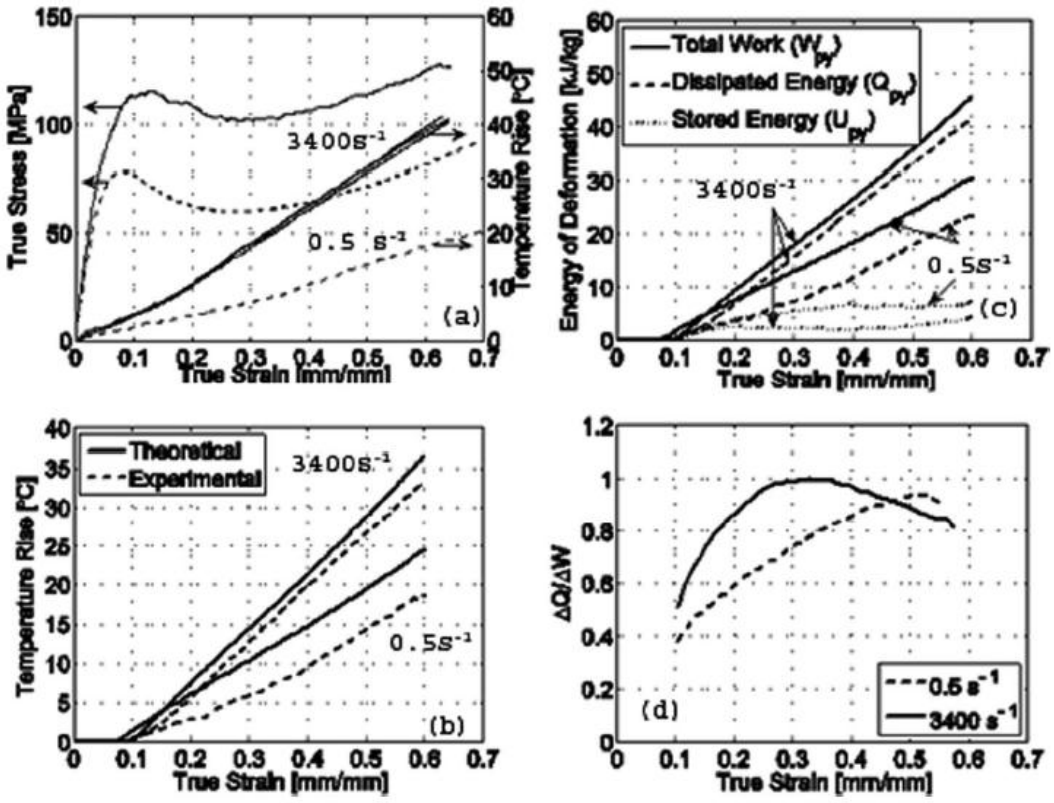

Figure 1-19: (a) True stress - true strain curve and temperature for PC under uniaxial compression (b) Increase of temperature (post-yield point), the upper bound assumes that 100% of the post-yield work to be dissipated as heat (c) Curve of three types of energy as a function of true strain (d) Ratio β as a function of true strain [48].

The dissipated energy, Q_{py}, is given by:

$$Q_{py} = \rho C_p \Delta T \tag{1-3}$$

Here, ρ is the materials' density. C_p is the heat capacity of materials. ΔT is the change of temperature during the test.

Figure 1-19 shows that the energy of plastic deformation was almost dissipated when the true strain reached 0.3 under the strain rate of 3400^{-1}.

Rittel [49] measured the variation of temperature by a thermocouple which was embedded into the samples (PC). The plastic work transferred into heat, β_{int}, is written as:

$$\beta = \frac{\rho C_p \Delta T}{\int dW_{py}} \tag{1-4}$$

Rittel observed that the temperature gradually rose and remained constant for several hundred of microseconds. The maximum elevation of temperature did not exceed 40 °C at a strain rate 2500 s^{-1}. For the value of β_{int} ratio, it was able to get to 1. It means that all the plastic deformation work dissipated as heat (β represents the plastic deformation work converted into heat). However, the maximum value of conversion rate, β_{diff}, was equal to 2.25, greater than 1. This could be explained by the fact that the dissipated energy contained a portion of stored energy in advance. Rittel found that both of them, β_{int} and β_{diff}, depended on the deformation level and strain rate.

1.3.2. Strain rate effect

The mechanical responses of neat polymers and polymer composites are sensitive to strain rate. More specifically, the yield stress and the Young's modulus increase for the high strain rates. In contrast, both yield stress and Young's modulus decrease for the low strain rates [23, 38-42, 51-53].

Ponçot et al. [54] performed the quasi static tensile test for PP/EPR and Polyethylene terephthalate (PET) by using a video-controlled mechanical testing method: VidéoTraction™ technique [55-57]. This system gives access to the true mechanical behavior of polymers for different deformation paths from video measurements performed locally in the middle of the sample. The quasi static tensile responses for PP/EPR and PET under different strain rates are shown in Figure 1-20. For both materials, an increase of the yield stress and Young's modulus is observed with increasing strain rates.

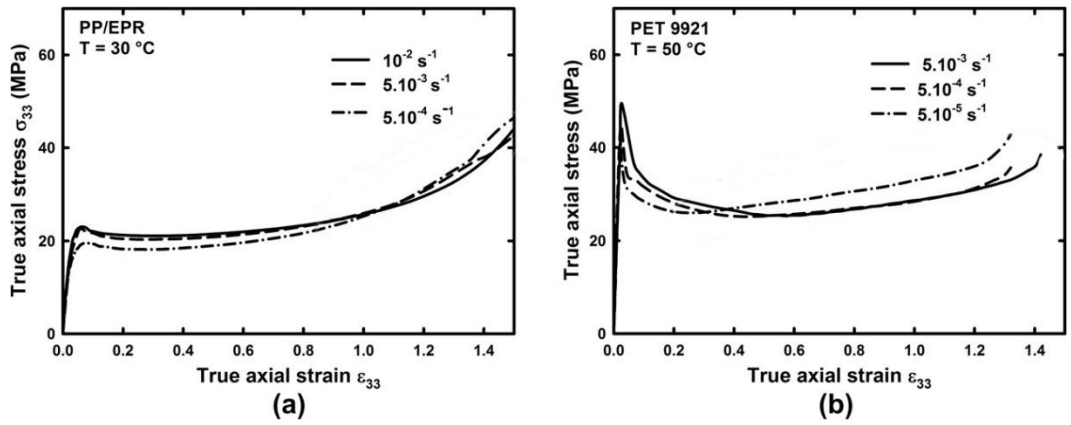

Figure 1-20: True tensile behaviours as a function of the true strain rate in the case of (a) PP/EPR and (b) PET [54].

Wang and Arruda obtained the mechanical responses of TPOs under a wide range of strain rates. Their results are shown in Figure 1-21 [23]. In Figure (a),

samples were tested at low strain rates by means of a MTS servohydraulic test system. The samples in (b) were tested at high strain rates using split Hopkinson pressure bar (SHPB) technique. The dependences of yield stress and Young's modulus on strain rate were plotted in figure (c) and figure (d).

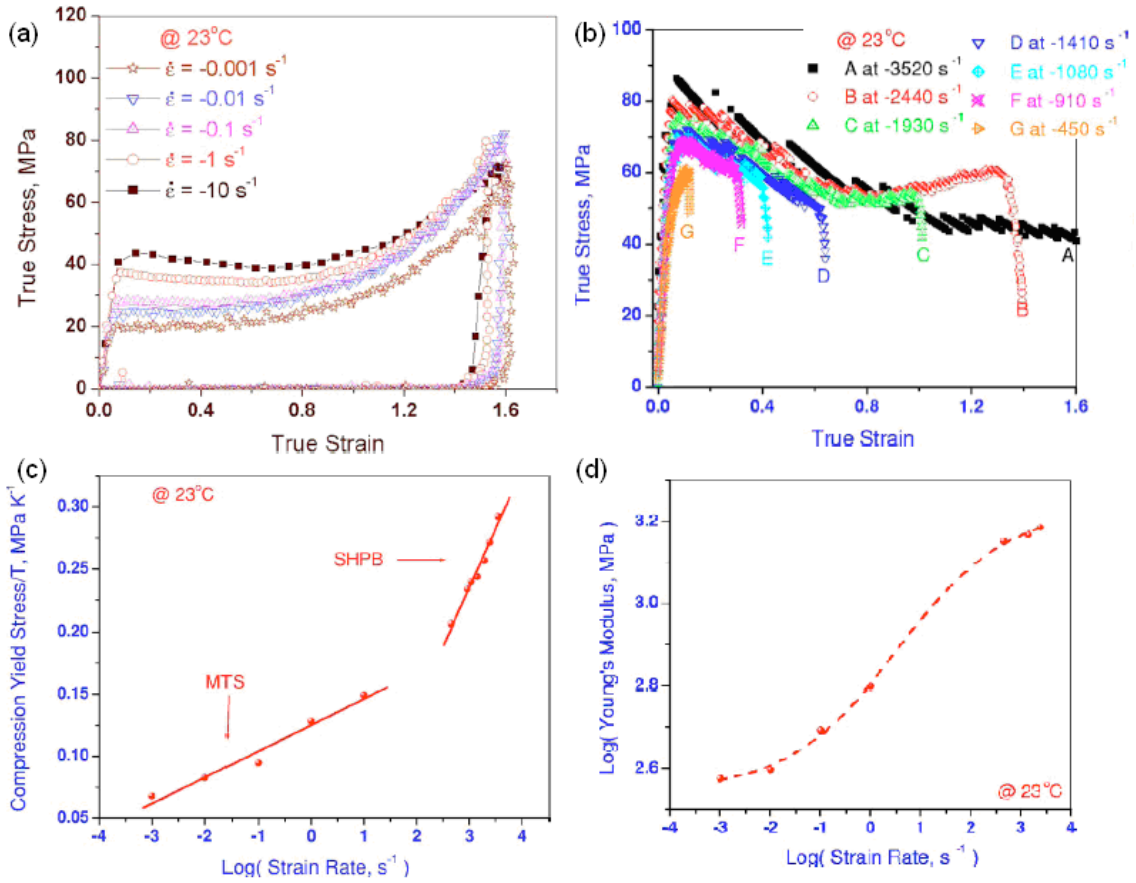

Figure 1-21: Mechanical response of TPOs (blended of PP, EPDM and HDPE) (a) under low strain rates (b) under high strain rates, (c) yield stress depends on strain rate, (d) Young's modulus depends on strain rate [23]

The strain rate increase leads to the hardening of the material due to less molecular chain mobility at large strain rates.

1.4. Recycling

One of the most relevant way to solve the environmental concerns of plastic wastes is implementing the strategy "3Rs", referring to reduce, reuse and recycle.

The giant molecules from plant and animal are naturally recycled. Others like thermosets and cross-linked materials cannot be recycled [9]. In the following, we reported the main existing results for recycling in order to introduce and comment our experimental studies.

1.4.1. Different recycling processes

The main treatment of waste plastics includes several aspects: landfill, energy recovery, feedstock recycling and mechanical recycling.

Landfill is a most used and relatively old treatment of waste plastics. Generally, the low density plastic materials need a large volume for landfill. Along with social progress, shortage of land resources induces an increasing cost. In addition, these plastic wastes are non-biodegradable, they will exist at least hundred years. The precipitation of additives in plastics would contaminate soil and ground water.

Energy recovery also means incineration. Plastics are made from oil. Plastic wastes have a high average calorific value as 35MJ/kg [58]. However, due to their high caloric value, the requirements of oven are complex. Moreover, the incineration of some plastics will release harmful gases like polychlorinated dibenzodioxins (PCDDs) and polychlorinated dibenzofurans (PCDFs) which have a negative effect on atmosphere.

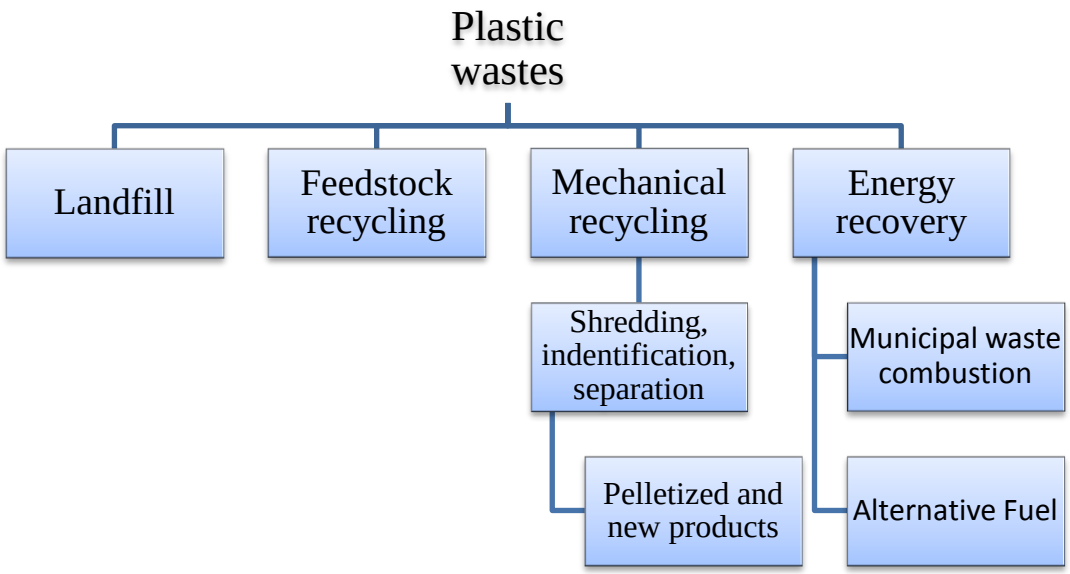

Figure 1-22: Recycling options for managing plastic wastes [59].

Feedstock recycling is also known as chemical recycling. The polymer chains are cleaved for using as raw materials or fossil fuel. Sakata et al. [60] used this method to get plastic-derived oil. Saito et al. [61] successful obtained gasoline and diesel from waste polyvinyl chloride (PVC). Masuda et al.[62] and Gersten et al. [63] found different methods to get high percentage of oil production with less residues from plastic wastes. Few applications of waste plastic or waste plastic mix with coal as fuel technology were done [64-66]. For polypropylene, its chemical formula of thermal decomposition under anaerobic conditions is written as below:

$$\left\{ CH\!=\!\underset{\displaystyle CH_3}{\underset{|}{C}} \right\}_n \xrightarrow[\Delta]{ZnCl_2} n\,(C + H_2 + CH_4 + C_2H_6 + C_3H_8 + \cdots + C_{20}H_{42} + C_{22}H_{46} + C_{25}H_{52})$$

where C_5 ~ C_{11} is gasoline fractions, C_{12} ~ C_{20} is diesel oil, C_1 ~ C_4 is flammable gas.

Mechanical recycling or named physical recycling is the simplest and relatively cheap recycling method for thermoplastics. It generally contains 2 options.

The first option means directly use. Waste plastics are cut and chopped into small flakes, washed contaminants, separated to get different types of plastics and put into an extruder to product new pellets. Finally, these new pellets are molded to manufacture new objects (Figure 1-21). However, the physical and mechanical properties of recycled materials are hardly controlled by this way. Therefore, the first option just uses to make simple productions with low requirement of mechanical properties.

The second mechanical recycling method proposes to use plastic wastes with some modifications. For physical modifications, we can add virgin polymers, rubbers, mineral fillers, alloys or other reinforcements to change the impact strength and toughness of recycled plastic. For chemical modifications, we use methods of crosslinking, grafting, chlorination etc. to improve the properties of recycled materials for required applications.

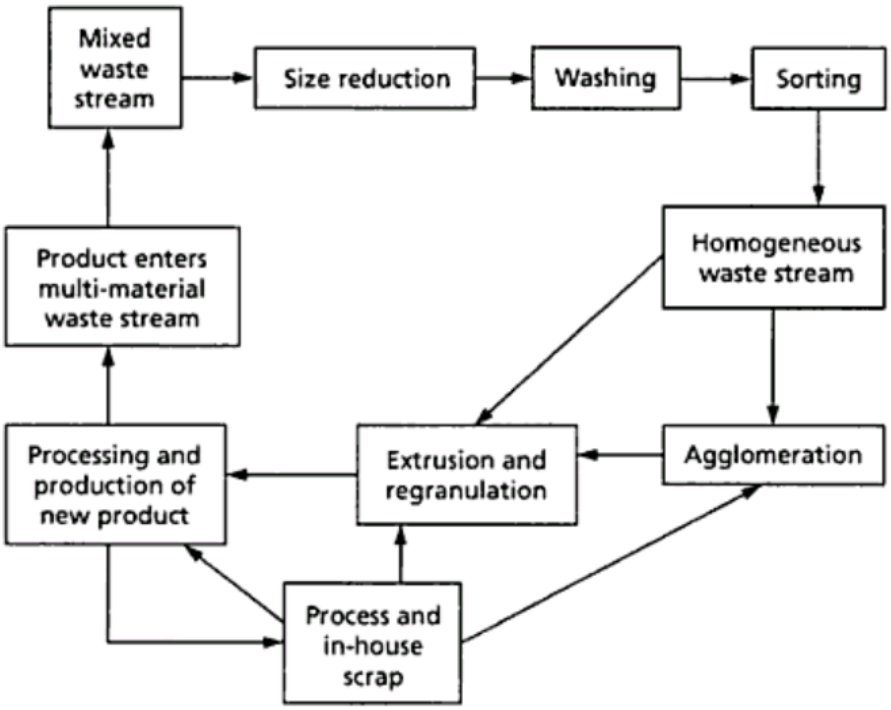

Figure 1-23: Mechanical recycling process for plastic materials [67].

1.4.2. Aspects of polymer degradations

Polymer degradation will lead to a change of the materials properties. These changes are usually undesirable. The property changes may be divided into physical and chemical ones. For physical properties, the degradation of polymer may induce a lower molecular weight, tensile and impact strength, elongation at break. For physical properties, the degradation of polymer may change the chemical structure-formation of functional groups. The mainly degradation processes of polymer are described as follows [68]:

1. Thermal: this occurs during processing or uses polymers at elevated temperatures. Polymers can be degraded by thermolysis at high temperatures to give monomers, oils, gases and water.

2. Mechanical: this occurs on the application of force or physical breakage. Chain scission may also occur here.

3. Ultrasonic: the application of sound at certain frequencies may induce the polymer chains to vibrate and split.

4. Hydrolytic: this occurs in polymers containing functional groups which are sensitive to the effect of water, especially those having a high moisture regain. Here de-esterification and the formation of acids and the original glycol are the main products.

5. Chemical: in this case corrosive chemicals or gases, e.g. ozone, may attack the basic structural functionalities in the polymers causing chain scission and oxidation.

6. Biological: this is specific to only a few polymers which contain functional groups that are attacked by microorganisms.

7. Radiation: on exposure to sunlight (UV) or high energy radiation (X-rays and gamma rays), either the polymer itself or impurities in the polymer will absorb the radiation and be degraded by photolysis resulting lower molecular weight molecules.

1.4.3. Recycling effects on different properties of polypropylene

In the literatures, it was found that the recycling of PP and PP-based composites is characterized by an increase of melt flow index (MFI) (Figure 1-24). This phenomenon is due to a reduction of molecular weight induced by chain scission mechanisms [69-73].

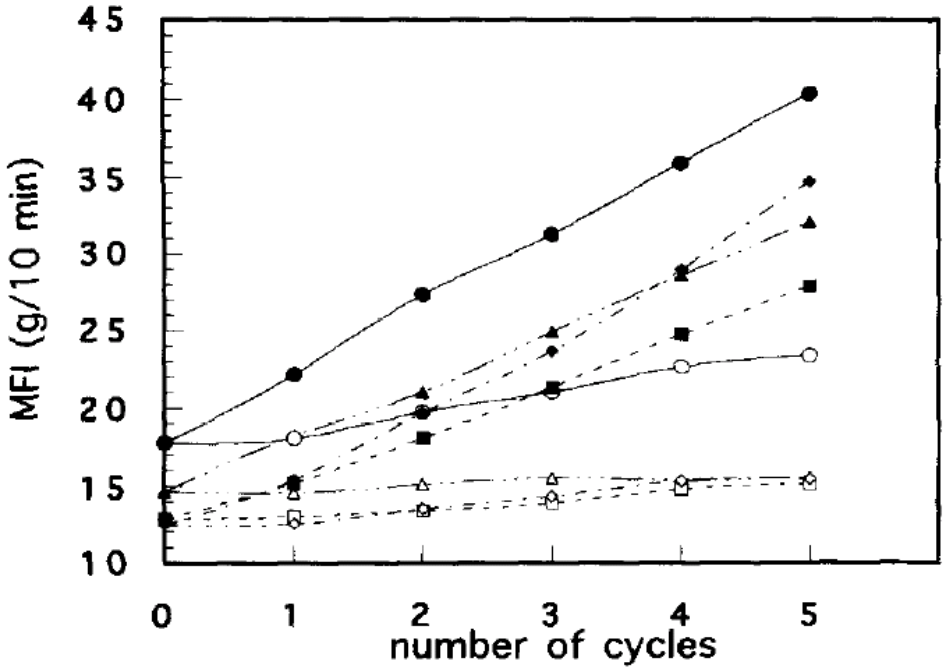

Figure 1-24 : MFI of PP-based materials processed as a function of the number of processing cycles: (●) neat PP, (■) PP-10% talc, (♦) PP-20% talc, (▲) PP-40% talc. Melt temperatures of 200°C (empty symbols) and 250°C (filled symbols) [71].

The lower molecular weight of recycled materials results in an increase in crystallinity of PP matrix [72, 74].

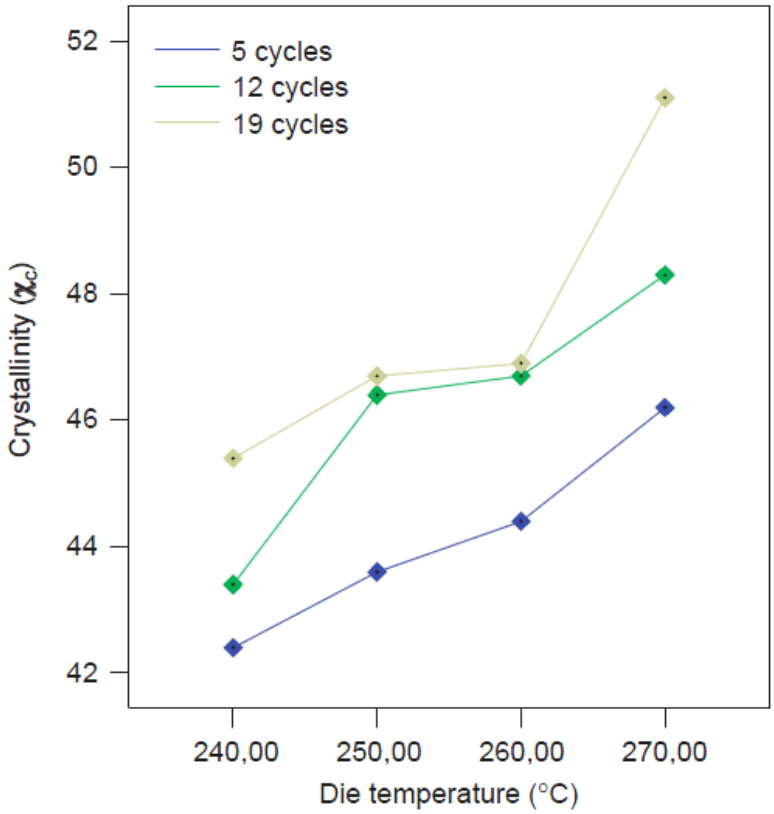

Figure 1-25: Variation of crystallinity (Xc) with die temperature and cycles of extrusion for polypropylene [74].

In the case of PP-based materials submitted to multiple extrusions procedures, Sarrionandia et al. [69], Guerrica-Echevarría et al. [71] and Aurrekoetxea et al. [75] did not observe any significant change in the chemical functional groups of the materials by Fourier transform infrared spectroscopy (FTIR). In particular, no oxidation was observed, which was attributed to the absence of oxygen in the polymer at the melted state [75]. Concerning the thermal stability of recycled PP composites, Jimenez et al. [76] demonstrated that the decomposition temperature of these materials was similar to that of the non-recycled ones. Therefore, recycled PP

composites can be used in the same temperature range than non-recycled PP composites. However, Camacho et al.[77] observed a drop of the degradation temperature of PP with the number of recycling procedure, indicating marked chains scission mechanisms. Concerning mechanical properties, Bahlouli et al. [32] found a continuous decrease of strength, stiffness and toughness of PP/EPR and PP/EPDM/talc composites with increasing the number of recycling up to 12 passes. Similar conclusions were proposed by Da Costa et al.[74] in the case of neat PP up to 19 recycling procedures. These decreases of mechanical properties were attributed to the degradation of the material during the recycling. Nevertheless, Sarrionandia et al. [69] found a constant stiffness and toughness for PP/EPDM/talc composites recycled up to 5 times. Last, Aurreboetxea et al.[75] demonstrated an increase of strength and stiffness in the case of PP recycled up to 8 times due to an increase of crystallinity. These previous works indicate that there is no general trend concerning the impact of recycling on the mechanical properties of neat PP and PP-based composites. Each investigated case has its own set of experimental conditions, and can only be compared with cases characterized by similar experimental conditions.

1.5. Mechanical behavior modeling of polymer-based composite

The materials properties are discussed above where we also represented the temperature and strain rate effects on the mechanical properties of polymeric materials. Although the mechanical behavior of the materials can be obtained by way of experimental test, a robust micromechanical model can be used to predict the materials responses avoiding numerous experimental tests. Conventional micromechanical models are widely used to predict the effective elastic modulus and the effective yield stress of composite materials. In these models, the effective properties are usually calculated as function of the properties of the matrix, the volume/weight fraction and properties of the fillers. The effects of temperature and strain rate on the mechanical properties of materials are not taken into account in these models [78]. In the following, we would like to give a brief introduction of the models for elastic and yield behaviors of polymer with temperature and strain rate dependence.

1.5.1. Temperature and strain rate dependence of elastic behavior

As discussed earlier, the mechanical behavior of both pure polymers and their composites are strongly influenced by the testing temperature and strain rate. Therefore, it is necessary to develop a constitutive model which accounts for these effects. Drozdov [79] proposed a relation for the temperature dependence of the elastic modulus (Equation 1-5):

$$E(T) = E_0 - \frac{E_1}{T_g - T} \tag{1-5}$$

In this model, E_0 and E_1 are the material parameters and T_g is the glass transition temperature of materials. Unfortunately, this equation can only be used below the glass transition temperature. For the temperatures at and above T_g, this model is not valid.

In the literature, few models exists for the prediction of the elastic properties of the rubbery region [80], but they are valid only for temperatures above the glass transition temperature. To cover the entire range below and above T_g, Mahieux and Reifsnider [81] developed a statistical model for modeling the stiffness of polymers under a wide range of temperatures. This model is described below:

$$E(T) = (E_1 - E_2) \cdot \exp\left(-\left(\frac{T}{T_\beta}\right)^{m_1}\right) + (E_2 - E_3) \cdot \exp\left(-\left(\frac{T}{T_g}\right)^{m_2}\right) + E_3 \cdot \exp\left(-\left(\frac{T}{T_f}\right)^{m_3}\right) \quad (1\text{-}6)$$

where the parameter E_1, E_2 and E_3 are the instantaneous stiffnesses of the polymer at the beginning of transition temperatures: β transition, glass transition and flow transition, respectively. Correspondingly, the parameters T_β, T_g and T_f are the β transition temperature, glass transition temperature and melting temperature of the polymer. The parameters m_i represent the Weibull moduli (i=1, 2, 3). The feasibility of this model was validated by applying the model to experimental data chosen at random from the literature. The behavior of six polymers of very different nature was successfully described. Figure 1-26 shows the prediction of the storage modulus by this approach and the experimental results for polyether ether ketone (PEEK) and polyvinylidene chloride (PVDC).

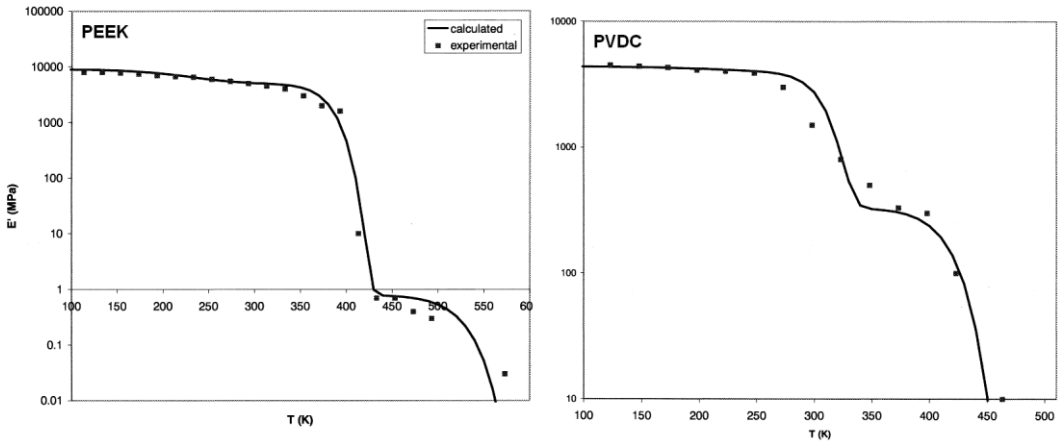

Figure 1-26: Experimental and theoretical results for the storage modulus of PEEK and PVDC [81].

Although this temperature dependence stiffness model can be used under a wide range of temperatures, there is no strain rate dependency in this model. Based on this statistical model, Richeton et al. [35] suggested an approach that includes both temperature and strain rate (or frequency) effects. For this, they incorporated the dependence on frequency (*f*) for each instantaneous stiffness and for each transition temperature as follows:

$$E(T,f)=\left(E_1(f)-E_2(f)\right)\cdot\exp\left(-\left(\frac{T}{T_\beta(f)}\right)^{m_1}\right)+\left(E_2(f)-E_3(f)\right)\cdot\exp\left(-\left(\frac{T}{T_g(f)}\right)^{m_2}\right)+E_3(f)\cdot\exp\left(-\left(\frac{T}{T_f(f)}\right)^{m_3}\right) \quad (1\text{-}7)$$

The parameters m_i remain the same as in Equation (1-6) and the modifications consist of taking the parameters $E_i(f)$ and $T_i(f)$ as frequency dependent. According to physical considerations [35], these frequency dependent parameters are described below [35]:

$$\frac{1}{T_\beta} = \frac{1}{T_\beta^{ref}} + \frac{k}{\Delta H_\beta} \ln\left(f^{ref} / f \right) \tag{1-8}$$

$$T_g = T_g^{ref} + \frac{-C_2^{ref} \cdot \log(f^{ref} / f)}{C_1^{ref} + \log(f^{ref} / f)} \tag{1-9}$$

$$T_f = T_f^{ref} \cdot (1 + 0.01 \cdot \log(f / f^{ref})) \tag{1-10}$$

$$E_i = E_i^{ref} \cdot (1 + s \cdot \log(f / f^{ref})) \tag{1-11}$$

In the above equations, f^{ref} represents the reference frequency, T_i^{ref} means the transition temperatures for a given reference frequency, k refers to the Boltzmann constant, ΔH_β is the β activation energy and C_1^{ref} and C_2^{ref} are the Williams-Landel-Ferry (WLF) equation parameters for a given reference frequency. In Equation (1-11), E_i^{ref} represents the instantaneous stiffness at a reference frequency and s represents sensitivity coefficient of the stiffness to frequency.

By using this new approach, Richeton et al. [35] found good agreement between the theoretical and experimental results of the Young's modulus and the storage modulus in a wide range of temperatures and strain rates for two amorphous polymers, PMMA and PC. Figure 1-27 shows the modeling results and experimental data from quasi-static uniaxial compression tests for the initial Young's modulus under four different strain rates for PC.

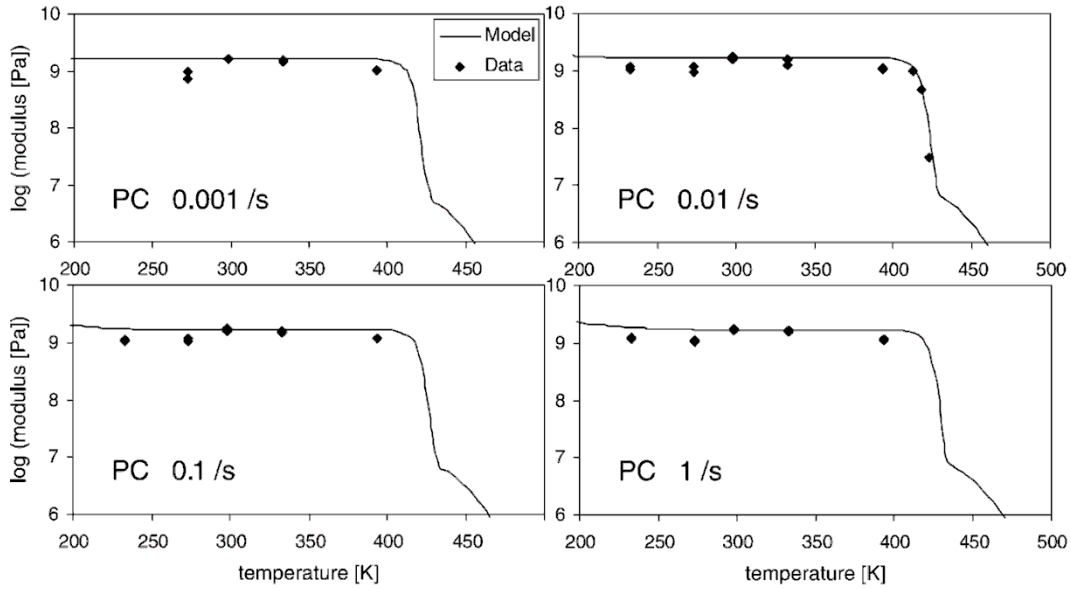

Figure 1-27: Experimental and theoretical results for the compressive modulus of PC [35].

Based on the Richeton model, Matadi et al. [82] extended this approach to PMMA/organoclay nanocomposites. The effect of clay concentration on the storage modulus has been introduced in the Equation (1-7) by replacing the instantaneous storage modulus present in Equation (1-7) by their effective values. The resulted formulation is given by:

$$E(T,f)=\left(E_{1eff}(f)-E_{2eff}(f)\right)\cdot\exp\left(-\left(\frac{T}{T_\beta(f)}\right)^{m_1}\right)+$$
$$\left(E_{2eff}(f)-E_{3eff}(f)\right)\cdot\exp\left(-\left(\frac{T}{T_g(f)}\right)^{m_2}\right)+E_{3eff}(f)\cdot\exp\left(-\left(\frac{T}{T_f(f)}\right)^{m_3}\right) \quad (1\text{-}12)$$

In this equation, the effective instantaneous moduli of nanocomposite $E_{ieff}(f)$ (i=1,2,3) were calculated by using Takayanagi homogenization method [83].

$$E_{ieff}=\frac{\varphi\cdot E_{ic}\cdot E_{im}}{\Omega\cdot E_{im}+(1-\Omega)\cdot E_{ic}}+(1-\varphi)\cdot E_{im} \quad (1\text{-}13)$$

Here, φ and Ω are parameters related to the organoclay and PMMA matrix volume fractions. E_{ic} and E_{im} with i from 1 to 3 represent the instantaneous storage moduli of the PMMA and the organoclay, respectively.

By using this extended Richeton model, Matadi et al. [82] successful predicted the storage moduli of two PMMA-based nanocomposites, for different frequencies, temperatures and for different clay concentrations (Figure 1-28).

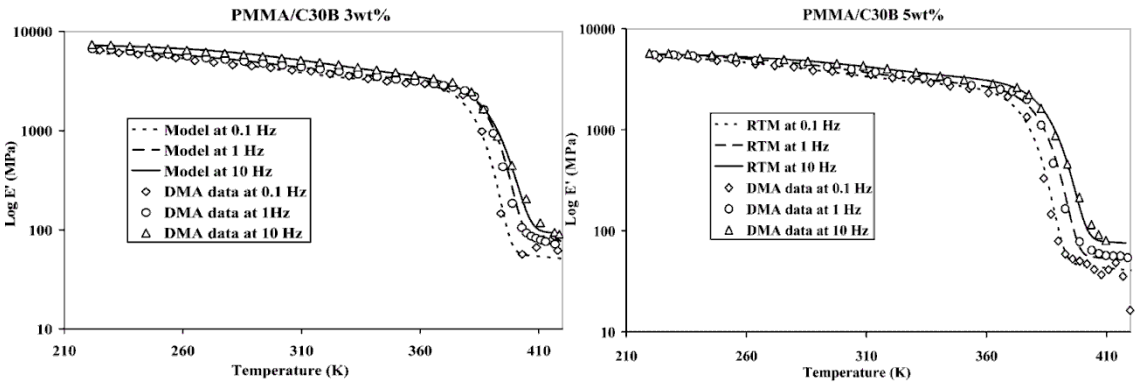

Figure 1-28: Model prediction and experimental data of the storage modulus as function of temperature for PMMA/organoclay nanocomposites with different clay concentrations at different frequencies [82].

Although Matadi et al. [82] proposed to extend Richeton model for the prediction of the stiffness of polymer nanocomposites by using two-phase composite homogenization methods. In a nanocomposite system, the presence of an interphase between the polymer matrix and the nanofillers cannot be neglected. Both exfoliated and intercalated structures result in a huge interfacial area compared to conventional microcomposites. Under this condition, Wang et al. [84] proposed to incorporate Ji's three-phase model [85] into Richeton's approach [35] to compute the effective instantaneous moduli (Equation 1-12) of nanocomposite. Ji model is given by the following equation:

$$\frac{E_{ic}}{E_{im}}=\left[(1-\alpha)+\frac{\alpha-\beta}{(1-\alpha)+\alpha(h-1)/ln(h)}+\frac{\beta}{(1-\alpha)+(\alpha-\beta)(h+1)/2+(E_{if}/E_{im})\beta}\right]^{-1} \quad (1\text{-}14)$$

$$\text{With}\ \begin{cases}\alpha=\sqrt{[2(\tau/t_c)+1]\varphi_f}\\ \beta=\sqrt{\varphi_f}\end{cases} \quad (1\text{-}15)$$

For the platelet-like particles that have the thickness t_c, the same length and width ξ_c, with $\xi_c \gg t_c$, the stiffness of their random orientation dispersion system is calculated according to Equation (1-13) where E_{ic}, E_{im} and E_{if} are the instantaneous elastic moduli of the nanocomposite, the matrix and the fillers, respectively. τ is the interphase thickness, φ_f is the volume fraction of the nanoparticles. Moreover, $h=E_i(0)/E_m$ is the ratio of the interphase modulus on the surface of the particle, $E_i(0)$, to that of the matrix E_m.

The new Richeton-Ji model took account of the temperature, frequency/strain-rate, volume fraction of filler and exfoliation extent of filler in the matrix. Figure 1-29 shows predictions by Richeton-Ji (RJ) model of the compressive modulus of PP/organoclay nanocomposites with different organoclay content.

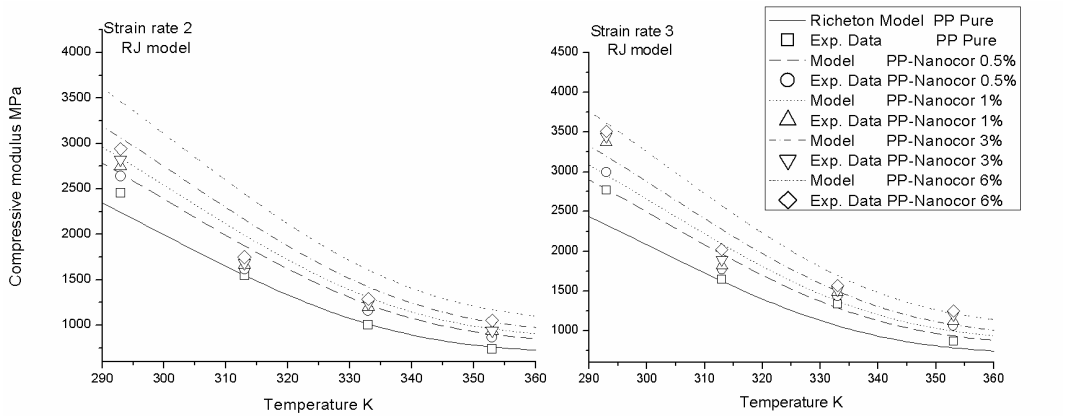

Figure 1-29: Experimental data and theoretical predictions for compressive modulus of pure PP and PP organoclay nanocomposites under strain-rate-2=816 s^{-1} and strain-rate-3=1450 s^{-1} [84].

By using the RJ model, the estimated average particle thicknesses increase with the increase of fillers' volume fraction. This continuous increase of estimated average particle thickness shows a decrease of exfoliation of fillers in the matrix. This exfoliation extent trend shows a good agreement with the TEM observations and XRD measurements.

1.5.2. Temperature and strain rate dependence of yield stress

The strain rate and temperature dependence of the yield behavior can be described by an Eyring's formulation in which the yielding is considered as an activated rate process. Accordingly, the reduced yield stress is given by:

$$\frac{\sigma_y}{T} = \frac{k}{V}\sinh^{-1}\left(\frac{\dot{\varepsilon}}{\dot{\varepsilon}_0 \exp\left(-\frac{\Delta H}{kT}\right)}\right) \tag{1-16}$$

where σ_y is the yield stress, T refers to the absolute temperature, k is the Boltzmann's constant, V is an activation volume, ΔH is an activation energy, $\dot{\varepsilon}$ is the strain rate and $\dot{\varepsilon}_0$ is a constant pre-exponential factor. Several authors [86, 87] indicated that the yield behavior of both amorphous and semi-crystalline polymers could not be represented by a single molecular process, but by rather at least two activated processes acting in parallel.

Richeton et al. [34, 36, 37] developed a new formulation of the cooperative model of Fotherigham and Cherry [86] starting from a strain rate/temperature superposition principle for the yield stress. The expression is given by:

$$\frac{\sigma_y}{T} = \frac{\sigma_i(0) - m \cdot T}{T} + \frac{2k}{\Delta V} \sinh^{-1}\left(\frac{\dot{\varepsilon}}{\dot{\varepsilon}_0 \exp\left(-\frac{\Delta H}{RT} \right)} \right)^{1/n} \tag{1-17}$$

Here, $\sigma_i(0)$ is the internal stress at 0 K, m is a material parameter equal to $\sigma_i(0)/T^*$, T^* being the compensation temperature, n describes the cooperative character of the yield process, ΔH and ΔV are the activation energy and activation volume, respectively. Other parameters have been defined previously.

This model gave good prediction of yield stress for a wide range of strain rates and temperatures, including the high strain rates and glass transition region. A comparison of the strain rate dependence for the compressive yield stress of PC and PMMA between the cooperative model and experimental data is shown in Figure 1-30. The cooperative model shows good agreement with the experimental data for different strain rates at different temperatures.

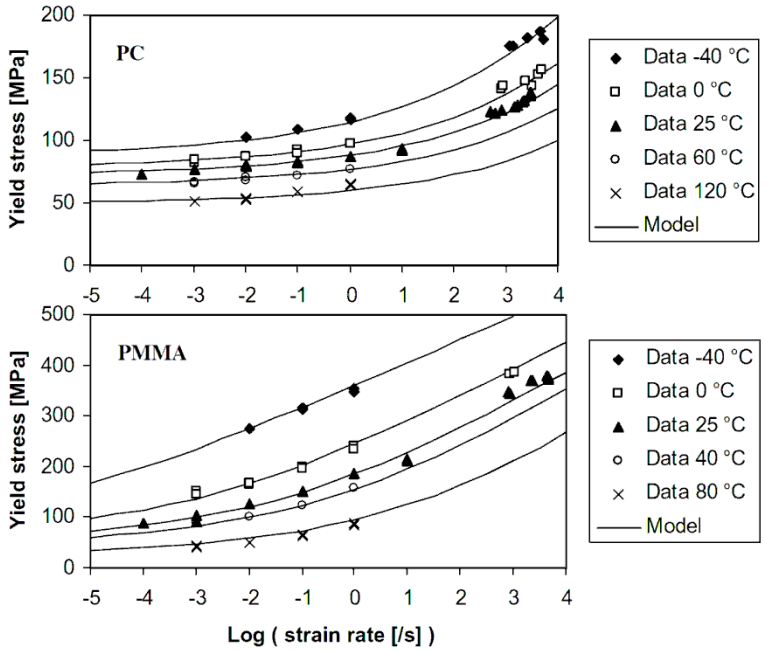

Figure 1-30: Strain rate dependence of the compression yield stress for PC and PMMA [36].

However, Richeton formulation [34] is only focused on amorphous polymers. Considering the semi-crystalline polymers as a two phase material, Gueguen et al. [88] developed an extended formulation for semi-crystalline polymers:

$$\frac{\sigma_y}{T} = \frac{\sigma_i(0) - m \cdot T}{T} + \frac{2k}{V_M} \sinh^{-1}\left(\frac{\dot{\varepsilon}}{\dot{\varepsilon}_0 \exp\left(-\frac{\Delta H_M}{RT} \right)} \right)^{1/n} \tag{1-18}$$

where ΔH_M and V_M are the effective activation energy and effective activation volume, respectively. These two parameters were obtained from the activation parameters of amorphous phase $\Delta H_{amorphous}$, $V_{amorphous}$, and of the crystalline phase, $\Delta H_{Crystalline}$ and $V_{Crystalline}$, following the Takayanagi micromechanical model [83]:

$$\Delta H_M = \frac{\varphi \cdot \Delta H_{Crystalline} \cdot \Delta H_{amorphous}}{\Omega \cdot \Delta H_{amorphous} + (1-\Omega) \cdot \Delta H_{Crystalline}} + (1-\varphi) \cdot \Delta H_{Amorphous}$$
$$V_M = \frac{\varphi \cdot V_{Crystalline} \cdot V_{amorphous}}{\Omega \cdot V_{amorphous} + (1-\Omega) \cdot V_{Crystalline}} + (1-\varphi) \cdot V_{amorphous} \quad (1\text{-}19)$$

Here, φ and Ω are parameters related to the volume fractions of the two phases.

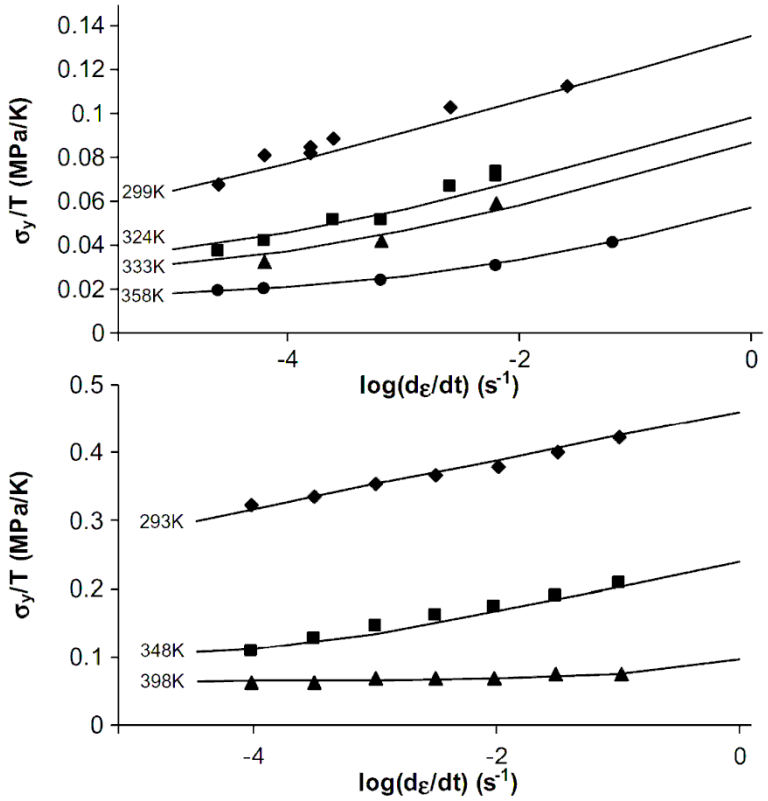

Figure 1-31: Variation of the tensile yield stress/temperature with strain rate for PE and PET [89].

By using Takayanagi homogenization, the effective activation parameters can be calculated by the volume fractions of the amorphous and crystalline phases. The predicted results are in good agreement with the experimental results for polyethylene (PE) and poly(ethylene terephthalate) (PET) in a wide range of temperatures and strain rates (Figure 1-31) [89].

In the work of Matadi et al. [90], the cooperative model was extended to polymer matrix based organoclay nanocomposites (PMMA/Cloisite) by introducing an effective activation energy ΔH_{eff} and an effective activation volume V_{eff}. These effective parameters can be computed using a multiscale theory such as the Takayanagi approach [83] which yields the following relations:

$$\begin{aligned} \Delta H_{eff} &= \frac{\varphi \cdot \Delta H_2 \cdot \Delta H_1}{\Omega \cdot \Delta H_1 + (1-\Omega) \cdot \Delta H_2} + (1-\varphi) \cdot \Delta H_1 \\ V_{eff} &= \frac{\varphi \cdot V_2 \cdot V_1}{\Omega \cdot V_1 + (1-\Omega) \cdot V_2} + (1-\varphi) \cdot V_1 \end{aligned} \tag{1-20}$$

Here φ and Ω are parameters related to the organoclay (f_c) and matrix (f_m) volume fractions:

$$\begin{cases} f_c = \varphi \cdot \Omega \\ f_m = 1 - \varphi \cdot \Omega \end{cases} \tag{1-21}$$

The polymer based organoclay nanocomposite was considered as a two-phase material where the yield processes is described by the activation parameters in the matrix, ΔH_1 and V_1, and in the organoclay phase, ΔH_2 and V_2. The resulted yield process is then expressed by [90]:

$$\frac{\sigma_{y,c}}{T} = \frac{\sigma_i(0) - m \cdot T}{T} + \frac{2k}{V_{eff}} \sinh^{-1}\left(\frac{\dot{\varepsilon}}{\dot{\varepsilon}_0 \exp\left(-\frac{\Delta H_{eff}}{RT} \right)} \right)^{1/n} \tag{1-22}$$

This formulation of the cooperative model gives accurate prediction for the yield stress of PMMA based organoclay nanocomposites (Figure 1-32). The authors also mentioned that the activation energy increases slightly with increasing organoclay

content. By contraries, the activation volume decreases slightly with increasing organoclay concentration.

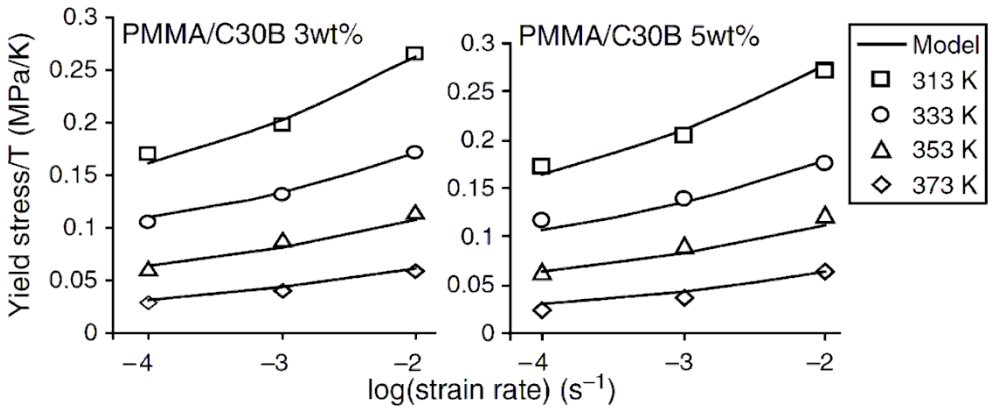

Figure 1-32: Yield stress/temperature versus strain rate of PMMA/organoclay nanocomposites with different clay concentrations [91].

However, this formulation doesn't include the exfoliation degree of organoclay in the matrix. In addition a three phase model, including an interphase between the filler and the matrix, is suited to correctly describe the mechanical properties of polymer based organoclay nanocomposite. Under this condition, Matadi et al. [92] continued to develop this approach to take into account strain rate and temperature effects as well as for the extent of exfoliation of the nanofillers. In this, the microstructure of polymer-based nanocomposite can be simplified into the following three phases: a homogenized semi-crystalline matrix, the nanofillers and the interphase between the matrix and the fillers. The exfoliation degree could be measured by the quantification of the extent of interfacial interaction. This extent of interfacial interaction can be quantitatively characterized by the following relation developed by Pukanszky et al. [93]:

$$\frac{\sigma_{y,c}}{\sigma_{y,M}} = \frac{1-\varphi_f}{1+2.5\varphi_f} Exp(B\varphi_f) \qquad (1\text{-}23)$$

where $\sigma_{y,c}$, $\sigma_{y,M}$ are the yield stresses of the nanocomposite and the polymer matrix, respectively, φ_f the fillers' volume fraction and B a parameter characterizing the interfacial interaction, including the interlayer thickness and interfacial strength.

By introducing this relation in the cooperative model, the yield stress of the nanocomposite as a function of strain rate, temperature, organoclay concentration, and extent of exfoliation can be expressed as:

$$\frac{\sigma_{y,c}}{T}=\left[\frac{1-\varphi_f}{1+2.5\varphi_f}\exp(B\varphi_f)\right]\times\left[\frac{\sigma_i(0)-m\cdot T}{T}+\frac{2k}{V_M}\sinh^{-1}\left(\frac{\dot{\varepsilon}}{\dot{\varepsilon}_0\exp\left(-\frac{\Delta H_M}{RT}\right)}\right)^{1/n}\right] \quad (1\text{-}24)$$

The theoretical predictions for compressive yield stress of PP/organoclay nanocomposites with different organoclay concentrations by this new formulation are shown in Figure 1-28. The simulated results are in good agreement with experimental measurements of the yield stress of PP/organoclay nanocomposites with the effect of exfoliation extent.

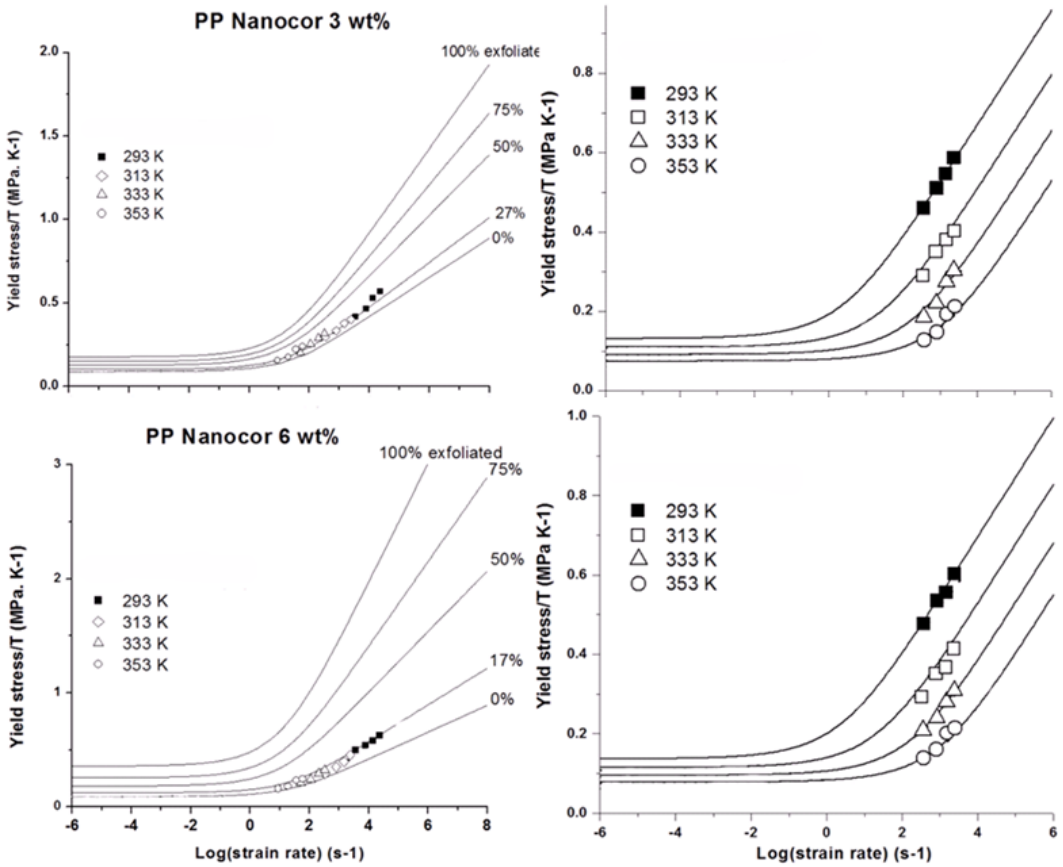

Figure 1-33: Master curve of PP/organoclay nanocomposites with different organoclay concentrations build at a reference temperature of 313K (left), yield stress/temperature versus strain rate of PP/organoclay nanocomposites (right) [92].

1.6. Conclusions

PP is one of the most used semi-crystalline thermoplastic materials. Due to the low cost, high thermal resistance and good mechanical properties, PP shares a large TPs market with a strong growth rate. However, neat PP is brittle at low temperature. For vehicle applications, PP is usually blended with elastomer and talc to improve the impact behavior and to balance the stiffness of materials. Both neat PP and its composites are sensitive to temperature and strain rate. Higher strain rate and low temperature lead to an increase of yield stress and Young's modulus of PP-based composites. After the lifespan of the TPs, the mechanical recycling is the simplest and ecological recycling method for TPs wastes. However, the reprocessing of plastics, conducts under important shear conditions at high temperature, and with the presence of oxygen and impurities, may lead to degradations of the materials and consequently to a loss of properties. Thus, it is necessary to identify the degradation mechanisms of polypropylene based composites resulting from the mechanical recycling. For the aspect of micro-mechanical modeling, we introduced the cooperative model for the yield stress predictions of materials with temperature and strain rate effects. A statistical stiffness model was also represented for the predictions of the elastic behavior with temperature and strain rate dependences.

References

[1] Rosato DV, Rosato MG, Rosato DV. Concise Encyclopedia of Plastics: Springer - Verlag; 2000.

[2] Xanthos M. Functional Fillers for Plastics: John Wiley & Sons; 2010.

[3] Oudet C. Polymères Structure et Propriétés Introduction1993.

[4] J.Richeton. modeling and validation of the finite strain response of amorphous polymers for a wide range of temperature and strain rate: University of Strasbourg; 2005.

[5] Halary J-L, Lauprêtre F, Monnerie L. Polymer materials macroscopic properties and molecular interpretations. Hoboken, N.J.: Wiley; 2011.

[6] Patrick Combette IE. Physique des polymères, Structure, Fabrication, Emploi. 2005;1.

[7] Sirotkin RO, Brooks NW. The effects of morphology on the yield behaviour of polyethylene copolymers. Polymer. 2001;42:3791-3797.

[8] Biron M. Thermoplastics and Thermoplastic Composites. Thermoplastics and Thermoplastic Composites. 2007.

[9] Charles E, Carraher J. Giant Molecules: Essential Materials for Everyday Living and Problem Solving. Journal of Chemical Education. 1990;67.

[10] Hans-Henning Kausch NH, Christopher John Plummer, Pierre Decroly. Traité des matériaux2001.

[11] DUVAL C. Polypropylènes (PP)2004.

[12] Patrick Combette IE. Physique des polymères: HERMANN EDITEURS; 2005.

[13] Rosato DV, Rosato MG, Rosato DV. Concise Encyclopedia of Plastics. Springer - Verlag; 2000.

[14] Sperling LH. Introduction to Physical Polymer Science. 4 ed. New Jersey: John Wiley & Sons, Inc.; 2006.

[15] C. Yu T. Mentallocane plastomer modification of polypropylenes. Polymer Engineering and Science. 2001;41:656-671.

[16] Yu TC, Davis DS. Metallocene Plastomer Modification of Clear Polypropylene for Impact Enhancement. Metallocene Catalyzed Polymers. Norwich, NY: William Andrew Publishing; 1998. p. 209-214.

[17] Massey LK. Polyolefin Plastomers (POP). Permeability Properties of Plastics and Elastomers (Second Edition). Norwich, NY: William Andrew Publishing; 2002. p. 249-250.

[18] Chum PS, Swogger KW. Olefin polymer technologies--History and recent progress at The Dow Chemical Company. Progress in Polymer Science. 2008;33:797-819.

[19] Rémi D, Gérard F. Introduction aux matériaux polymères: Tech.& Doc./Lavoisier; 1997.

[20] Utracki LA. Polymer Blends Handbook: Kluwer Academic Publishers; 2002.

[21] Rosato D. Reinforced Plastics Handbook. 3 ed: ELSEVIER; 2004.

[22] Karger-Kocsis J. Polypropylene - An A-Z Reference. Springer - Verlag; 1999.

[23] Wang Y, Arruda EM. Constitutive Modeling of a Thermoplastic Olefin Over a Broad Range of Strain Rates. Journal of Engineering Materials and Technology. 2006;128:551-558.

[24] Zebarjad SM, Bagheri R, Reihani SMS, Lazzeri A. Deformation, yield and fracture of elastomer-modified polypropylene. Journal of Applied Polymer Science. 2003;90:3767-3779.

[25] Zebarjad SM. Fracture mechanism under dynamic loading of elastomer-modified polypropylene. Materials Letters. 2003;57:2733-2741.

[26] Zhou Y, Mallick PK. Effects of temperature and strain rate on the tensile behavior of unfilled and talc-filled polypropylene. Part I: Experiments. Polymer Engineering and Science. 2002;42:2449-2460.

[27] Zhou Y, Rangari V, Mahfuz H, Jeelani S, Mallick PK. Experimental study on thermal and mechanical behavior of polypropylene, talc/polypropylene and polypropylene/clay nanocomposites. Materials Science and Engineering: A. 2005;402:109-117.

[28] Pessey D, Bahlouli N, Ahzi S, Khaleel M. Strain rate effects on the mechanical response of polypropylene-based composites deformed at small strains. Polymer Science Series A. 2008;50:690-697.

[29] Pessey D, Bahlouli N, Pattofatto S, Ahzi S. Polymer composites for the automotive industry: Characterisation of the recycling effect on the strain rate sensitivity. International Journal of Crashworthiness. 2008;13:411-424.

[30] Pessey D, Bahlouli N, Raveyre C, Guillet J, Ahzi S, Hiver J-M, Dahoun A. Characterization of Contamination Effects for Two Polypropylene-Based Materials. Polymer Engineering and Science. 2010;50:1-9.

[31] Rogueda-Berriet C, Bahlouli N, Pessey D, Rémond Y. Mechanical behavior of recycled polypropylene composites under tensile, bending, and creep loading: Experimental and modeling. Journal of Engineering Materials and Technology. 2011;133:030907.

[32] Bahlouli N, Pessey D, Raveyre C, Guillet J, Ahzi S, Dahoun A, Hiver JM. Recycling effects on the rheological and thermomechanical properties of polypropylene-based composites. Materials and Design. 2012;33:451-458.

[33] Öksüz M, Eroglu M, Yıldırım H. Effect of talc on the properties of polypropylene/ethylene/propylene/diene terpolymer blends. Journal of Applied Polymer Science. 2006;101:3033-3039.

[34] Richeton J, Ahzi S, Daridon L, Remond Y. A formulation of the cooperative model for the yield stress of amorphous polymers for a wide range of strain rates and temperatures. Polymer. 2005;46:6035-6043.

[35] Richeton J, Schlatter G, Vecchio KS, Rémond Y, Ahzi S. A unified model for stiffness modulus of amorphous polymers across transition temperatures and strain rates. Polymer. 2005;46:8194-8201.

[36] Richeton J, Ahzi S, Vecchio KS, Jiang FC, Adharapurapu RR. Influence of temperature and strain rate on the mechanical behavior of three amorphous polymers: Characterization and modeling of the compressive yield stress. International Journal of Solids and Structures. 2006;43:2318-2335.

[37] Richeton J, Ahzi S, Vecchio KS, Jiang FC, Makradi A. Modeling and validation of the large deformation inelastic response of amorphous polymers over a wide range of temperatures and strain rates. International Journal of Solids and Structures. 2007;44:7938-7954.

[38] Brown EN, Rae PJ, Gray GT. The influence of temperature and strain rate on the tensile and compressive constitutive response of four fluoropolymers. J Phys IV France. 2006;134:935-940

[39] Cady CM, Blumenthal WR, III GTG, Idar DJ. Determining the constitutive response of polymeric materials as a function of temperature and strain rate. J Phys IV France. 2003;110:27-32.

[40] Gray GT, Blumenthal WR, Trujillo CP, Carpenter RW. Influence of temperature and strain rate on the mechanical behavior of Adiprene L-100. J Phys IV France. 1997;7:523.

[41] Brown EN, Willms RB, Gray GT, Rae PJ, Cady CM, Vecchio KS, Flowers J, Martinez MY. Influence of Molecular Conformation on the Constitutive Response of Polyethylene: A Comparison of HDPE, UHMWPE, and PEX. Experimental Mechanics. 2007;47:381-393.

[42] YIN, N. Z, WANG, J. T. Deformation of PC/ABS alloys at elevated temperatures and high strain rates. Kidlington, ROYAUME-UNI: Elsevier; 2008.

[43] Chou S, Robertson K, Rainey J. The effect of strain rate and heat developed during deformation on the stress-strain curve of plastics. Experimental Mechanics. 1973;13:422-432.

[44] Farren WS, Taylor GI. The Heat Developed during Plastic Extension of Metals. Proceedings of the Royal Society of London Series A. 1925;107:422-451.

[45] Taylor GI, Quinney H. The Latent Energy Remaining in a Metal after Cold Working. Proceedings of the Royal Society of London Series A. 1934;143:307-326.

[46] Mason JJ, Rosakis AJ, Ravichandran G. On the strain and strain rate dependence of the fraction of plastic work converted to heat: an experimental study using high speed infrared detectors and the Kolsky bar. Mechanics of Materials. 1994;17:135-145.

[47] Hodowany J, Ravichandran G, Rosakis AJ, Rosakis P. Partition of plastic work into heat and stored energy in metals. Experimental Mechanics. 2000;40:113-123.

[48] Garg M, Mulliken AD, Boyce MC. Temperature Rise in Polymeric Materials During High Rate Deformation. Journal of Applied Mechanics. 2008;75:011009-011008.

[49] Rittel D. On the conversion of plastic work to heat during high strain rate deformation of glassy polymers. Mechanics of Materials. 1999;31:131-139.

[50] Li Z, Lambros J. Strain rate effects on the thermomechanical behavior of polymers. International Journal of Solids and Structures. 2001;38:3549-3562.

[51] Jordan JL, Siviour CR, Foley JR, Brown EN. Compressive properties of extruded polytetrafluoroethylene. Polymer. 2007;48:4184-4195.

[52] Lauro F, Oudin J. Static and dynamic behaviour of a polypropylene for bumpers. International Journal of Crashworthiness. 2003;8:553-558.

[53] Morin D, Haugou G, Bennani B, Lauro F. Experimental characterization of a toughened epoxy adhesive under a large range of strain rates. Journal of Adhesion Science and Technology. 2011;25:1581-1602.

[54] Ponçot M, Addiego F, Dahoun A. True intrinsic mechanical behaviour of semi-crystalline and amorphous polymers: Influences of volume deformation and cavities shape. International Journal of Plasticity. 2013;40:126-139.

[55] Addiego F, Dahoun A, G'Sell C, Hiver JM. Volume variation process of high-density polyethylene during tensile and creep tests. Oil and Gas Science and Technology. 2006;61:715-724.

[56] Addiego F, Dahoun A, G'Sell C, Hiver JM, Godard O. Effect of microstructure on crazing onset in polyethylene under tension. Polymer Engineering and Science. 2009;49:1198-1205.

[57] Martin J, Ponç M, Bourson P, Dahoun A, Hiver JM. Study of the crystalline phase orientation in uniaxially stretched polypropylene by Raman spectroscopy:

Validation and use of a time-resolved measurement method. Polymer Engineering and Science. 2011;51:1607-1616.

[58] Goodship V. Introduction to plastic recycling. Warwick University: Woodhead; 2007.

[59] Kang H-Y, Schoenung JM. Electronic waste recycling: A review of U.S. infrastructure and technology options. Resources, Conservation and Recycling. 2005;45:368-400.

[60] Sakata Y, Bhaskar T, Uddin MA, Muto A, Matsui T. Development of a catalytic dehalogenation (Cl, Br) process for municipal waste plastic-derived oil. Journal of Material Cycles and Waste Management. 2003;5:113-124.

[61] Saito K, Narita H. Studies on the dechlorination and oil-production technology of waste plastics. Journal of Material Cycles and Waste Management. 2001;3:93-98.

[62] Masuda T, Kushino T, Matsuda T, Mukai SR, Hashimoto K, Yoshida S-i. Chemical recycling of mixture of waste plastics using a new reactor system with stirred heat medium particles in steam atmosphere. Chemical Engineering Journal. 2001;82:173-181.

[63] Gersten J, Fainberg V, Garbar A, Hetsroni G, Shindler Y. Utilization of waste polymers through one-stage low-temperature pyrolysis with oil shale. Fuel. 1999;78:987-990.

[64] Kato K, Nomura S, Uematsu H. Waste plastics recycling process using coke ovens. Journal of Material Cycles and Waste Management. 2003;5:98-101.

[65] Haghseresht F, Lu GQ. Adsorption Characteristics of Phenolic Compounds onto Coal-Reject-Derived Adsorbents. Energy and Fuels. 1998;12:1100-1107.

[66] Luo M, Curtis CW. Effect of reaction parameters and catalyst type on waste plastics liquefaction and coprocessing with coal. Fuel Processing Technology. 1996;49:177-196.

[67] Goodship V. Introduction to Plastics Recycling, 2nd Edition: Smithers Rapra; 2007.

[68] Allen NS. Fundamentals of Polymer Degradation and Stabilization: Springer; 1992.

[69] Sarrionandia M, Lopez-Arraiza A, Aurrekoetxea J, Arostegui A. Structure and mechanical properties of a talc-filled polypropylene/ethylene-propylene-diene composite after reprocessing in the melt state. Journal of Applied Polymer Science. 2009;114:1195-1201.

[70] Ramírez-Vargas E, Navarro-Rodríguez D, Blanqueto-Menchaca AI, Huerta-Martínez BM, Palacios-Mezta M. Degradation effects on the rheological and mechanical properties of multi-extruded blends of impact-modified polypropylene

and poly(ethylene-co-vinyl acetate). Polymer Degradation and Stability. 2004;86:301-307.

[71] Guerrica-Echevarría G, Eguiazábal JI, Nazábal J. Effects of reprocessing conditions on the properties of unfilled and talc-filled polypropylene. Polymer Degradation and Stability. 1996;53:1-8.

[72] Martins MH, De Paoli MA. Polypropylene compounding with post-consumer material: II. Reprocessing. Polymer Degradation and Stability. 2002;78:491-495.

[73] Strömberg E, Karlsson S. The design of a test protocol to model the degradation of polyolefins during recycling and service life. Journal of Applied Polymer Science. 2009;112:1835-1844.

[74] Da Costa HM, Ramos VD, De Oliveira MG. Degradation of polypropylene (PP) during multiple extrusions: Thermal analysis, mechanical properties and analysis of variance. Polymer Testing. 2007;26:676-684.

[75] Aurrekoetxea J, Sarrionandia MA, Urrutibeascoa I, Maspoch ML. Effects of recycling on the microstructure and the mechanical properties of isotactic polypropylene. Journal of Materials Science. 2001;36:2607-2613.

[76] Jiménez A, Torre L, Kenny JM. Processing and properties of recycled polypropylene modified with elastomers. Plastics, Rubber and Composites. 2003;32:357-367.

[77] Camacho W, Karlsson S. Assessment of thermal and thermo-oxidative stability of multi-extruded recycled PP, HDPE and a blend thereof. Polymer Degradation and Stability. 2002;78:385-391.

[78] Fu S-Y, Feng X-Q, Lauke B, Mai Y-W. Effects of particle size, particle/matrix interface adhesion and particle loading on mechanical properties of particulate-polymer composites. Composites Part B: Engineering. 2008;39:933-961.

[79] Drozdov AD. Viscoelastoplasticity of amorphous glassy polymers. European Polymer Journal. 2000;36:2063-2074.

[80] Murayama T, Bell JP. Relation between the network structure and dynamic mechanical properties of a typical amine-cured epoxy polymer. journal of polymer science part b-polymer physics. 1970;8:437-445.

[81] Mahieux CA, Reifsnider KL. Property modeling across transition temperatures in polymers: a robust stiffness-temperature model. Polymer. 2001;42:3281-3291.

[82] Matadi Boumbimba R, Said A, Nadia B, David R, José G. Dynamic mechanical properties of PMMA/Organoclay Nanocomposite:Experiments and Modeling. Journal of Engineering Materials and Technology. 2011;133:030908

[83] Takayanagi M. Mem Fac Eng. Kyushu Univ. 1963;23:1.

[84] Wang K, Ahzi S, Matadi Boumbimba R, Bahlouli N, Addiego F, Rémond Y. Micromechanical modeling of the elastic behavior of polypropylene based organoclay nanocomposites under a wide range of temperatures and strain rates/frequencies. Mechanics of Materials. 2013.

[85] Ji XL, Jing JK, Jiang W, Jiang BZ. Tensile modulus of polymer nanocomposites. Polymer Engineering and Science. 2002;42:983-993.

[86] Fotheringham D, Cherry BW, Bauwens-Crowet C. Comment on "the compression yield behaviour of polymethyl methacrylate over a wide range of temperatures and strain-rates". Journal of Materials Science. 1976;11:1368-1371.

[87] Bauwens-Crowet C, Bauwens JC. Effect of thermal history on the tensile yield stress of polycarbonate in the β transition range. Polymer. 1983;24:921-924.

[88] Gueguen O, Richeton J, Ahzi S, Makradi A. Micromechanically based formulation of the cooperative model for the yield behavior of semi-crystalline polymers. Acta Materialia. 2008;56:1650-1655.

[89] Gueguen O, Richeton J, Ahzi S, Makradi A. Micromechanically based formulation of the cooperative model for the yield behavior of semi-crystalline polymers. Acta Materialia. 2008;56:1650-1655.

[90] Matadi R, Gueguen O, Ahzi S, Gracio J, Muller R, Ruch D. Investigation of the stiffness and yield behaviour of melt-intercalated poly(methyl methacrylate)/organoclay nanocomposites: Characterisation and modelling. Journal of Nanoscience and Nanotechnology. 2010;10:2956-2961.

[91] Matadi R, Gueguen O, Ahzi S, Gracio J, Muller R, Ruch D. Investigation of the Stiffness and Yield Behaviour of Melt-Intercalated Poly(methyl methacrylate)/Organoclay Nanocomposites: Characterisation and Modelling. Journal of Nanoscience and Nanotechnology. 2010;10:2956-2961.

[92] Matadi Boumbimba R, Wang K, Bahlouli N, Ahzi S, Rémond Y, Addiego F. Experimental investigation and micromechanical modeling of high strain rate compressive yield stress of a melt mixing polypropylene organoclay nanocomposite. Mechanics of Materials. 2012;52:58-68.

[93] Pukánszky Jr B, Bagdi K, Tóvölgyi Z, Varga J, Botz L, Hudak S, Dóczi T, Pukánszky B. Nanophase separation in segmented polyurethane elastomers: Effect of specific interactions on structure and properties. European Polymer Journal. 2008;44:2431-2438.

Chapter 2:

Effects of fillers content on the recycled polypropylene-based composites

2. Effects of fillers content on the recycled polypropylene-based composites

2.1. Introduction

Our work is focused on the impact of recycling on the properties of PP/ethylene octene copolymer (EOC)/talc composites that are novel composite systems for car bumper application. To understand the impact of recycling on these composites, we decided to investigate the effect of recycling on the neat PP, PP/EOC and PP/talc. Thus, the elementary degradation mechanisms of the PP-based materials induced by EOC and talc could be easily assessed by this material decoupling.

The purpose of this chapter is to identify the thermomechanical degradation mechanisms of PP/EOC and PP/talc blends, as a function of fillers' content, occurring during recycling procedures consisting of grinding steps and re-extrusion steps. To this end, gel permeation chromatography (GPC) was used to measure the molecular weight of materials. Melt flow index measurements (MFI) were conducted to obtain information about the rheological properties of composites. The thermal stability of the materials was characterized by thermogravimetric analysis (TGA). Fourier transform infrared spectroscopy (FTIR) was used to analyze the chemical properties of the materials. The crystalline properties of composites were identified by differential scanning calorimetry (DSC) and wide-angle X-ray scattering (WAXS). The morphology of the materials was analyzed by scanning electron microscopy (SEM). Finally, the mechanical behavior of PP blends was investigated by dynamic mechanical analysis (DMA) and tensile testing.

2.2. Materials and processing

2.2.1. Materials

The polypropylene (PP) selected for this study is a homopolymer reference Moplen HP500N that is a highly isotactic grade produced by Lyondellbasell (Frankfurt am Main, Germany). This PP is characterized by a MFI of 12 g/ 10 min and a density of 0.9 g/cm^3 [1]. The impact modifier of polypropylene is a metallocene ethylene octene copolymer (EOC) Exact TM 8230 supplied by Exxonmobil (Brussels, Belgium). EOC has a MFI of 30 g/10 min and a density of 0.882 g/ cm^3, while it contains 72 wt. % of ethylene and 28 wt. % of octene. The talc powder, referenced Steamic T1 CF, was kindly offered by Luzenac (Toulouse, France) and has a density of 2.78 g/cm^3 and a median diameter (D50) of 1.9 μm (based on sedimentation analyses).

2.2.2. Processing

PP blends containing 0 wt. %, 10 wt. % and 20 wt. % of EOC (PP/EOC, 100/0, 90/10, 80/20, respectively) and PP blends containing 0 wt. %, 10 wt. % and 20 wt. % of talc (PP/talc, 100/0, 90/10, 80/20, respectively) were prepared by melt processing. For PP/EOC, the raw materials of PP and EOC in form of pellet were first carefully compounded by hand. For PP/talc, the talc powder was dried for 12h at 80 °C and then carefully compounded by hand with PP pellet. Materials were mixed within a BUSS Kneader extruder model PR46 (Pratteln, Switzerland) at 200 °C and 50 rpm. Extrusion was conducted with a single screw (diameter of 46.5 mm and L/D=11) and under air conditions. The obtained melted filaments (extrudates) of composites were quenched by means of a cold water bath and were subsequently pelletized using a

rapid granulator. The obtained pellets were dried in an air-circulating oven during 60 min to eliminate water, and hence, to minimize the moisture for the subsequent step [2]. To simulate recycling procedures, both neat PP, PP/EOC, PP/talc blends were subjected to multiple extrusion procedures using the same extruder and the same processing conditions, up to 6 recycling procedures. We present in this study the results obtained for the recycling number 1, 3 and 6. We note that 6 processing passes are enough to identify the degradation mechanisms [3].

Finally, dumbbell-shaped tensile samples for all materials (ASTM D638, type Ⅰ) were injected by Billion 90 tons injection molding machine (Bellignat, France) with a temperature profile ranging from 190°C to 220°C (from the hopper to the nozzle) and a screw rotation speed of 180 rpm. The duration of molding was 60 s under a constant mould temperature of 60 °C and a constant pressure of 70 bars (Figure 2-1). In the following, neat PP, PP/EOC and PP/talc blends were denoted as PP neat, PP/EOC x/y and PP/talc x/y, respectively, where x, y are the weight percent of PP, EOC and talc, respectively. Concerning the recycling number, it was denoted as 0P, 1P, 3P and 6P.

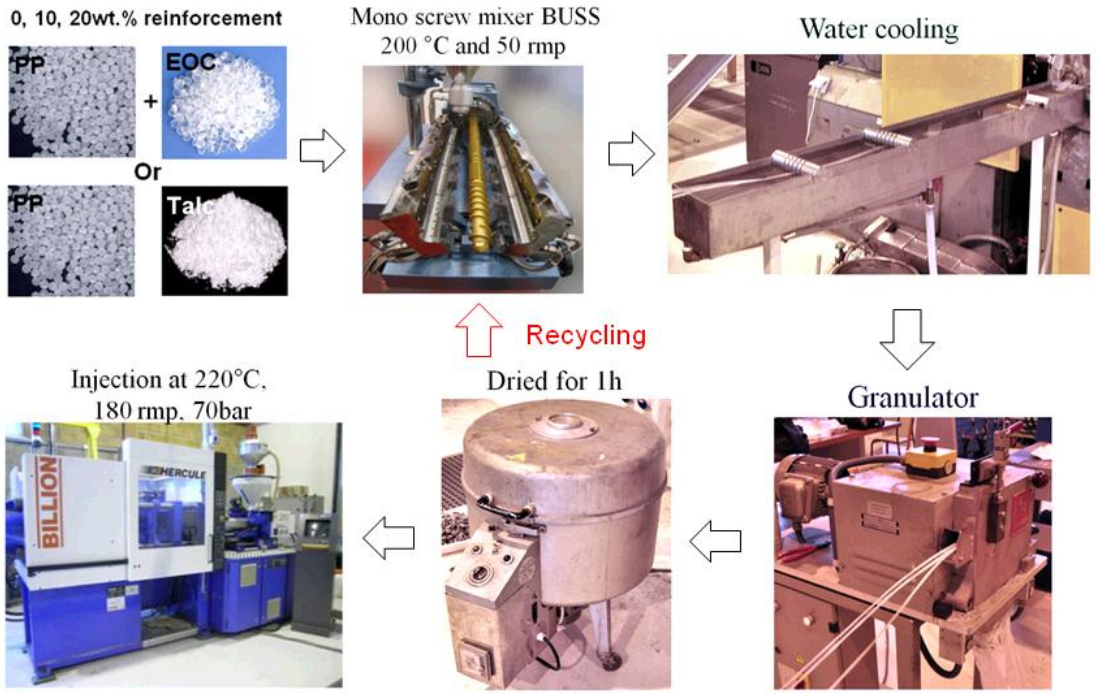

Figure 2-1: Reprocessing of PP-based composites.

2.3. Experimental characterization

2.3.1. Molecular weight characterization

The molecular weight determinations were performed in trichlorobenzene using a gel permeation chromatography (GPC) system with a differential refractive index detector (DRI). For PP/talc composites, talc was filtered before being injected into the system of GPC. We measured the number-average (Mn), weight-average (Mw), and z-average (Mz) molecular weights of EOC, the non-recycled and recycled neat PP and PP blends. The molecular weight distribution of EOC was computed using a universal calibration for polyethylene where the molecular weight distribution of neat PP and PP blends was computed using a universal calibration for polypropylene. Each GPC measurement was repeated on 2 samples, and hence, we report here averaged values.

2.3.2. Rheological characterization

The melt flow index (MFI) was measured by a melt flow indexer Davenport serial number 1211 (London, United Kingdom), based on the standard ISO 1133 at 230°C with a load of 2.16 kg. MFI is an assessment of average molecular weight and is an inverse measure of the melt viscosity. A low molecular weight normally leads to a high fluidity, and hence corresponds to a high MFI. For this reason, the MFI measurement is a rapid method to obtain qualitative changes of molecular weight of polymer during multiple extrusions. MFI values were averaged from 5 measurements for each material.

2.3.3. Thermal characterization

The thermal stability of the materials was investigated by thermogravimetric analysis (TGA) using a Netzsch STA 409 PC/PG instrument (Selb, Germany). To this end, samples with mass 20±1 mg were introduced in alumina crucibles and were heated up to 800°C with a heat rate of 10°C/min under nitrogen atmosphere. We measured the decomposition temperature (T_{onset}) and the temperature corresponding to a weight loss of 5 % (T_5). TGA investigation reported representative curves and values of T_{onset} and T_5.

2.3.4. Chemical characterization

To characterize the oxidation state of the non-recycled and recycled PP blends, Fourier transform infrared spectroscopy (FTIR) measurements were done with a Bruker Tensor 27 (Ettlingen, Germany). Tests were conducted with the reflection mode and with a resolution 4 cm^{-1}. A total of 50 scans was conducted for each material, and the results are shown by the average representative scans. To verify the

possible chemical structure modifications of talc at the temperature of extrusion, the talc powder was heated for 7h at 200 °C in an air-circulating oven and then was tested by FTIR. We considered that 7h was much longer than the effective time corresponding to 6 re-extrusions.

2.3.5. Physical characterization

To identify changes in crystallinity of the blends with the recycling number, differential scanning calorimetry (DSC) testing was carried out using a Netzsch DSC 204 F1 instrument (Selb, Germany). Under a nitrogen circulation, samples with mass of 10 ± 1 mg were first heated from 25 °C to 200 °C with a heating rate of 10 °C/min, then were cooled from 200 °C to 25 °C at -10 °C/min, and last were subjected to a second heating step with the same conditions than the first one. The first heating step was done to eliminate the thermal history of the materials, while the crystallization peaks observed during cooling step were analyzed to calculate the crystallization temperature of PP ($T_{c,\ PP}$) and EOC ($T_{c,\ EOC}$) and the crystallization enthalpy of PP ($\Delta H_{c,PP}$). The crystallinity degree of PP matrix was determined by using the crystallization enthalpy and was corrected by the content of fillers using the following equation [4]:

$$X_{c,DSC,PP} = \frac{\Delta H_{c,PP}}{(1-w)\Delta H_{100\%}} \tag{2-1}$$

where *w* is the EOC or talc weight fraction and $\Delta H_{100\%}$ is the heat of fusion for a pure crystalline isotactic polypropylene, 209J/g [1]. The melting peaks occurring during the second heating step were analyzed to determine the melting temperatures of PP

and EOC phase ($T_{m,PP}$ and $T_{m,EOC}$, respectively). Each DSC measurement was repeated on 3 samples, and hence, we report here averaged values.

To get complementary information about the crystalline properties of the materials, we performed wide-angle X-ray scattering (WAXS) experiments using a Panalytical X'Pert Pro MPD diffractometer (Almelo, Netherlands). We utilized the Kα radiation of Copper (wavelength λ = 1.54 Å) generated at 40kV and 40mA. The diffractometer was configured with its transmission mode. Diffractograms were recorded at room temperature and in the 2 theta (2θ) range 7°- 45°. As incident optics, we used a focusing mirror, as sample holder we used a spinner, and as secondary optics we used the PIXcel detector (Panalytical, Almelo, Netherlands). The diffractograms were analyzed by means of the software PeakFit (Systat, San Jose, USA) that enabled to perform the deconvolution the scattered intensity I – 2θ curves. The deconvolution was done using Gaussian functions to fit both crystalline and amorphous peaks [5].

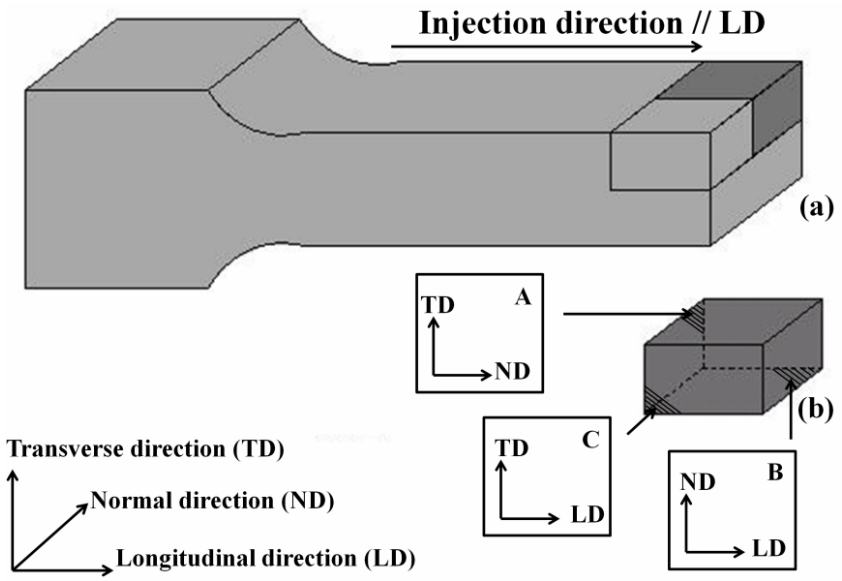

Figure 2-2: Sample preparation for the WAXS and SEM observation: (a) a half of slice was cut from the center of the sample, (b) definition of the planes of interest.

For PP/EOC, the investigations were performed on 10 mm × 10 mm ×3 mm samples cut from the injected tensile specimens. Attention is focused on the amount of the β crystalline phase of PP that is quantified by means of the empirical model (equation (2-2)) of Jones et al. [6]:

$$K_\beta = \frac{I_{(300)}}{I_{(300)} + (I_{(110)} + I_{(040)} + I_{(130)})} \quad (2\text{-}2)$$

where $I_{(300)}$ is the amplitude of the peak related to the (300) planes of β phase, and $I_{(110)}$, $I_{(040)}$, and $I_{(130)}$ are the amplitudes of the peaks related to the (110), (040), and (130) planes of α phase, respectively. Note that the amplitudes of the peaks considered in the equation (2-2) correspond to those of the peaks used for the deconvolution.

For PP/talc, the investigations were performed with the TD-ND plane (shown in Figure 2-2) positioned perpendicular to the X-ray beam. To this end, rectangular specimens with a thickness of 3 mm were carefully cut from the injected tensile specimens. Attention is focused on the b-axis orientation index of PP crystals. The definition of the b-axis orientation index was shown in Figure 2-3. This index is determined by the ratio of the intensity of α phase planes (040) and (110). These intensities were measured as the amplitude of the peak after the deconvolution.

For each condition, WAXS measurement was done on 3 specimens and we reported averaged values and representative diffractograms.

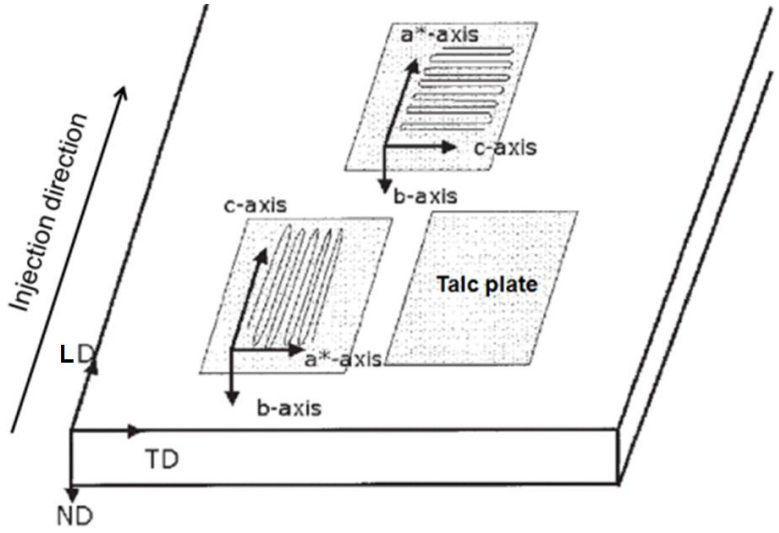

Figure 2-3: Definition of the b-axis orientation index.

2.3.6. Morphological characterization

The microstructure of the materials was studied by means of a pressure-controlled scanning electron microscope (SEM) FEI Quanta FEG 200 (Hillsboro, Oregon, USA). Attention was focused on the dimension and dispersion of inclusions with recycling that have an important effect on the mechanical properties of PP blends [7, 8].

In PP/EOC blends, there is no chemical contrast between PP and EOC due to a similar chemical composition, it is hence necessary to stain one of these two components. Ruthenium tetroxide (RuO_4) is typically used for staining elastomer through an oxidation mechanism of ester groups that produces crosslinked esters, while its reaction with PP is quite limited [9]. To this end, a 3 mm-thick material slice was cut from the center of the tensile specimen, and was subsequently cut in its middle to form two samples (Figure 2-2). These samples were examined parallel, plane A, and perpendicular, plane C, to the injection direction (Figure 2-2). The areas of interest were carefully polished down to a roughness of about 1 µm and then the

specimens were introduced into a glass vial for the RuO_4 staining procedure. During this procedure, the specimens were exposed 2.5 hours to the vapor of a lab-made aqueous solution of RuO_4 at the room temperature [10]. The areas of interest were then microtomed at -50°C by means of a cryo-ultramicrotome Leica EM UC6/UF6 instrument (Wetzlar, Germany) using a trimming diamond blade to remove the over stained skin [11]. For each surface of interest, 6 representative images were recorded and analyzed from the skin to the center of the materials.

In PP/talc blends, the chemical contrast between PP and talc is enough to be observed directly. Thus, 3 mm thick slices were cut from the center of the injected tensile specimens (Figure 2-2 a), and were subsequently cut in their middle to get two samples (Figure 2-2 b). The areas of interest, namely TD-ND, TD-LD and ND-LD, were carefully polished with a roughness of about 1 µm and observed. On each area of interest, 4 representative images were recorded from the center to the edge of the area.

Finally, these images were analyzed by means of the software Image-J (National Institutes of Health, Bethesda, Maryland, USA) to quantify the talc particle morphological characteristics.

2.3.7. Mechanical characterization

2.3.7.1.Viscoelastic characterization

The viscoelastic properties of the materials were characterized by dynamic mechanical analysis (DMA) using a NETZSCH DMA 242C instrument (Selb, Germany). Specimens of dimensions of 16 mm × 10 mm × 3 mm were carefully cut from the tensile specimens, tested with the single – cantilever bending mode at the

frequency of 1 Hz and with a constant static force of 0.5 N. During this procedure, the materials were tested from -100 °C to 140 °C with a heating rate of 2°C/min. For DMA, we report averaged values and representative curves resulting from 3 experiments per tested material.

2.3.7.2. Tensile characterization

Mechanical properties for both virgin and recycled materials were evaluated using uniaxial tension with a servohydraulic Instron testing machine model 8031 (Norfolk, Massachusetts, USA) at the room temperature (25±1°C). Based on the standard ASTM D638, the Young's modulus and yield stress were determined at a crosshead speed of 1 mm/min and the strain at break was determined at the crosshead speed of 50 mm/min. The Young's modulus and the yield stress were calculated from the initial slop of stress-strain curves and the maximum stress of stress-strain curves during the transition between viscoelastic and viscoplastic stages, respectively. Since the tensile specimens have a gauge length of 50 mm, the corresponding strain rates are 0.0033 s^{-1} for 1 mm/min and 0.017 s^{-1} for 50 mm/min. The engineering stress (σ_{eng}) and strain (ε_{eng}) were determined from the measured load (F) and displacement (Δl) using the original specimen cross-sectional area (S_0) and length (l_0). σ_{eng} and ε_{eng} can be used to determine the true stress (σ_{true}) -true strain (ε_{true}) curves from equations (2-2) and (2-3) below. At least 5 tests were performed per strain rate, which allows determining the averaged values of each mechanical parameter.

$$\varepsilon_{true} = \ln(1+\varepsilon_{eng}) \quad (2\text{-}3)$$

$$\sigma_{true} = \sigma_{eng}(1+\varepsilon_{eng}) \quad (2\text{-}4)$$

2.4. Results and discussions

2.4.1. Molecular weight

Table 2-1: Molecular weight of the non-recycled materials (0P) and recycled materials (0P and 6P).

	Mn	*Mw*	*Mz*	*PDI*
EOC	24700±0	68550±780	144150±210	2.8
PP neat 0P	44550±1200	214000±5230	653050±34290	4.8
PP neat 6P	46450±212	192300±2550	542600±2120	4.1
PP/EOC 80/20 0P	35300±3540	189550±500	636150±8130	5.4
PP/EOC 80/20 6P	28000±1700	157300±420	493900±16260	5.6
PP/talc 80/20 0P	44300±1270	206900±3540	637400±5091	4.7
PP/talc 80/20 6P	42600±1700	203900±2400	622150±13220	4.8

The possible changes of molecular weight of the non-recycled materials (0P) and recycled materials due to the recycling procedures are shown in Table 2-1. We only present here the measurements of the extreme cases, i.e. the non-recycled case and the case corresponding to 6 recycling procedures. In Table 2-1, EOC shows lower number-average (Mn), weight-average (Mw), and z-average (Mz) molecular weights and narrower molecular weight distribution (polydispersity index (PDI)) compared to PP. The lower molecular weight of EOC allows having lower peak melting points and free flowing pellets for continuous compounding. The narrow molecular weight

distribution of EOC demonstrated by the low PDI indicates that EOC has a high degree of chain-to-chain uniformity of composition. This property makes it possible to produce polymers with relatively low molecular weight (high melt index) without a significant low molecular weight tail [12]. For non-recycled PP/EOC 80/20, the molecular weights of PP in PP/EOC 80/20 composite are lower than them in non-recycled neat PP and PP/talc 80/20. This is probably due to the difficulty of separation of the PP and EOC during the GPC measurements. The molecular weight of EOC overlapped the molecular weight of PP and resulted in a lower apparent molecular weight of PP.

Comparing with the non-recycled PP, PP/EOC 80/20 and PP/talc 80/20 composites, the molecular weight of the recycled materials slightly decreased after six reprocessing passes. The decrease of molecular weight of materials can be attributed to the chain scissions mechanism because the recycled materials were underwent high temperature and intensive shearing reprocessing condition. However, the number-average molecular weight for neat PP increased after six reprocessing passes. This increase is probably due to the experimental error. Attention is also focused on the change of PDI between the non-recycled and recycled materials. The molecular weight distribution of PP matrix in the recycled PP/EOC and PP/talc composites is larger than the non-recycled one, as shown by the increase of PDI. This is due to the reprocessing results in more molecules with different chain lengths. However, the molecular weight distribution of recycled neat PP is narrower than the virgin neat PP. This is probably due to the measurement with experimental error for the number-average molecular weight of neat PP.

2.4.2. Rheological properties

The melt flow index of each sample is shown in Table 2-2. For the non-recycled neat PP, one notes a MFI of 12.5 g/10min that is near to the value of 12g/10min reported by the datasheet of the supplier. With increasing the content of EOC, the MFI of the non-recycled blends gradually increases from 12.5 g/10 min to 18.2 g/ 10 min, which is due to the inherent high MFI of EOC. As a consequence, the addition of EOC to PP leads to higher processability compared to neat PP. However, the addition of talc led to a continuous decrease of the MFI with increasing the talc content. This is due to the fact that the incorporation of talc hinders plastic flow and increases the viscosity of PP composites at the melt state [13]. Whatever the material, the recycling up to 6 grinding/re-extrusion procedures implies an increase of MFI. In particular, a 49 % increase of MFI is noted for neat PP. For PP/EOC composites, a 99 % increase of MFI is noted for PP/EOC 90/10, and a 74 % increase of MFI is noted for PP/EOC 80/20. For PP/talc composites, it is in a less marked manner. A 24% increase of MFI is noted for PP/talc 90/10, and a 15 % increase of MFI is noted for PP/talc 80/20. It is supposed that the presence of talc does not significantly influence the degradation mechanisms of the matrix, as shown previously [19]. The less marked increase of MFI of PP/talc composites compared to neat PP may be due to a gradual increase of delamination and dispersion of talc particles or agglomerates during the successive extrusions. This mechanism would result in an increased number of particles and a decreased particle size, hindering the melt flow of the PP. The evolution of talc particle dimensions with the re-extrusion procedures is investigated in a next section of the present chapter. The continuous increase of MFI with the recycling number indicates a decrease of molecular weight due to chain scissions mechanisms of PP during multiple extrusions which is in agreement with the GPC

measurements although the decrease of molecular weight are quite weak [14-18]. Therefore, PP composites suffer from continuous thermo-mechanical degradation during the recycling (according to the Newtonian viscosity, $\eta=A\cdot(Mw)^a$, where η is the viscosity, Mw is the molar weight, A is a constant and a is a power equal to 3.4, we can see that a small decrease of molecular weight normally leads to a large increase of viscosity of materials. This can explain the more significant increased MFI values). It is to be mentioned that thermal degradation of PP is characterized by random chain scission mechanisms, followed by radical transfer process, without involving chain branching or crosslinking mechanisms as in polyethylene [19].

Table 2-2: Melt flow index (MFI) of the non-recycled materials (0P) and recycled materials (1P to 6P).

MFI (g/10min)	*0P*	*1P*	*3P*	*6P*
Neat PP	12.5±0.2	12.8±0.1	14.9±0.4	18.6±0.4
PP/EOC 90/10	13.9±0.7	14.9±0.4	18.6±0.4	27.6±0.6
PP/EOC 80/20	18.2±0.3	19.4±0.7	22.7±0.1	31.6±0.3
PP/talc 90/10	12.3±0.03	12.6±0.1	13.9±0.2	15.3±0.2
PP/talc 90/10	11.8±0.12	12.1±0.1	12.4±0.1	13.6±0.7

2.4.3. Thermal properties

Representative TGA curves of EOC, neat PP, PP/EOC and PP/talc composites (non-recycled and recycled) are shown in Figure 2-4 and Figure 2-5. All curves exhibit one-step degradation that can be attributed to the radical random scission

mechanism of the thermal degradation of the polyolefins [20-22]. This mechanism occurs in PP and EOC since these two materials have a similar chemical composition and structure [20, 21]. The decomposition temperature (T_{onset}) and the 5% weight lost temperature (T_5) of the materials were listed in Table 2-3.

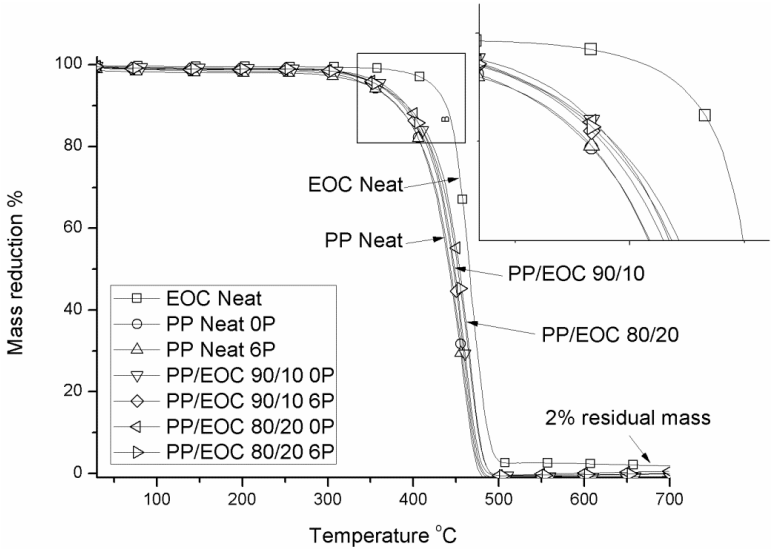

Figure 2-4: TGA curves of neat PP, neat EOC and PP/EOC composites (0P: virgin, 6P: 6 recycling procedures).

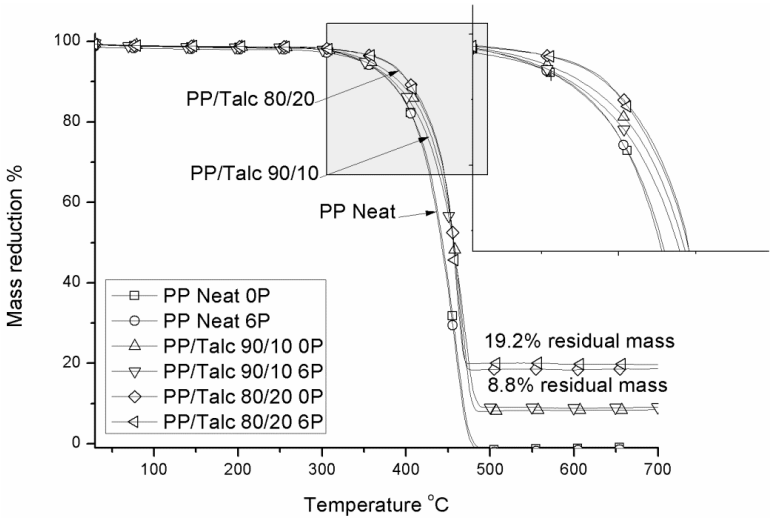

Figure 2-5: TGA curves of neat PP and PP/talc composites (0P: virgin, 6P: 6 recycling procedures).

For PP/EOC (Figure 2-4), it can be observed that EOC has a higher degradation temperature than neat PP (443 °C vs. 412 °C). This result can be explained by the fact that compared to EOC, PP has a higher density of tie molecules. Indeed, tie molecules have a high degree of stored energy and therefore are more susceptible to chain scission than the other chains [23]. We note an increase of the decomposition temperature of PP with increasing the content of EOC. Indeed, T_{onset} varies from 412 °C for neat PP to 427 °C for PP/EOC 80/20. The same result was found by Mano et al. [24] in the case of PP blended with 20 % of EPDM for which the degradation temperature was 18 °C higher than that of neat PP. This result demonstrates that increasing the amount of EOC induces an increase of the blend thermo stability. In addition, we note that when EOC was heated up to 700 °C, a 2% residual mass is still present and is probably due to the presence of catalytic residues. These residues can also contribute to increase the decomposition temperature of EOC compared with neat PP.

For PP/talc (Figure 2-5), the addition of talc filler increased the degradation temperature of PP/talc composites because talc has a much higher decomposition temperature than PP. In addition, the decomposition temperature of PP/talc composites increases with the increase of the talc content (Table 2-3). Thus, the talc addition can improve the thermal stability of PP. When PP/talc composites were heated up to 700 °C, the residual weight fraction was 8.8 % for PP/talc 90/10 and 19.2 % for PP/talc 80/20. Therefore, a small quantity of talc powder was lost during the compounding and extrusion steps of the processing.

Comparing with the non-recycled PP, PP/EOC and PP/talc composites, the degradation temperatures and the 5% weight fraction lost temperature of recycled

materials were slightly lower due to chain scission mechanisms of PP matrix during the reprocessing [22, 25]. However, the slight decrease of these two temperatures (around 2°C-4°C for T_{onset} and 1°C-6°C for T_5) demonstrates that the recycled materials have a quite good thermal stability despite the re-extrusion-induced thermo-mechanical degradation [26]. Therefore, recycled neat PP and PP composites can be used in the same temperature range than the non-recycled ones.

Table 2-3: Decomposition temperature (T_{onset}) and 5% weight lost temperature (T_5) for virgin and recycled neat PP, PP/EOC and PP/talc composites.

	T_{onset} *(°C)*		T_5 *(°C)*	
	0P	6P	0P	6P
EOC Neat	443	—	421	—
PP Neat	412	410	348	346
PP/EOC 90/10	419	417	357	355
PP/EOC 80/20	427	424	360	359
PP/talc 90/10	424	420	356	350
PP/talc 80/20	429	426	377	376

2.4.4. Chemical properties

The possible changes in the chemical functions of the materials due to the recycling procedures are shown in Figure 2-6 and Figure 2-7 where FTIR curves are

displayed. We only present here the curves of the extreme cases, i.e. the non-recycled case and the case corresponding to 6 recycling procedures, because chemical function changes are quite limited.

For neat PP and PP/EOC blends (Figure 2-6), recycling does not cause the formation of peak attributed to oxidation. The same result was obtained by Sarrionandia et al. [14] in a PP/EPDM/talc composite after five reprocessing procedures. Guerrica-Echevarría et al. [16] did not find any chemical structure change for PP after five injection molding cycles. Aurrekoetxea et al. [27] explained the absence of oxidation by the absence of oxygen in the polymer matrix at the melted state during the recycling. We also observed that recycling caused the disappearance of a peak centered at 1745 cm^{-1}. This peak, centered at 1745 cm^{-1}, is not present in the FTIR spectrum of EOC, which means that it is attributed to PP. According to Jansson et al. [28] and Luda et al.[29, 30], this peak is attributed to ester groups and may be linked to the presence of anti-oxidants in the PP matrix that can contain such a function. After 6 recycling procedures, these residual antioxidants are partially lost as shown by the negligible absorption around 1745 cm^{-1} for neat PP and PP/EOC blends 6P (see Figure 2-6) resulting no remarkable different in the chemical structures between the non-recycled and recycled neat PP and PP/EOC blends. Note the disappearance of the anti-oxidant peak can be due to a chemical transformation of ester groups and/or to a physical disappearance of the anti-oxidant (evaporation, diffusion) [31]. As we see on Figure 2-6 for wavenumbers higher than 1745 cm-1, the FTIR spectra seem to be the same for recycled and non-recycled neat PP and PP/EOC blends suggesting negligible differences in the chemical structures of these materials.

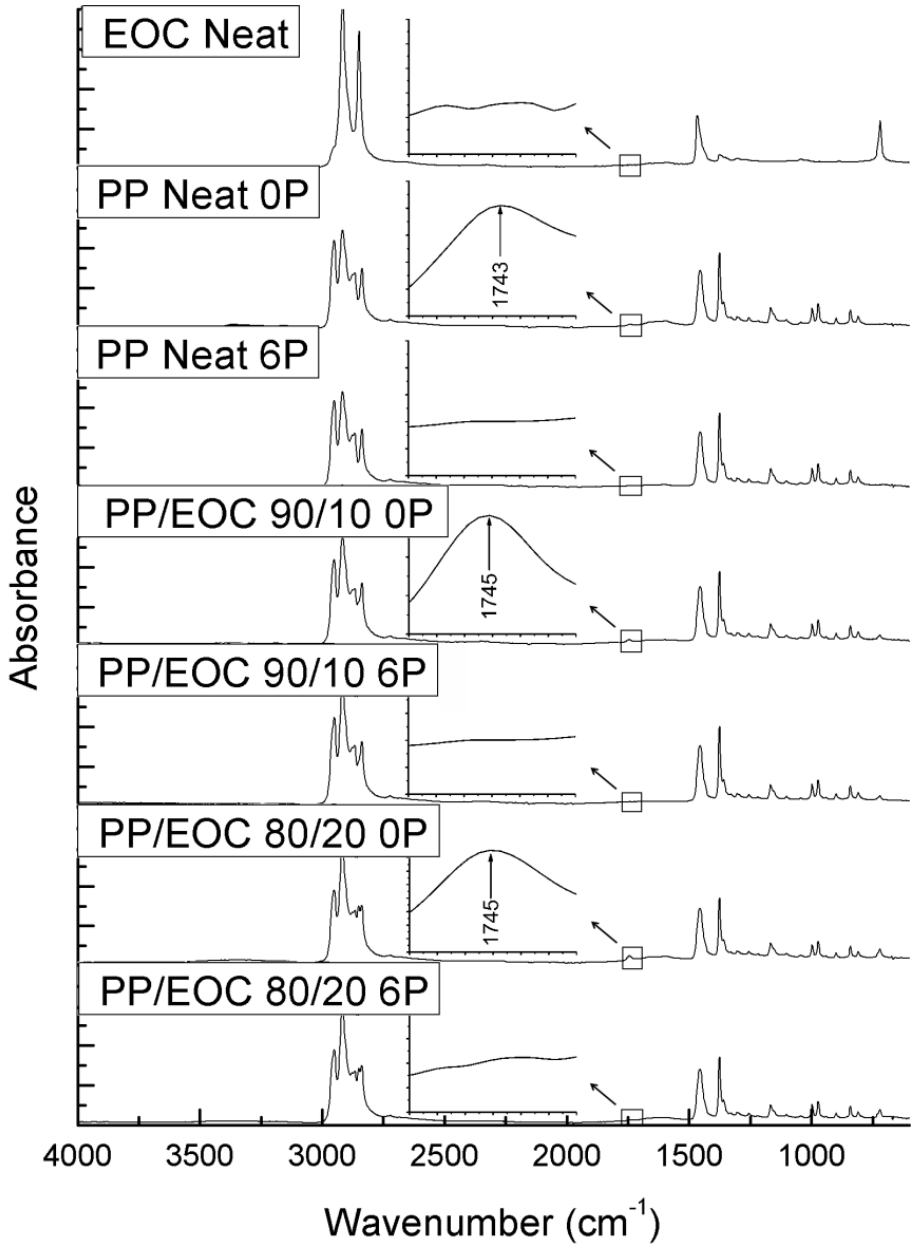

Figure 2-6: FTIR spectra of EOC, neat PP and PP/EOC blends (0P: virgin, 6P: 6 recycling procedures).

For PP/talc composites, attention is first focused on the talc powder. For the non-heated talc powder, the peaks situated between 3600 cm^{-1} and 3700 cm^{-1} and between 1550 cm^{-1} and 1700 cm^{-1} were assigned to the –OH stretching region and to the -OH bending region, respectively (see Figure 2-7). These spectral peaks correspond to the presence of water molecules induced by sorption mechanisms

(adsorption and absorption) of water by the talc [32-35]. Although the talc powder was heated 7 hours, no significant change was noted on the spectra in comparison with the non-heated one. We however observed that the heating treatment caused the formation of new small peaks between 1700 cm^{-1} and 1900 cm^{-1} demonstrating that this treatment induced a chemical modification of talc whose origin is unknown. It is thought that the heating treatment may modify the chemical structure of some talc impurities.

When mixing PP with talc, the FTIR spectra show the presence of the –OH stretching region and the –OH bending region for the two non-recycled composites. Furthermore, the intensity of the –OH bending significantly increases with the recycling (Figure 2-7).This can probably be attributed to the modification of talc morphology during the reprocessing that is studied in the next section [32]. It is also to be noted that the absorption peak at around 1745 cm^{-1} was detected for PP/talc composites 6P. This indicated that the anti-oxidant was not entirely lost or that new ester groups were formed during the reprocessing [30]. It is also believed that talc particles may physically prevent the evaporation or diffusion of the anti-oxidants, indicating that the chemical transformation of ester groups may be weak or inactive without talc.

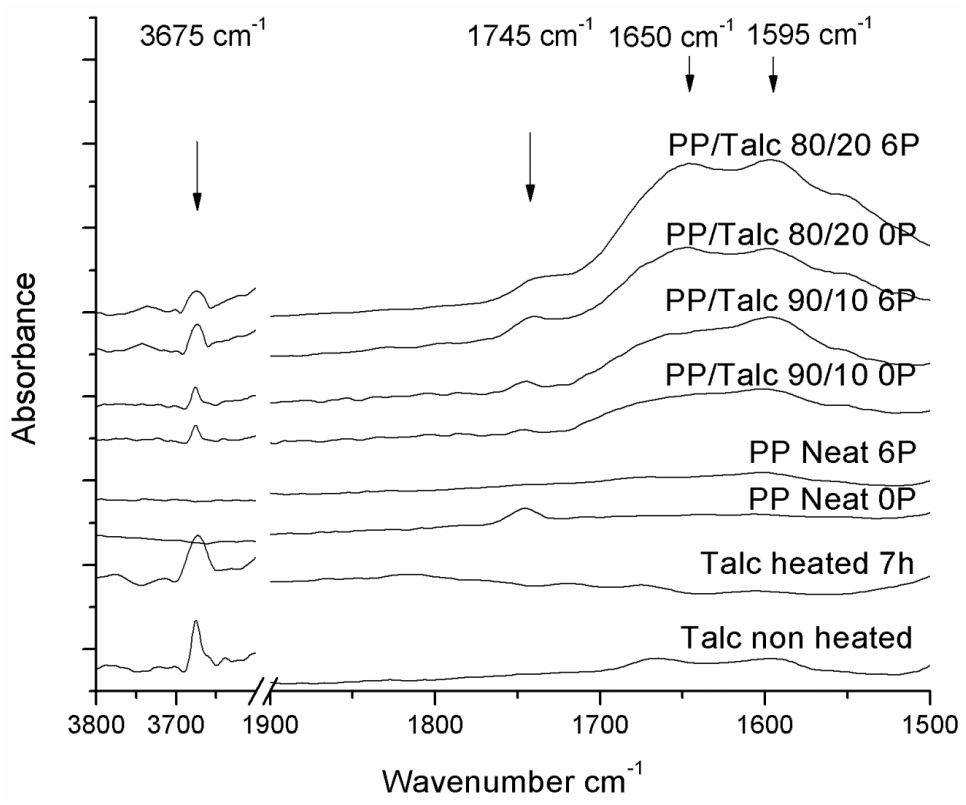

Figure 2-7: FTIR spectra of talc powder, neat PP and PP/talc composites (0P: virgin, 6P: 6 recycling procedures).

2.4.5. Physical properties

The DSC results of non-recycled and recycled neat PP, PP/EOC and PP/talc composites are summarized in Table 2-4.

We found that the presence of EOC has no significant effect on the melting temperature (Tm PP), crystallization temperature (Tc PP) and crystallinity index (Xc DSC PP) of PP matrix of the non-recycled materials, which is consistent with results reported in other works [36, 37]. In particular, Xc DSC PP is estimated to be of about 49 % in both neat PP and PP/EOC blends. Concerning the EOC phase, the DSC thermograms exhibit small peaks centered at 77 °C and 59 °C, corresponding to its melting and crystallization processes, respectively. The position of these peaks

provides the melting temperature (Tm EOC) and the crystallinity temperature (Tc EOC) of EOC (see Table 2-4).

Table 2-4: Crystaline properties of the non-recycled and the recycled materials obtained by DSC.

		$T_{m\ EOC}$ (°C)	$T_{m\ PP}$ (°C)	$T_{c\ EOC}$ (°C)	$T_{c\ PP}$ (°C)	$X_{c,DSC,PP}$ (%)
Neat PP	0P	—	168.1±0.4	—	115.6±0.2	49.2±0.2
	1P	—	168.0±0.2	—	114.2±0.3	49.8±0.3
	3P	—	167.2±0.2	—	113.9±0.1	50.2±0.1
	6P	—	166.9±0.4	—	112.3±0.3	50.6±0.1
PP/EOC	0P	77.0±0.1	167.2±0.3	58.8±0.2	116.1±0.2	49.5±0.1
90/10	1P	77.1±0.1	167.1±0.2	58.8±0.2	115.2±0.1	49.9±0.1
	3P	77.0±0.1	166.8±0.3	58.8±0.2	114.1±0.1	51.2±0.1
	6P	76.9±0.2	166.5±0.5	58.9±0.2	113.9±0.1	51.9±0.2
PP/EOC	0P	77.1±0.1	167.1±0.4	58.9±0.2	115.3±0.2	48.9±0.2
80/20	1P	77.1±0.1	166.8±0.1	58.8±0.2	115.1±0.1	49.4±0.1
	3P	77.0±0.1	166.5±0.4	58.9±0.2	114.4±0.1	49.5±0.3
	6P	77.0±0.1	166.1±0.1	58.9±0.2	113.8±0.2	50.3±0.1
PP/talc	0P	—	168.9±0.1	—	124.3±0.1	50.3±0.1
90/10	1P	—	169.2±0.2	—	124.2±0.2	50.4±0.2
	3P	—	169.0±0.5	—	124.4±0.2	50.9±0.3
	6P	—	169.3±0.4	—	124.3±0.2	51.4±0.2
PP/talc	0P	—	169.0±0.4	—	127.1±0.1	51.2±0.1
80/20	1P	—	169.3±0.2	—	127.1±0.4	51.6±0.1
	3P	—	169.3±0.4	—	127.4±0.3	51.8±0.2
	6P	—	169.1±0.4	—	127.4±0.2	52.2±0.2

For PP/talc composites, the addition of talc has no or a limited effect on the melting temperature ($T_{m\,PP}$) of PP matrix (about 1°C). At the same time, the presence of talc filler significantly increases the crystallization temperature ($T_{c\,PP}$) of PP matrix, in particular, this effect is more substantial for the high content of talc. (increase of 9°C for PP/talc 90/10 and increase of 12°C for PP/talc 80/20). Similar results are published by Velasco et al. [38], where the melting temperature ($T_{m\ PP}$) of PP remained almost constant with the presence of talc and the crystallization temperature ($T_{c\,PP}$) of PP matrix increased with the introduction of talc. The slight increase of the melting temperature could be attributed to the higher thermal conductivity of talc and may also be attributed to the development of thicker lamellae of PP dictated by an increased crystallinity [39]. The significant increase of the crystallization temperature is explained by a nucleating effect of the talc particles, which generally leads to numerous but small spherulites [40-43]. In particular, PP could be transcrystallized on the talc cleavage surface, with PP crystals oriented perpendicular to the talc surface [41, 43]. At the same time, the index of crystallinity of PP increased with the addition of talc, indicating that both the nucleation and the growth PP crystal are enhanced by the addition of talc [42].

Concerning the recycling effects, for neat PP and PP/EOC composites, it can be observed that with increasing the recycling number up to 6, $T_{m\ EOC}$ and $T_{c\,EOC}$ are constant, while $T_{m\,PP}$ and $T_{c\ PP}$ gradually decrease. Note that the decrease of $T_{m\,PP}$ indicates a decrease of the average lamella thickness. In the same time, $X_{c\ DSC\ PP}$ slightly increases from about 49 % to about 51 % with the recycling procedures. These findings that demonstrate thermomechanical degradation mechanisms occur in the PP matrix, while EOC inclusions appear stable with recycling. As mentioned above, chain scission mechanisms are active in PP blends and induce smaller

macromolecules and a larger molecular weight distribution compared to the non-recycled materials (Table 2-1), as well as the formation of defect groups [44] (dangling chain, voids etc. [45]). The gradual formation of a molecular network containing more defects than the initial one may explain the decrease of the crystallization temperature and melting temperature of PP with the number of recycling. However, in the same time, the reduction of the length of PP chains may increase their mobility and hence, facilitate their rearrangement during the crystallization. This higher mobility may cause the observed small increase of crystallinity with the reprocessing [16]. However, for PP/talc composites, $T_{m\,PP}$ and $T_{c\,PP}$ remained constant with the recycling number up to 6 cycles, while the crystallinity index increased slightly. These results are in good agreement with those reported by Sarrionandia et al. [14]. The stabilization of the crystallization temperature during the recycling was probably due to a competition between the breaking of talc particles faciliting the nucleation process of PP (increase of $T_{c\ PP}$) and the formation of a molecular network containing numerous defects (decrease of $T_{c\ PP}$).. As mentioned above, the thermal degradation caused a decrease of molecular weight that slightly increases the ability to fold of the chain, which may explain the slight increase of crystallinity of PP/talc composites during the recycling. Concerning the average lamella thickness, it is unchanged by the recycling, explaining the constant values of $T_{m\,PP}$ (Table 2-2).

We performed WAXS experiments to get complementary information about the crystalline properties of the PP blends. The WAXS diffractograms of neat EOC, non-recycled and recycled neat PP, PP/EOC and PP/talc composites are displayed in Figure 2-8 and Figure 2-9.

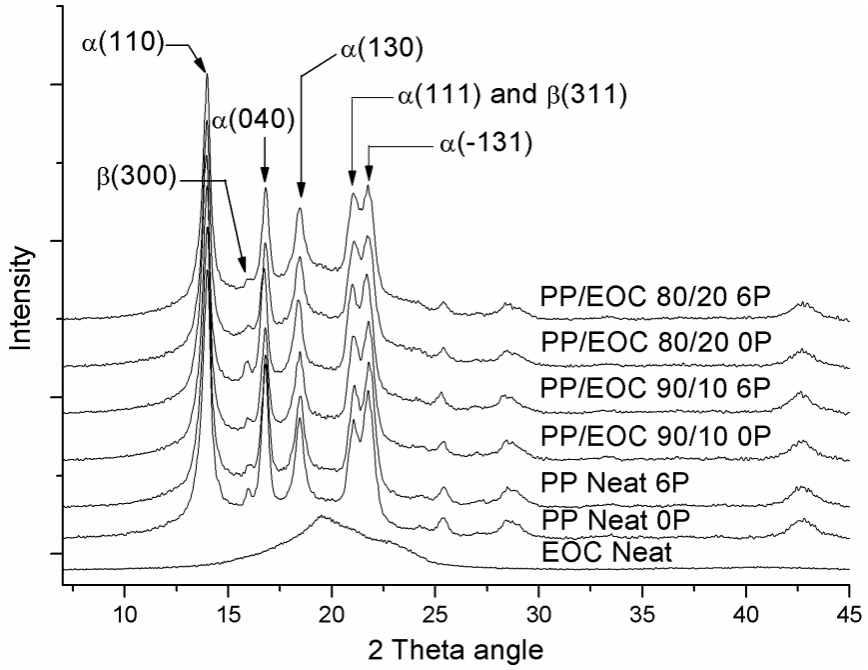

Figure 2-8: WAXS diffractograms of neat EOC, non-recycled and recycled neat PP and PP/EOC composites.

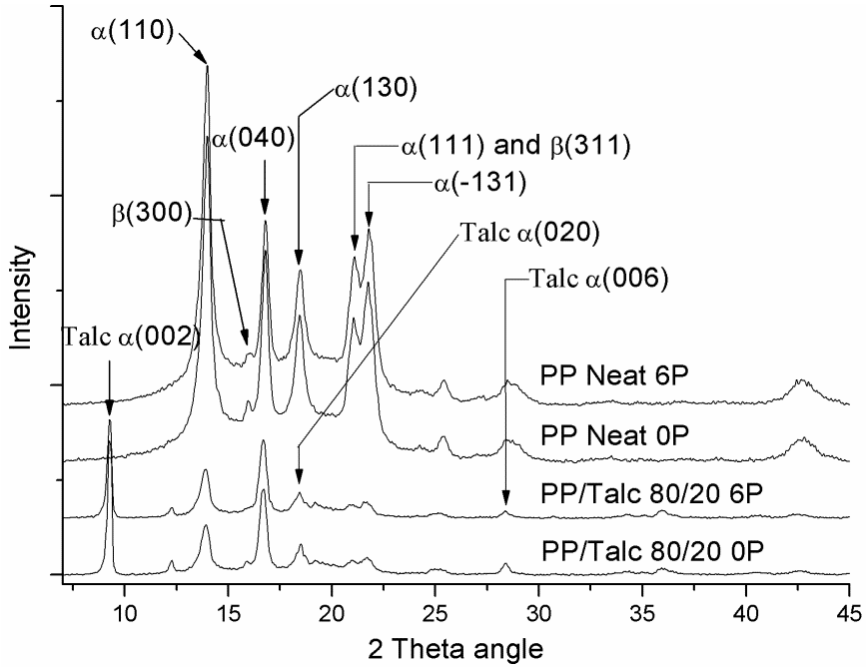

Figure 2-9: WAXS diffractograms of non-recycled and recycled neat PP and PP/talc 80/20 composites.

Table 2-5: Amount of β phase in non-recycled and recycled neat PP, PP/EOC blends obtained by WAXS.

EOC content (wt. %)		K_β *(%)*
0	0P	2.5±0.4
	6P	1.9±0.2
10	0P	3.7±0.4
	6P	3.9±0.1
20	0P	3.1±0.1
	6P	3.1±0.4

We found the characteristic peaks of the α crystalline phase of PP centered at the 2θ angles of 14.1° (110), 16.9° (040), 18.5° (130), 21.4° (111) and 21.8° (-131). We also found the main reflection of the β crystalline phase centered at 16° (300) (see Figure 2-8 and Figure 2-9). In Figure 2-9, the diffraction peaks at a 2θ angle of 9.4° (002), 18.8° (020) and 28.5° (006) correspond to the talc fillers.

For PP/EOC composites, attention is focused on the amount of β phase in PP that is usually calculated by Equation (2-2) [5, 6, 46]. In Table 2-5, we can observe that the amount of the β phase, K_β, increases from 2.5±0.4 % for neat PP to 3.7±0.4% for PP/EOC 90/10 blend. This is because the presence of EOC has synergistic toughening effects on PP matrix [47]. For a higher content of EOC, K_β decreases. We also note that recycling has no impact on K_β, excepted for neat PP for which K_β decreases from 2.5±0.4 % to 1.9 ±0.2 %. As shown by Aboulfaraj et al. [48], β

spherulites allow the initiation and propagation of plasticity, while α spherulites are much more brittle and have a limited plasticity. As a result, increasing the content of β spherulites is suitable to increase the ductility of PP, which indicates that the blends probably have a higher ductility than neat PP. Tensile testing of the material are reported in the next section to verify this hypothesis. β metastable phase generally forms under specific thermal, nucleation/crystallization or rheological conditions [48-50]. The most common way to form β phase is the use of β-nucleating agents [49, 50]. The most stable phase of PP is the α phase that is favored above a crystallization temperature of 132°C and is characterized by a low growth rate. The β phase is a metastable phase that is favored below a crystallization temperature of 132 °C and is characterized by a high growth rate [50]. It appears that the addition of EOC to PP facilitates the nucleation of β phase, this phenomenon being more important in the case of PP/EOC 90/10 than in the case of PP/EOC 80/20.

Table 2-6: Intensity ratio I (040)/I (110) for non-recycled and recycled neat PP, PP/talc 80/20 composite obtained by WAXS.

	I(040)/I(110)	
	0P	6P
Neat PP	0.65±0.02	0.52±0.01
PP/Talc 80/20	1.85±0.06	2.23±0.15

For PP/talc composites, the diffractograms of PP/talc 90/10 are not shown in Figure 2-9 because they exhibit the same characteristics than those of PP/talc 80/20. Comparing with the neat PP, the characteristic peaks of β crystal of PP in PP/talc

composites are less intense (K_β is not shown here). This result proves that the talc is a strong nucleation agent of the α crystalline phase of PP. Therefore, the addition of talc particles within the PP matrix results in a lower ductility of PP. Attention is focused on the ratio between the intensity of the planes (040) and (110) of α crystalline phase of PP. These ratios are listed in Table 2-6. Concerning the non-recycled materials, the addition of talc increased the degree of b-axis orientation of the PP crystal. This is due to the preferred orientation of plate-like talc fillers along the injection plane (LD-TD), and the PP lamellae growth perpendicular to the talc surface along the normal direction (ND) (see Figure 2-2). For the neat PP, after 6 recycling cycles, the b-axis orientation of the PP crystal slightly decreased from 0.65 to 0.52. This is probably due to the increase of the mobility of polymer chains inducing more PP lamellae which are parallel to the injection direction.

In Table 2-6, for PP/talc 80/20, it can be observed that I(040)/I(110) increased from 1.85 to 2.23, which is probably due to the break of talc during the multiple extrusions. Obata et al.[51] reported that the smaller the talc size, the higher was the degree of b-axis orientation of the PP crystals for a given talc content. The decrease of talc dimension may allow an increase of the interaction between talc particles and PP matrix, which may hence enhance the growth of PP lamellae perpendicular to the talc surface. SEM will be used to analyze the evolution of fillers' dimension with the re-extrusion procedures.

2.4.6. Morphological properties

The SEM investigation of the inclusions morphology during the recycling procedures is shown in Figures 2-10 to Figure 2-12 in the case of PP/EOC 80/20 and is shown in Figure 2-13 to Figure 2-15 in the case of PP/talc 80/20. We selected to show the result for PP blended with 20 wt. % fillers only because we believe the results will be the same for PP blended with 10 wt. % fillers.

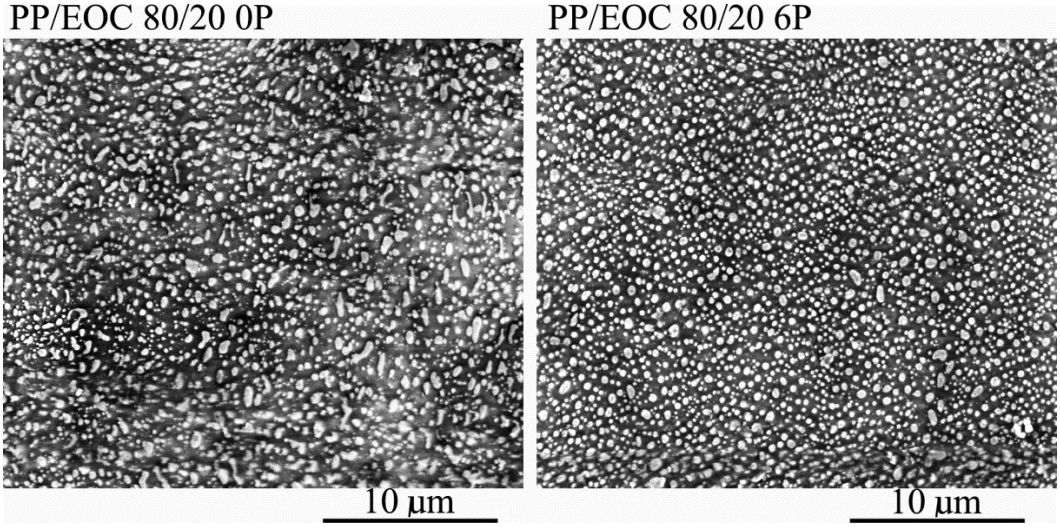

Figure 2-10: SEM micrographs of non-recycled (0P) and recycled (6P) PP/EOC 80/20 recorded at a low magnification.

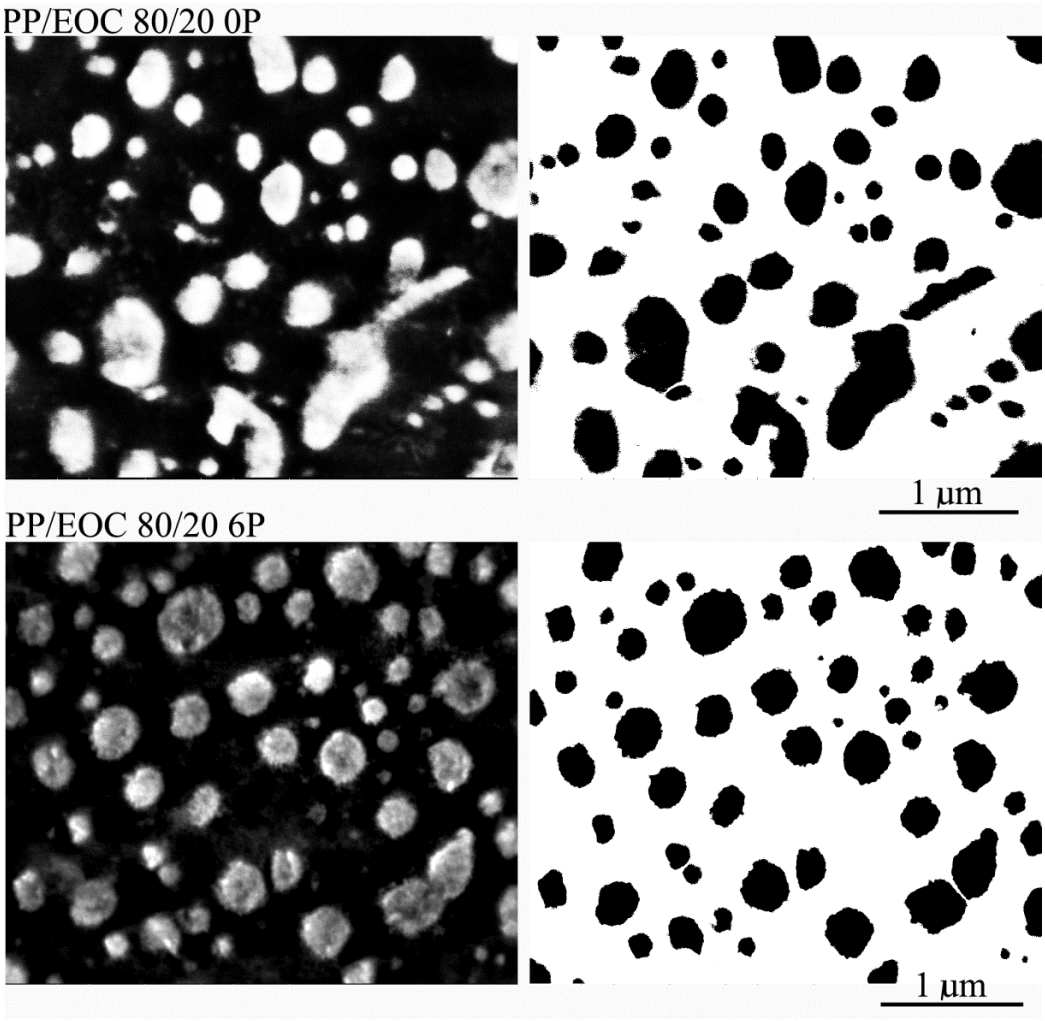

Figure 2-11: SEM micrographs of non-recycled (0P) and recycled (6P) PP/EOC 80/20 recorded at a high magnification, initial image (left) and thresholded image (right).

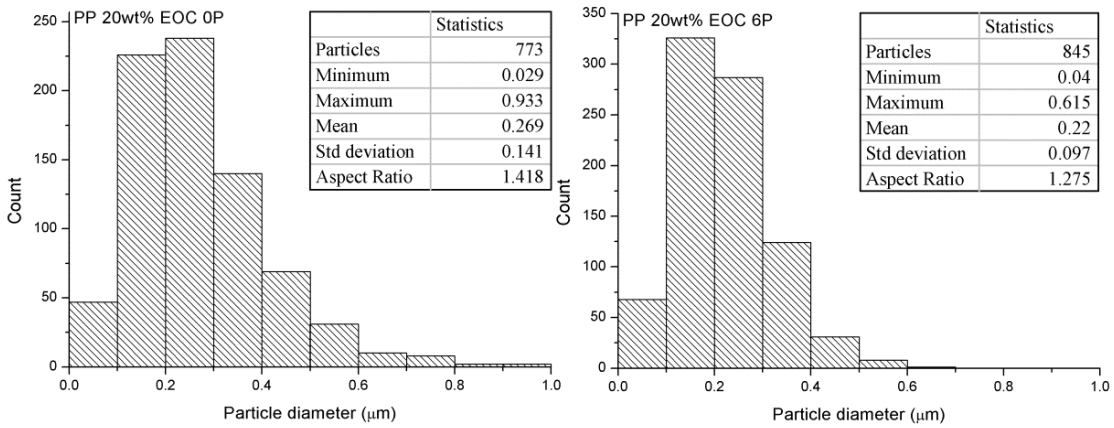

Figure 2-12: Statistical investigation of the EOC inclusions size distribution in the case of non-recycled (0P) and recycled (6P) PP/EOC 80/20

For PP/EOC composites, at low magnification, we note an optimal distribution of elastomeric inclusions within the PP matrix for both non-recycled and recycled composites (Figure 2-10). With increasing the magnification (Figure 2-11), EOC inclusions have a heterogeneous shape at the non-recycled state, while after 6 recycling procedures, their shape is more homogeneous. The micrographs were treated by means of the image treatment software Image-J. To this end, 12 images recorded from the skin to the center of the sample along two spatial directions (Figure 2-2) for the non-recycled and the recycled materials.

The statistics of the image analysis procedure are reported in Figure 2-12. The diameter D_i of each particle is calculated from average between the length of the major axis D_{major} and that of the minor axis D_{minor} of each identified object, based on equation (2-5). Then, the average particle diameter D_{mean} is obtained by equation (2-6) where n is the total number of objects.

$$D_i = (D_{major} + D_{minor}) / 2 \tag{2-5}$$

$$D_{mean} = \sum D_i / n \tag{2-6}$$

Finally, the average aspect ratio of the particles was assessed as the average ratio length of major object axis to length of minor object axis based on the following Equation:

$$Aspect\ \ ratio = \sum (D_{i,major} / D_{i,minor}) / n \tag{2-7}$$

In the case of PP/EOC 80/20, 6 recycling procedures induce a narrower inclusions size distribution, a decrease of the average inclusions size from 0.27 µm to 0.22 µm, and a decrease of the average aspect ratio from 1.42 to 1.27, compared to the

non-recycled state. The initial heterogeneous shape of the inclusions seems to be due to coalescence phenomena of EOC particles. The multiple extrusions tend to break these imperfect inclusions into smaller and more spherical particles due to the repeated shear and elongational flows [15, 52].

For PP/talc composites, at a low magnification (Figure 2-13), the high contrast images clearly show the talc fillers appearing with a bright contrast and PP matrix appearing with a dark contrast. The SEM images observed on the three surfaces show a good dispersion of talc micro-particles within PP matrix for the non-recycled and the recycled composites. On surfaces A and B (defined in Figure 2-2), talc particles appear as sticks while on surface C, they appear as plates, demonstrating an orientation of talc major axis along the injection direction. These observations are consistent with the results provided by Frihi et al. [53]. At the low magnification, we did not observe any impact of the recycling on the morphology of talc particles. In Figure 2-14, high magnification SEM images were recorded and analyzed to obtain the statistical information about the impact of recycling on the talc inclusion dimensions. On the surface C, the minor axis of talc is difficult to measure. The statistical measurements were only carried out on the surfaces A and B (Figure 2-2). To this end, 8 images of each sample were analyzed by means of the software Image-J on different areas taken on the surfaces A and B. These statistical results are reported in Figure 2-15 by using Equation (2-5) to Equation (2-7).

In Figure 2-15, the major number of talc particles has a length less than 2 μm for the non-recycled and the recycled PP/talc 80/20 composites. For the non-recycled material, we found an average length of 1.9 μm that is exactly equal to the median diameter of 1.9 μm given by the talc supplier. PP/talc 80/20 6P is characterized by

more talc particles than the non-recycled material. This is due to a break of the particles with the recycling that obviously leads to an increased number of particles. Both the averaged length and thickness of talc inclusions in the recycled composite slightly decreased compared to the non-recycled composite. Similar observations were done by Guerrica-Echevarría et al.[16] for PP/talc composite after five recycling passes. In their study, this reduction of talc size was explained by intensive shearing reprocessing condition [16]. It is thought that the decrease of talc size and the increase of talc particles number during the recycling were at the origin of the increased sorption of water molecules observed on FTIR spectra (Figure 2-7). This may be explained by an increase of the surface area of talc particles and by an increase of the dispersion state of talc particles, which may facilitate the sorption of water molecules by the talc during the reprocessing. Furthermore, although both talc length and thickness slightly decreased after 6 reprocessing cycles, the mean aspect ratio of talc increases by 23% from 3.06 to 3.77. We measured the complex viscosity of the PP/talc 80/20 0P using the Physica MCR Rheometer and found the viscosity at 200°C and 50 rmp to be $\eta^*_{PP/talc} = 2413\, Pa \cdot s$. Using this value, we estimated the applied shear stress in the extruder and we found a value about 0.5 MPa. This applied shear stress is enough to break the talc particles with a peeling angle larger than 6 ° (see detailed estimation in Appendix A1) [16, 54-59]. These changes of talc dimensions are expected to impact the mechanical properties of the PP/talc composites that are studied in the next section.

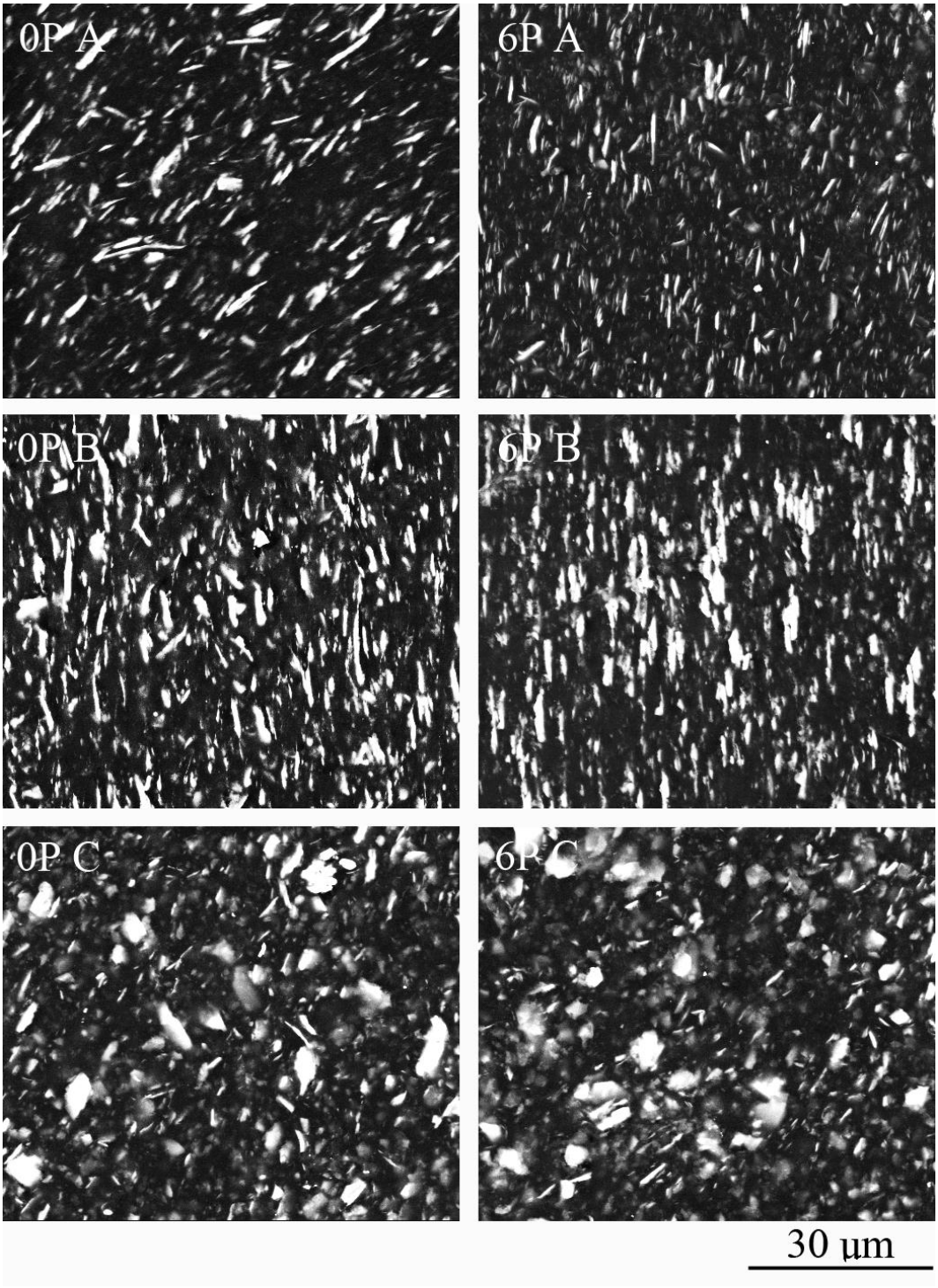

Figure 2-13: SEM micrographs of non-recycled (0P) and recycled (6P) PP/Talc 80/20 recorded at a low magnification (A, B, C are defined in Figure 2-2).

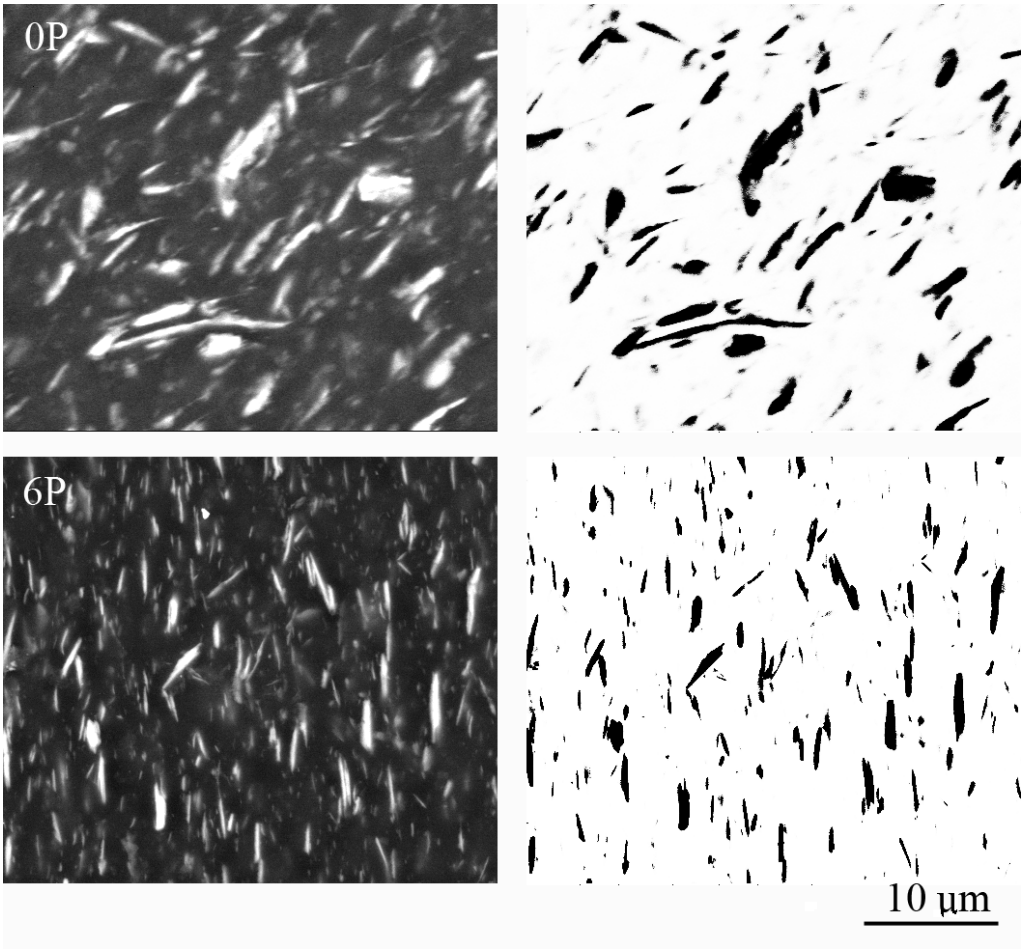

Figure 2-14: SEM micrographs (plane A) of non-recycled (0P) and recycled (6P) PP/Talc 80/20 recorded at a high magnification, initial image (left) and thresholded image (right).

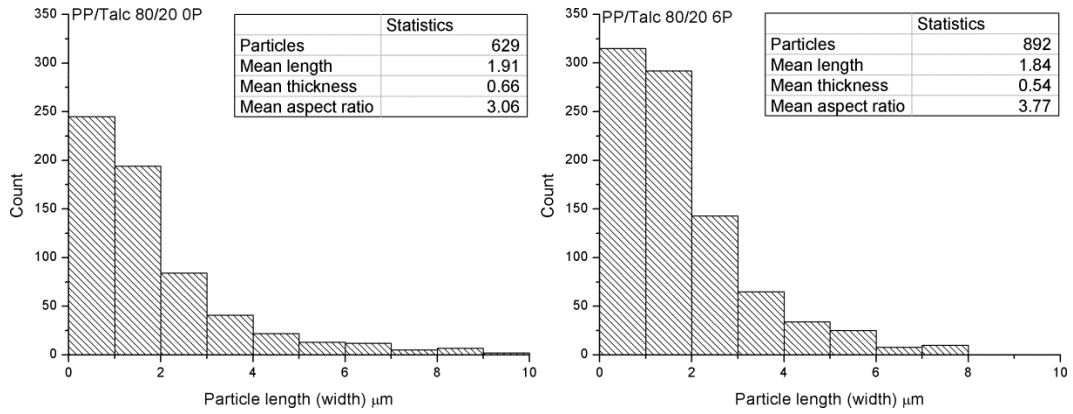

Figure 2-15: Statistical investigation of the talc particle size distribution in the case of non-recycled (0P) and recycled (6P) PP/talc 80/20 composites.

2.4.7. Mechanical properties

2.4.7.1. Viscoelastic properties

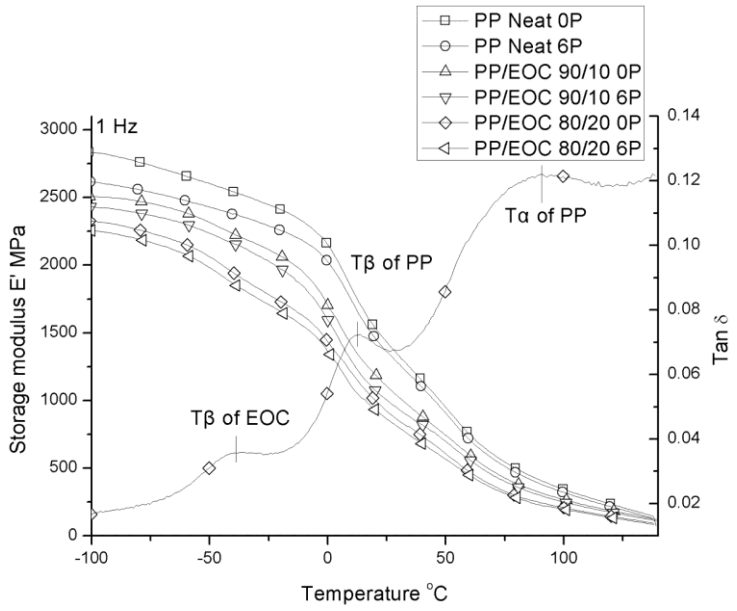

Figure 2-16: Storage modulus of non-recycled and recycled neat PP and PP/EOC composites as a function of temperature at 1 Hz.

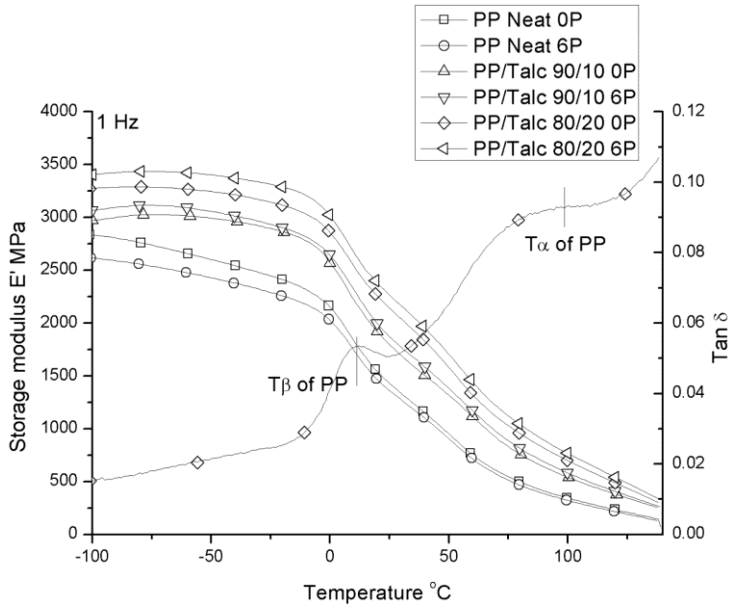

Figure 2-17: Storage modulus of non-recycled and recycled neat PP and PP/talc composites as a function of temperature at 1 Hz.

Attention is first focused on the impact of recycling on the viscoelastic properties of the PP blends characterized by DMA, and in particular on the storage modulus (Figure 2-15 and Figure 2-16).

For PP/EOC composites (Figure 2-16), in the case of the non-recycled materials, the storage modulus decreases with the content of EOC due to the increased amount of soft rubber phase. We also note that the storage modulus of the recycled materials slightly decreases because of the thermomechanical degradation of the materials by chain scission. For the evolution of the damping factor *tan* δ with temperature (Figure 2-16), we observed three relaxation peaks: 1) the glass transition of EOC (β_{EOC}), 2) the glass transition of PP (β_{PP}), and 3) the crystalline phase relaxation of PP (α_{PP}). It is to be noted that the crystalline phase relaxation of EOC (α_{EOC}) was not detected due to the overlapping of the α_{EOC} relaxation with the much more intense β_{EOC} relaxation [60-62]. The peak position of each relaxation process provided the corresponding relaxation temperature (Table 2-7). We note that recycling causes an increase of the glass transition temperature of PP (T_β of PP) and a decrease of the crystalline phase relaxation temperature of PP (T_α of PP), while the glass transition temperature of EOC (T_β of EOC) is constant with recycling. As mentioned above, the thermomechanical degradation induces the formation of a molecular network containing shorter chains but more defective than the initial one. Such a molecular network induces a higher crystallinity index, but thinner lamellae than the non-recycled molecular network. The presence of thinner PP lamellae in the recycled materials may explain the decrease of the relaxation temperature of PP crystalline phase (Table 2-7) [63]. Concerning the amorphous phase of PP, we consider that reprocessing leads to a more constrained amorphous phase due to the important defects and the higher crystallinity, which may explain the increase of the β_{PP}

relaxation temperature of PP [64]. The glass transition temperature of EOC phase is constant with the recycling number demonstrating that the mechanical recycling has no significant effect on the EOC phase. This observation is also in line with our DSC results (Table 2-4).

Table 2-7: Relaxation temperatures of PP matrix and EOC reinforcement in the case of non-recycled and recycled blends at 1Hz.

		T_β of EOC (°C)	T_β of PP(°C)	T_α of PP(°C)
Neat PP	0P	—	12.2±0.2	94.9±0.9
	6P	—	13.0±0.4	91.6±0.7
PP/EOC	0P	-43.5±0.8	12.2±0.1	92.5±0.1
90/10	6P	-43.6±0.9	13.0±0.1	87.3±0.9
PP/EOC	0P	-43.3±0.3	12.2±0.6	92.5±0.9
80/20	6P	-43.4±0.4	13.1±0.5	87.0±0.9
PP/talc	0P	—	11.7±0.6	99.4±1.5
90/10	6P	—	11.4±0.5	96.0±1.1
PP/talc	0P	—	11.3±0.6	101.6±0.7
80/20	6P	—	10.5±0.3	98.0±0.2

For PP/talc composites (Figure 2-17), concerning the non-recycled materials, the storage modulus increased with the addition of talc due to the presence of rigid talc fillers. The increase in rigidity was also explained by the formation of an interphase between the PP matrix and the rigid talc fillers, having an intermediate

rigidity between that of talc and that of PP [65]. Different from PP/EOC composites, the storage modulus of PP/talc composites increased for the two talc concentrations with the recycling number. The reason is that the intensive shear reprocessing condition produced smaller talc particles as concluded previously. Indeed, finer talc particles led to larger PP/talc interfaces, and hence led to a higher rigidity of the composite. Furthermore, the higher aspect ratio of talc filler in PP matrix after 6 recycling passes is also one of the main reasons of the increase of the storage modulus [66].

Comparing with the glass transition temperature of PP phase for non-recycled neat PP and PP/talc composites (Table 2-7), we found that the addition of talc filler slightly decreased the glass transition temperature of PP. The talc particles acted as nucleation agents of PP, and hence, the presence of talc within PP matrix resulted in a faster crystallization rate that caused an amorphous phase with a higher motion in comparison with neat PP [65]. On the contrary, the α_{PP} relaxation temperature of PP increased with the presence of talc. This is attributed to the fact that talc fillers increased the lamella thickness of PP.

We should note that the glass transition temperature of PP phase in PP/talc composites decreased with the reprocessing cycles. Indeed, the break of talc filler produced greater interfaces for the nucleation of PP resulting in more amorphous phase with greater motion. Concerning the α_{PP} transition temperature of PP, it decreased from the non-recycled to recycled materials in PP/talc composites.

2.4.7.2. Tensile properties

The nominal stress-strain curves with the zoomed true stress - true strain curves of the non-recycled PP, PP/EOC and PP/talc blends are shown in Figure 2-18 and Figure 2-19 for two strain rates. Because we are interested only in the elastic and yield behaviors of the materials, the tensile tests under 1mm/min stopped after the yield stress. In addition, under tensile speed of 50mm/min, equations (2-3) and (2-4) were used to calculate the true strain- true stress curves before the necking.

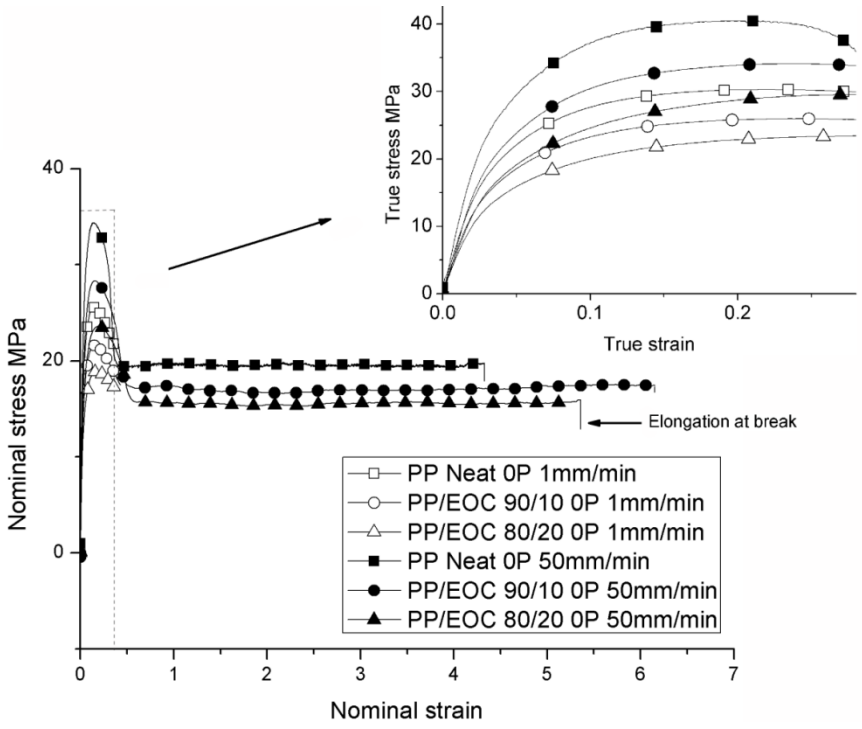

Figure 2-18: Tensile stress strain curves of non-recycled neat PP and PP/EOC composites.

In Figure 2-18 and 2-19, both neat PP and PP blends exhibit strain rate sensitivity, where the yield stress and the Young's modulus obtained at 50 mm/min were higher than those obtained at 1 mm/min for all materials [66].

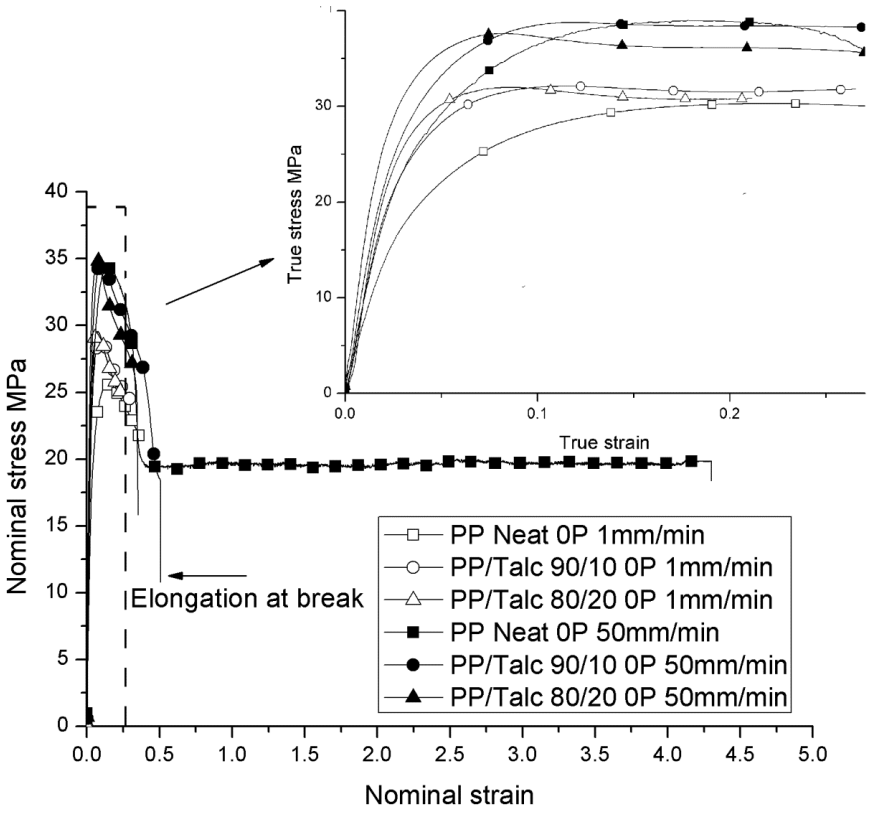

Figure 2-19: Tensile stress strain curves of non-recycled neat PP and PP/talc composites.

For PP/EOC composites (Figure 2-18), the addition of EOC inclusions decreases the yield stress and Young's modulus of neat PP, which is consistent with the storage modulus of PP and PP/EOC blends assessed by DMA (Figure 2-16).

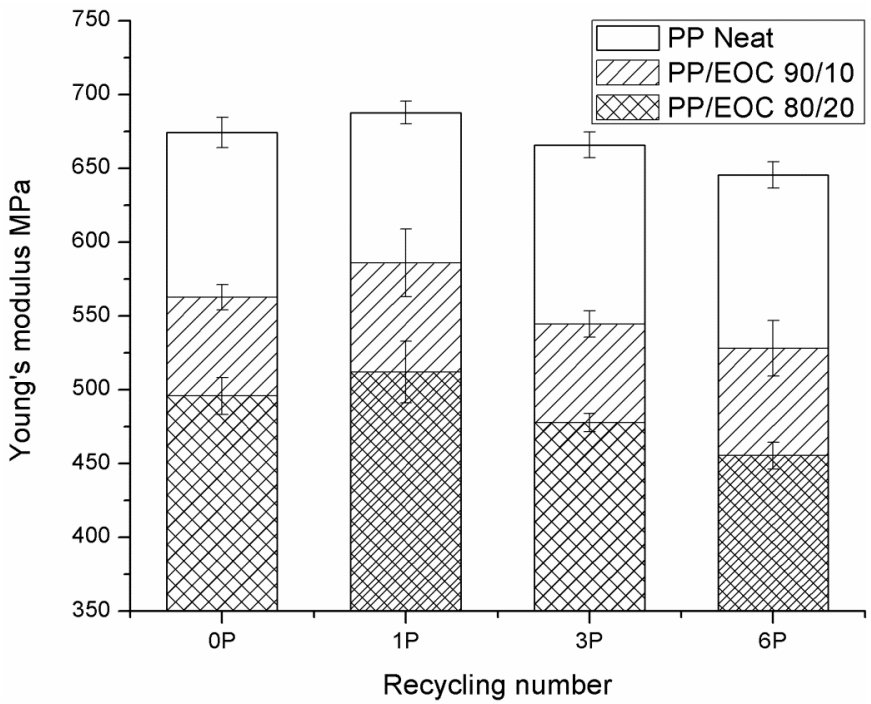

Figure 2-20: Tensile modulus of neat PP and PP/EOC composites as a function of the recycling number.

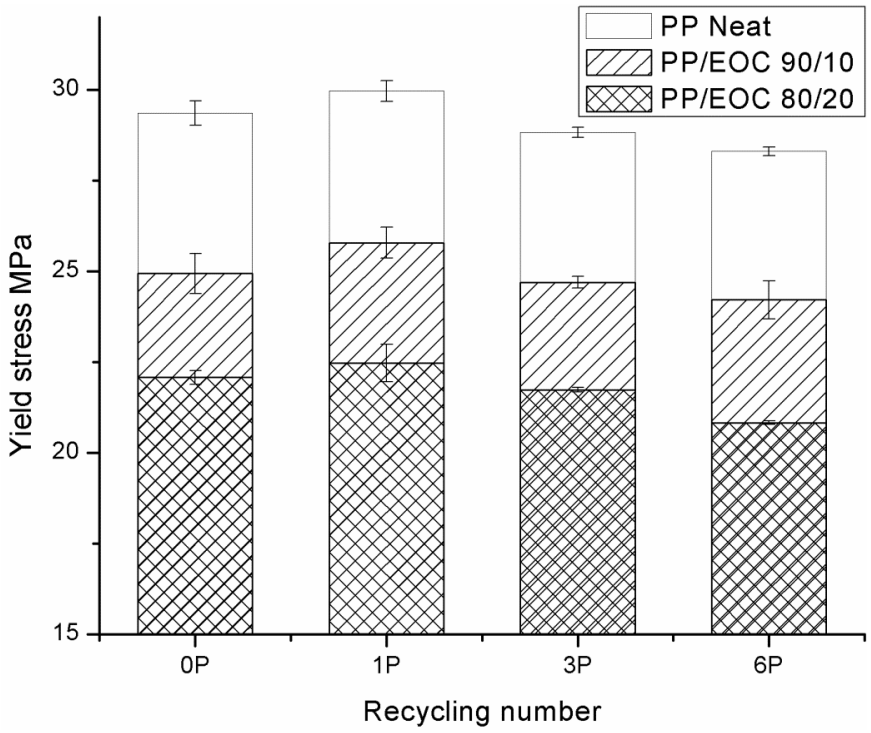

Figure 2-21: Tensile yield stress of neat PP and PP/EOC composites as a function of the recycling number.

The evolution of the Young's modulus and yield stress with the recycling number of neat PP and PP/EOC blends is presented in Figure 2-20 and Figure 2-21. These two mechanical parameters slightly increase after the first recycling procedure due to the increase of PP crystallinity that makes the material more stiffer [27]. For higher recycling numbers, it can be seen that the recycling produces a slight reduction of the yield stress and Young's modulus of neat PP and PP/EOC blends. This result suggests that the initial stiffening effect due to the increase of crystallinity is overcome by the important chain scission mechanisms and the increase of amorphous chain defects that soften the materials. We also measured the elongation at break of the materials as a function of the recycling number (Figure 2-22). Firstly, the elongation at break of non-recycled material increases in the following order: PP < PP/EOC 80/20 < PP/EOC 90/10. It was expected that neat PP had a lower elongation at break than the PP / EOC blends due to the toughening effect of the rubber particles, but surprisingly elongation behavior seems not to increase with the increasing content of EOC.

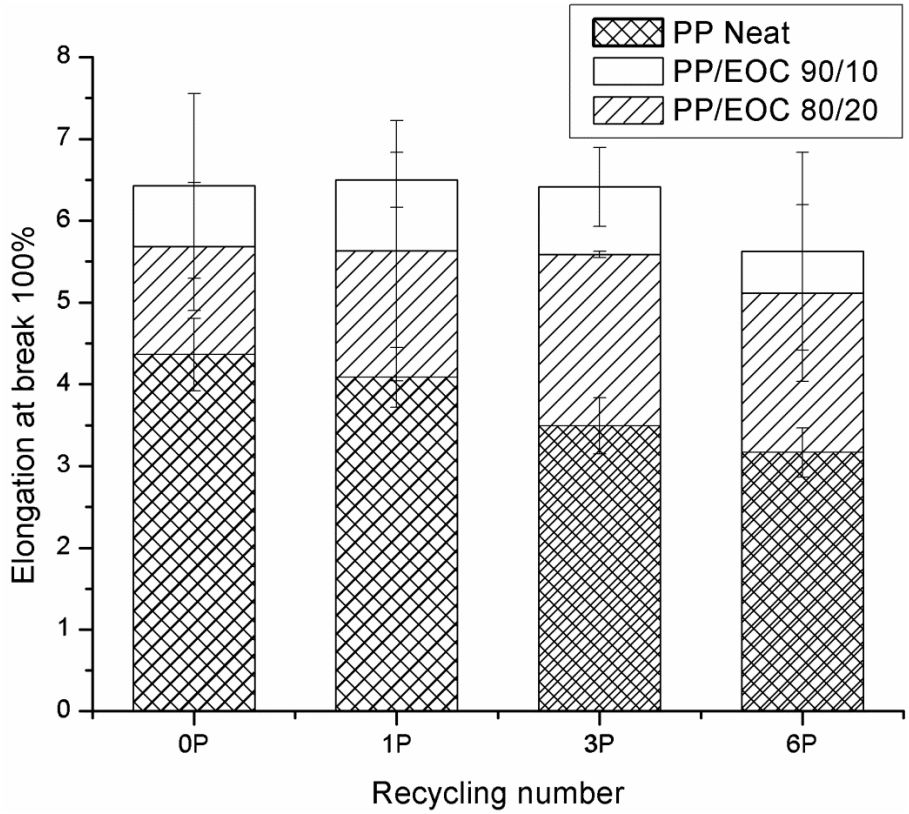

Figure 2-22: Elongation at break of neat PP and PP/EOC composites as a function of the recycling number.

According to the currently accepted toughening theories during loading, the rubbery particles act as sites of stress concentration. Therefore, as soon as the stress around the particles overcomes the yield stress of the matrix, the deformation mechanism such as crazing and/or shear yielding become active [29, 67]. Consequently, the ductility behavior of neat PP is improved by the addition of EOC dispersed phase. It should be noted that the ductility behavior of PP/rubber blends is not persistent increasing with the increasing of the rubber concentration. This behavior is influenced by both the nature of matrix and the rubber volume fraction. At low volume fraction of rubber, the generation of crazing around the rubber particles eliminates the tendency of the matrix to strain hardening. The whitening of the specimen and the inconspicuous cross-sectional areas change between the yield stress

and the failure point indicate that crazing, rather than shear yielding, is the main energy dissipation mechanism [29]. For high volume fraction of rubber, the shear bands around rubber particles interact, and microcracks develop at the areas of high mechanical constraints, leading to a reduce the elongation at break [7]. On the other hand, the elongation at break appears related to the amount of β phase (Table 2-5): the higher the amount of β phase, the higher the ductility of PP blends. These two mechanisms can be used to explain why the elongation at break of PP/EOC 90/10 is higher than that of PP/EOC 80/20 in our case.

For recycled materials, the elongation at break of neat PP gradually decreases with the recycling number, while that of the blends is constant during the first three recycling procedures, then it decreases. In the case of neat PP the repeated recycling procedures gradually shorten the molecular chains, which decreases both chain entanglements in the amorphous phase and tie molecules density. As a result, plasticity is limited due to reduced optimal stress transfer from amorphous chain to crystalline lamellae and the amorphous network is rapidly disentangled. In the case of PP blends, the elongation is strongly influenced by both particles size and particles distribution [8]. For recycled PP/EOC blends, the elongation at break is constant until the third recycling number. This is probable due to the homogenous distribution of the inclusions with reduced inclusions size caused by recycling as shown by SEM images in Figure 2-12 (we note that Figure 2-12 shows only the microstructure for six recyclings). For higher recycling numbers, this mechanism is overcome by the thermomechanical degradation of the PP matrix, which explains the final decrease of elongation at break for the blends.

For PP/talc composites (Figure 2-19), the introduction of the talc filler significantly increased the Young's modulus of neat PP For the two crosshead speeds. However, the presence of talc increased the tensile yield stress of neat PP at the lower rate (1 mm/min), but decreased the tensile yield stress at the higher rate (50 mm/min). When the talc was mixed with PP, it may accommodate one part of macroscopic stress, with limited or delayed cavitation mechanisms by debonding. In the case of a low strain rate, the accommodation of stress by the talc particles is important, resulting in an increase of yield stress and limited cavitation. For the case of high strain rates, the accommodation of stress by the talc particles is low, which results in marked cavitation mechanisms and a low yield stress [11, 68-70]. Besides this, Zhou et al.[71] attributed the decrease of PP/talc composite yield stress compared to neat PP to the presence of thermal residual stresses in the case of the composite. In particular, the coefficients of thermal expansion of PP matrix and talc are quite different, which may induce important thermal residual stresses within the composites and hence may decrease the yield stress during the tensile test in comparison with neat PP.

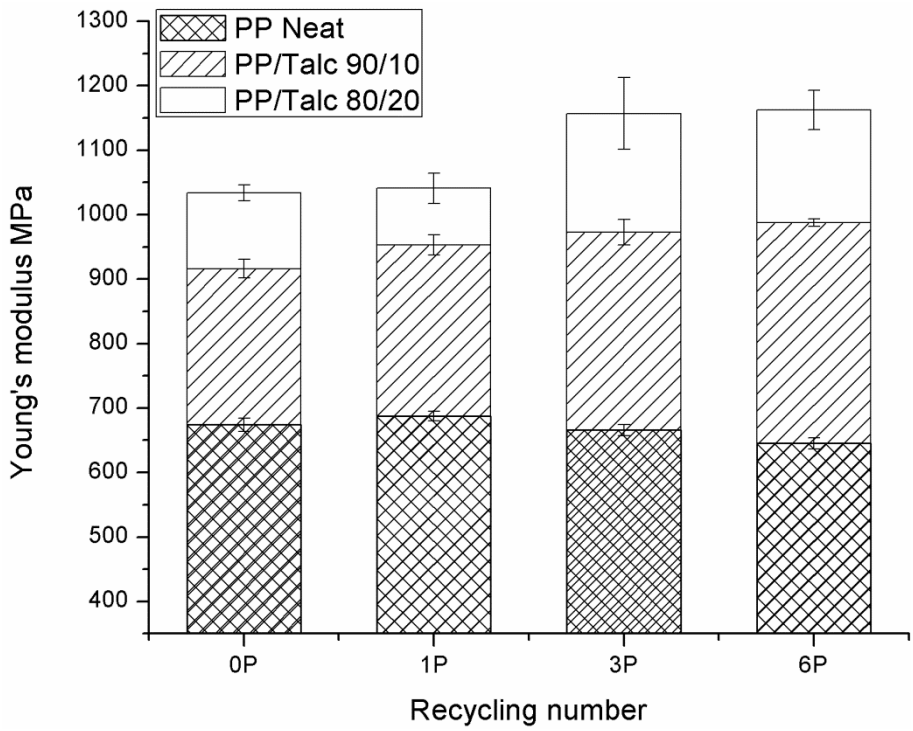

Figure 2-23: Tensile modulus of non-recycled and recycled neat PP and PP/talc composites.

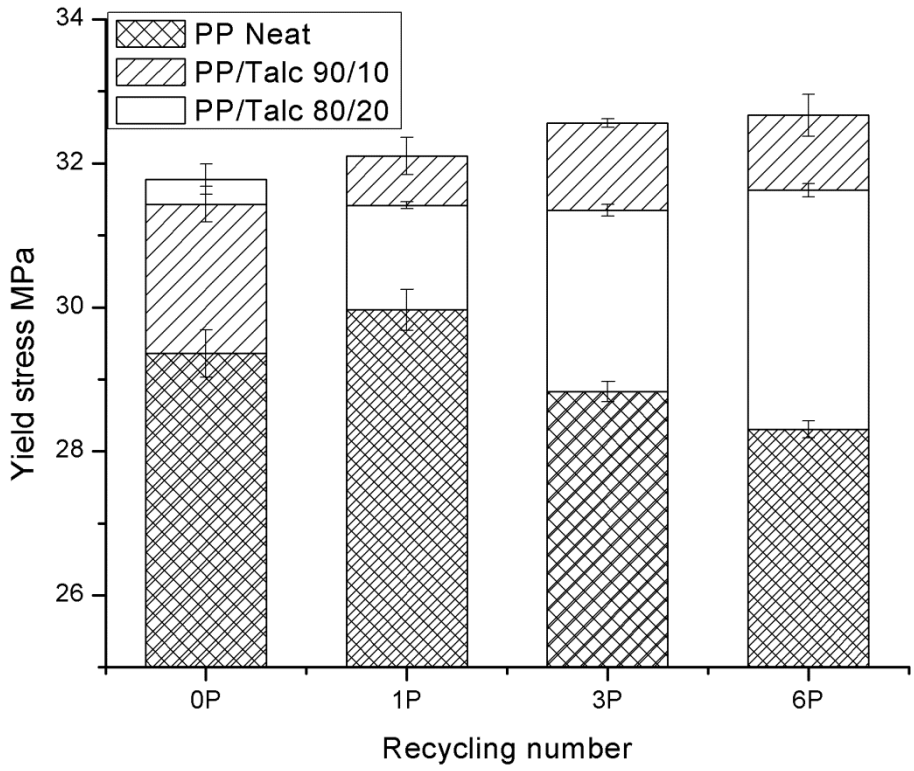

Figure 2-24: Yield stress of virgin and recycled neat PP and PP/talc composites.

The reprocessing effect on the mechanical behavior in terms of Young's modulus and yield stress for non-recycled and recycled neat PP and PP/talc composites are presented in Figure 2-23 and Figure 2-24. With the recycling cycles, the yield stress of PP/talc 90/10 composites increased slightly, while that of PP/talc 80/20 composites remained constant. A competition between self-reinforcement mechanisms and damage mechanisms by debonding may be active in the two composites during the recycling. Self-reinforcement mechanisms may be due to the reduction of talc particle dimensions with the recycling that increased the interphase size, and hence the ability to accommodate stress by the talc. However, if the concentration of talc is too important, damage mechanisms by matrix/filler debonding may be active, which may prevent the self-reinforcement effect. The first mechanisms may be predominant in PP/talc 90/10, while the two mechanisms may be in equilibrium in the case of PP/talc 80/20 composites. These hypotheses may explain why the yield stress increased for PP/talc 90/10, and why it remained constant for PP/talc 80/20, with the recycling number.

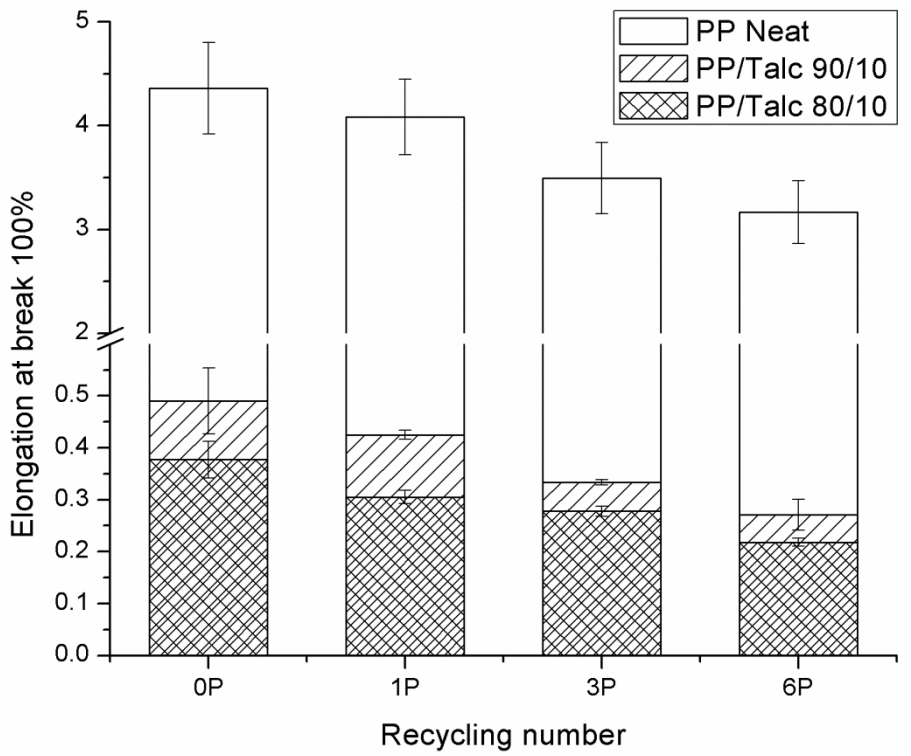

Figure 2-25: Elongation at break of non recycled and recycled neat PP and PP/talc composites.

The impact of recycling on the elongation at break of PP and PP/talc composites is shown in Figure 2-25. The elongation at break continuously decreased with the recycling number for PP/talc composites. Indeed, talc particles induced cavitation mechanisms by matrix/filler debondings. This mechanism further reduces the elongation at break of the PP-based materials, especially with increasing the recycling number due to the increase of particle number (Figure 2-15).

2.5. Conclusions

We investigated the thermomechanical degradation mechanisms of polypropylene (PP), PP/ethylene octene copolymer (EOC) and PP/talc blends resulting from recycling procedures consisting of grinding steps and re-extrusion steps. Different contents of fillers (0 wt. %, 10 wt. %, and 20 wt. %) were tested. Up to 6 recycling procedures, it is found that thermomechnical degradation induces chains scission mechanisms in PP matrix without significant oxidation.

For neat PP:

Recycling caused slight changes of different properties: 1) an increase of the melt flow index, 2) a decrease of the melting and crystallization temperatures, 3) an increase of the crystallinity, 4) an increase of the glass transition temperature and 5) a decrease of the crystalline phase relaxation temperature of PP. Young's modulus and tensile yield stress increase at the first recycling procedures, and then decrease for the rest recycling passes, while the elongation at break has a continuous decrease.

Effects of EOC:

The addition of EOC to PP induces also slight changes in properties : 1) it increases the processability of PP by decreasing its viscosity, 2) increases the thermal stability of PP, 3) enhances the formation of the ductile β crystalline phase and 4) increases the inherent low toughness of PP. The recycling does not modify the crystalline properties of EOC, nor its relaxation processes, which indicates a high resistance of EOC toward thermomechanical degradation due to mechanical recycling. However, the EOC inclusions show a narrower size distribution, a decrease of their average size, and a decrease of their average aspect ratio. As a consequence,

during the first three recyclings, the strain at break of the blends is stable, while that of PP decreases.

Effects of talc:

The addition of talc fillers to the PP matrix led to the following: 1) an increase of the thermal stability, 2) an increase of the melting temperature, crystallization temperature and crystallinity content, 3) a decrease of the β crystal phase content, 4) an increases of b-axis orientation, 5) a decrease of the glass transition temperature, 6) an increase of the α transition temperature, 7) an increase of the Young's modulus, 8) an increase of the yield stress at low tensile speed and a decrease of it at high tensile speed, 9) a decrease of the elongation behavior, for non-recycled materials.

During the recycling, the addition of talc filler to the PP matrix 1) keeps the melting temperature and the crystallinity temperature of PP constant, 2) continuously increases b-axis orientation of PP, 3) continuously decreases the glass transition temperature of PP, 4) continuously increases the Young's modulus, 5) slightly increases the yield stress of PP/talc 90/10 and keeps the yield stress of PP/talc 80/20 constant.

References

[1] Wang K, Boumbimba RM, Bahlouli N, Ahzi S, Muller R, Bouquey M. Dynamic behaviour of a melt mixing polypropylene organoclay nanocomposites. Journal of Engineering Materials and Technology. 2012;134:010905 http://dx.doi.org/010910.011115/010901.4005420.

[2] Matadi R, Hablot E, Wang K, Bahlouli N, Ahzi S, Avérous L. High strain rate behaviour of renewable biocomposites based on dimer fatty acid polyamides and cellulose fibres. Composites Science and Technology. 2011;71:674-682.

[3] Bahlouli N, Pessey D, Raveyre C, Guillet J, Ahzi S, Dahoun A, Hiver JM. Recycling effects on the rheological and thermomechanical properties of polypropylene-based composites. Materials and Design. 2012;33:451-458.

[4] Hablot E, Matadi R, Ahzi S, Avérous L. Renewable biocomposites of dimer fatty acid-based polyamides with cellulose fibres: Thermal, physical and mechanical properties. Composites Science and Technology. 2010;70:504-509.

[5] Somani RH, Hsiao BS, Nogales A, Fruitwala H, Srinivas S, Tsou AH. Structure development during shear flow induced crystallization of i-PP: In situ wide-angle X-ray diffraction study. Macromolecules. 2001;34:5902-5909.

[6] Jones AT, Aizlewood JM, Beckett DR. Crystalline forms of isotactic polypropylene. Die makromolekulare Chemie. 1964;75:134-158.

[7] Jancar J, DiAnselmo A, DiBenedetto AT, Kucera J. Failure mechanics in elastomer toughened polypropylene. Polymer. 1993;34:1684-1694.

[8] Van der Wal A, Verheul AJJ, Gaymans RJ. Polypropylene-rubber blends: 4. The effect of the rubber particle size on the fracture behaviour at low and high test speed. Polymer. 1999;40:6057-6065.

[9] Sawyer LC, Grubb DT, Meyers GF. Polymer microscopy. 3 ed. New York: Springer; 2008.

[10] Brown GM, Butler JH. New method for the characterization of domain morphology of polymer blends using ruthenium tetroxide staining and low voltage scanning electron microscopy (LVSEM). Polymer. 1997;38:3937-3945.

[11] Addiego F, Di Martino J, Ruch D, Dahoun A, Godard O, Lipnik P, Biebuyck J-J. Cavitation in unfilled and nano-CACO3 filled HDPE subjected to tensile test: Revelation, localization, and quantification. Polymer Engineering and Science. 2010;50:278-289.

[12] C. Yu T. Mentallocane plastomer modification of polypropylenes. Polymer Engineering and Science. 2001;41:656-671.

[13] Leong YW, Abu Bakar MB, Ishak ZAM, Ariffin A, Pukanszky B. Comparison of the mechanical properties and interfacial interactions between talc, kaolin, and

calcium carbonate filled polypropylene composites. Journal of Applied Polymer Science. 2004;91:3315-3326.

[14] Sarrionandia M, Lopez-Arraiza A, Aurrekoetxea J, Arostegui A. Structure and mechanical properties of a talc-filled polypropylene/ethylene-propylene-diene composite after reprocessing in the melt state. Journal of Applied Polymer Science. 2009;114:1195-1201.

[15] Ramírez-Vargas E, Navarro-Rodríguez D, Blanqueto-Menchaca AI, Huerta-Martínez BM, Palacios-Mezta M. Degradation effects on the rheological and mechanical properties of multi-extruded blends of impact-modified polypropylene and poly(ethylene-co-vinyl acetate). Polymer Degradation and Stability. 2004;86:301-307.

[16] Guerrica-Echevarría G, Eguiazábal JI, Nazábal J. Effects of reprocessing conditions on the properties of unfilled and talc-filled polypropylene. Polymer Degradation and Stability. 1996;53:1-8.

[17] Martins MH, De Paoli MA. Polypropylene compounding with post-consumer material: II. Reprocessing. Polymer Degradation and Stability. 2002;78:491-495.

[18] Strömberg E, Karlsson S. The design of a test protocol to model the degradation of polyolefins during recycling and service life. Journal of Applied Polymer Science. 2009;112:1835-1844.

[19] Peterson JD, Vyazovkin S, Wight CA. Kinetics of the Thermal and Thermo-Oxidative Degradation of Polystyrene, Polyethylene and Poly(propylene). Macromolecular Chemistry and Physics. 2001;202:775-784.

[20] Navarro R, Torre L, Kenny JM, Jiménez A. Thermal degradation of recycled polypropylene toughened with elastomers. Polymer Degradation and Stability. 2003;82:279-290.

[21] Liu Z, Chen S, Zhang J. Photodegradation of ethylene–octene copolymers with different octene contents. Polymer Degradation and Stability. 2011;96:1961-1972.

[22] Wang K, Addiego F, Bahlouli N, Ahzi S, Rémond Y, Toniazzo V, Muller R. Analysis of thermomechanical reprocessing effects on polypropylene/ethylene octene copolymer blends. Polymer Degradation and Stability. 2012;97:1475–1484.

[23] Tortorella N, Beatty CL. Morphology and mechanical properties of impact modified polypropylene blends. Polymer Engineering and Science. 2008;48:2098-2110.

[24] Mano E, Martins A, Mendes L. Thermal Analysis Applied to Discarded Car Bumpers. Journal of Thermal Analysis and Calorimetry. 2000;59:425-432.

[25] Camacho W, Karlsson S. Assessment of thermal and thermo-oxidative stability of multi-extruded recycled PP, HDPE and a blend thereof. Polymer Degradation and Stability. 2002;78:385-391.

[26] Jiménez A, Torre L, Kenny JM. Processing and properties of recycled polypropylene modified with elastomers. Plastics, Rubber and Composites. 2003;32:357-367.

[27] Aurrekoetxea J, Sarrionandia MA, Urrutibeascoa I, Maspoch ML. Effects of recycling on the microstructure and the mechanical properties of isotactic polypropylene. Journal of Materials Science. 2001;36:2607-2613.

[28] Jansson A, Möller K, Gevert T. Degradation of post-consumer polypropylene materials exposed to simulated recycling - Mechanical properties. Polymer Degradation and Stability. 2003;82:37-46.

[29] Luda MP, Ragosta G, Musto P, Pollicino A, Camino G, Recca A, Nepote V. Natural Ageing of Automotive Polymer Components: Characterisation of New and Used Poly(propylene) based Car Bumpers. macromolecular materials and engineering. 2002;287:404-411.

[30] Luda MP, Ragosta G, Musto P, Acierno D, Di Maio L, Camino G, Nepote V. Regenerative Recycling of Automotive Polymer Components: Poly(propylene) Based Car Bumpers. macromolecular materials and engineering. 2003;288:613-620.

[31] Colin X, Verdu J, Rabaud B. Stabilizer thickness profiles in polyethylene pipes transporting drinking water disinfected by bleach. Polymer Engineering and Science. 2011;51:1541-1549.

[32] Othman N, Ismail H, Jaafar M. Preliminary study on application of bentonite as a filler in polypropylene composites. Polymer - Plastics Technology and Engineering. 2004;43:713-730.

[33] Butylina S, Hyvärinen M, Kärki T. A study of surface changes of wood-polypropylene composites as the result of exterior weathering. Polymer Degradation and Stability. 2012;97:337-345.

[34] Qiao X, Zhang Y, Zhang Y, Zhu Y. Ink-eliminated waste paper sludge flour-filled polypropylene composites with different coupling agent treatments. Journal of Applied Polymer Science. 2003;89:513-520.

[35] Pandey KK, Pitman AJ. FTIR studies of the changes in wood chemistry following decay by brown-rot and white-rot fungi. International Biodeterioration and Biodegradation. 2003;52:151-160.

[36] Da Silva ALN, Rocha MCG, Coutinho FMB, Bretas R, Scuracchio C. Rheological, mechanical, thermal, and morphological properties of polypropylene/ethylene-octene copolymer blends. Journal of Applied Polymer Science. 2000;75:692-704.

[37] Zebarjad SM, Bagheri R, Reihani SMS, Lazzeri A. Deformation, yield and fracture of elastomer-modified polypropylene. Journal of Applied Polymer Science. 2003;90:3767-3779.

[38] Velasco JI, De Saja JA, Martínez AB. Crystallization behavior of polypropylene filled with surface-modified talc. Journal of Applied Polymer Science. 1996;61:125-132.

[39] Gafur MA, Nasrin R, Mina MF, Bhuiyan MAH, Tamba Y, Asano T. Structures and properties of the compression-molded istactic-polypropylene/ talc composites: Effect of cooling and rolling. Polymer Degradation and Stability. 2010;95:1818-1825.

[40] Monasse B, Ferrandez P, Delamare F, Montmitonnet P, Haudin JM. Crystallization temperature effect on the solid-state rheology of a high-density polyethylene under compression. Polymer Engineering and Science. 1997;37:1684-1693.

[41] Kim JH, Koo CM, Choi YS, Wang KH, Chung IJ. Preparation and characterization of polypropylene/layered silicate nanocomposites using an antioxidant. Polymer. 2004;45:7719-7727.

[42] Ferrage E, Martin F, Boudet A, Petit S, Fourty G, Jouffret F, Micoud P, De Parseval P, Salvi S, Bourgerette C, Ferret J, Saint-Gerard Y, Buratto S, Fortune JP. Talc as nucleating agent of polypropylene: morphology induced by lamellar particles addition and interface mineral-matrix modelization. Journal of Materials Science. 2002;37:1561-1573.

[43] Naiki M, Fukui Y, Matsumura T, Nomura T, Matsuda M. The effect of talc on the crystallization of isotactic polypropylene. Journal of Applied Polymer Science. 2001;79:1693-1703.

[44] Da Costa HM, Ramos VD, De Oliveira MG. Degradation of polypropylene (PP) during multiple extrusions: Thermal analysis, mechanical properties and analysis of variance. Polymer Testing. 2007;26:676-684.

[45] Sperling LH. Introduction to Physical Polymer Science. 4 ed. New Jersey: John Wiley & Sons, Inc.; 2006.

[46] Zhang RH, Shi DA, Tsui CP, Tang CY, Tjong SC, Li RKY. The formation of β-polypropylene crystals in a compatibilized blend of isotactic polypropylene and polyamide-6. Polymer Engineering and Science. 2011;51:403-410.

[47] Bai H, Wang Y, Song B, Han L. Synergistic toughening effects of nucleating agent and ethylene–octene copolymer on polypropylene. Journal of Applied Polymer Science. 2008;108:3270-3280.

[48] Aboulfaraj M, G'Sell C, Ulrich B, Dahoun A. In situ observation of the plastic deformation of polypropylene spherulites under uniaxial tension and simple shear in the scanning electron microscope. Polymer. 1995;36:731-742.

[49] Shangguan Y, Song Y, Peng M, Li B, Zheng Q. Formation of β-crystal from nonisothermal crystallization of compression-molded isotactic polypropylene melt. European Polymer Journal. 2005;41:1766-1771.

[50] Lotz B. α and β phases of isotactic polypropylene: A case of growth kinetics 'phase reentrency' in polymer crystallization. Polymer. 1998;39:4561-4567.

[51] Obata Y, Sumitomo T, Ijitsu T, Matsuda M, Nomura T. The effect of talc on the crystal orientation in polypropylene/ethylene-propylene rubber/talc polymer blends in injection molding. Polymer Engineering and Science. 2001;41:408-416.

[52] Varghese H, Bhagawan SS, Prabhakaran N, Thomas S. Tearing behavior and recyclability of nitrile rubber/poly(ethylene-co-vinyl acetate) blends. Materials Letters. 1995;24:333-339.

[53] Frihi D, Masenelli-Varlot K, Vigier G, Satha H. Mixed percolating network and mechanical properties of polypropylene/talc composites. Journal of Applied Polymer Science. 2009;114:3097-3105.

[54] Rondin J. Apports des écoulements élongationnels lors de la mise en œuvre de mélanges PP/EPDM réticulés dynamiquement et chargés à base de graphène: University of Strasbourg; 2012.

[55] Suh CH, White JL. Talc-thermoplastic compounds: particle orientation in flow and rheological properties. Journal of Non-Newtonian Fluid Mechanics. 1996;62:175-206.

[56] Knittel FL. Compounding Technologies, Advantages and Applications of Buss Kneaders. 2011.

[57] Borse NK, Kamal MR. Estimation of stresses required for exfoliation of clay particles in polymer nanocomposites. Polymer Engineering and Science. 2009;49:641-650.

[58] Médout-Marère V. A Simple Experimental Way of Measuring the Hamaker Constant A11 of Divided Solids by Immersion Calorimetry in Apolar Liquids. Journal of Colloid and Interface Science. 2000;228:434-437.

[59] Ma Q, Tibbenham PC, Lai X, Glogovsky T, Su X. Micromechanical modeling of the mechanical behavior of thermoplastic olefin. Polymer Engineering and Science. 2010;50:536-542.

[60] Jaziri M, Mnif N, Massardier-Nageotte V, Perier-Camby H. Rheological, thermal, and morphological properties of blends based on poly(propylene), ethylene propylene rubber, and ethylene-1-octene copolymer that could result from end of life vehicles: Effect of maleic anhydride grafted poly(propylene). Polymer Engineering and Science. 2007;47:1009-1015.

[61] Al-Malaika S, Peng X, Watson H. Metallocene ethylene-1-octene copolymers: Influence of comonomer content on thermo-mechanical, rheological, and thermo-oxidative behaviours before and after melt processing in an internal mixer. Polymer Degradation and Stability. 2006;91:3131-3148.

[62] Benavente R, Pérez E, Yazdani-Pedram M, Quijada R. Viscoelastic relaxations in poly(ethylene-co-1-octadecene) synthesized by a metallocene catalyst. Polymer. 2002;43:6821-6828.

[63] Mnif N, Massardier V, Kallel T, Elleuch B. New (PP/EPR)/nano-CaCO3 based formulations in the perspective of polymer recycling. Effect of nanoparticles properties and compatibilizers. Polymers for Advanced Technologies. 2010;21:896-903.

[64] Zhao J, Wang J, Li C, Fan Q. Study of the Amorphous Phase in Semicrystalline Poly(ethylene terephthalate) via Physical Aging. Macromolecules. 2002;35:3097-3103.

[65] Díez-Gutiérrez S, Rodríguez-Pérez MA, De Saja JA, Velasco JI. Dynamic mechanical analysis of injection-moulded discs of polypropylene and untreated and silane-treated talc-filled polypropylene composites. Polymer. 1999;40:5345-5353.

[66] Weon JI, Sue HJ. Mechanical properties of talc- and CaCO3- reinforced high-crystallinity polypropylene composites. Journal of Materials Science. 2006;41:2291-2300.

[67] Greco R, Mancarella C, Martuscelli E, Ragosta G, Yin J. Polyolefin blends: 2. Effect of EPR composition on structure, morphology and mechanical properties of iPP/EPR alloys. Polymer. 1987;28:1929-1936.

[68] Hadal RS, Misra RDK. The influence of loading rate and concurrent microstructural evolution in micrometric talc- and wollastonite-reinforced high isotactic polypropylene composites. Materials Science and Engineering: A. 2004;374:374-389.

[69] Azizi H, Faghihi J. An investigation on the mechanical and dynamic rheological properties of single and hybrid filler/polypropylene composites based on talc and calcium carbonate. Polymer Composites. 2009;30:1743-1748.

[70] Addiego F, Dahoun A, G'Sell C, Hiver JM, Godard O. Effect of microstructure on crazing onset in polyethylene under tension. Polymer Engineering and Science. 2009;49:1198-1205.

[71] Zhou Y, Rangari V, Mahfuz H, Jeelani S, Mallick PK. Experimental study on thermal and mechanical behavior of polypropylene, talc/polypropylene and polypropylene/clay nanocomposites. Materials Science and Engineering: A. 2005;402:109-117.

Chapter 3:

Dynamic mechanical analysis of the recycled polypropylene-based composites

3. Dynamic mechanical analysis of the recycled polypropylene-based composites

3.1. Introduction

The impact of reprocessing on the properties of PP-based composite are now partially studied. In this, most of the investigations characterized the evolution of rheological, chemical, physical and quasi-static mechanical properties of materials with reprocessing cycles [1-8]. In the previous chapter, we characterized the impact of the reinforcements on the degradation of re-extruded polypropylene-based composites. The considered fillers consisted of EOC and talc. The degradation mechanisms of the composites were studied by a multiphysical approach [9]. To the best of our knowledge, the influence of mechanical recycling on the dynamic behavior of PP-based composites is less investigated. In automotive industry, PP-based composites are generally used in the manufacturing of bumpers [15,18,19]. In such a case, a detailed study of high strain rate and temperature sensitivities of PP-based composites is essential since the bumpers undergo compressive impact loading in a wide range of temperatures.

The aim of this chapter is to study the impact of the reinforcements on the dynamic compression behavior of re-extruded PP-based composites. The dynamic compression behavior is investigated by using split Hopkinson pressure bars in a wide range of temperatures and strain rates. The mechanical properties are correlated with the morphology of the studied composites by using the optical microscopy (OM).

3.2. Experiments

3.2.1. Materials

The materials used in this chapter are the same the ones investigated in chapter 2. In order to investigate the impact of the reinforcement on the dynamic behavior of re-extruded PP/EOC/talc composites, we prepared a ternary-phase material by using 70 wt. % of PP, 20 wt.% of EOC and 10 wt.% of talc. We note that the material processing and reprocessing were the same as in the previous chapter.

In the following, neat PP, PP/EOC, PP/talc and PP/EOC/talc blends were denoted as PP neat, PP/EOC x/y, PP/talc x/y and PP/EOC/talc x/y/z, respectively, where x, y, z are the weight percent of each component. In this chapter, we investigated the recycling number of 0P, 3P and 6P. It is to be mentioned that the recycling cycle 1P did not markedly affect the materials properties (see Chapter 2).

For the dynamic testing, cylindrical specimens with a diameter of 8 mm and with a thickness of 3mm were cut from the injection samples by a die cutter [10].

3.2.2. Mechanical Investigation at High Strain Rates

3.2.2.1. Split Hopkinson pressure bar technique

A split Hopkinson pressure bar (SHPB) set-up is an apparatus which typically consists in a striker bar, an incident bar and a transmitted bar (Figure 3-1). The incident and the transmitted bars of our home made SHPB are made of 316L steel with the same length of 3 m and a diameter of 22 mm. Strikers 0.5m and 1m in length are made of the same steel. The strain gages are glued on the middle of the incident and the transmitted bars with a distance of 1.5m from the interface of specimen and

bars. A furnace with two symmetrical resistance heaters is installed for high-temperature tests. Liquid nitrogen is used for low temperature tests.

Cylindrical specimens are sandwiched between the incident bar and the transmitted bar to determine their dynamic responses under compression. The striker is used to generate a longitudinal compressive wave. Once this compressive wave reaches the incident bar, strain gages cemented on this bar record an incident wave $\varepsilon_I(t)$. The difference in the mechanical impedances at the interface between the incident bar and the specimen results in the fact that a part of the incident wave reflects back along the incident bar while the other part transmits through the specimen and then in the transmitted bar. The reflected wave $\varepsilon_R(t)$ is measured by the same strain gages cemented on the incident bar. The transmitted wave $\varepsilon_T(t)$ can be obtained by the same type of strain gages glued on the transmitted bar. In addition, two speed sensors are used to measure the velocity of the striker.

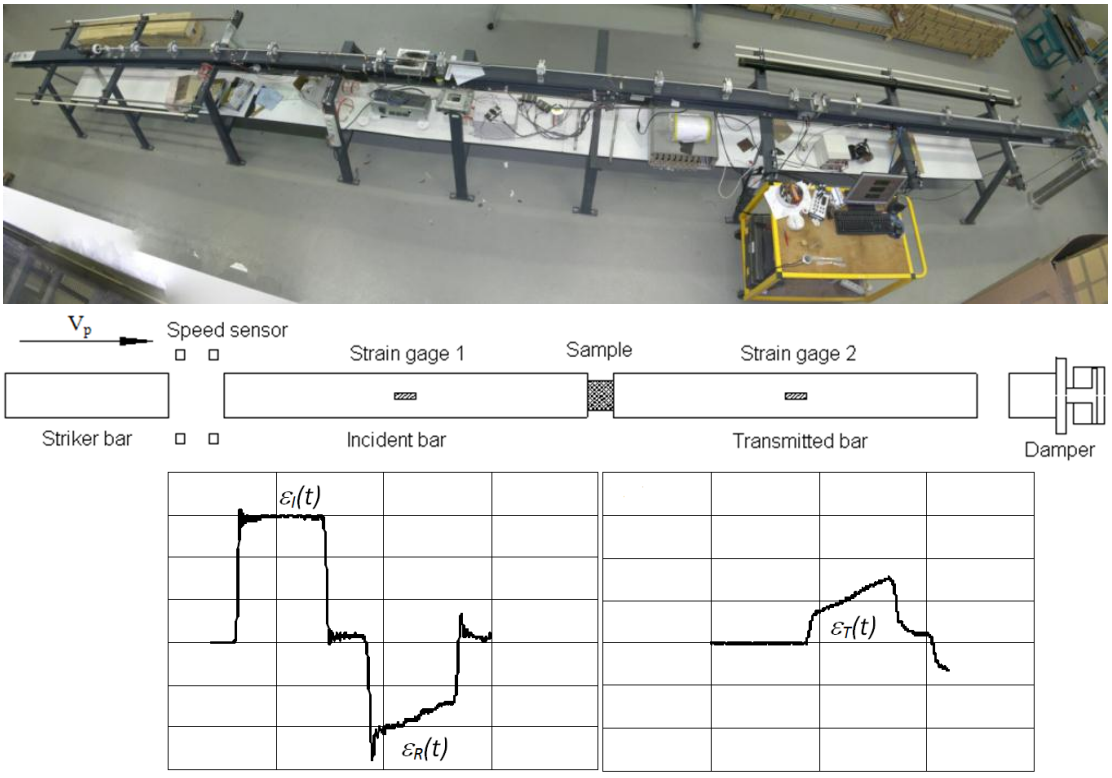

Figure 3-1: Schematic representation of a typical compression split Hopkinson pressure bar.

According to the classical elastic wave propagation theory, the nominal stress (σ_n), the nominal strain (ε_n) and the nominal strain rate ($\dot{\varepsilon}_n$) of the tested materials can be computed by the following expressions [11]:

$$\dot{\varepsilon}_n = \frac{2C_b}{L} \cdot \varepsilon_R(t) \tag{3-1}$$

$$\varepsilon_n = \frac{2C_b}{L} \int \varepsilon_R(t) dt \tag{3-2}$$

$$\sigma_n = E \cdot (\frac{A}{A_s}) \cdot \varepsilon_T(t) \tag{3-3}$$

Here, C_b is the elastic wave speed in the incident and the transmitted bars (bars are made of the same materials); E is the Young's modulus of the bars; L represents the initial thickness of specimen; A and A_s are the cross sectional area of the bars and the specimen, respectively. The nominal strain and stress can be used to derive the true ones (with the subscript *t*) by the following equations [12]:

$$\dot{\varepsilon}_t(t) = \frac{\dot{\varepsilon}_n(t)}{1-\varepsilon_n(t)} \tag{3-4}$$

$$\varepsilon_t(t) = -\ln(1-\varepsilon_n(t)) \tag{3-5}$$

$$\sigma_t(t) = \sigma_n(t)\exp(-2\upsilon\varepsilon_t(t)) \tag{3-6}$$

These equations are written for compression when strains are taken positive. In equation (6), υ is the Poisson's ratio of the tested material. In this work, a value of $\upsilon = 0.4$ is used for both neat PP and PP-based composites.

In this study, dynamic tests were carried out at various temperatures, from -30°C to 85°C (-30°C, 0°C, 25°C, 50°C and 85°C), and various strain rates from 592 s^{-1} to 3346 s^{-1} ($\dot{\varepsilon}_1 = 592$, $\dot{\varepsilon}_2 = 1276$, $\dot{\varepsilon}_3 = 2221$ and $\dot{\varepsilon}_4 = 3346$).

3.2.2.2. Assumption of Split Hopkinson pressure bar

Split Hopkinson pressure bar technique is based on four major simplifying assumptions [10, 13]: (1) The waves in elastic bars propagate in one-dimension ; (2) In the axial direction, the stress and strain fields in the specimen are uniform; (3) The inertia effect on the specimen is neglected; (4) The friction effect on the interface between the specimen and bars is neglected.

The first assumption is generally accepted when the incident wave is much longer than the length of specimens [10, 14].

Applying to the second assumption, Equation (3-4) becomes correct only when the stress and strain fields are uniform in the specimen. However, it is not valid at the beginning of the impact test. Actually, when the first wave reaches the interface of the specimen and the incident bar, the interface of the specimen and the transmitted bar is not yet loaded. For a given material, the duration of the wave propagation through the specimen depends upon the sample thickness. Therefore, this effect is even more severe for thick samples [15]. In order to minimize this effect, thin specimens are more appropriated [16-18].

During a high strain rate compressive test, besides the axial particle velocity of the specimen, both radial and tangential particle velocities would achieve high values. The resulting necessary accelerations require high compressive stresses in all the three directions. Therefore, the hydrostatic part of the stress tensor is high. Consequently, the specimen remains constrained, showing a greater apparent resistance to compression than that in the ideal one-dimensional compressive test [19]. Even though the inertia effect is one of the major error sources in the impact tests [20, 21], some authors reported that this effect is still limited [22]. Song et al. [17] noted that the induced inertia just led to a low increase of the intrinsic yield stress of the material. Trautmann et al. [23] showed that the inertial stresses of PC were lower than 0.2 MPa for the thin specimen (0.5 mm) and lower than 1 MPa for the thick specimens (5 mm) during the acceleration phase under a strain rate of 2500 s^{-1}. Thus, the inertia effect on the measured yield stresses can be neglected when thin specimens are used.

Friction effect is considered to be the largest source of error in SHPB technique [24]. During the high strain rate compression tests, friction between the surfaces of the sample and the bars tends to constrain the lateral flow of the sample. This constraint generates a hydrostatic stress that is superimposed upon the axial stress, resulting in a triaxial stress state. Therefore, the measured mechanical responses of tested materials tend to exaggerate their apparent behaviors [24]. Moreover, this error is more marked for thin specimens than for thick specimens which results in high measured yield stresses [19]. Different lubricant layers were used to reduce the interfacial friction, such as silicone grease [22], oleamide [25], stearamide [25], petroleum jelly [22, 23, 25-27], molybdenum [10, 23, 28] and polytetrafluoroethylene [23]. Petroleum jelly is a suitable lubricant for polymeric materials which can effectively reduce the frictional effect on SHPB tests at low temperature (- 60 °C) and at room temperature [16, 22, 23, 25, 29].

As discussed above, thin specimens are desirable to minimize the effects of the non-uniform stress field and inertia of specimens in SHPB approach. However, thin specimens tend to increase friction stresses.

In our previous study [30], we investigated the lubrication of polypropylene and polypropylene based composite in split Hopkinson pressure bar at high temperatures. In this study, the samples with two different geometries of neat PP, PP-Nanocor (rigid fillers) and PP-EPR (soft fillers) were used to investigate the frictional effect on SHPB under two strain rates ($\dot{\varepsilon}_1 = 1247$ and $\dot{\varepsilon}_2 = 2247$.) and at three temperatures (20°C, 40°C and 60°C). The experimental responses for all the materials without lubricant shown evident frictional effects on the impact tests. The lubricant of petroleum jelly can effectively reduce the friction effect on the dynamic behavior of

the materials to zero with experimental error at room temperature as well as high temperatures [30].

Therefore, in the present work, our samples (diameter = 8 mm, thickness = 3 mm) for dynamic tests will be lubricated by petroleum jelly at all test conditions.

3.3. Results and Analysis

Figure 3-2 shows the experimental true stress–strain curves in compression of non-recycled neat polypropylene and its composites at different temperatures and under strain rate 2 which is mentioned above. We note that non-recycled neat PP and non-recycled PP/talc composites are brittle at -30°C and 0 °C. This is due to the glass transition temperature of non-recycled PP which is about 12°C (see section 2.4.7). At -30°C, the dynamic responses of neat PP 0P and PP/talc composites 0P show a rapid decrease of stress before the yield point. However, this decrease of stress is less marked for neat PP 0P and PP/talc composites 0P at 0 °C than at -30°C. This phenomenon is probably due to the increase of mobility with increasing temperature that delays the material rupture. For PP/EOC 0P and PP/EOC/talc 0P, the dynamic response do not show a fragile behavior as PP 0P and PP/talc composites 0P at low temperatures (-30°C and 0 °C). This is due to the addition of the EOC that modifies the impact behavior of the materials. In Figure 3-2, for PP/EOC composites 0P, the Young's modulus and the yield stress decrease with the content of EOC due to the increased amount of soft rubber phase. For PP/talc composites 0P, the Young's modulus increases with the increasing of talc content due to the presence of rigid talc fillers. However, the yield stresses of PP/talc 90/10 0P at 25°C and 85°C are higher than those of PP/talc 80/20 0P at the same temperatures. This is probably due to the damage mechanisms by matrix/filler debonding during the dynamic test in PP/talc

80/20 0P is more important than that in PP/talc 90/10 0P. In addition, we note that the Young's modulus of PP/EOC/talc 70/20/10 0P is slightly higher than that of PP/EOC 90/10 0P whereas the yield stress of PP/EOC/talc 70/20/10 0P is lower than that of PP/EOC 90/10 0P for our investigated test conditions.

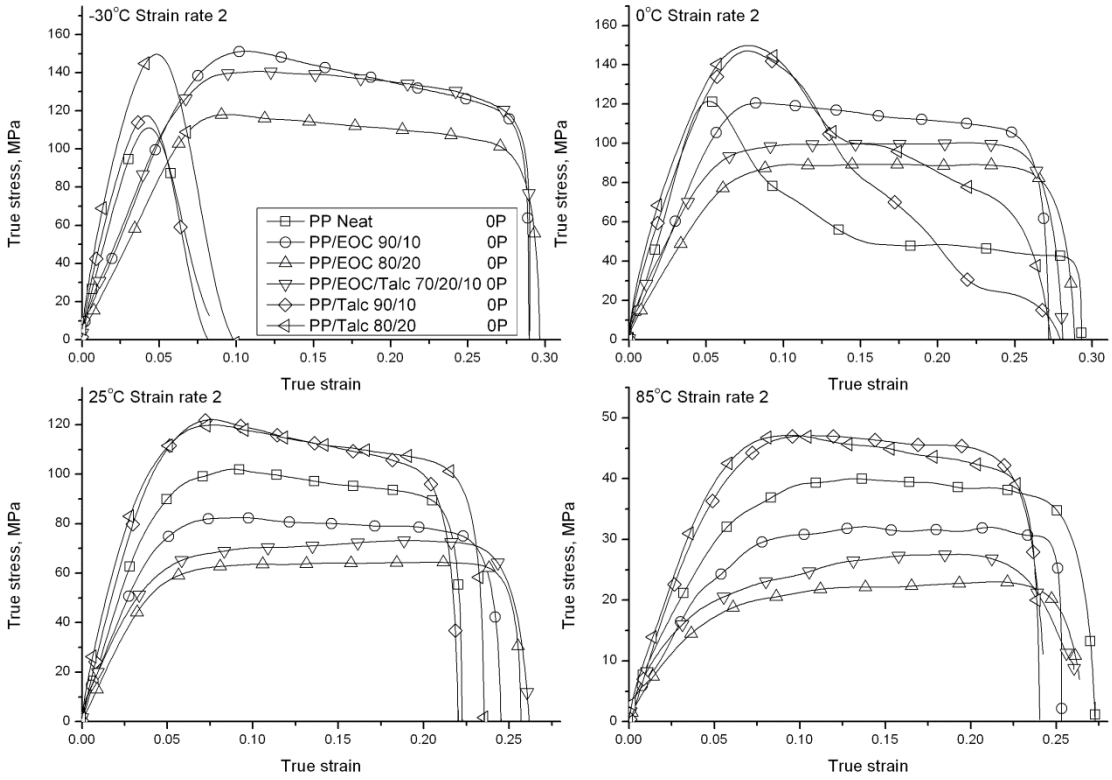

Figure 3-2: True stress - true strain curves in compression of non-recycled neat PP and its composites at different temperatures and under strain rate 2 (strain-rate-2 =1276 s^{-1}).

As pointed out by previous works [31], the mechanical response of neat polymers or composite polymers is sensitive to temperature and strain rate. In particular, the yield stress and the Young's modulus increase with decreasing temperature and increasing strain rates. When the temperature rises, the distance between the structural units increases due to thermal agitation and in consequence, interaction forces decrease which imply a degradation of mechanical properties. The

increase of strain rate leads to the hardening of the material due to less molecular chain mobility at large strain rates. The experimental true-stress versus true-strain curves under uniaxial compression loading of non-recycled neat PP and PP-based composites at -30 °C, 25 °C and 85 °C for strain rate 2 and strain rate 4 are shown in Figure 3-3. The zoom-in view of the initial parts of the true stress - true strain curves are shown on the right side of each figure. In these curves, effects of temperature and strain rate can be clearly observed for non-recycled neat PP or non-recycled PP-based composites. Obviously, the Young's modulus and yield stress increase with the increase of strain rate. As expected, both Young's modulus and yield stress decrease as the temperature increases.

At -30 °C, neat PP 0P and PP/talc 80/20 0P exhibit a brittle behavior for both strain rates while PP/EOC 80/20 0P and PP/EOC/talc 70/20/10 0P show ductility. In addition, PP/EOC 80/20 0P and PP/EOC/talc 70/20/10 0P show strain-softening after the yield point under strain rate 4. In this stage of the stress-strain curve, PP/EOC/talc 70/20/10 0P has a greater amplitude of strain softening than PP/EOC 80/20 0P.

For the testing at 25 °C and under strain rate 4, the mechanical response of neat PP 0P shows a typical feature of stress–strain curves in which the curves can be divided into five parts: linear elasticity, non-linear transition to yield, strain softening, flow at almost constant stress and strain-hardening [32, 33]. For PP/EOC 80/20 0P and PP/EOC/talc 70/20/10 0P under the same test condition, the true stress-strain curves show a limited strain softening but a significant strain-hardening. However, the dynamic behavior of PP/talc 80/20 0P at 25 °C and under strain rate 4 shows a significant strain softening after the yield point and following by a strain hardening.

By comparing the dynamic response of materials under these two strain rates (strain rate 2 and 4 in Figure 3-3), we observe that the true stress-strain curves for

PP/EOC 80/20 0P and PP/EOC/talc 70/20/10 0P at -30 °C under strain rate 2 have a smaller amplitude of strain softening than at strain rate 4 at the same temperature. A similar result is obtained for PP/talc 80/20 0P and neat PP 0P at 25 °C where the true stress-strain curves of strain rate 4 has a more significant strain softening.

When polymers are subjected to high strain rates, the effects of strain hardening, strain rate and temperature sensitivity play important roles in the behavior of materials [34]. The dynamic behavior of materials is based on the competition between strengthening at high strain rates and softening with the temperature increase under adiabatic loading conditions [35]. For PP/EOC 80/20 0P and PP/EOC/talc 70/20/10 0P tested at -30 °C, and for neat PP 0P and PP/talc 80/20 0P tested at 25 °C, the adiabatic condition may induce failure by adiabatic shear banding which overcomes the high strain rate strengthening effect and result in the post-yield softening [36]. The amplitude of this phenomenon increases with the strain rate. For PP/EOC 80/20 0P and PP/EOC/talc 70/20/10 0P tested at 25 °C, the failure is mainly associated to a craze-like damage, identified as a highly shear localized type of dilatational bands. This craze-like mechanisms can occur when shear bandings coalesce with cavitated EOC particles [37, 38]. Lazzeri [38] reported that for blends with good rubber/matrix adhesion, after the cavitation, a rubber layer forms which is strongly attached to the inner surface of the newly formed void. This rubber layer could stabilize dilatational band propagation by delaying strain localization and premature failure of the ligaments [38]. This may probably results in the post-yield hardening of PP/EOC and PP/EOC/talc composites at 25 °C.

For the dynamic responses of materials at high temperature (85 °C) for both strain rates, the post-yield softening and hardening phenomenon are reduced. The true stress-strain curves of neat PP 0P and PP/talc 80/20 0P under strain rate 4 exhibit a

very small strain softening and then a flow at almost constant stress. For PP/EOC 80/20 0P and PP/EOC/talc 70/20/10 0P, the true stress – strain curves show a less important post-yield strain hardening compared to 25 °C. These observations are mainly attributed to the softening of the material at high temperatures. We do not show the dynamic responses of PP/EOC 90/10 0P and PP/talc 90/10 0P here, because they have similar behavior as PP/EOC 80/20 0P and PP/talc 80/20 0P, respectively.

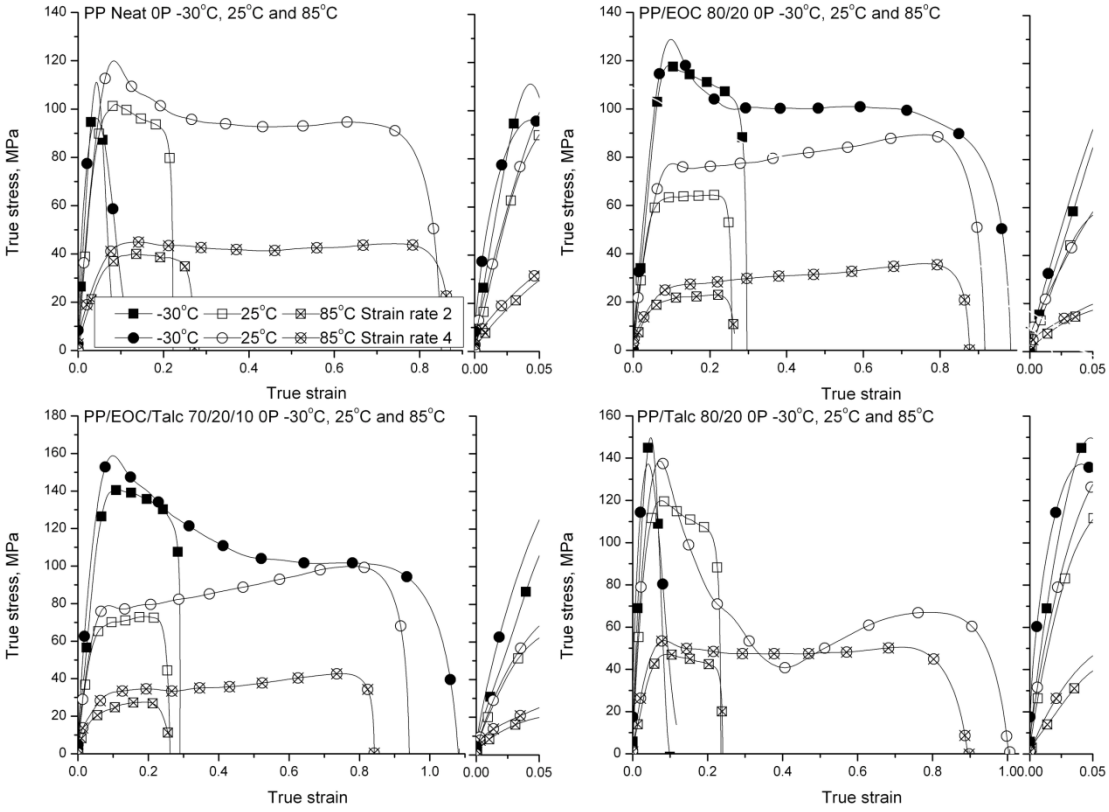

Figure 3-3: Experimental true stress versus true strain curves under uniaxial compression loading of non-recycled neat PP and PP-based composites at different temperatures for two true strain rates with the zoom-in view of the initial part of the curves on the right side.

The effect of recycling on the dynamic responses for non-recycled and recycled neat PP and PP-based composites at 25 °C and under strain rate 2 are presented in Figure 3-4. In this Figure, with the increasing of recycling cycles, the

Young's modulus and the yield stresses of neat PP and PP/EOC 80/20 decrease. This result is attributed to the chain scission mechanisms and the increase of amorphous chain defects that soften the materials as mentioned in section 2.4.7. However, for PP/talc 80/20 these two mechanical properties increase with the reprocessing number. This is due to the more important self-reinforcement mechanisms by the reduction of talc particle dimensions than the chain scission mechanisms (see section 2.3.6). Attention is focused on the dynamical responses of PP/EOC/talc 70/20/10 with the recycling number, the Young's modulus and the yield stresses of non-recycled and recycled PP/EOC/talc 70/20/10 are almost constant with the recycling cycles. This is probably due to the presence of EOC that increased the fluidity of the material (see Section 2.4.2). This higher fluidity of material resulted in a lower shear stress in the extruder (see section 2.3.6) which broke less talc particles to stiffen the material. Consequently, equilibrium is found between the degradation of materials due to the chain scission mechanisms and the self-reinforcement mechanisms. The materials' behaviors under other testing conditions are not shown here because they have similar responses. In addition, the dynamic responses for non-recycled and recycled PP/EOC 90/10 and PP/talc 90/10 are similar to those of non-recycled and recycled PP/EOC 80/20 and PP/talc 80/20, respectively.

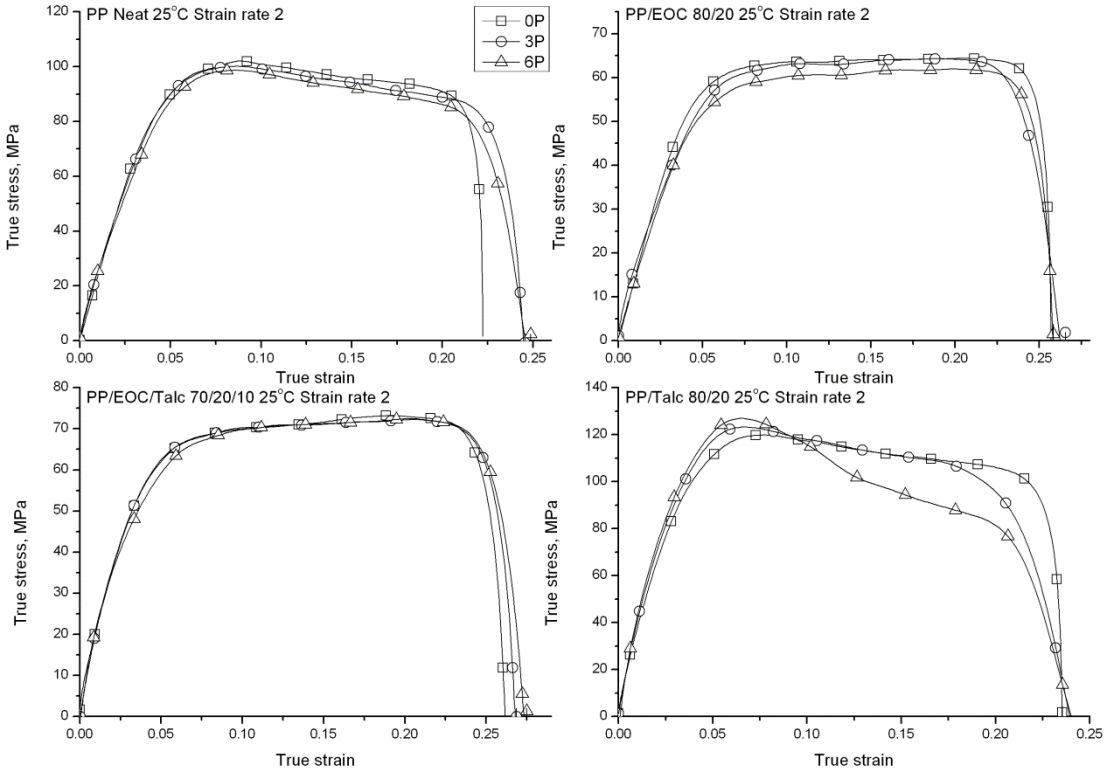

Figure 3-4: Experimental true stress versus true strain curves under uniaxial compression loading of non-recycled and recycled neat PP and PP-based composites at 25 °C for four true strain rates.

The maximum stresses on the true stress – true strain curves were chosen as the yield stress for the materials with a significant post-yield softening. In the case of the materials with a significant post-yield hardening, the point of the intersection of two slopes (elastic and post yield part) was selected as the yielding point. Table 3-1 and Table 3-2 list the yield stress and the Young's modulus of considered materials obtained for different temperatures, different strain rates, various filler concentrations and for different recycling number.

Table 3-1: Strain-rate, filler content, temperature and recycling effects on the yield stress of materials.

Materials	**Temperature (°C)**	**Recycling Number**	**Yield stress (MPa)**			
			Strain rate (s^{-1})			
			1	2	3	4
PP Neat	-30°C	0P	-	-	-	-
		3P	-	-	-	-
		6P	-	-	-	-
	0°C	0P	-	-	-	-
		3P	-	-	-	-
		6P	-	-	-	-
	25 °C	0P	92.3±1.3	102.5±1.5	111.3±2.5	120.5±1.4
		3P	91.3±0.7	99.8±1.4	109.0±2.9	116.0±3.0
		6P	90.3±0.6	98.7±0.8	106.0±2.0	114.0±1.1
	50°C	0P	58.3±1.2	66.7±0.7	73.3±2.6	77.0±1.0
		3P	57.0±1.3	64.5±1.9	69.1±1.3	72.4±1.8
		6P	54.2±2.3	60.0±2.0	68.2±0.7	70.1±1.6
	85°C	0P	35.4±1.7	40.1±0.9	43.0±1.0	44.5±1.3
		3P	34.8±0.7	39.3±0.9	40.6±0.8	43.7±1.9
		6P	33.0±0.4	37.2±1.0	39.5±1.3	42.5±0.5
PP/EOC 90/10	-30°C	0P	143.2±1.4	151.4±2.0	155.8±1.0	163.0±3.6
		3P	139.1±2.0	148.1±1.0	152.1±1.6	158.2±3.6
		6P	136.2±1.5	143.0±2.0	148.0±1.0	151.9±2.4
	0°C	0P	114.0±1.4	120.1±1.1	125.0±2.0	131.0±3.0
		3P	111.0±1.7	117.0±1.0	120.0±0.9	127.1±1.4
		6P	106.1±0.9	112.0±2.1	115.3±1.4	123.0±2.7
	25 °C	0P	77.5±2.5	83.2±1.0	91.3±1.1	96.1±5.4

		3P	76.0±0.9	80.7±1.4	86.6±2.3	94.7±0.6
		6P	74.2±0.5	79.1±1.7	82.6±1.1	89.7±0.7
	50°C	0P	46.9±0.4	52.0±1.1	56.3±0.3	60.3±0.4
		3P	45.0±0.7	50.6±1.1	53.1±2.3	58.3±0.3
		6P	42.0±1.5	49.0±1.2	51.5±0.4	56.8±2.5
	85°C	0P	25.9±0.8	30.8±0.4	35.3±0.1	38.3±1.5
		3P	24.0±0.5	30.4±1.1	34.3±1.1	37.2±2.2
		6P	23.7±0.6	30.0±1.0	33.0±0.3	35.8±0.9
PP/EOC	-30°C	0P	108.1±0.9	118.2±1.5	123.0±0.4	128.0±1.5
80/20		3P	105.1±0.7	113.0±1.0	118.0±1.6	124.0±2.0
		6P	100.0±0.8	109.0±2.5	112.5±1.5	121.0±1.4
	0°C	0P	80.3±1.1	88.2±0.8	94.5±0.5	99.5±2.0
		3P	75.3±0.2	83.8±0.7	89.7±0.7	98.1±1.7
		6P	72.2±1.1	82.8±0.9	85.7±0.8	93.4±1.1
	25 °C	0P	54.1±0.7	61.8±1.4	67.1±0.6	77.3±2.0
		3P	50.1±1.1	61.1±0.8	64.7±1.4	74.4±0.6
		6P	49.5±0.5	57.8±0.7	63.1±0.7	67.5±3.3
	50°C	0P	32.6±1.1	39.2±1.2	45.4±0.7	47.5±0.9
		3P	30.8±0.9	38.2±1.7	43.4±0.5	44.8±0.6
		6P	29.1±0.4	36.4±0.6	41.5±0.4	43.1±0.4
	85°C	0P	19±0.3	21.4±0.4	23.0±1.1	26.9±1.9
		3P	18.0±0.2	20.5±0.7	22.1±1.2	25.7±0.2
		6P	17.4±0.6	19.6±0.6	21.1±0.6	24.8±1.1
PP/EOC/Talc	-30°C	0P	127.0±0.6	140.4±0.9	152.1±2.7	156.5±2.2
70/20/10		3P	126.1±1.6	140.3±1.0	150.0±2.8	151.1±0.4
		6P	127.6±1.2	141.5±1.1	146.0±0.4	151.1±0.7
	0°C	0P	92.3±1.7	98.0±0.8	106.1±1.2	113.1±0.7
		3P	91.4±1.3	97.7±1.5	107.0±0.3	113.2±0.1

		6P	91.1±1.9	97.7±0.8	106.0±1.4	113.1±1.9
	25 °C	0P	66.2±0.3	70.0±0.8	76.4±1.1	79.7±0.6
		3P	64.0±1.0	68.0±1.1	76.8±1.0	78.7±0.8
		6P	64.0±1.0	67.8±1.1	79.0±1.2	81.7±2.0
	50°C	0P	40.2±0.5	44.0±1.4	47.6±1.1	53.1±0.4
		3P	38.6±0.7	43.9±1.1	46.4±2.2	53.8±0.3
		6P	39.0±1.5	44.5±0.4	47.5±0.5	54.8±1.1
	85°C	0P	22.1±0.4	24.8±1.1	29.3±1.5	33.6±0.8
		3P	20.8±1.1	25.5±0.7	28.5±1.4	31.5±0.8
		6P	21.6±0.5	24.8±0.7	30.0±0.5	32.6±1.7
PP/Talc	-30°C	0P	-	-	-	-
90/10		3P	-	-	-	-
		6P	-	-	-	-
	0°C	0P	-	-	-	-
		3P	-	-	-	-
		6P	-	-	-	-
	25 °C	0P	115.1±1.1	122.0±1.3	134.4±0.9	140.1±3.0
		3P	116.0±0.9	123.1±1.8	137.0±0.6	144.1±1.7
		6P	119.0±2.1	128.9±1.2	141.9±0.5	148.0±1.0
	50°C	0P	75.3±0.6	85.9±1.6	91.5±0.9	99.2±1.1
		3P	77.9±0.7	89.8±0.8	94.9±1.1	103.0±0.6
		6P	80.7±0.7	91.5±2.1	96.7±0.7	107.9±3.7
	85°C	0P	43.3±0.7	46.9±0.7	51.1±1.1	55.1±0.4
		3P	44.4±0.3	48.8±0.7	53.2±1.2	59.0±0.4
		6P	45.4±0.4	50.8±1.1	56.2±1.5	62.9±1.0
PP/Talc	-30°C	0P	-	-	-	-
80/20		3P	-	-	-	-
		6P	-	-	-	-

	0°C	0P	-	-	-	-
		3P	-	-	-	-
		6P	-	-	-	-
	25 °C	0P	112.0±1.4	120.0±0.8	131.0±1.7	138.7±0.5
		3P	113.0±1.0	123.0±0.7	134.9±2.7	143.1±1.2
		6P	114.5±0.7	127.1±1.3	140.0±2.0	148.2±0.6
	50°C	0P	72.4±1.3	81.3±0.6	90.0±0.8	95.0±1.0
		3P	74.0±0.8	84.0±1.0	92.9±1.7	101.0±0.7
		6P	74.9±1.1	85.8±0.3	95.0±0.1	105.0±1.4
	85°C	0P	42.6±0.4	47.1±1.0	49.3±1.2	53.4±0.6
		3P	43.5±0.4	48.6±0.4	51.8±1.6	57.6±1.1
		6P	44.5±0.8	50.7±1.4	55.3±0.1	62.6±1.0

Table 3-2: Strain-rate, filler content, temperature and recycling effects on the Young's modulus of materials.

Materials	**Temperature (°C)**	**Recycling Number**	**Young's modulus (MPa)**			
			Strain rate (s^{-1})			
			1	2	3	4
PP Neat	-30°C	0P	3493±303	3536±366	3650±560	3940±560
		3P	3348±351	3463±229	3596±499	3856±333
		6P	3229±151	3265±390	3459±472	3589±256
	0°C	0P	2964±289	3067±225	3171±53	3279±216
		3P	2876±170	2948±244	3039±253	3183±206
		6P	2800±318	2838±272	2841±406	3097±259
	25 °C	0P	2227±127	2362±43	2448±107	2714±231
		3P	2142±163	2237±161	2422±210	2674±425
		6P	2071±279	2246±114	2331±110	2499±123

	50°C	0P	1381±85	1607±120	1667±97	2032±188
		3P	1281±34	1449±186	1541±98	1993±126
		6P	1241±124	1393±159	1609±230	1903±356
	85°C	0P	649±42	796±36	958±70	1028±99
		3P	598±78	716±81	908±22	990±34
		6P	612±45	715±12	890±78	926±199
PP/EOC	-30°C	0P	3009±132	3093±174	3169±336	3213±541
90/10		3P	2957±135	2968±251	3105±100	3193±452
		6P	2748±147	2904±174	3081±193	3135±413
	0°C	0P	2375±169	2436±261	2519±224	2699±120
		3P	2267±203	2362±203	2495±132	2545±64
		6P	2144±411	2271±212	2334±322	2474±324
	25 °C	0P	1800±142	1933±113	1954±129	2162±259
		3P	1674±196	1775±231	1872±123	2005±147
		6P	1716±97	1867±244	1873±197	1984±192
	50°C	0P	983±56	1372±127	1430±262	1519±135
		3P	1054±78	1283±42	1386±91	1501±101
		6P	949±70	1150±159	1314±190	1356±322
	85°C	0P	521±40	619±78	806±97	849±81
		3P	528±56	566±39	785±9	832±112
		6P	469±72	506±97	698±129	780±158
PP/EOC	-30°C	0P	2455±159	2485±302	2598±340	2782±405
80/20		3P	2184±132	2217±169	2344±165	2549±328
		6P	2080±384	2255±270	2327±154	2649±337
	0°C	0P	2058±101	2150±225	2378±158	2397±178
		3P	1946±156	2063±52	2184±77	2282±187
		6P	1878±285	1941±222	2027±505	2183±124
	25 °C	0P	1483±71	1752±162	1814±136	1902±188

		3P	1491±63	1704±279	1745±56	1913±155
		6P	1371±272	1640±269	1791±305	1841±194
	50°C	0P	891±67	1134±177	1243±129	1311±70
		3P	857±64	1047±197	1225±193	1291±137
		6P	769±72	867±235	1109±130	1243±125
	85°C	0P	411±66	603±89	653±105	762±98
		3P	392±60	590±81	621±91	743±108
		6P	380±32	485±150	546±117	683±87
PP/EOC/Talc	-30°C	0P	3003±441	3071±206	3295±278	3396±40
70/20/10		3P	3102±119	5153±166	3331±342	3422±276
		6P	3032±188	3110±274	3248±248	3349±129
	0°C	0P	2245±222	2500±290	2690±420	2873±560
		3P	2257±170	2552±262	2677±516	2880±117
		6P	2273±309	2455±328	2737±181	2904±291
	25 °C	0P	1759±178	1980±101	2133±102	2349±263
		3P	1748±225	2012±372	2107±112	2448±135
		6P	1711±152	2008±168	2151±218	2424±235
	50°C	0P	1051±71	1401±124	1517±202	1619±110
		3P	1024±116	1334±264	1559±279	1662±308
		6P	1075±119	1313±188	1528±114	1636±254
	85°C	0P	558±76	735±221	737±76	842±198
		3P	583±152	712±83	738±68	848±63
		6P	592±51	741±83	748±171	860±126
PP/Talc	-30°C	0P	4135±345	4402±364	4530±316	4640±246
90/10		3P	4197±105	4523±179	4605±270	4812±258
		6P	4254±294	4548±257	4657±260	4838±378
	0°C	0P	3110±181	3337±404	3509±281	3698±439
		3P	3189±167	3529±252	3722±128	3929±431

		6P	3268±323	3589±241	3770±466	3972±340
	25 °C	0P	2363±95	2814±195	2861±341	3148±178
		3P	2508±331	2838±270	2884±290	3176±247
		6P	2608±138	3026±314	3031±295	3288±277
	50°C	0P	1604±138	1706±155	1755±85	2087±74
		3P	1718±130	1756±346	1859±277	2113±193
		6P	1746±265	1824±99	1898±169	2255±78
	85°C	0P	764±61	916±27	1085±81	1289±96
		3P	785±123	988±196	1107±214	1325±117
		6P	829±123	1003±46	1155±208	1396±155
PP/Talc	-30°C	0P	4623±599	5099±405	5192±425	5261±237
80/20		3P	4680±558	5173±249	5312±171	5388±207
		6P	4847±297	5236±387	5356±114	5438±320
	0°C	0P	3574±212	4091±296	4339±370	4439±125
		3P	3659±197	4198±242	4395±587	4558±124
		6P	3771±265	4310±496	4674±351	4940±490
	25 °C	0P	2572±134	2973±145	3202±363	3539±226
		3P	2723±81	3115±226	3308±362	3471±376
		6P	2821±145	3169±287	3420±171	3667±128
	50°C	0P	1743±105	1978±157	2186±83	2470±140
		3P	1772±209	2057±144	2211±103	2570±185
		6P	1937±165	2116±223	2279±209	2698±13
	85°C	0P	950±44	1163±57	1457±132	1490±22
		3P	993±14	1205±119	1519±62	1535±142
		6P	1087±69	1296±57	1613±182	1634±167

In order to show the strain rate dependence of yield stress and Young's modulus, the Young's modulus and yield stress versus strain rates curves of non-recycled neat PP and non-recycled PP-based composite are plotted for the five temperatures (Figure 3-5 and Figure 3-6). Note that the recycled materials have similar strain rate dependencies of yield stress and Young's modulus compared to non-recycled materials. In Figure 3-5, the variations of Young's modulus are not perfectly linear with the strain rate. This effect is more significant with increasing temperature. In Figure 3-6, plots of yield stress/T against log(strain rate) gives for all the materials a series of parallel straight lines showing that the yield can be considered as an activated rate process [39-41]. For all the materials these lines decrease with decreasing strain rate tests and with increasing temperature as a consequence of two rate processes being involved in the yield behavior.

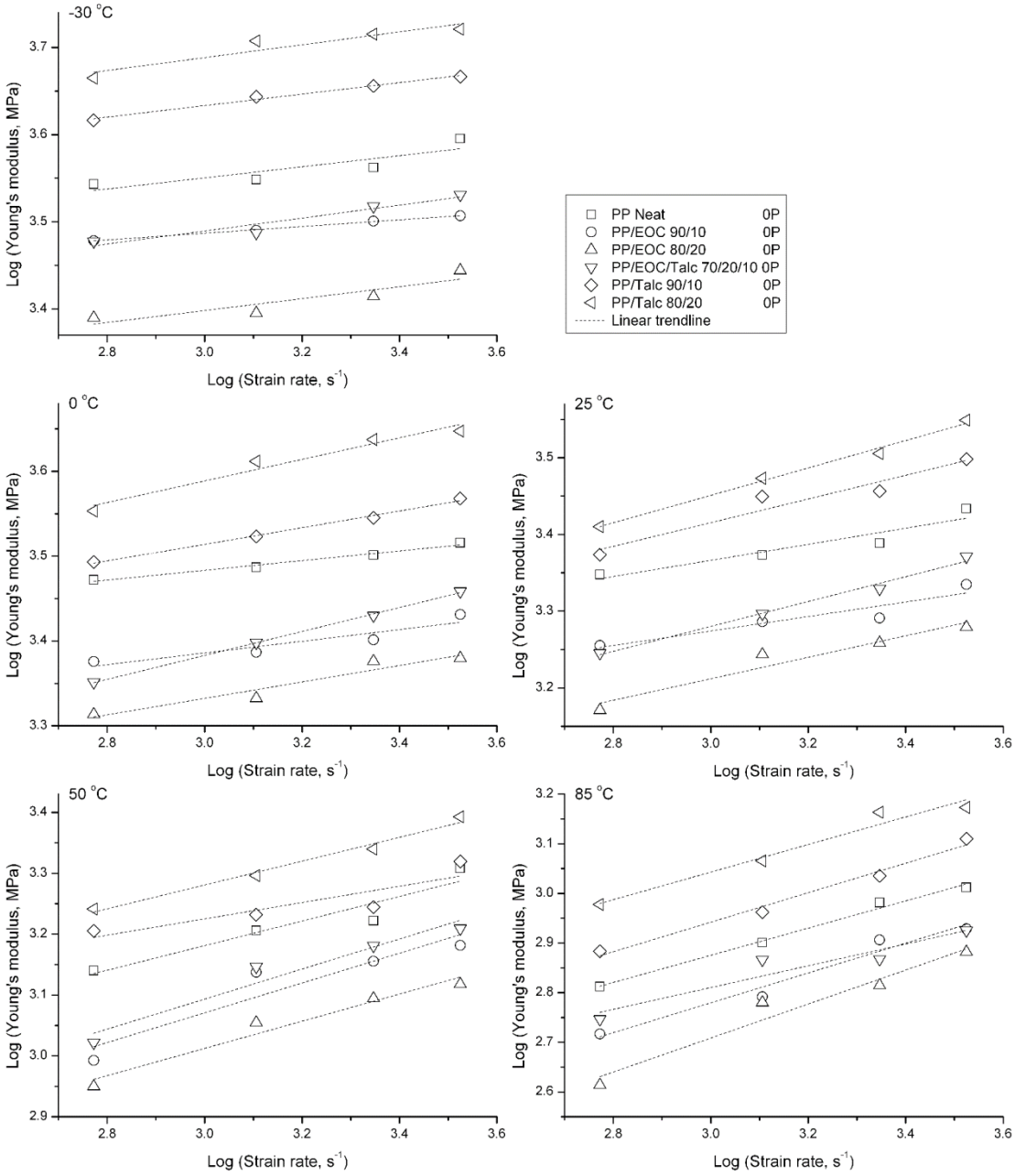

Figure 3-5: The dependence of Young's modulus in dynamic compression on strain rate at five temperatures.

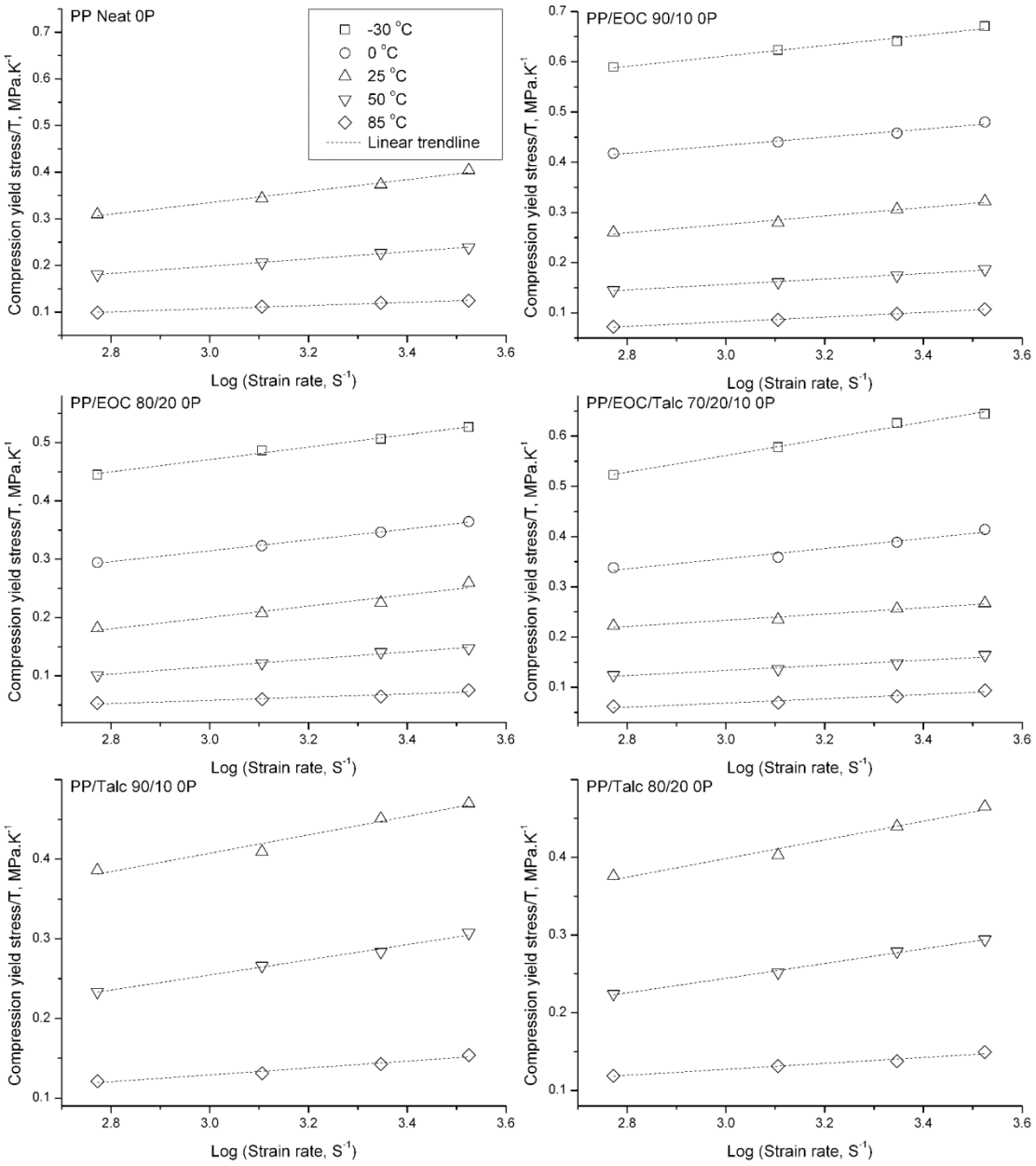

Figure 3-6: The dependence of yield stress in dynamic compression on strain rate at five temperatures.

The morphological investigation by optical microscopy (OM) for the non-recycled and recycled materials before and after the dynamic compressive tests is shown in Figures 3-7 to Figure 3-10. In these four figures, we do not show the results for PP blended with 10 wt. % fillers because we believe that the results will be the same than for PP blended with 20 wt. % of fillers. In addition, we only present here

the images of the extreme cases, i.e. the non-recycled case (0P) and the case corresponding to 6 recycling procedures (6P). We believe that the possible change of materials' morphology with the recycling numbers 3 (3P) has the same tendencies. Furthermore, we only show the OM images for tested materials under strain rate 4.

OM images obtained under different magnifications for non-tested materials are shown in Figure 3-7. For all considered materials, there is no significant difference between the non-recycled (0P) and recycled (6P) materials in our investigated magnifications.

PP Neat 0P

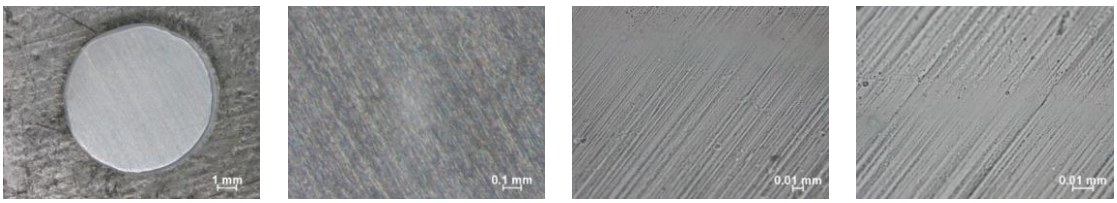

PP Neat 6P

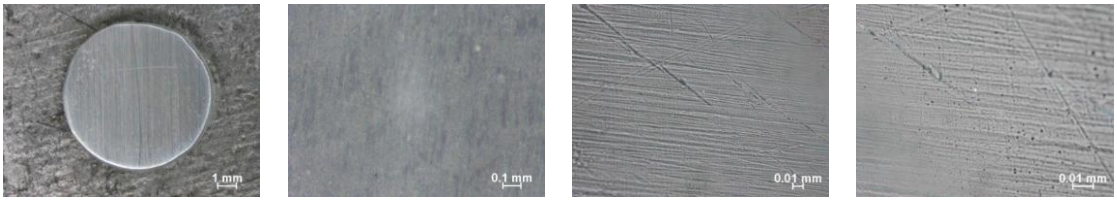

PP/EOC 80/20 0P

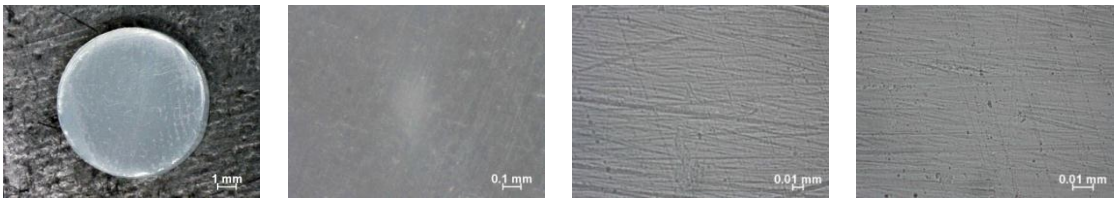

PP/EOC 80/20 6P

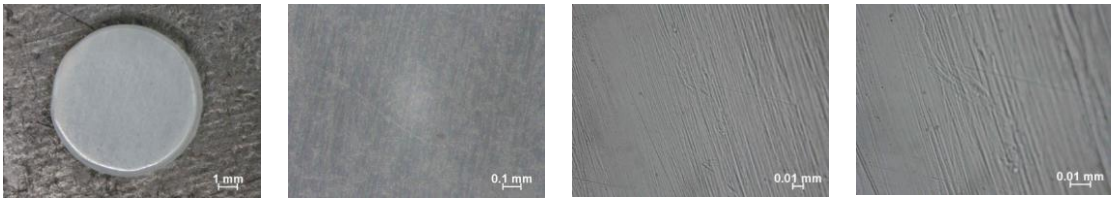

PP/EOC/Talc 70/20/10 0P

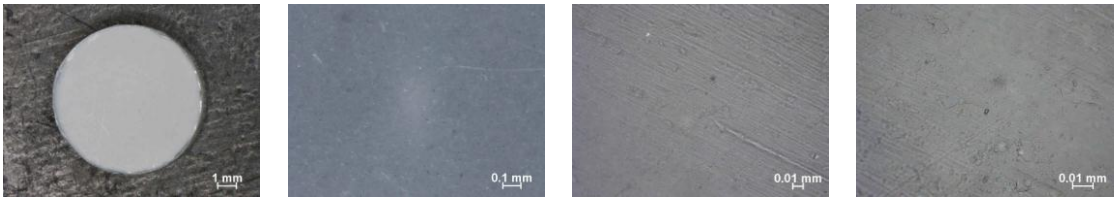

PP/EOC/Talc 70/20/10 6P

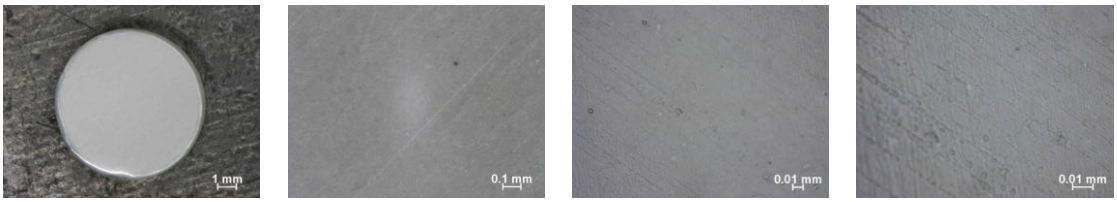

PP/Talc 80/20 0P

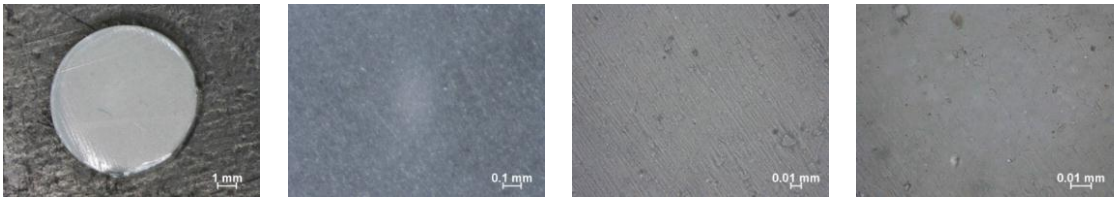

PP/Talc 80/20 6P

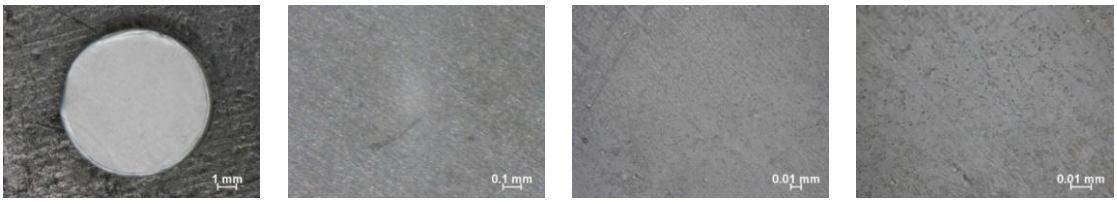

Figure 3-7: OM images of non-recycled and recycled neat PP and PP-based composites before the dynamic compressive test (initial dimensions: diameter = 8 mm, thickness = 3 mm).

Figure 3-8 shows the morphology of materials after the dynamic mechanical test at -30 °C and under strain rate 4. We note that all the materials were overflowing the edge of the anvils of Hopkinson bars during the test. In this, neat PP (0P and 6P) and PP/talc 80/20 (0P and 6P) failed in an almost explosive manner by shear banding and cracking mechanisms [22, 42]. For PP/EOC 80/20 (0P and 6P), the detachment of fragments at the periphery by cracking is shown at low magnification. This can use to

explain the strain softening of PP/EOC 80/20 0P at -30 °C in Figure 3-3. For PP/EOC/talc 70/20/10 (0P and 6P), besides the peripheral fragments, the OM images also show the internal fragmentation of materials. This may be the reason why PP/EOC/talc 70/20/10 0P show greater amplitude of strain softening compared to PP/EOC 80/20 0P at -30 °C in Figure 3-3.

PP Neat 0P

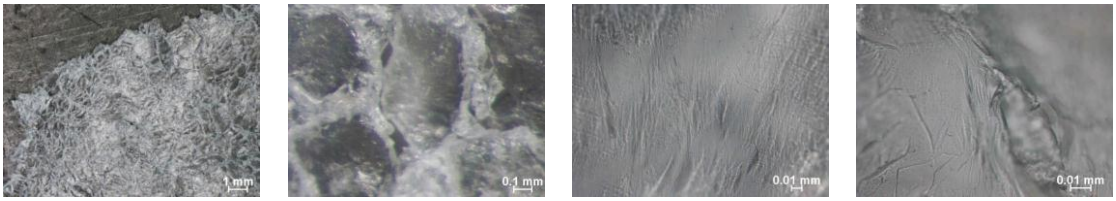

PP Neat 6P

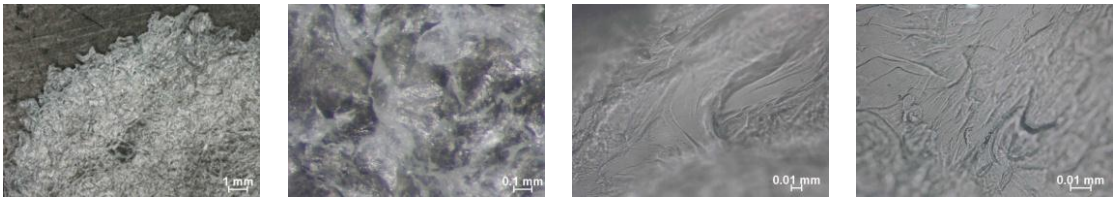

PP/EOC 80/20 0P

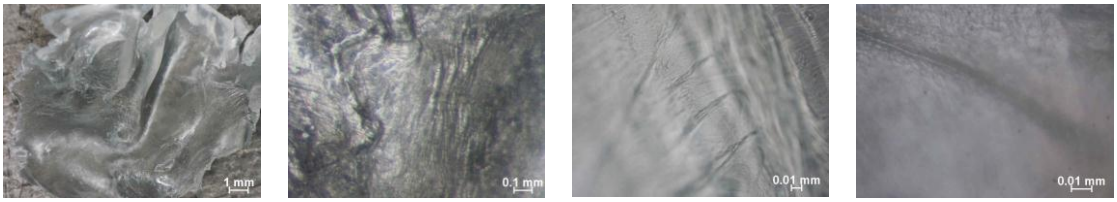

PP/EOC 80/20 6P

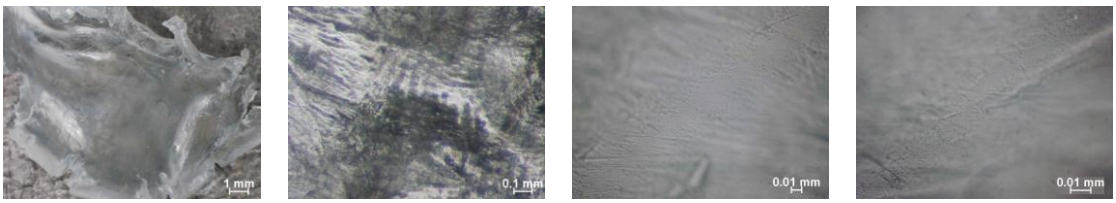

PP/EOC/Talc 70/20/10 0P

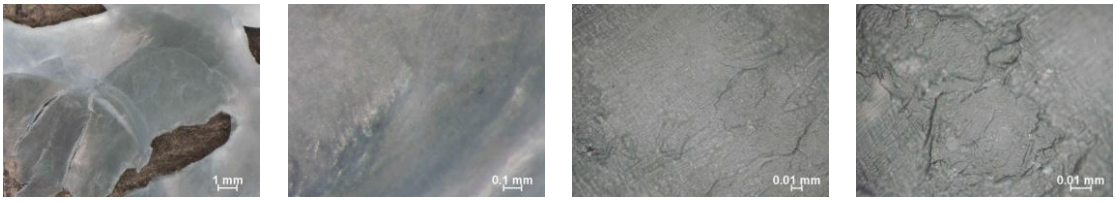

PP/EOC/Talc 70/20/10 6P

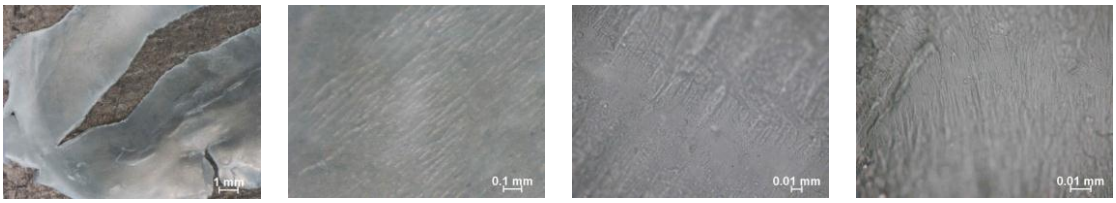

PP/Talc 80/20 0P

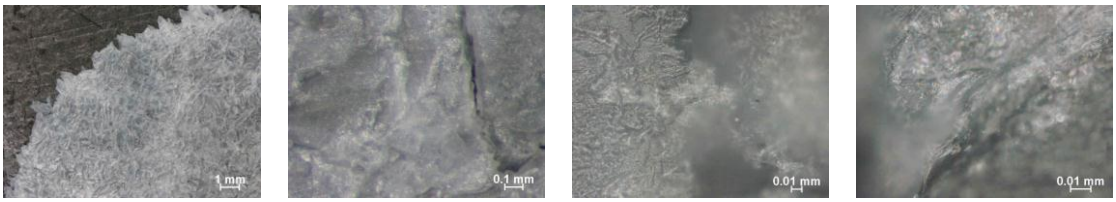

PP/Talc 80/20 6P

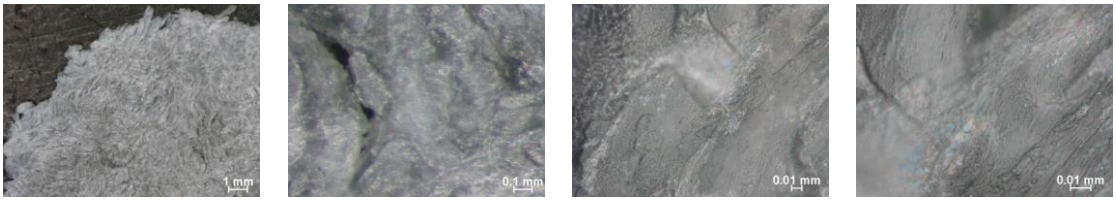

Figure 3-8: OM images of non-recycled and recycled neat PP and PP-based composites after the dynamic compressive test at -30 °C and under strain rate 4.

OM images of non-recycled and recycled neat PP and PP-based composites after the dynamic compressive test at 25 °C and under strain rate 4 are presented in Figure 3-9. In this figure, neat PP (0P and 6P) only shows peripheral fragments while PP/talc 80/20 (0P and 6P) shows both peripheral and internal fragmentations of materials by cracks. These fragmentations of PP/talc 80/20 result in an important strain softening of the materials in Figure 3-3. For PP/EOC 80/20 (0P and 6P) and PP/EOC/talc 70/20/10 (0P and 6P), although the materials overflowed the edge of the

bars anvils, they do not show a peripheral crack leading to partial separation of a piece of the materials. However, OM images at higher magnification for PP/EOC 80/20 (0P and 6P) and PP/EOC/talc 70/20/10 (0P and 6P) exhibit shearing bands. This finding can explain the limited post-yield strain-softening effect of PP/EOC 80/20 0P and PP/EOC/talc 70/20/10 0P at 25 °C (see Figure 3-3).

PP Neat 0P

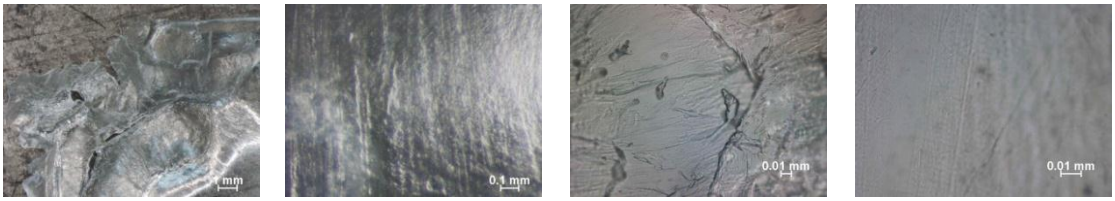

PP Neat 6P

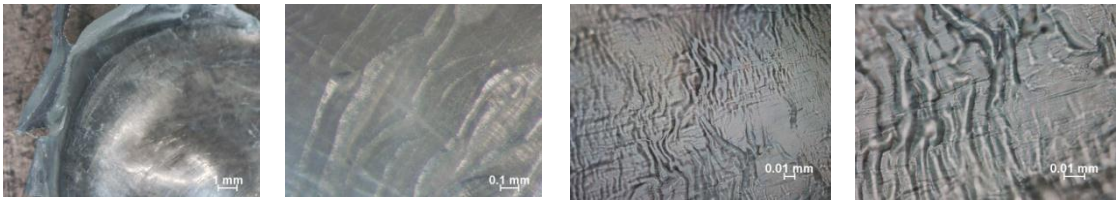

PP/EOC 80/20 0P

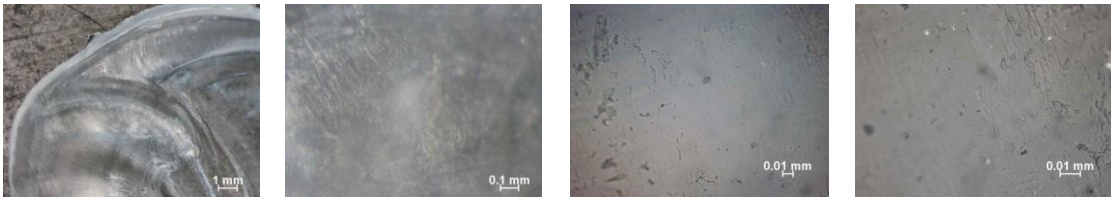

PP/EOC 80/20 6P

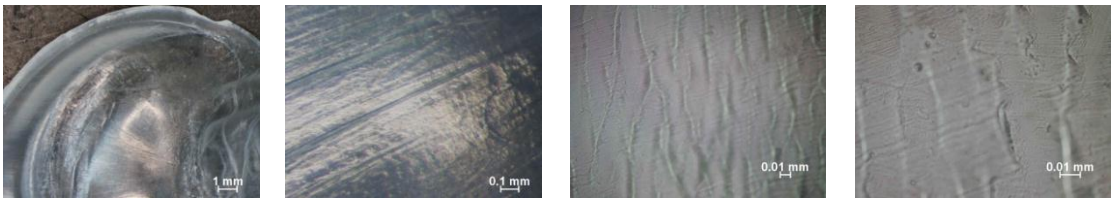

PP/EOC/Talc 70/20/10 0P

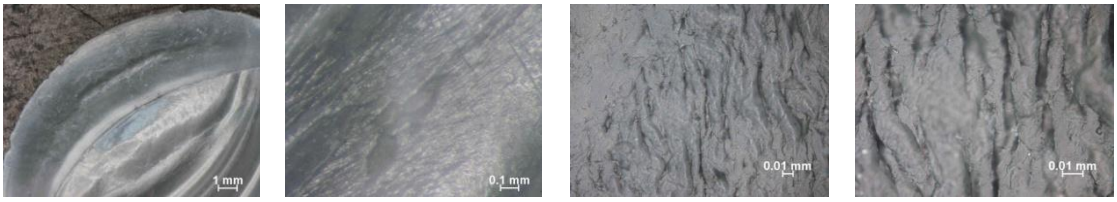

PP/EOC/Talc 70/20/10 6P

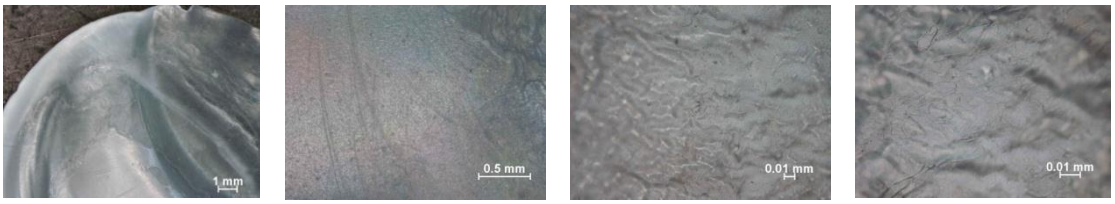

PP/Talc 80/20 0P

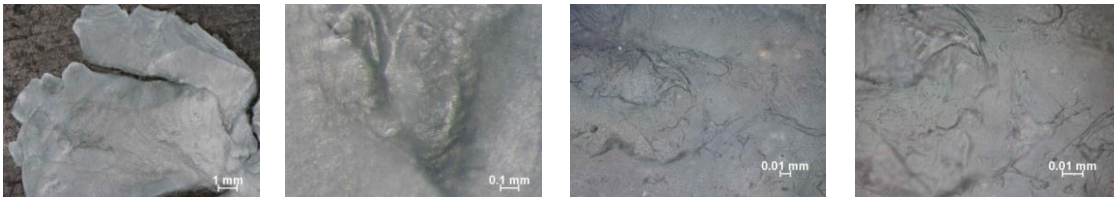

PP/Talc 80/20 6P

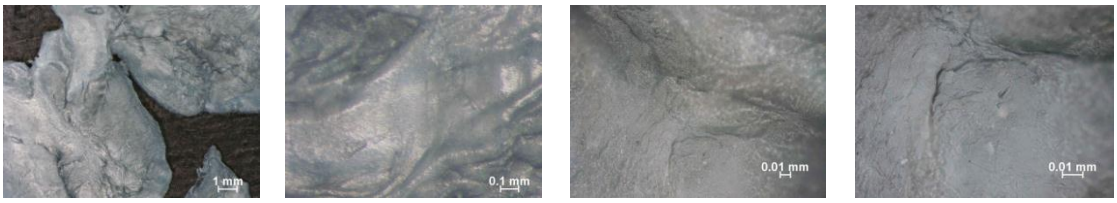

Figure 3-9: OM images of non-recycled and recycled neat PP and PP-based composites after the dynamic compressive test at 25 °C and under strain rate 4.

For the dynamic mechanical testing at 85 °C and under strain rate 4, the materials deformed more homogeneously out to large compressive strains than them of -30 °C and 25 °C (Figure 3-10). No significant cracks were observed for all the considered materials in our investigated magnifications. However, the shear bandings still exist for all the materials. Note that the differences of morphology between the non-recycled (0P) and recycled (6P) materials after dynamic mechanical testing are

not significant for all test temperatures in our investigated magnifications (see Figure 3-8 to Figure 3-10)

PP Neat 0P

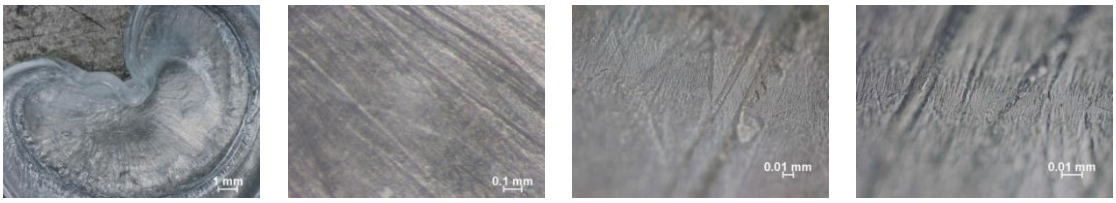

PP Neat 6P

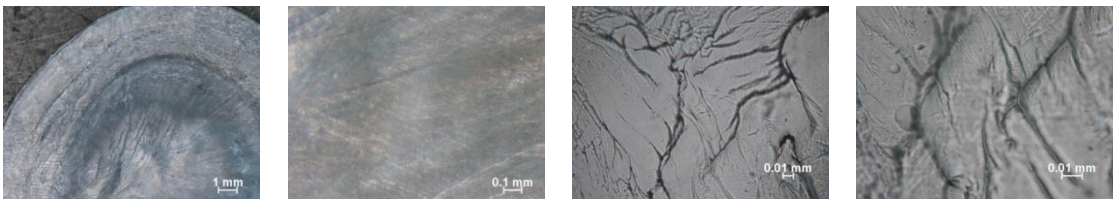

PP/EOC 80/20 0P

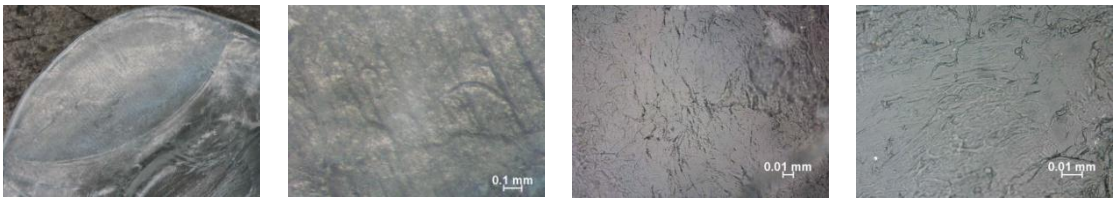

PP/EOC 80/20 6P

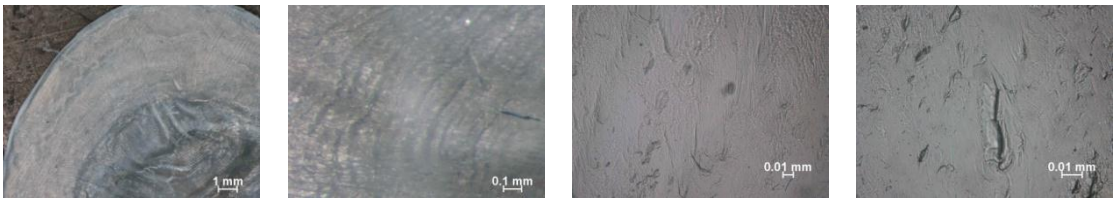

PP/EOC/Talc 70/20/10 0P

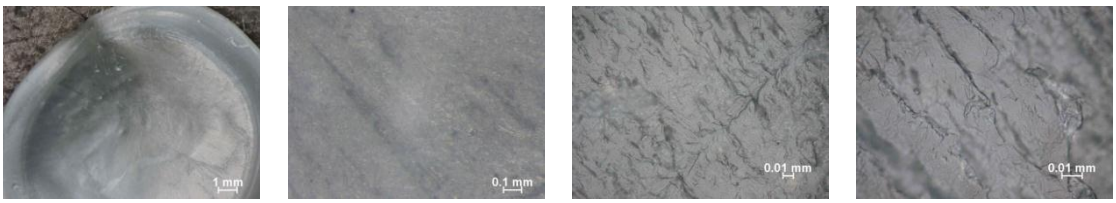

PP/EOC/Talc 70/20/10 6P

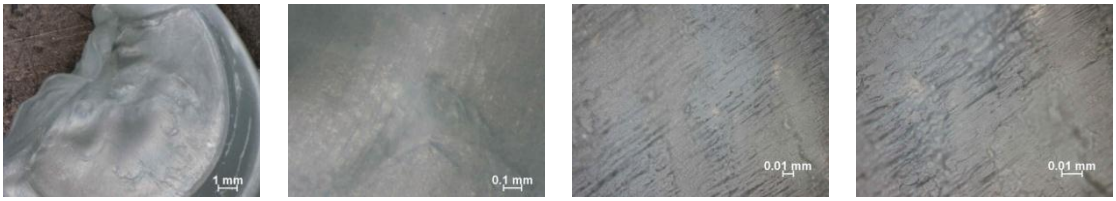

PP/Talc 80/20 0P

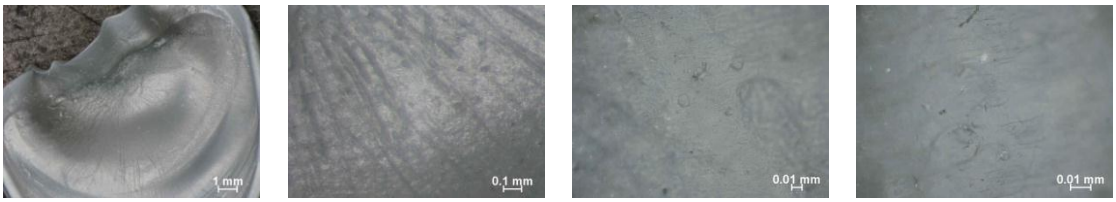

PP/Talc 80/20 6P

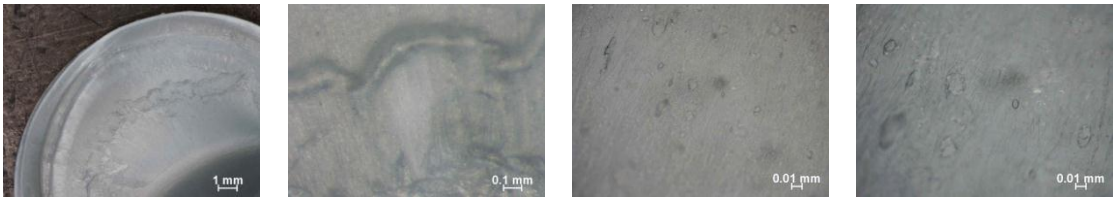

Figure 3-10: OM images of non-recycled and recycled neat PP and PP-based composites after the dynamic compressive test at 85 °C and under strain rate 4.

Table 3-3: Mechanical response and the morphology of materials under strain rate 4 ($\dot{\varepsilon}_4 = 3346$)

Materials	Mechanical response			Morphology		
	-30 °C	25 °C	85 °C	-30 °C	25 °C	85 °C
Neat PP	Brittle	Post-yield strain-softening	Post-yield constant flow	Explosive failure	Peripheral fragment	No significant crack
PP/EOC 80/20	Ductility Post-yield strain-softening	Post-yield strain-hardening	Post-yield strain-hardening	Detachment of fragment	No peripheral crack	No significant crack
PP/EOC/Talc 70/20/10	Ductility Post-yield strain-softening	Post-yield strain-hardening	Post-yield strain-hardening	Detachment of fragment and internal fragmentation	No peripheral crack	No significant crack
PP/Talc 80/20	Brittle	Post-yield strain-softening	Post-yield constant flow	Explosive failure	Peripheral and internal fragment	No significant crack

3.4. Conclusions

Dynamic compressive behaviors of non-recycled and recycled neat PP and PP-based composites are investigated by using split Hopkinson pressure bars in a wide range of temperatures and strain rates. The results showed that the considered materials are strain-rate and temperature sensitive. The addition of EOC decreased the yield strength and Young's modulus of PP whereas the presence of talc fillers increased the Young's modulus of PP. However, the yield strength for PP/talc 80/20 was lower than that of PP/talc 90/10 due to the more important damage by matrix/filler debonding in PP/talc 80/20 during the test. With the increasing of recycling number, the dynamic behaviors of neat PP and PP/EOC composite decreased due to the chain scission mechanism. The dynamic responses of PP/talc increased with increasing of reprocessing cycle due to a more important self-reinforcement mechanism by talc particle reduction. For PP/EOC/talc composites, the dynamic responses were less modified with the reprocessing cycles. This is explained by chain scission mechanism and self-reinforcement mechanism involved for PP/EOC/talc composites. Equilibrium was found between these two mechanisms.

The dynamic behaviors of the materials are correlated with their morphology by using optical microscopy (OM) (Table 3-3). At low temperature (-30 °C), neat PP and PP/talc composites shown explosive failure where other materials shown partial failure by peripheral or internal fragmentations. These failures were caused by crack and shear banding mechanisms. At room temperature (25 °C), these failures were less marked where neat PP and PP/talc shown partial fragmentations. At high temperature (85 °C), the materials deformed more homogeneously without significant cracks. The observed failures of materials by OM are in good accordance with the dynamic responses of our considered materials.

References

[1] Navarro R, Torre L, Kenny JM, Jiménez A. Thermal degradation of recycled polypropylene toughened with elastomers. Polymer Degradation and Stability. 2003;82:279-290.

[2] Hinsken H, Moss S, Pauquet JR, Zweifel H. Degradation of polyolefins during melt processing. Polymer Degradation and Stability. 1991;34:279-293.

[3] Aurrekoetxea J, Sarrionandia MA, Urrutibeascoa I, Maspoch ML. Effects of recycling on the microstructure and the mechanical properties of isotactic polypropylene. Journal of Materials Science. 2001;36:2607-2613.

[4] Valenza A, La Mantia FP. Recycling of polymer waste: Part II - Stress degraded polypropylene. Polymer Degradation and Stability. 1988;20:63-73.

[5] Hamskog M, Klügel M, Forsström D, Terselius B, Gijsman P. The effect of base stabilization on the recyclability of polypropylene as studied by multi-cell imaging chemiluminescence and microcalorimetry. Polymer Degradation and Stability. 2004;86:557-566.

[6] González-González VA, Neira-Velázquez G, Angulo-Sánchez JL. Polypropylene chain scissions and molecular weight changes in multiple extrusion. Polymer Degradation and Stability. 1998;60:33-42.

[7] Guerrica-Echevarría G, Eguiazábal JI, Nazábal J. Effects of reprocessing conditions on the properties of unfilled and talc-filled polypropylene. Polymer Degradation and Stability. 1996;53:1-8.

[8] Guerrica-Echevarría G, Eguiazábal JI, Nazábal J. Influence of molding conditions and talc content on the properties of polypropylene composites. European Polymer Journal. 1998;34:1213-1219.

[9] Wang K, Addiego F, Bahlouli N, Ahzi S, Rémond Y, Toniazzo V, Muller R. Analysis of thermomechanical reprocessing effects on polypropylene/ethylene octene copolymer blends. Polymer Degradation and Stability. 2012;97:1475–1484.

[10] Malinowski JZ, Klepaczko JR. A unified analytic and numerical approach to specimen behaviour in the Split-Hopkinson pressure bar. International Journal of Mechanical Sciences. 1986;28:381-391.

[11] Gray GT. Classic split-Hopkinson pressure bar testing: ASM International; 2000.

[12] Instruction manual of David, SHPB tests analysis software, https://www.sites.google.com/site/hopkinsonbars/home/david.

[13] Zhao H, Gary G. On the use of SHPB techniques to determine the dynamic behavior of materials in the range of small strains. International Journal of Solids and Structures. 1996;33:3363-3375.

[14] Bertholf LD, Karnes CH. Two-dimensional analysis of the split hopkinson pressure bar system. Journal of the Mechanics and Physics of Solids. 1975;23:1-19.

[15] Zhao H. A study of specimen thickness effects in the impact tests on polymers by numeric simulations. Polymer. 1998;39:1103-1106.

[16] Buckley CP, Harding J, Hou JP, Ruiz C, Trojanowski A. Deformation of thermosetting resins at impact rates of strain. Part I: Experimental study. Journal of the Mechanics and Physics of Solids. 2001;49:1517-1538.

[17] Song B, Chen W, Montgomery ST, Forrestal MJ. Mechanical response of an alumina-filled epoxy at various strain rates. Journal of Composite Materials. 2009;43:1519-1536.

[18] Lee O, Kim D, Han Y, Park Y. Dynamic deformation of hot temperature degraded POM and PP using a modified SHPB with pulse shaper technique. Journal of Mechanical Science and Technology. 2008;22:1692-1698.

[19] Dharan C, Hauser F. Determination of stress-strain characteristics at very high strain rates. Experimental Mechanics. 1970;10:370-376.

[20] Gorham DA. Specimen inertia in high strain-rate compression. Journal of Physics D: Applied Physics. 1989;22:1888.

[21] Davies EDH, Hunter SC. The dynamic compression testing of solids by the method of the split Hopkinson pressure bar. Journal of the Mechanics and Physics of Solids. 1963;11:155-179.

[22] Walley SM, Field JE, Pope R, Safford NA. The rapid deformation behaviour of various polymers. J Phys III France. 1991;1:1889-1925.

[23] Trautmann A, Siviour CR, Walley SM, Field JE. Lubrication of polycarbonate at cryogenic temperatures in the split Hopkinson pressure bar. International Journal of Impact Engineering. 2005;31:523-544.

[24] Hartley RS, Cloete TJ, Nurick GN. An experimental assessment of friction effects in the split Hopkinson pressure bar using the ring compression test. International Journal of Impact Engineering. 2007;34:1705-1728.

[25] Briscoe BJ, Nosker RW. The influence of interfacial friction on the deformation of high density polyethylene in a split hopkinson pressure bar. Wear. 1984;95:241-262.

[26] Dioh NN, Leevers PS, Williams JG. Thickness effects in split Hopkinson pressure bar tests. Polymer. 1993;34:4230-4234.

[27] Siviour CR, Walley SM, Proud WG, Field JE. The high strain rate compressive behaviour of polycarbonate and polyvinylidene difluoride. Polymer. 2005;46:12546-12555.

[28] Gray GT, Blumenthal WR, Trujillo CP, Carpenter RW. Influence of temperature and strain rate on the mechanical behavior of Adiprene L-100. J Phys IV France. 1997;7:523.

[29] Walley SM, Field JE, Pope PH, Safford NA. A Study of the Rapid Deformation Behaviour of a Range of Polymers. Philosophical Transactions of the Royal Society of London A Mathematical and Physical Sciences. 1989;328:1-33.

[30] Wang K, Bahlouli N, Matadi R, Addiego F, Ahzi S, Rémond Y. Lubrication of polypropylene and polypropylene based composite in split Hopkinson pressure bar tests in a wide range of temperature. International Journal of Crashworthiness. 2012.

[31] Pessey D, Bahlouli N, Pattofatto S, Ahzi S. Polymer composites for the automotive industry: Characterisation of the recycling effect on the strain rate sensitivity. International Journal of Crashworthiness. 2008;13:411-424.

[32] Richeton J, Ahzi S, Vecchio KS, Jiang FC, Makradi A. Modeling and validation of the large deformation inelastic response of amorphous polymers over a wide range of temperatures and strain rates. International Journal of Solids and Structures. 2007;44:7938-7954.

[33] Richeton J, Ahzi S, Vecchio KS, Jiang FC, Adharapurapu RR. Influence of temperature and strain rate on the mechanical behavior of three amorphous polymers: Characterization and modeling of the compressive yield stress. International Journal of Solids and Structures. 2006;43:2318-2335.

[34] Rodríguez-Martínez JA, Rusinek A, Arias A. Relation between strain hardening of steel and critical impact velocity in tension. Journal of Theoretical and Applied Mechanics. 2009;47:645-665.

[35] Rosenberg Z, Ashuach Y, Kreif R. The effect of specimen dimensions on the propensity to adiabatic shear failure in Kolsky bar experiments. Matéria (Rio de Janeiro). 2010;15:283-290.

[36] Dodd B, Bai Y. Adiabatic Shear Localization: Frontiers and Advances: Elsevier Limited, Oxford; 2012.

[37] Inberg JPF. Fracture of polycarbonate/ABS blends: University of Twente, Enschede, The Netherlands; 2001.

[38] Zebarjad SM. Fracture mechanism under dynamic loading of elastomer-modified polypropylene. Materials Letters. 2003;57:2733-2741.

[39] Truss RW, Clarke PL, Duckett RA, Ward IM. The dependence of yield behavior on temperature, pressure, and strain rate for linear polyethylenes of different molecular weight and morphology. Journal of Polymer Science: Polymer Physics Edition. 1984;22:191-209.

[40] Richeton J, Ahzi S, Daridon L, Remond Y. A formulation of the cooperative model for the yield stress of amorphous polymers for a wide range of strain rates and temperatures. Polymer. 2005;46:6035-6043.

[41] Hablot E, Matadi R, Ahzi S, Vaudemond R, Ruch D, Avérous L. Yield behaviour of renewable biocomposites of dimer fatty acid-based polyamides with cellulose fibres. Composites Science and Technology. 2010;70:525-529.

[42] S. M. Walley, J. E. Field, P. H. Pope, N. A. Safford. A study of the rapid deformation behaviour of a range of polymers. London, ROYAUME-UNI: Royal Society of London; 1989.

Chapter 4:

Micromechanical modeling of polypropylene-based composites

4. Micromechanical modeling of polypropylene-based composites

4.1. Introduction

For the modeling of the effective elastic stiffness, some existing works have reported the prediction of stiffness of polymer-based composites with a good agreement in comparison to the experimental results [1-4]. However, these models account only for the volume fraction of fillers, aspect ratio (AR), shape and orientation of the particles. They do not consider any temperature and strain rate dependence. Nevertheless, it is well known that both neat polymers and polymer-based composites are very sensitive to these factors. Recently, we extended Richeton model [5] to describe the dependence of the elastic modulus on the test temperature, frequency/strain rate, volume fraction of nanofiller and on the extent of exfoliation [6]. The predictions of the nanocomposite elastic modulus by our modified models showed a good agreement with experimental results [5].

For the modeling of the yield behavior for polymer composite, we proposed a three-phase approach to model the yield behavior of the polymer nanocomposite. This approach is based on the micromechanical formulation of the cooperative model for the yield behavior of semi-crystalline polymers combined with the effect of nanoparticles and their distribution on yielding. In this, our proposed approach accounts for strain rate and temperature effects as well as for the extent of exfoliation of the organoclay fillers. Our model predictions were compared to the experimental results and a good agreement was found [6].

However, modeling of the mechanical responses for recycled materials is less investigated. Although above mentioned stiffness model and yield model can well predict the elastic behavior and yield strength of polymer-based composites. They are used for polymer with single filler. In addition, they are used for non-recycled materials.

In this chapter, for the prediction of the Young's modulus of PP-based composites, we propose to improve the statistical stiffness model of Richeton et al. [5] by incorporating a Mori-Tanaka based approach and a two-population model by using Mori-Tanaka model [7]. In particular, we implemented the aspect ratio of the fillers (depending on the reprocessing cycle)in the prediction of the compressive stiffnesses of neat PP. This new approach can use to estimate the effective modulus of the recycled PP-based composites with single or double fillers. The predicted elastic behavior depends on the frequency (or strain rate) and temperature as well as on the volume fraction of fillers and recycling cycles.

For the prediction of the yield stress of PP-based composites, we propose to incorporate the Pukanszhy approach and a two-population model by using Pukanszhy approach [8] into the Gueguen model [9]. It is to be noted that we assume linear evolutions of the internal stress of neat PP and the parameter B with reprocessing cycles. The modified model can estimate the effective yield stress of the recycled PP-based composite with one or two inclusions. The predicted yield stress depends on the strain rate and temperature as well as on the filler content and reprocessing number.

Our proposed models were validated on PP-based composites with different weight percentage of fillers and with different recycling number. In our approach, we compared the predicted results with experimental ones. The experimental tests

consisted in both dynamic mechanical analysis (Section 2.4.7) and dynamic mechanical compressive tests by the split Hopkinson pressure bars (Section 3.3).

4.2. Materials and experiments used for the modeling

Dynamic mechanical analysis (DMA) was conducted to investigate the elastic behavior of neat PP and PP-based composites as mentioned in Section 2.3.7. In order to study the frequency sensitivity of non-recycled and recycled PP-based composites, materials were subjected to deformation at the frequency of 1 Hz and 10 Hz. Previous results from high strain rate uniaxial compression tests (split Hopkinson pressure bar) are also used in this chapter.

4.3. Modeling of the elastic modulus of materials

4.3.1. Composite models for elastic modulus

4.3.1.1. Mori-Tanaka and Chow models with filler content effect

- *Mori-Tanaka model:*

Mori-Tanaka (MT) model [10] derived by the use of Eshelby's inclusion model is widely used to evaluate the effective properties of composites. Mori-Tanaka considered the behavior of composites that contain a non-dilute reinforcement consisting of many identical spheroidal particles via dilute inhomogeneities that are subjected to effective matrix fields rather than the macroscopic fields [11].

On the basis of the MT model, Tandon and Weng [7] proposed an analytical solution for the elastic modulus of an isotropic matrix filled with aligned spheroidal inclusions. In particular, Eshelby tensor takes into account the aspect ratio (AR) of

ellipsoidal inclusions. In an injected polymer-based composite, the preferred orientation of filler along the injection direction results in an anisotropic microstructure [12]. In the previous study (section 2.4.6), our scanning electron microscope (SEM) micrograph for PP/talc 80/20 demonstrated an orientation of talc major axis along the injection direction. Given this oriented microstructure of the considered polymer composite, the TW model can be used to estimate the effective elastic properties. The longitudinal and transverse Young's moduli, $E_{c//}^{MT}$ and $E_{c\perp}^{MT}$, are given by following equations [7]:

$$\frac{E_{c//}^{MT}}{E_m} = \frac{1}{1+\varphi_f (A_1 + 2\upsilon_m A_2)/A} \tag{4-1}$$

$$\frac{E_{c\perp}^{MT}}{E_m} = \frac{1}{1+\varphi_f [-2\upsilon_m A_3 + (1-\upsilon_m)A_4 + (1+\upsilon_m)A_5 A]/2A} \tag{4-2}$$

Here, E_m is the elastic modulus of the matrix, φ_f is the volume fraction of filler, υ_m denotes the Poisson ratio of PP matrix. A_i and A are related to the Eshelby tensor components and the properties of the inclusions and the matrix, specifically elastic constants, inclusion volume fraction and aspect ratio (Appendices A2) [7, 13].

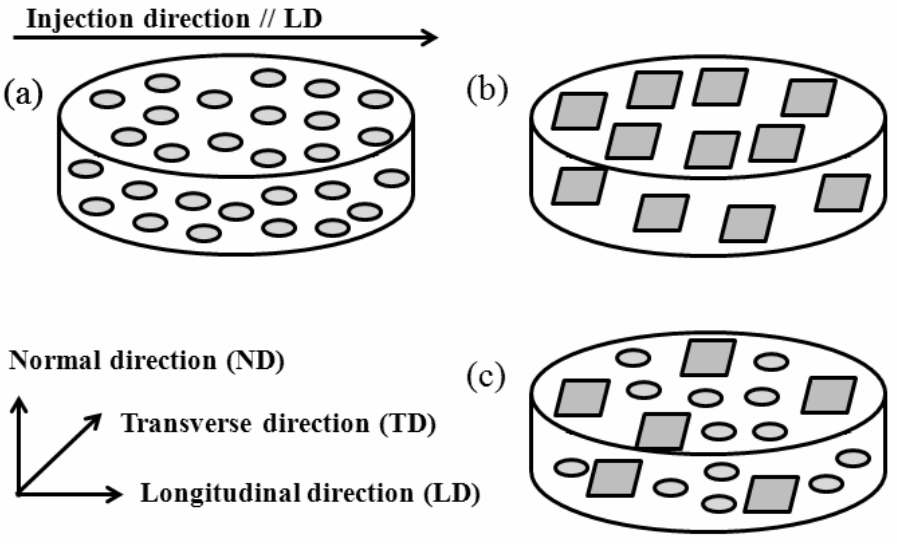

Figure 4-1: Physical representations and coordinate system for (a) PP/EOC, (b) PP/talc, and (c) PP/EOC/talc composites.

In our experimental investigations, the loading direction is perpendicular to the LD-TD plane of samples (Figure 4-1) and therefore, equation (4-1) is used to estimate the effective stiffness of the composites [7].

- *Chow model:*

Chow developed a simplified model for computing the effective properties of filled polymer composites containing aligned ellipsoidal particles at finite concentrations, φ_f. The anisotropic particle shape is characterized by an aspect ratio of the major to the minor axes [14, 15]. The effective elastic properties of composites, $E_{c//}^{Ch}$ and $E_{c\perp}^{Ch}$, can be calculated by following equations:

$$\frac{E_{c//}^{Ch}}{E_m} = 1 + \frac{(k_f / k_m - 1)G_1 + 2(\mu_f / \mu_m - 1)K_1}{2K_1G_3 + G_1K_3}\varphi_f \tag{4-3}$$

$$\frac{E_{c\perp}^{Ch}}{E_m} = 1 + \frac{(k_f / k_m - 1)G_3 + (\mu_f / \mu_m - 1)(G_3\xi + K_1\zeta)}{2K_1G_3 + G_1K_3}\varphi_f \tag{4-4}$$

where $E_{c//}^{Ch}$ and $E_{c\perp}^{Ch}$, are the longitudinal and transverse Young's moduli of composites. k_f and k_m are the bulk moduli and μ_f and μ_m are the shear moduli of the inclusions and matrix, respectively. Other parameters (K_i , G_i , ξ and ζ) related to the Eshelby tensor components and the properties of the inclusions and the matrix are defined in Appendices A2. Taking the same reason for the loading direction, Equation (4-3) of Chow model is used to estimate the effective stiffness of our materials.

4.3.1.2. Two population models for polymer with two fillers

Mori-Tanaka and Chow model are usually used for polymer composites with single filler. However, in our study, the PP/EOC/talc composite consisted both EOC and talc reinforcements. Indeed, EOC and talc fillers have different effects on the mechanical properties of the composites. Thus, separate models are useful to predict their contributions to the properties of the composites. Paul et al. [16, 17] proposed a two-population model to take into account the existence of two fillers in a single composite. In this model, two types of fillers were considered separately to get a more accurately predicted effective modulus of the materials. A two-population model can be considered to have an additive approach or a multiplicative approach.

- *Additive approach:*

In the additive approach, the effect of each filler on the properties of composite are computed separately and then summed together. The additive approach is given by the following equation:

$$\frac{E_C^{add}}{E_m} = \frac{E_{PP/EOC}}{E_m} + \frac{E_{PP/Talc}}{E_m} - 1 \qquad (4\text{-}5)$$

where E_m, $E_{PP/EOC}$ and $E_{PP/Talc}$ are the moduli for PP matrix, PP/EOC and PP/Talc composites, respectively. E_C^{add} is the effective modulus of PP/EOC/talc composite estimated by the additive approach.

- *Multiplicative approach:*

For the multiplicative approach, there are two ways to compute the effective modulus of a ternary-phase material. The first way is to take into account the effect of talc filler at first. Then the PP/Talc composite is considered to be the matrix for the EOC inclusions. The contribution of EOC is computed using the calculated modulus of PP/talc composite as the matrix rather than those of the neat PP matrix. The first way of the multiplicative approach is described below:

$$\frac{E_C^{mult}}{E_m} = \frac{E_{PP/Talc}}{E_m} \cdot \frac{E_C}{E_{PP/Talc}} \tag{4-6}$$

Here, E_C^{mult} is the effective modulus of PP/EOC/talc composite calculated by the multiplicative approach. E_C is the modulus of PP/EOC composite for a given filler volume fraction. Other parameters are defined as before.

The second way is to take into account the effect of EOC inclusion at first. Then the PP/EOC blend is considered to be the matrix for the talc fillers. The contribution of talc is calculated using the modulus of PP/EOC composite as the matrix rather than those of the neat PP matrix. The second way of the multiplicative approach is shown as below:

$$\frac{E_C^{mult}}{E_m} = \frac{E_{PP/EOC}}{E_m} \bullet \frac{E_C}{E_{PP/EOC}} \tag{4-7}$$

Here, E_C is the modulus of PP/talc composite for a given filler volume fraction. Other parameters are depicted as before.

4.3.1.3. Richeton model

Mori-Tanaka, Chow and the two-population models account only for the volume fraction of fillers, aspect ratio, shape and orientation of the particles. There is no temperature and strain rate (or frequency) dependence. In order to take into account these two factors, Richeton et al. [5] proposed to extended the statistical model of Mahieux and Reifsnider [18, 19] with both temperature and strain rate/frequency effects (See Section 1.5.1). Richeton model is described below:

$$E(T,f)=\left(E_1(f)-E_2(f)\right)\cdot\exp\left(-\left(\frac{T}{T_\beta(f)}\right)^{m_1}\right)+\left(E_2(f)-E_3(f)\right)\cdot\exp\left(-\left(\frac{T}{T_g(f)}\right)^{m_2}\right)+E_3(f)\cdot\exp\left(-\left(\frac{T}{T_f(f)}\right)^{m_3}\right) \tag{4-8}$$

$$\frac{1}{T_\beta}=\frac{1}{T_\beta^{ref}}+\frac{k}{\Delta H_\beta}\ln\left(f^{ref}/f\right) \tag{4-9}$$

$$T_g=T_g^{ref}+\frac{-C_2^{ref}\cdot\log(f^{ref}/f)}{C_1^{ref}+\log(f^{ref}/f)} \tag{4-10}$$

$$T_f=T_f^{ref}\cdot(1+0.01\cdot\log(f/f^{ref})) \tag{4-11}$$

$$E_i=E_i^{ref}\cdot(1+s\cdot\log(f/f^{ref})) \tag{4-12}$$

The detailed information about Richeton model and the definition of its parameters has been reported in Section 1.5.1.

4.3.2. Recycling effect on the elastic modulus

As shown in chapter 2, the compressive Young's modulus, *E*, of neat PP had a continuous decrease with the reprocessing cycles. Therefore, we assumed linear evolution of Young's modulus for neat PP with reprocessing dependences:

$$E(N_P) = k_1 N_P + E_0 \tag{4-13}$$

where N_p is the number of reprocessing. k_1 is the reprocessing strengthening coefficient of Young's modulus. E_0 is the Young's modulus for non-recycled neat PP.

For PP/EOC and PP/talc composites, we observed the changes of AR of EOC and talc particles with the reprocessing cycles (See Section 2.4.6). Therefore, we also assumed linear evolutions of fillers' AR with the reprocessing number as follows:

$$AR(N_P) = k_2 N_P + AR_0 \tag{4-14}$$

Here, k_2 is the reprocessing strengthening coefficient of fillers' AR. AR_0 is the aspect ratio of fillers in non-recycled PP-based composites.

4.3.3. Modeling results and discussion

4.3.3.1. Mori-Tanaka and Chow models comparisons

Table 4-1 lists the elastic modulus, density and Poisson's ratio of EOC and talc. For neat PP, $\upsilon_m = 0.4$ and $\rho_m = 0.9 g/cm^3$ are used in this study (see Section 2.2.1 and Section 4.3.1.1) The volume fraction of the fillers, φ_f, can be computed from their weight fraction according to the following equation [20].

$$\varphi_f = w_f (w_f + (1 - w_f)\rho_C / \rho_m)^{-1} \quad (4\text{-}15)$$

where ρ_C and ρ_m are the densities of the fillers and PP matrix, respectively, and w_f is the filler weigh fraction.

Table 4-1: Inclusion properties for composite modeling [16, 21-24].

Inclusion	Modulus (GPa)	Density (g/cm^3)	Poisson's ratio
EOC	0.0076	0.882	0.499
Talc	170	2.78	0.22

Figure 4-2 and Figure 4-3 compare the predicted effective modulus by the MT and Chow models with the experiment data for non-recycled PP/EOC and non-recycled PP/talc composites. The experiment data are chosen from Table 3-2 for the materials tested at 25 °C and strain rate 4. In Figure 4-2, we reporte the predicted effective modulus from the MT and Chow models with three different aspect ratios (ARs) of EOC inclusion. In this part, the results from the classical bounds are also reported. The experimental data for non-recycled PP/EOC blends lie on the both side of the predicted curve with AR=1.42. Note this AR=1.42 is the same value as our measurement of EOC inclusion in section 2.4.6. In Figure 4-2, the difference between the predicted effective moduli of non-recycled PP/EOC composites by the MT model and Chow models with AR=1.42 is very weak. However, the predicted effective moduli for non-recycled PP/talc composites by the Chow model are significantly lower than those of the MT model (Figure 4-3). The predicted effective moduli obtained by the Chow model are very close to the lower bound predictions. We note

that the best fit AR of talc particles is equal to 17 for non-recycled PP/talc composites. This estimated AR of talc is higher than that measured by SEM for PP/talc 80/20 0P in the previous study (Section 2.4.6). This is probably due to the measurement error for the average talc particle thickness in our previous investigation where a lower AR of talc particles was measured.

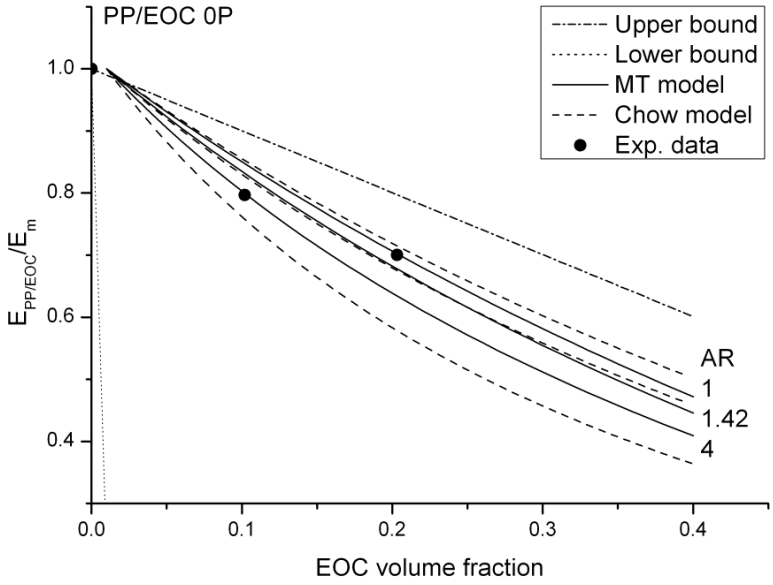

Figure 4-2: Comparison of the predicted effective modulus by the MT and Chow models with the experiment data for non-recycled PP/EOC.

The comparison between the predicted effective modulus by the MT and Chow models and the experiment data for the recycled PP/EOC 6P and recycled PP/talc 6P are shown in Figure 4-4 and Figure 4-5, respectively. We selected to show the results for the recycling number six only because we believed that the results for the recycling number three will have similar tendencies. In Figure 4-4 and Figure 4-5, the experimental data are chosen from Table 3-2 for the recycled materials tested at 25 °C and strain rate 4. For PP/EOC 6P, AR=1.2 (obtained by statistical investigation in Section 2.4.6) for the EOC inclusion yields reasonably good predictions of the effective modulus of recycled PP/EOC composites by both MT and Chow models.

However, Chow model underestimates the effective modulus for recycled PP/talc composite (Figure 4-5). Note the AR=35 of talc better fit with the experimental result with increasing talc content by using the MT model. Although this AR is larger than our measured one, it increases with recycling number that is in good accordance with our statistical results (Section 2.4.6).

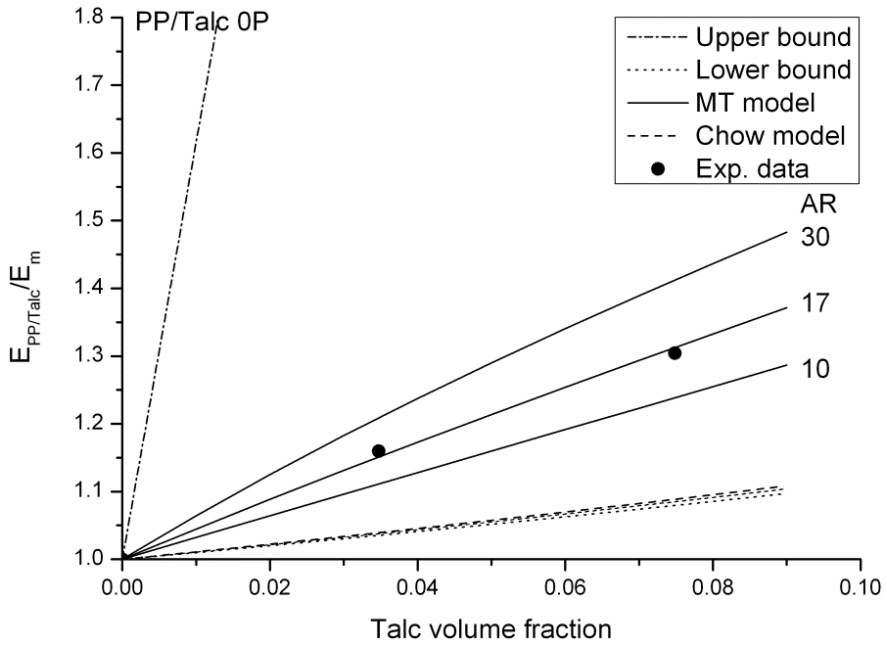

Figure 4-3: Comparison of the predicted effective modulus by the MT and Chow models with the experiment data for non-recycled PP/talc.

Due to the lower estimated effective modulus by Chow model for both non-recycled and recycled PP/talc composites, the MT model will be selected for the subsequent effective modulus modeling.

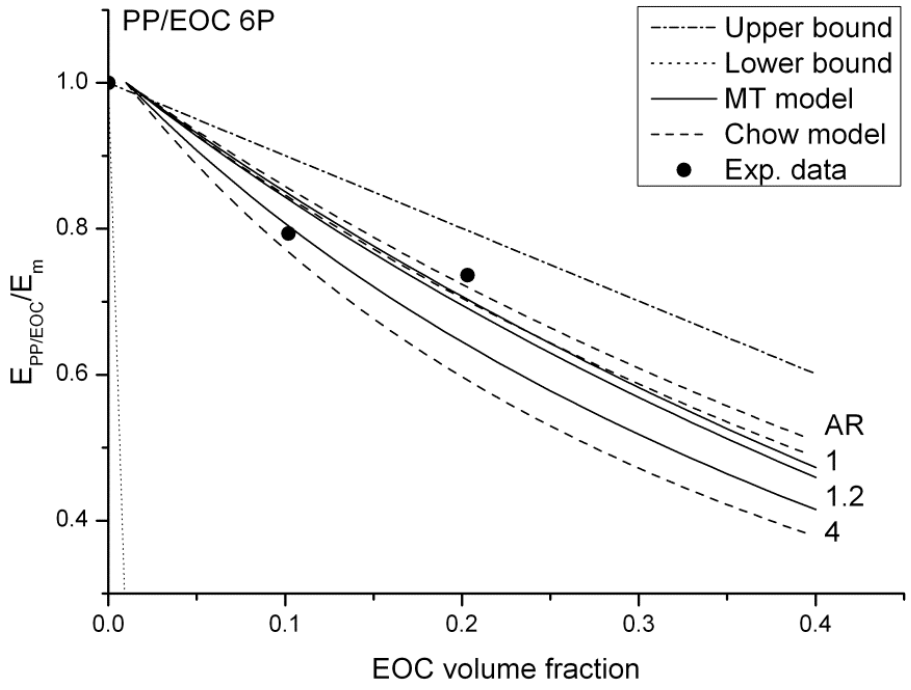

Figure 4-4: Comparison of the predicted effective modulus by the MT and Chow models with the experiment data for recycled PP/EOC.

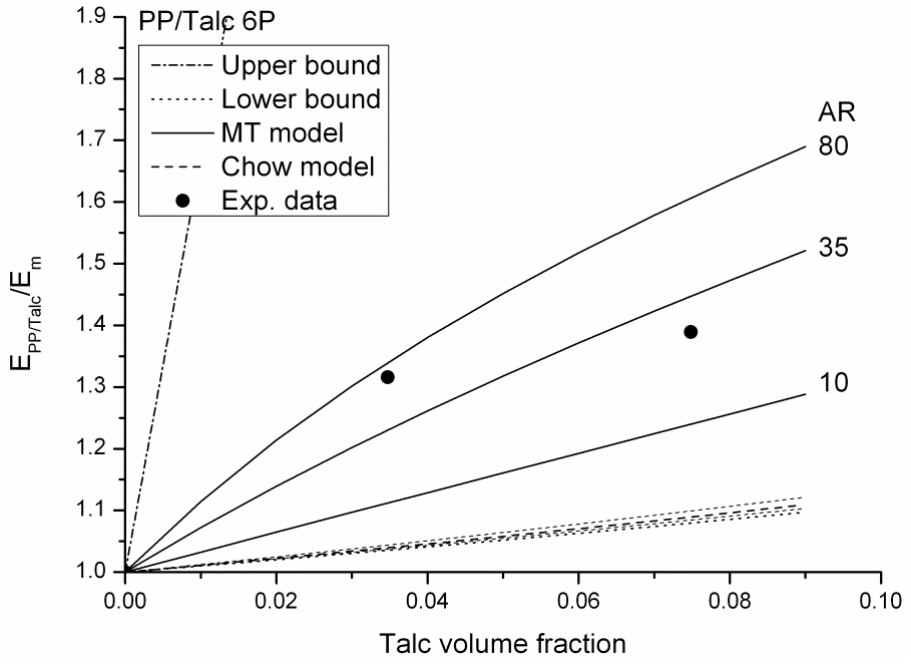

Figure 4-5: Comparison of the predicted effective modulus by the MT and Chow models with the experiment data for recycled PP/talc.

4.3.3.2. Two-population model comparisons

Figure 4-6 and Figure 4-7 compare the additive and multiplicative two-population models for the prediction of the effective modulus of non-recycled PP/EOC/talc composites by the MT approach. The ARs of EOC and talc particles kept the same value reported in Figure 4-2 and Figure 4-3 (AR=1.42 for EOC and AR=17 for talc). The dynamic compressive moduli for non-recycled materials tested at 25 °C and strain rate 4 are used as experimental data (see Table 3-2). When PP/talc is considered to be the matrix the EOC contribution for the effective modulus of composite is shown in Figure 4-6. The predicted effective moduli by both additive and multiplicative approaches decrease with increasing of EOC volume fraction. In this, the multiplicative model seems to incorrectly predict the effective modulus of materials. The additive model underestimates the compressive modulus of composites. The lower predicted modulus by the additive method can be attributed to the lower estimated modulus of PP/talc 90/10 0P by using the AR=17 of talc in Figure 4-3.

Taking the PP/EOC as matrix, the talc contribution for the effective modulus of composite is shown in Figure 4-7. In this Figure, both additive and multiplicative approaches match the experimental data fairly well. The multiplicative method appears to better fit the compressive moduli for the PP/EOC 80/20 0P and PP/EOC/Talc 70/20/10 0P. The slightly lower predicted effective modulus by the multiplicative method is due to the underestimation of the modulus for PP/EOC 0P by MT model with the AR=1.42 (See Figure 4-2).

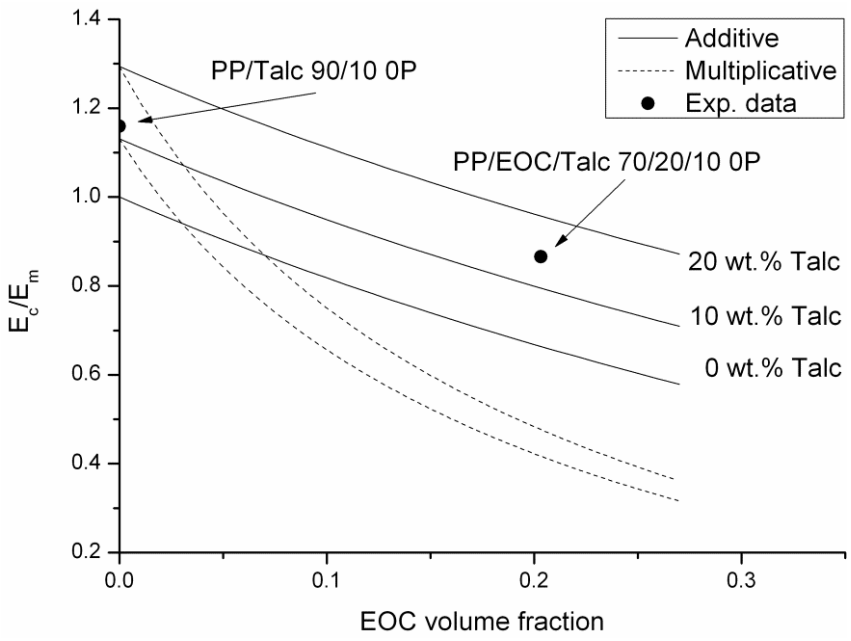

Figure 4-6: Comparison of the predicted effective modulus by the MT theory using the additive and multiplicative two-population model for non-recycled PP/EOC/talc composite, PP/talc is considered to be the matrix for the EOC inclusions.

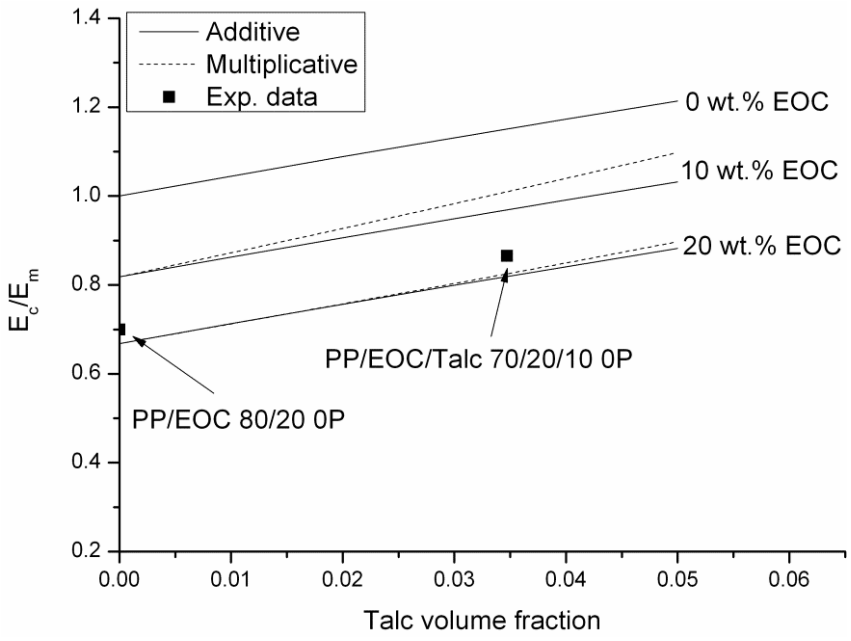

Figure 4-7: Comparison of the predicted effective modulus by the MT theory using the additive and multiplicative two-population model for non-recycled PP/EOC/talc composite, PP/EOC is considered to be the matrix for the talc particles.

Note that the two-population model comparison results for the recycled materials are not shown here, because this comparison gave similar results. In the following, the multiplicative method will use to predict the effective modulus of PP/EOC/talc composite by taking the PP/EOC as matrix.

4.3.3.3. Modeling of storage modulus

The experimental results of dynamic mechanical analysis (DMA) for non-recycled neat PP, PP/EOC, PP/EOC/talc and PP/talc composites are plotted in Figure 4-8 for two frequencies (1Hz and 10Hz). In this figure, both temperature and frequency effects are shown on the storage modulus for both neat PP and PP-based composites. These results for the storage modulus show similar sensitivities of the neat PP, PP/EOC and PP/talc composites to frequency and temperature where a shift is obtained for the higher frequency. The shift due to frequency and the slopes due to temperature effects are similar to all considered materials. However, the storage modulus of PP/EOC/talc composite is close to those of PP/EOC 90/10 0P with temperature above 250K. For temperature lower than 250K, the storage modulus of PP/EOC/talc composite is higher than those of PP/EOC 90/10 0P for both frequencies. This is probably due to the experimental error. The storage modulus of recycled materials is shown previously (Section 2.4.7). Note the storage modulus for the recycled materials has similar sensitivities to frequency and temperature. The storage modulus of PP/EOC decreased with the reprocessing while the storage modulus of PP/talc increased. In addition, the storage modulus of PP/EOC/talc composite has limited change with reprocessing for both frequencies. The probable reason is explained in Section 3.3.

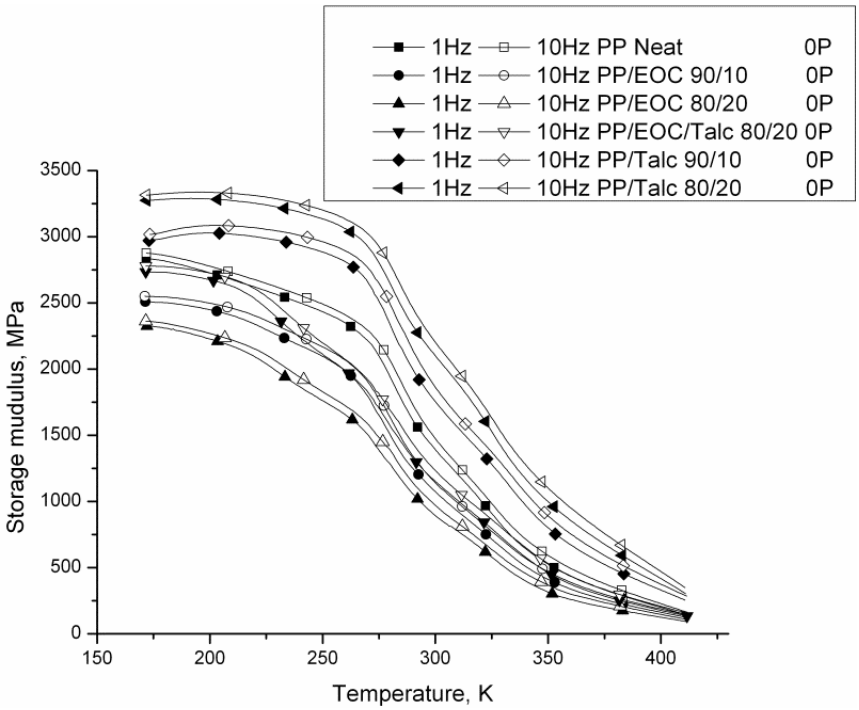

Figure 4-8: DMA results for non-recycled materials for two frequencies.

Equation (4-8) could be used to predict the storage modulus of non-recycled and recycled neat PP (0P and 6P) [5]. However for the non-recycled and recycled PP/EOC, PP/talc and PP/EOC/talc composites, this model cannot be directly applied because of the presence of fillers. Therefore, we suggest incorporating MT model (Equation (4-1)) into Richeton model (Equation (4-8)) for evaluating the three effective instantaneous moduli where the Tandon-Weng equation is modified as follows:

$$\frac{E_{ic}^{ref}}{E_{im}^{ref}} = \frac{1}{1+\varphi_f (A_{i1} + 2\upsilon_m A_{i2}) / A_i} \tag{4-16}$$

Here, E_{im}^{ref} correspond to the three reference instantaneous moduli of non-recycled and recycled neat PP ($i=1,2,3$) at a reference frequency. Once these three moduli are determined, the three reference instantaneous moduli E_{ic}^{ref} of the non-recycled and

recycled PP/EOC and PP/talc composites could be calculated by Equation (4-16) for different filler volume fractions φ_f and the corresponding AR. Then E_{ic} are obtained from E_{ic}^{ref} by using Eq. (4-12) which will be used to replace the instantaneous moduli (E_i) in Equation (4-8). Finally, the storage modulus of the non-recycled and recycled PP/EOC and PP/talc composites could be predicted by this modified statistical model (Equation (4-8)). It should be noted that A_{i1}, A_{i2}, and A_i are calculated from each instantaneous modulus E_{im}^{ref} of non-recycled and recycled neat PP. In the following, this new model is denoted as Richeton-MT (RMT) model.

For non-recycled and recycled PP/EOC/talc composite, the multiplicative approach (Equation (4-7)) was incorporated into the Richeton model (Equation (4-8)) by using the MT approach (Equation (4-16)) to calculate the three moduli $E_{ic\_mult}^{ref}$ of PP/EOC/talc composite according to our new approach:

$$\frac{E_{ic\_mult}^{ref}}{E_{im}^{ref}} = \frac{E_{PP/EOCi}^{ref}}{E_{im}^{ref}} \frac{E_{ic}^{ref}}{E_{PP/EOCi}^{ref}} \tag{4-17}$$

Here, E_{ic}^{ref} is the reference instantaneous moduli of PP/talc composite for a given filler volume fraction. $E_{PP/EOCi}^{ref} / E_{im}^{ref}$ is calculated at first by using Equation (4-16). Then, the contribution of talc on the stiffness of PP/EOC/talc is obtained by considering the PP/EOC as the matrix. Once the $E_{ic\_mult}^{ref}$ is computed, E_{ic} could be determined (Equation (4-12)) and incorporated in the Richeton model (Equation (4-8)) as E_i for computing the effective storage modulus of the non-recycled and recycled PP/EOC/talc composite. In the following, this model is denoted as Richeton-Multiplicative model (RM) model.

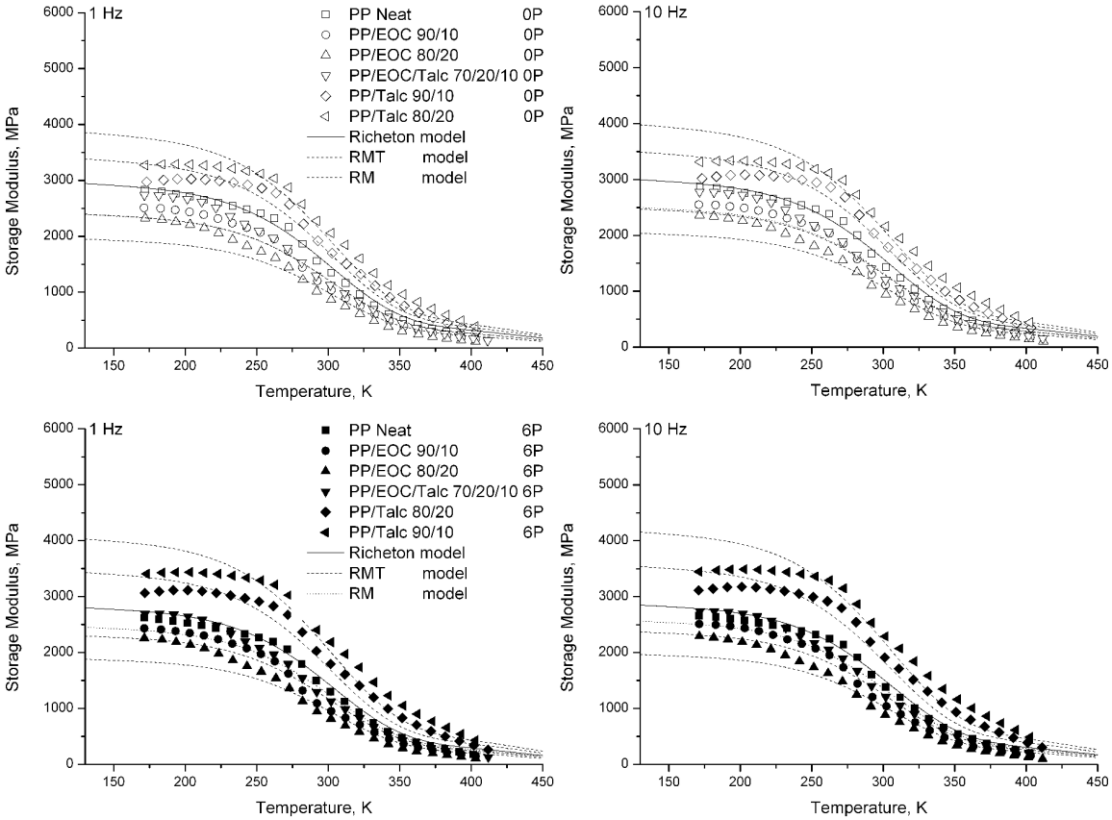

Figure 4-9: Comparison between the theoretical and the experimental (from DMA measurements) storage modulus for non-recycled (0P) and recycled (6P) neat PP, PP/EOC, PP/talc and PP/EOC/talc composites.

Figure 4-9 shows the predicted results of the storage modulus as a function of temperature under two different frequencies (1Hz and 10Hz). The storage modulus of neat PP (0P and 6P) is predicted by Richeton model and those of PP/EOC and PP/talc are estimated by the RMT model. The storage modulus of PP/EOC/talc is predicted by RM model. The predictions of these models show reasonably good agreements with the DMA measurements. Note the underestimation of storage modulus for PP/EOC composites below 250 K is probably due to the glass transition of EOC inclusion at low temperature (see Section 2.4.7). Indeed, EOC is sensitive to temperature and frequency. In our approach, we kept the constant elastic modulus for

EOC as well as talc particle. In addition, the overestimated storage modulus for PP/talc composite above 250 K is probably due to the experimental error.

Tables 4-2 and 4-3 exhibit the parameters of Richton model used for non-recycled and recycled neat PP at a reference frequency of 1 Hz, respectively. The reference parameters (E_i^{ref} , T_i^{ref} , m_i (i=1, 2, 3)) are physical quantities which were determined according to the description of Mahieux and Reifsnider [18] and Richeton [5]. For this calculation, the WLF equation parameters C_1^g and C_2^g were chosen from Shea [25]. For the β activation energy, $\triangle H_\beta$, we took the values which would be discussed in the next section (Section 4.4). The sensitivity factor, *s*, for storage modulus was calculated from the average value of the DMA data. For non-recycled and recycled PP/EOC and PP/talc, the parameters E_i^{ref} were determined by the modified Tandon-Weng equation (Equation (4-16)). For non-recycled and recycled PP/EOC/talc composite, the parameters E_i^{ref} were computed by the modified multiplicative approach (Equation (4-17)) as mentioned above. In order to reduce the number of parameters which need to be identified, we assumed that the parameters C_i^g and m_i are constant for all the materials and taken equal those of non-recycled neat PP. For the PP-based composites (non-recycled and recycled ones), the parameters T_i^{ref} and *s* were determined by the same method as described above for neat PP, and $\triangle H_\beta$ is taken from the next section. In the RMT model, and as mentioned earlier, the ARs of EOC inclusions for the non-recycled and recycled PP/EOC were chosen AR=1.42 and AR=1.2, respectively. The ARs of talc particles for the non-recycled and recycled PP/talc were chosen AR=17 and AR=35, respectively. These parameters are summarized in Table 4-2.

Table 4-2: Parameters for the modeling of storage modulus of non-recycled (0P) and recycled (6P) materials by the Richeton, RMT and RM models.

	PP neat		PP/EOC 90/10		PP/EOC 80/20		PP/EOC/talc 70/20/10		PP/talc 90/10		PP/talc 80/20	
	0P	6P	0P	6P	0P	6P	0P	6P	0P	6P	0P	6P
f^{ref} (Hz)	1	1	1	1	1	1	1	1	1	1	1	1
E_1^{ref} (MPa)	3350	3130	-	-	-	-	-	-	-	-	-	-
E_2^{ref} (MPa)	2650	2560	-	-	-	-	-	-	-	-	-	-
E_3^{ref} (MPa)	305	295	-	-	-	-	-	-	-	-	-	-
T_β^{ref} (K)	173	173	173	173	173	173	173	173	173	173	173	173
T_g^{ref} (K)	309	310	309	309	309	309	309	309	309	308	309	309
T_f^{ref} (K)	441	440	440	440	440	440	440	440	442	442	442	442
m_1	0.7	0.7	0.7	0.7	0.7	0.7	0.7	0.7	0.7	0.7	0.7	0.7
m_2	7.3	7.3	7.3	7.3	7.3	7.3	7.3	7.3	7.3	7.3	7.3	7.3
m_3	10	10	10	10	10	10	10	10	10	10	10	10
s	0.018	0.018	0.032	0.032	0.045	0.045	0.035	0.035	0.048	0.048	0.036	0.036
$\triangle H_\beta$ (kJ/mol)	83	84.4	83	84.4	83	84.4	83	84.4	83	84.4	83	84.4
C_1^g	18.2	18.2	18.2	18.2	18.2	18.2	18.2	18.2	18.2	18.2	18.2	18.2
C_2^g	47.6	47.6	47.6	47.6	47.6	47.6	47.6	47.6	47.6	47.6	47.6	47.6
RMT model												
AR	-	-	1.42	1.2	1.42	1.2	-	-	17	35	17	35

4.3.3.4. Modeling of the compressive Young's modulus obtained by SHPB

For modeling the dynamic compressive modulus obtained by SHPB in Section 3, we proposed a similar method as that used for storage modulus. In Equation (4-8), we replaced the dependence on frequency f by strain rate $\dot{\varepsilon}$ as shown in Equation. (4-18) below [5]. Other parameters are depicted as before.

$$E(T,\dot{\varepsilon}) = \left(E_1(\dot{\varepsilon}) - E_2(\dot{\varepsilon})\right)\cdot\exp\left(-\left(\frac{T}{T_\beta(\dot{\varepsilon})}\right)^{m_1}\right) + \left(E_2(\dot{\varepsilon}) - E_3(\dot{\varepsilon})\right)\cdot\exp\left(-\left(\frac{T}{T_g(\dot{\varepsilon})}\right)^{m_2}\right) + E_3(\dot{\varepsilon})\cdot\exp\left(-\left(\frac{T}{T_f(\dot{\varepsilon})}\right)^{m_3}\right) \tag{4-18}$$

As reported by Richeton et al. [5], the direct relationship between the frequency of DMA and the strain rate for common mechanical tests is given by Equation (4-19):

$$\frac{f^{ref}}{f} = \frac{\dot{\varepsilon}^{ref}}{\dot{\varepsilon}} \tag{4-19}$$

Consequently, the dependence on strain rate of the three transition temperatures and three instantaneous moduli can be determined by equation (4-20) given below.

$$\begin{cases} \dfrac{1}{T_\beta} = \dfrac{1}{T_\beta^{ref}} + \dfrac{k}{\Delta H_\beta}\ln\left(\dot{\varepsilon}^{ref}/\dot{\varepsilon}\right) \\ T_g = T_g^{ref} + \dfrac{-c_2^{ref}\cdot\log\left(\dot{\varepsilon}^{ref}/\dot{\varepsilon}\right)}{c_1^{ref} + \log\left(\dot{\varepsilon}^{ref}/\dot{\varepsilon}\right)} \\ T_f = T_f^{ref}\cdot\left(1 + 0.01\cdot\log\left(\dot{\varepsilon}/\dot{\varepsilon}^{ref}\right)\right) \\ E_i = E_i^{ref}\cdot\left(1 + s\cdot\log\left(\dot{\varepsilon}/\dot{\varepsilon}^{ref}\right)\right) \end{cases} \tag{4-20}$$

Equation (4-18) can be used for predicting the Young's modulus of neat PP. For extending the application to PP-based composites, MT and multiplicative models

were incorporated to calculate the reference instantaneous stiffnesses E_i^{ref} of the composites as described in Section 4.3.3.3.

For the determination of the parameters, a reference strain rate $\dot{\varepsilon}^{ref} = 1\, s^{-1}$ is first chosen for both non-recycled and recycled neat PP and PP-based composites. We note that a reference strain rate of 1 s^{-1} corresponds to a reference frequency value of 25 Hz in our case (the maximum strain of our DMA measurements is 1%) [26]. Furthermore, it is well known that a high strain rate/frequency leads to an increase of the three transition temperatures of the polymer [27]. Therefore, the three reference temperatures of neat PP and PP-based composites increase slightly (Equation (4-9) to Equation (4-11)).

The resulting shift of the glass transition temperature between the DMA and compressive test (CT) leads to a change in the WLF parameters which can be expressed as follows [5]:

$$\begin{cases} C_2^{DMA} - T_g^{DMA} = C_2^{CT} - T_g^{CT} \\ C_1^{DMA} C_2^{DMA} = C_1^{CT} C_2^{CT} \end{cases} \tag{4-21}$$

In this relationship, C_i^{DMA} corresponds to the WLF equation parameters associated to T_g^{DMA} of the DMA measurements at a reference frequency of 1Hz. Similarly, C_i^{CT} are the parameters of WLF equation for the compressive test at a reference strain rate of 1 s^{-1}.

The initial compressive stiffnesses E_i^{ref} and the three reference temperatures T_i^{ref} of neat PP 0P and neat PP 6P are computed from the storage modulus of neat PP 0P and neat PP 6P with a frequency of 25 Hz by using Equation (4-9) to Equation (4-

12), respectively. In the RMT model, the ARs for EOC inclusions and for talc particles in PP/EOC (0P and 6P) and PP/talc (0P and 6P) composites are taken the same value as those used for the storage modulus predictions (Table 4-2).

For neat PP 3P, we suggest computing the initial compressive stiffnesses E_i^{ref} with reprocessing dependences where the linear evolution of the compressive modulus is described based on Equation (4-13):

$$E_i^{ref}(N_P) = k_{1i} N_P + E_{0i} \tag{4-22}$$

where k_{1i} are the reprocessing strengthening coefficients of the three initial compressive stiffnesses. E_{0i} are the three compressive moduli for non-recycled neat PP. Similarly, the reprocessing dependent fillers' ARs were calculated by using Equation (4-14). Other parameters like the sensitivity factor of the Young's modulus, *s*, was kept the same as those of materials 0P. We also assumed that C_i^g, m_i and $\triangle H_\beta$ were the same as those of non-recycled neat PP. All the parameters for modeling the Young's modulus are summarized in Table 4-3 for different recycling number. Table 4-4 shows the reprocessing parameters in Equation (4-22) and Equation (4-14).

Table 4-3: Parameters for the modeling of compressive modulus of non-recycled (0P) and recycled (3P and 6P) materials by the Richeton, RMT and RM models.

	PP neat			PP/EOC 90/10			PP/EOC 80/20			PP/EOC/talc 70/20/10			PP/talc 90/10			PP/talc 80/20		
	0P	3P	6P	0P	3P	6P	0P	3P	6P	0P	3P	6P	0P	3P	6P	0P	3P	6P
ε^{ref} (Hz)	1	1	1	1	1	1	1	1	1	1	1	1	1	1	1	1	1	1
E_1^{ref} (MPa)	3434	3322	3209	-	-	-	-	-	-	-	-	-	-	-	-	-	-	-
E_2^{ref} (MPa)	2717	2670	2624	-	-	-	-	-	-	-	-	-	-	-	-	-	-	-
E_3^{ref} (MPa)	313	307	302	-	-	-	-	-	-	-	-	-	-	-	-	-	-	-
T_β^{ref} (K)	173	173	173	173	173	173	173	173	173	173	173	173	173	173	173	173	173	173
T_g^{ref} (K)	313	313	314	313	313	313	313	313	313	313	313	313	313	313	313	313	313	313
T_f^{ref} (K)	447	447	446	446	446	446	447	447	447	447	447	447	447	447	447	447	447	447
m_1	0.7	0.7	0.7	0.7	0.7	0.7	0.7	0.7	0.7	0.7	0.7	0.7	0.7	0.7	0.7	0.7	0.7	0.7

n_2	7.3	7.3	7.3	7.3	7.3	7.3	7.3	7.3	7.3	7.3	7.3	7.3	7.3	7.3	7.3	7.3
n_3	10	10	10	10	10	10	10	10	10	10	10	10	10	10	10	10
s	0.093	0.093	0.09	0.096	0.096	0.09	0.10	0.10	0.12	0.035	0.035	0.1	0.048	0.048	0.036	0.1
$\triangle H_{\beta}$ (kJ/mol)	85.3	85.3	83.7	85.3	85.3	83.7	85.3	85.3	83.7	85.3	85.3	83.7	85.3	83.7	85.3	83.7
C_1^g	18.2	18.2	18.2	18.2	18.2	18.2	18.2	18.2	18.2	18.2	18.2	18.2	18.2	18.2	18.2	18.2
C_2^g	47.6	47.6	47.6	47.6	47.6	47.6	47.6	47.6	47.6	47.6	47.6	47.6	47.6	47.6	47.6	47.6
AR	-	-	-	1.42	1.31	1.2	1.42	1.31	1.2	-	-	-	17	26	35	17	26	35

RMT model

Table 4-4: Reprocessing parameters for modeling the Young's modulus of materials.

Reprocessing parameters	
E_{01}	3434 MPa
E_{02}	2717 MPa
E_{03}	313 MPa
k_{11}	-37.5
k_{12}	-15.5
k_{13}	-1.83
$AR_{0\ talc}$	17
$k_{2\ talc}$	3
$AR_{0\ EOC}$	1.42
$k_{2\ EOC}$	-0.037

The modeling curves were compared with the experimental data of neat PP and PP-based composites with different recycling number in Figures 4-10 to 4-13. The experimental data were obtained by the SHPB apparatus at four different strain rates and five different temperatures (See Chapter 3). The Young's modulus of neat PP was predicted by Richeton model whereas those of the PP/EOC and PP/talc composites were estimated by the RMT model. For PP/EOC/talc composite, the Young's modulus was predicted by RM model using MT approach. In Figure 4-10, the experimental compressive modulus of neat PP, PP/EOC 80/20, PP/EOC/talc 70/20/10 and PP/talc 80/20 under strain-rate-2 with different recycling number are

plotted. In this figure, we also show the results from the modeling where the Richeton model yields satisfactory predictions of the Young's modulus of neat PP with recycling effect. Furthermore, the RMT and RM models yield reasonably good predictions of the Young's modulus of non-recycled and recycled PP/EOC 80/20, PP/talc 80/20 and PP/EOC/talc composites, respectively.

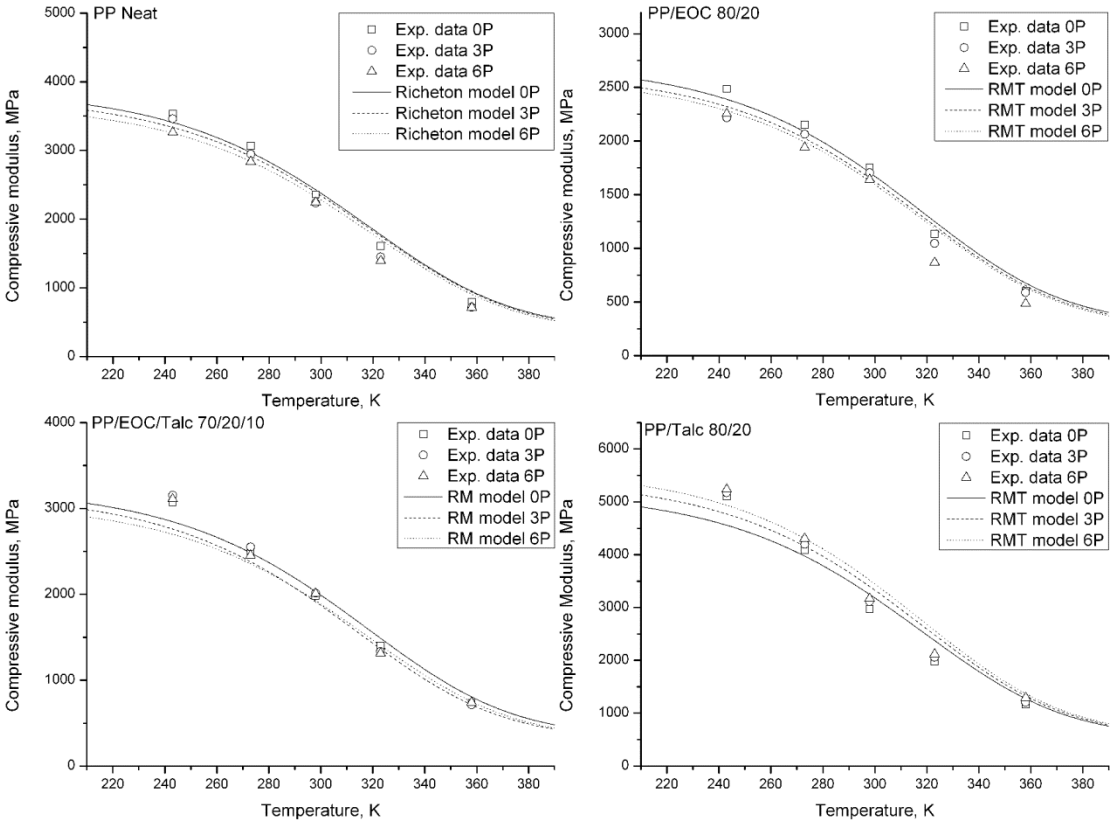

Figure 4-10: Comparison between the experimental data (obtained by SHPB) and the theoretical predictions for compressive modulus of neat PP and PP-based composites with different recycling number, under strain rate 2 and under a wide range of temperatures.

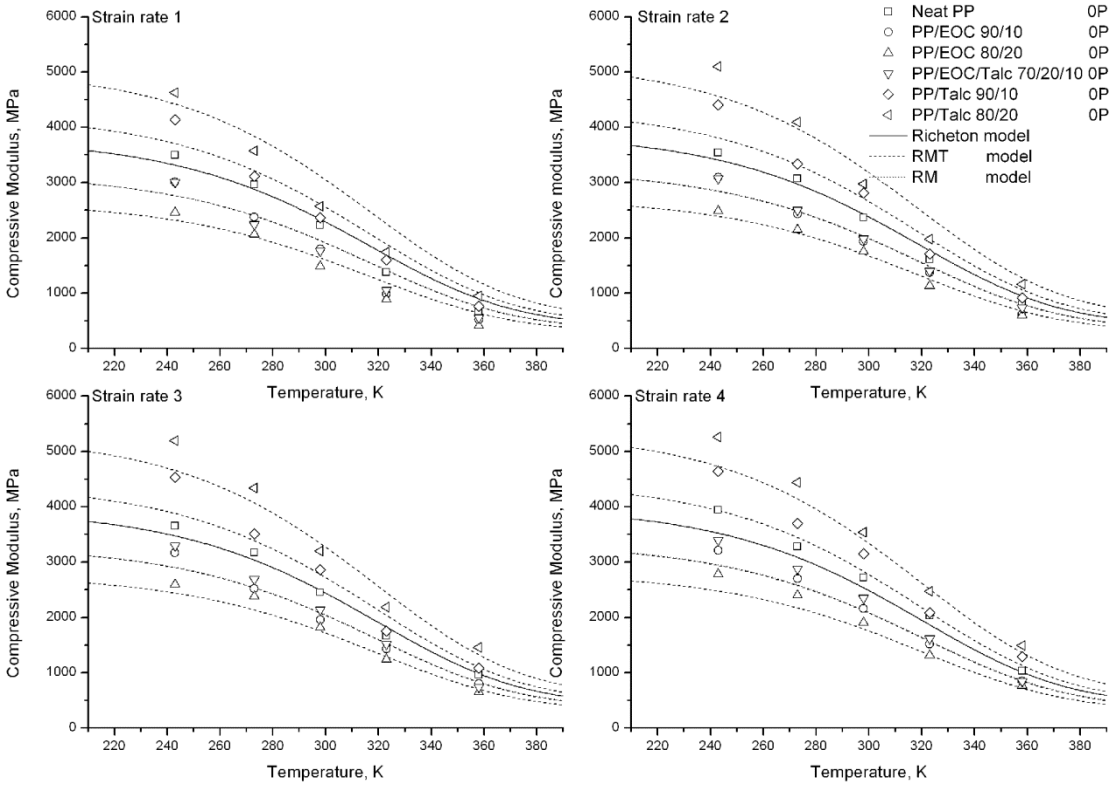

Figure 4-11: Experimental data (obtained by SHPB) and theoretical predictions for compressive modulus of non-recycled neat PP and PP–based composites under four strain rates.

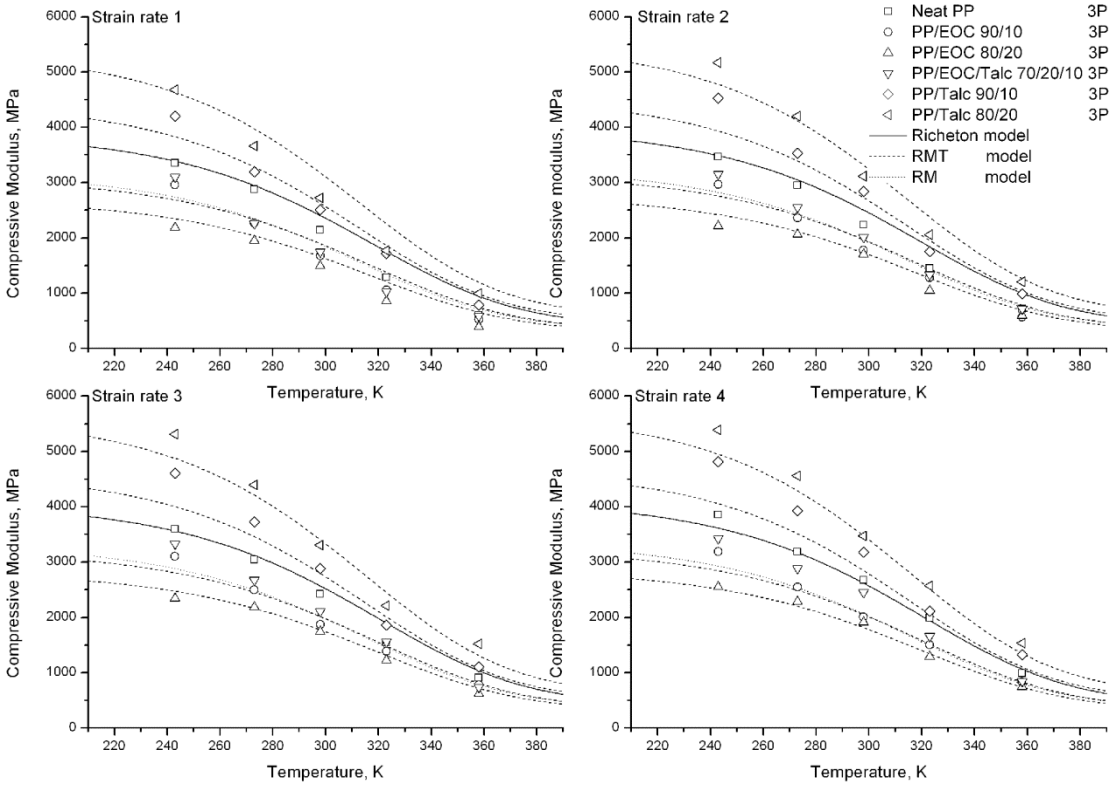

Figure 4-12: Experimental data (obtained by SHPB) and theoretical predictions for compressive modulus of recycled neat PP and PP–based composites (3P) under four strain rates.

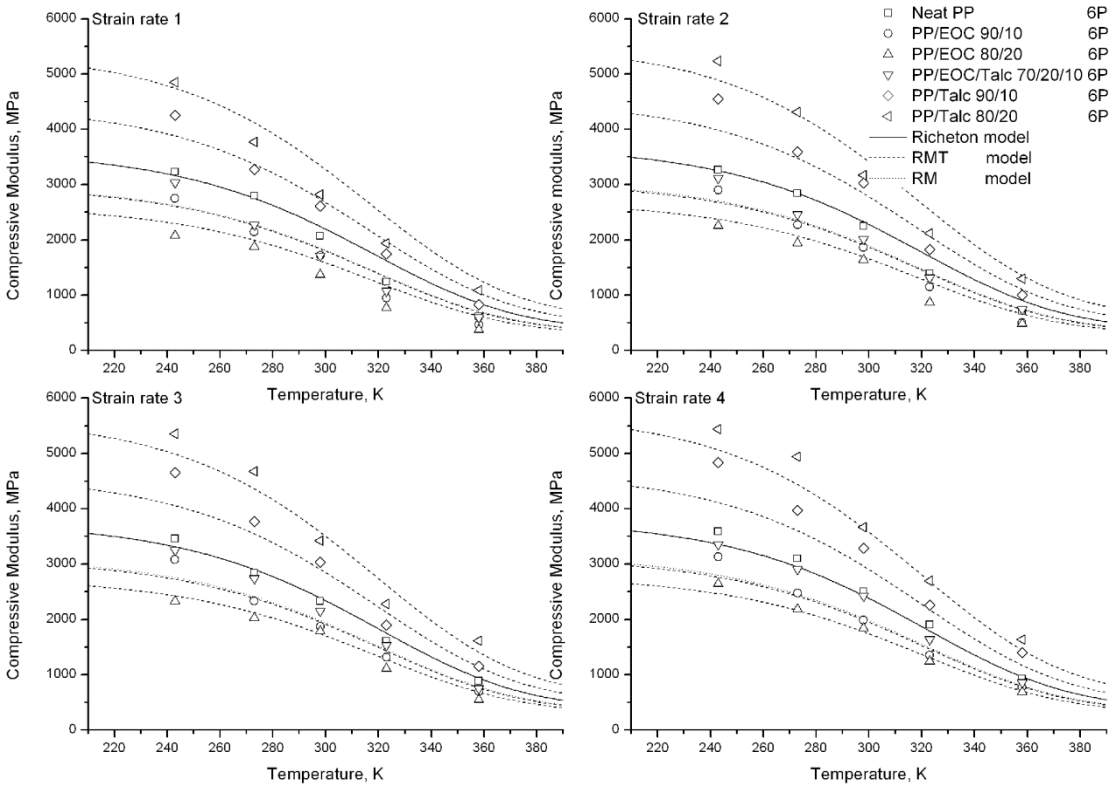

Figure 4-13: Experimental data (obtained by SHPB) and theoretical predictions for compressive modulus of recycled neat PP and PP–based composites (6P) under four strain rates.

In Figures 4-11 to 4-13, the experimental data at five different temperatures and four different strain rates are compared to the theoretical predictions in the temperature range from 210K to 390K. Although the modeling results for the compressive modulus of non-recycled and recycled neat PP and PP-based composites are not perfectly in accord with the experimental data, particularly for the lower strain rates, we still can conclude that the RMT and RM models yield results with fair agreements between the predictions and the experimental data with the recycling effect. Note the predicted compressive moduli of PP/EOC/talc 70/20/10 are very close to those of PP/EOC 90/10 for all recycling numbers.

4.4. Modeling of high strain rate compressive yield stress of materials

4.4.1. Composite models for yield stress

As introduced in Chapter 1, by considering the semi-crystalline polymers as a two phase material, Gueguen et al. [9] extended Richeton [28] model to describe the yield stress for semi-crystalline polymers with the strain rate and temperature dependences:

$$\frac{\sigma_y}{T} = \frac{\sigma_i(0) - m \cdot T}{T} + \frac{2k}{\Delta V_{eff}} \sinh^{-1}\left(\frac{\dot{\varepsilon}}{\dot{\varepsilon}_0 \exp\left(-\frac{\Delta H_{eff}}{RT} \right)} \right)^{1/n} \tag{4-23}$$

where σ_y is the yield stress. T refers to the absolute temperature. $\sigma_i(0)$ is the internal stress at 0 K. m is a material parameter which roughly equal to $\sigma_i(0)/T^*$, T^* being the compensation temperature. k is the Boltzmann's constant. $\dot{\varepsilon}$ is the strain rate. $\dot{\varepsilon}_0$ is a constant pre-exponential factor. ΔH_{eff} and ΔV_{eff} are the effective activation energy and the effective activation volume, respectively. R is the gas constant. n describes the cooperative character of the yield process.

In Equation (4-23), the effective activation energy and effective activation volume are obtained from the activation parameters of amorphous phase $\Delta H_{amorphous}$, $\Delta V_{amorphous}$, and of the crystalline phase, $\Delta H_{Crystalline}$ and $\Delta V_{Crystalline}$, following the Takayanagi micromechanical model [29]:

$$\begin{aligned}\Delta H_{eff} &= \frac{\varphi \cdot \Delta H_{Crystalline} \cdot \Delta H_{amorphous}}{\Omega \cdot \Delta H_{amorphous} + (1-\Omega) \cdot \Delta H_{Crystalline}} + (1-\varphi) \cdot \Delta H_{Amorphous} \\ \Delta V_{eff} &= \frac{\varphi \cdot V_{Crystalline} \cdot V_{amorphous}}{\Omega \cdot V_{amorphous} + (1-\Omega) \cdot V_{Crystalline}} + (1-\varphi) \cdot V_{amorphous}\end{aligned} \tag{4-24}$$

$$\begin{cases} f_c = \varphi \cdot \Omega \\ f_m = 1 - \varphi \cdot \Omega \end{cases} \tag{4-25}$$

Here, Ω and φ are parameters associated with the Takayanagi model. These two parameters represent the state of mixing (amorphous phase and crystalline phase in parallel-series version of the Takayanagi model [30]), but only one is independent. The product $f_c = \varphi \cdot \Omega$ is the volume fraction of the crystalline phase (Equation (4-25)). f_m is the volume fraction of the amorphous phase.

$$\frac{\sigma_{y,c}}{\sigma_{y,M}} = \frac{1-\varphi_f}{1+2.5\varphi_f} exp(B\varphi_f) \tag{4-26}$$

Based on the Gueguen model, Matadi et al. [31] developed a new approach to describe the yield stress for polymer nanocomposite by introducing the Pukanszky [8] approach (Equation (4-26)) in the Gueguen model (Equation (4-23)). This new approach can described the yield stress of the nanocomposite as a function of strain rate, temperature, filler concentration, and extent of exfoliation:

$$\frac{\sigma_{y,c}}{T} = \left[\frac{1-\varphi_f}{1+2.5\varphi_f}\exp(B\varphi_f)\right] \times \left[\frac{\sigma_i(0) - m \cdot T}{T} + \frac{2k}{V_M}\sinh^{-1}\left(\frac{\dot{\varepsilon}}{\dot{\varepsilon}_0 \exp\left(-\frac{\Delta H_M}{RT}\right)}\right)^{1/n}\right] \tag{4-27}$$

In Equation (4-26), $\sigma_{y,c}$, $\sigma_{y,M}$ are the yield stresses of the composite and the polymer matrix, respectively, φ_f the fillers' volume fraction. B is a parameter characterizing

the interfacial interaction, including the interphase thickness, the surface area between the fillers and the matrix and interfacial strength [8]. For poor interfacial bonding, the particles do not carry any load, so that B=0. Therefore, it is expected that B should be decreasing with increasing filler content, since the low content generally leads to a higher exfoliation microstructure where interfacial adhesion between the fillers and the polymer matrix is expected to be high. In contrast, high filler concentrations always lead to agglomeration and therefore to a poor interfacial adhesion.

In previous chapters, we found that the compressive yield stress of PP-based composites did not decrease or increase in the same proportion with the increasing content of EOC or talc fillers, respectively (See Section 3.3). In addition, the morphology characterization of materials had shown an increased AR of talc filler and a decreased aspect ratio (AR) of EOC inclusion with recycling cycles. These experimental results indicate that although the fillers such as EOC and talc have their dimensions in micro-scale, the filler content and recycling have important effects on the microstructure and the properties of materials. Under this condition, Equation (4-27) will be used to describe the temperature and strain rate effects on the yield stress of PP/EOC and PP/talc composites. In the following, this model will be called GP model (Gueguen- Pukanszky model).

For PP/EOC/talc composite, we proposed to incorporate the modified multiplicative approach (based on Equation (4-7)) into the Gueguen model (Equation (4-23)) to compute the yield stress, σ_{yC}^{mult}, of PP/EOC/talc composite by using Pukanszky approach (the comparison results for the yield stress by using the single-population and two-population models are not shown here where the multiplicative

model shown better match to the experimental results by considering the PP/EOC as matrix (see Section 4.3.3)):

$$\frac{\sigma_{y,C}^{mult}}{\sigma_{y,m}} = \frac{\sigma_{y,PP/EOC}}{\sigma_{y,m}} \cdot \frac{\sigma_{y,C}}{\sigma_{y,PP/EOC}} \tag{4-28}$$

Here, $\sigma_{y,C}$ is the yield stress of PP/talc composite for a given filler volume fraction. $\sigma_{y,PP/EOC} / \sigma_{y,m}$ is calculated at first by using Equation (4-26). Then, the contribution of talc on the yield stress of PP/EOC/talc composite is obtained by considering the PP/EOC as the matrix. In the following, this model is denoted as GM model (Gueguen-Multiplicative model).

4.4.2. Recycling effect on the modeling of the yield stress

As mentioned in section 2.5.4, chain scission mechanisms are active in PP blends and induce smaller macromolecules and a larger molecular weight distribution during the reprocessing, as well as the formation of defect groups. In Gueguen model (Equation (4-23)), the internal stress, $\sigma_i(0)$, is a structural parameter which depicts the arrangement of defects inherited from past thermal history [9]. Therefore, we assume linear evolution of the internal stress for neat PP with reprocessing dependences:

$$\sigma_i(0)(N_P) = k_3 N_P + \sigma_i(0)_0 \tag{4-29}$$

where N_p in the number of reprocessing. k_3 is the reprocessing strengthening coefficient of the internal stress . $\sigma_i(0)_0$ is the internal stress at 0 K for non-recycled neat PP.

The changes of the AR of EOC and talc particles with the reprocessing cycles were observed in section 2.4.6. These changes may affect the interfacial interaction, including the interphase thickness, the surface area between the fillers and the matrix and interfacial strength which is characterized by the parameter B. Thus, we assume linear evolutions of parameter B with reprocessing number as follows:

$$B(N_P) = k_4 N_P + B_0 \tag{4-30}$$

Here, k_4 is the reprocessing strengthening coefficient of parameter B. B_0 characterizes the interfacial interaction between the fillers and the matrix for non-recycled PP-based composite.

4.4.1. Modeling results and discussion

The cooperative model formulation (Equation (4-23)) for semi-crystalline polymers proposed by Gueguen [32] is first used to predict the yield behavior of neat PP 0P and neat PP 3P. Neat PP is considered as a two phase material, composed by an amorphous and a crystalline phase. The parameters are then obtained according to Equation (4-23). In summary, the experimental data have first to be superposed horizontally and vertically in an Eyring plot ($\frac{\sigma_y}{T}$ versus $\log(\dot{\varepsilon})$) at a chosen reference temperature of $T_{ref} = 298K$.

$$\begin{cases} \Delta(\log(\dot{\varepsilon}) = \dfrac{\Delta H_M}{R\ln 10}\left(\dfrac{1}{T} - \dfrac{1}{T_{ref}}\right) \\ \Delta\left(\dfrac{\sigma_y}{T}\right) = -\sigma_i(0)\left(\dfrac{1}{T} - \dfrac{1}{T_{ref}}\right) \end{cases} \tag{4-31}$$

Once the master curve is built, the parameters ΔH_{eff} and $\sigma_i(0)$ could be determined in line with Equation (4-31). Knowing ΔH_{eff}, the parameters $\Delta H_{amorphous}$, $\Delta H_{crystalline}$ could be estimated through Equation (4-24) for a given crystallinity degree (measured by DSC in Section 2.4.5). The other parameters $m, n, \dot{\varepsilon}_0$, are obtained after having the best fit of the master curve [32].

For neat PP 6P, Equation (4-29) was used to estimate the internal stress from those of neat PP 0P and neat PP 3P. Other parameter for neat PP 6P kept the same as those of neat PP 3P. Then, Equation (4-23) was used to predict the yield behavior of neat PP 6P. The Gueguen model [32] parameters obtained from the master curves for neat PP 0P, neat PP 3P and neat PP 6P are given in Table 4-5.

Table 4-5: Gueguen models parameters.

Parameters	***Pure PP* 0P**	***Pure PP* 3P**	***Pure PP* 6P**
n	2.3	2.3	2.3
φ	0.83	0.83	0.83
$\dot{\varepsilon}_0$	1.55E+16	1.55E+16	1.55E+16
$\sigma_i(0)$ (Mpa)	80	75	70
m	0.165	0.165	0.165
$\rho_{m\,(}\, g/cm^3)$	0.90	0.90	0.90
T_{ref} (K)	298	298	298
Cristallinity degree (%)	49.2	50.2	50.2
$\Delta H_{amorphous}$ *(kJ/mol)*	47.5	47.5	47.5
$\Delta V_{amorphous}$ m^3	1.45E-28	1.45E-28	1.45E-28
$\Delta H_{cristalline}$ *(kJ/mol)*	236.7	236.7	236.7
$\Delta V_{Crystalline}$ m^3	7.40E-28	7.40E-28	7.40E-28
ΔV_{eff} (m^3)	2.55E-28	2.59E-28	2.59E-28
ΔH_{eff} *(kJ/mol)*	83.0	84.40	84.40
k_3	-	-	-1.67

Figure 4-23 shows the master curve of neat PP built at a reference temperature of 298 K (left side) and the predicted evolution of the reduced yield stress (σ_y / T) versus log($\dot{\varepsilon}$) for the neat PP at different temperatures with different recycling numbers (right side). In Figure 4-23, the predicted results are compared to our experimental results. The cooperative model predictions of the yield stress are in good agreement with the experimental data for different reprocessing cycles, showing that

the plastic flow is controlled by the cooperative motion of the chain segments, and obey to strain rate and temperature superposition principle.

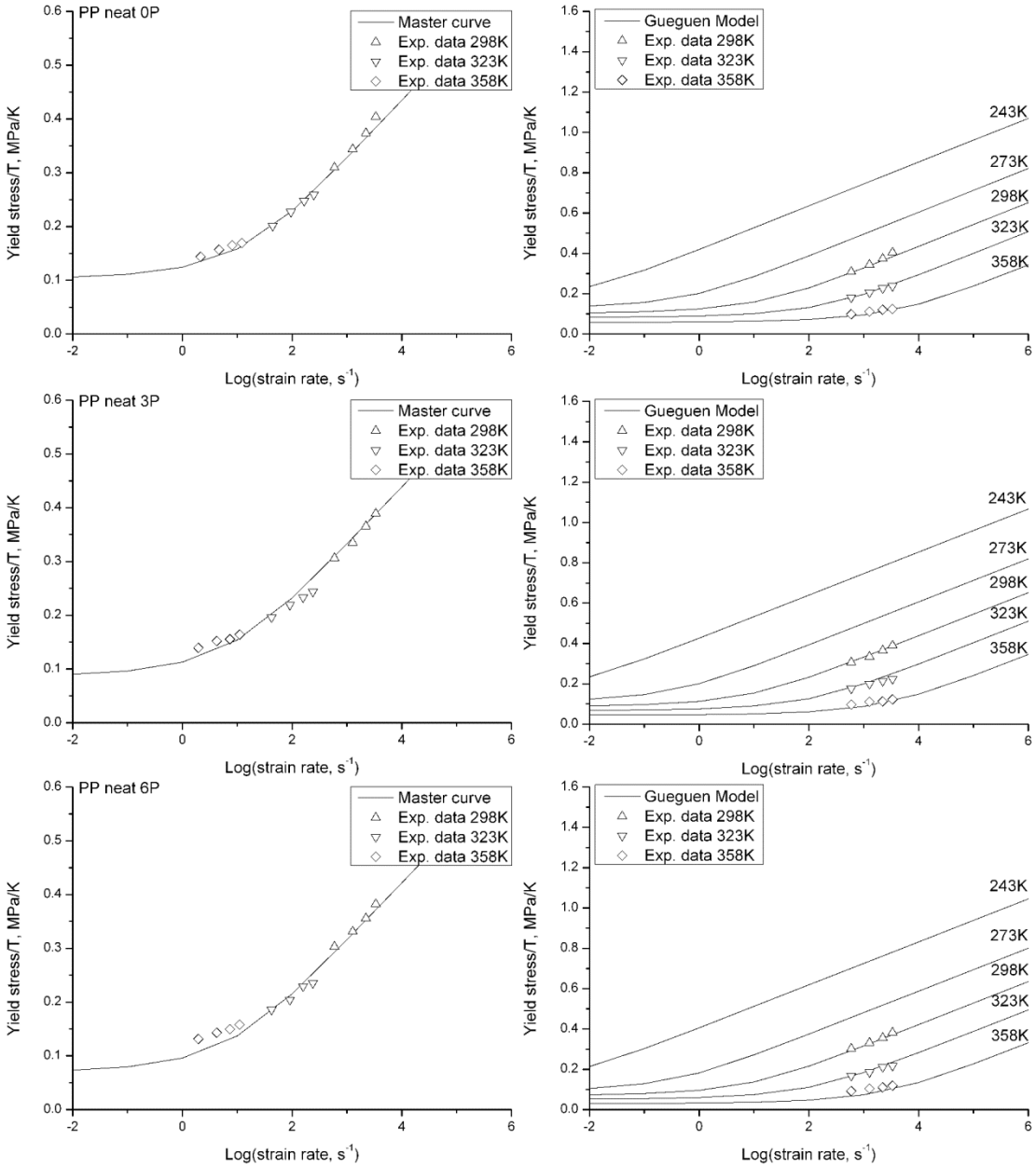

Figure 4-23: Master curve of neat PP build at a reference temperature of 298K (left side), yield stress/temperature versus strain rate of neat PP (right side).

Knowing the parameters for the non-recycled and recycled neat PP matrix estimated previously, the yield stress of PP-based composites can be calculated for a given fillers content by using the GP and GM models with different parameter B.

4.4.1.1. **Study of the parameter B**

According to the work of Aït Hocine et al. [33], the parameter B can be estimated by the following physically-based expression:

$$B = (1 + \tau \rho_f S_f) \ln(\sigma_{y,i} / \sigma_{y,M}) \quad (4\text{-}32)$$

where the quantities τ , ρ_f , S_f and $\sigma_{y,i}$ represent the thickness of the interphase between the matrix and the fillers, the density of the fillers, the surface area of the fillers and the yield stress of interphase, respectively. Since it seems to be impossible to obtain exact values of absolute thickness τ and the interphase yield stress $\sigma_{y,i}$, we chose to determine the parameter B by using the following approximation [33]:

$$B = \frac{1}{\varphi} \ln\left(\frac{\sigma_{y,c}}{\sigma_{y,M}} \frac{1 + 2.5\varphi}{1 - \varphi}\right) \quad (4\text{-}33)$$

Here, $\sigma_{y,M}$ and $\sigma_{y,c}$ are the experimentally measured matrix and composite yield stresses, respectively. Using our experimental results for neat PP and PP-based composites 0P and 3P (see Section 3.3), we can therefore estimate B.

Table 4-6 shows the evolution of the parameter B as a function of EOC and talc content for different strain rates. The parameter B was averaged from different temperatures. The recycling effect on the parameter B is also shown in this table. As expected the parameter B decreases with increasing filler content. This decrease of parameter B for PP/talc composites is more important than that of PP/EOC. It

indicates that the PP/talc system probably had higher exfoliated extent at low talc content corresponding to a larger specific surface area.

Table 4-6: the averaged values of parameter B of materials 0P and 3P for different strain rates, filler contents.

	Recycling number	Filler content wt. %	Averaged B from different temperatures				Averaged B from different strain rate
			$\dot{\varepsilon}_1$	$\dot{\varepsilon}_2$	$\dot{\varepsilon}_3$	$\dot{\varepsilon}_4$	
EOC	0P	10	0.96	0.93	1.12	1.25	1.07±0.15
		20	0.29	0.41	0.50	0.80	0.5±0.22
	3P	10	0.69	0.96	1.11	1.38	1.04±0.29
		20	0.07	0.41	0.52	0.76	0.44±0.29
Talc	0P	10	9.92	9.04	9.01	9.35	9.33±0.42
		20	5.97	5.64	5.57	5.70	5.72±0.17
	3P	10	11.06	10.67	11.25	11.77	11.19±0.46
		20	6.45	6.38	6.68	6.98	6.62±0.27

Concerning the recycling effect, the parameter B shows less change between PP/EOC 0P and PP/EOC 3P for a given EOC content. This is probably due to the less changed aspect ratio of EOC inclusion during the reprocessing. However, the higher parameter B of recycled PP/talc composites is observed compared to that of non-recycled one for a given talc content. It indicates that the recycled PP/talc system

probably had greater specific surface area. This observation is in accord with our morphology investigation where the break of the particles was found. The break of the particles led to an increased number of particles resulting in a larger interface between the fillers and the matrix.

Therefore, the determination of the parameter B allows for the evaluation of the interfacial interaction between the fillers and the matrix which depends on factors including the type and amount of surfactant used for sample preparation, the polymer matrix, the presence of coupling agents, processing conditions, etc… For these raisons we chose to use the average values of the parameter B (reported in Table 4-6), for calculating the effective yield stress of the composites with recycling effect.

Figure 4-24 and Figure 4-25 represent the master curve of PP-based composites built at a reference temperature of 298 K (left side) and the predicted evolution of the reduced yield stress (σ_y / T) versus log($\dot{\varepsilon}$) for the PP-based composites at different temperatures (right side) with the GP and GM models. Figure 4-24 shows the predictions of yield stress for materials 0P while Figure 4-25 exhibits the estimated yield stress for materials 3P. For GP model, the averaged parameter B is chosen from Table 4-6. As illustrated in Figure 4-24 and Figure 4-25, the GP and GM models are able to fairly predict the experimental data within the investigated range, excepted for PP/EOC/talc 70/20/10 3P where the predictions overestimates the compressive yield stress.

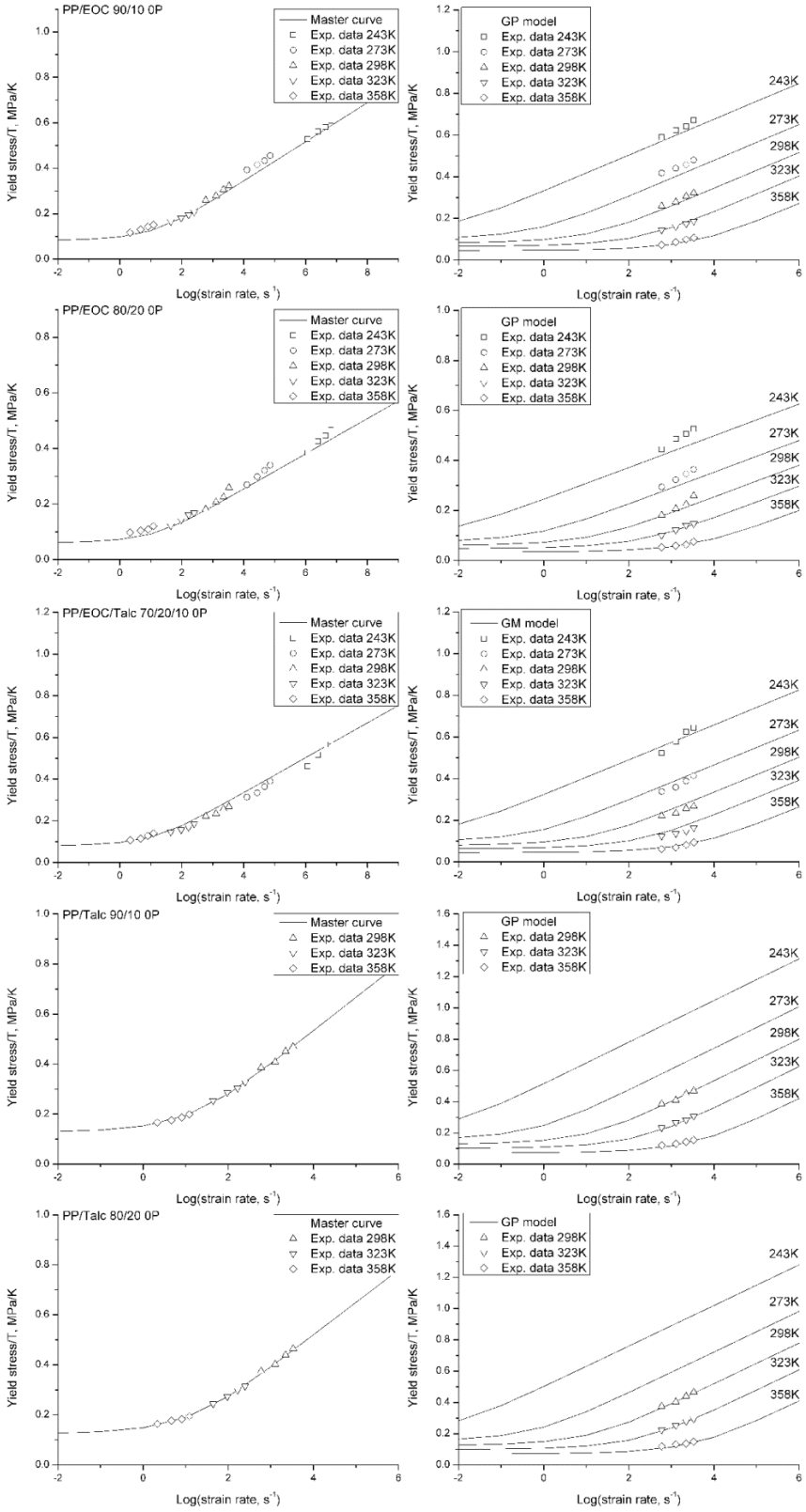

Figure 4-24: Master curve of PP-based composites 0P build at a reference temperature of 298K (left side), yield stress/temperature versus strain rate of PP-based composites 0P (right side).

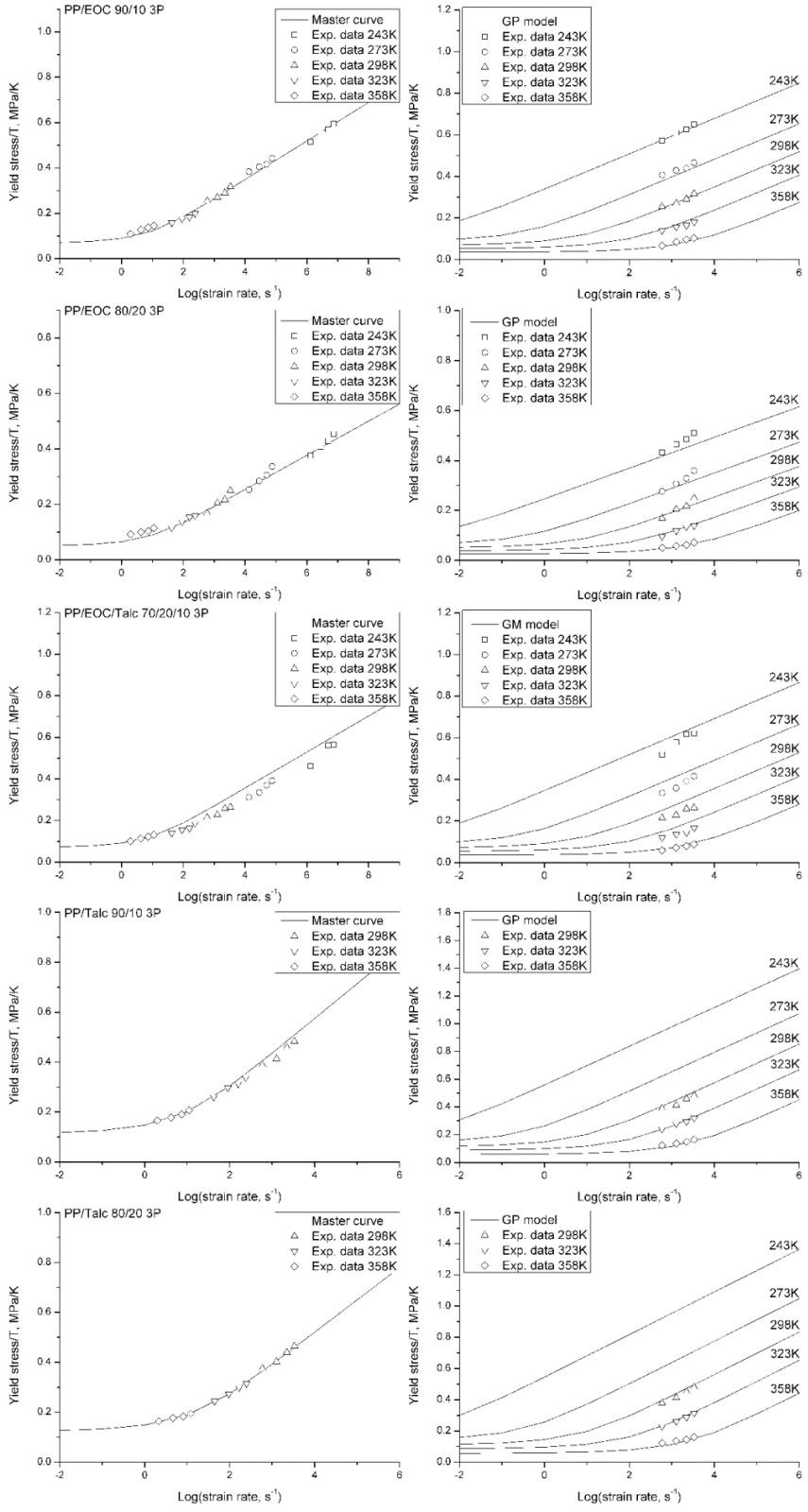

Figure 4-25: Master curve of PP-based composites 3P build at a reference temperature of 298K (left side), yield stress/temperature versus strain rate of PP-based composites 3P (right side).

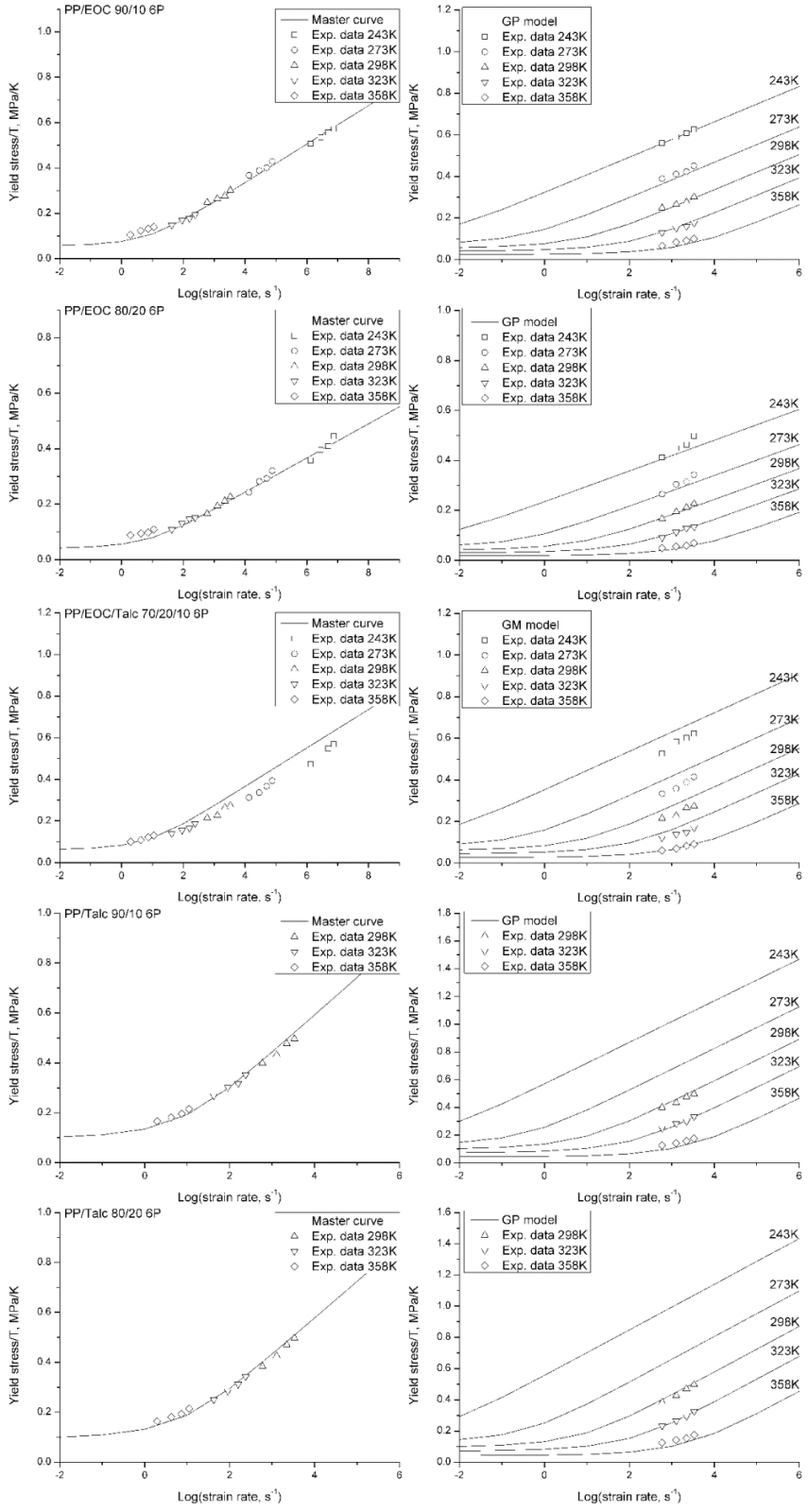

Figure 4-26: Master curve of PP-based composites 6P build at a reference temperature of 298K (left side), yield stress/temperature versus strain rate of PP-based composites 6P (right side).

For PP-based composites 6P, we suggest computing the parameter B with reprocessing dependences where the linear evolution of the parameter B is calculated by using Equation (4-30) with the experimental estimated parameter B (Table 4-6). Because the parameter B for PP/EOC is less changed with the recycling cycles, for simplicity, we assume that the parameter B for PP/EOC 90/10 6P and PP/EOC 80/20 6P keep constant as those for PP/EOC 80/20 3P and PP/EOC 90/10 3P, respectively. Table 4-7 shows the reprocessing parameters of the parameter B for PP/talc 90/10 and PP/talc 80/20. By using the predicted parameter B for PP/talc 90/10 6P and PP/talc 80/20 6P, The GP and GM models can be used to estimate the compressive yield stress for PP-based composites 6P.

Table 4-7: Reprocessing parameters for modeling the yield stress of PP/talc composites.

	B_0	k_4
PP/talc 90/10	9.33	0.62
PP/talc 80/20	5.72	0.3

Figure 4-26 shows comparisons of strain rate dependency for the compressive yield stress between GP model predictions, GM model predictions, and the experimental data for PP-based composites 6P. The GP model provides an excellent agreement with experimental data for different strain rates and temperatures with the estimated parameter B. In the case of GM model predictions, the yield stress dependence on strain rate for PP/EOC/talc 70/20/10 6P is also fair described for different temperatures. The slight overestimation of the yield stress by the GM model

is probably due to the assumed constant parameter B for PP/EOC composites. Besides this, the agreement between the experimental data and the modeling validates the strain rate/temperature superposition principle for reduced yield stress within the investigated range of temperatures and strain rates. This good agreement obtained with the GP and GM models validates our assumption for the linear evolution of the parameter B with the reprocessing number.

4.5. Conclusions

We proposed to extend the statistical stiffness model of Richeton et al. [5] by incorporating a Mori-Tanaka based approach and a two-population model by using Mori-Tanaka model [7]. By considering the initial compressive stiffnesses of neat PP and the aspect ratios of fillers with reprocessing dependences, the predicted elastic behavior depended on the frequency (or strain rate) and temperature as well as on the volume fraction of fillers and the recycling cycles. We also suggested incorporating the Pukanszhy model and a two-population model by using Pukanszhy approach [8] into the Gueguen model [9] to model the yield behavior of PP-based composites. In this, we computed the internal stress for neat PP and the parameter B for PP-based composites with reprocessing dependences. The predicted yield stress by our new approach depended on the strain rate and temperature as well as on the filler content and reprocessing numbers.

Our proposed models for the stiffness and the yield behaviors yield fair predictions of the experimental data within the investigation range for the considered PP-based composites by taking the filler content and recycling effects.

References

[1] Weon JI. Mechanical and thermal behavior of polyamide-6/clay nanocomposite using continuum-based micromechanical modeling. Macromolecular Research. 2009;17:797-806.

[2] Anoukou K, Zaïri F, Naït-Abdelaziz M, Zaoui A, Messager T, Gloaguen JM. On the overall elastic moduli of polymer-clay nanocomposite materials using a self-consistent approach. Part II: Experimental verification. Composites Science and Technology. 2011;71:206-215.

[3] Rodolfo A, Innocentini-Mei LH. Poly(vinyl chloride)/metallic oxides/organically modified montmorillonite nanocomposites: Preparation, morphological characterization, and modeling of the mechanical properties. Journal of Applied Polymer Science. 2010;116:422-432.

[4] Mesbah A, Zaïri F, Boutaleb S, Gloaguen JM, Naït-Abdelaziz M, Xie S, Boukharouba T, Lefebvre JM. Experimental characterization and modeling stiffness of polymer/clay nanocomposites within a hierarchical multiscale framework. Journal of Applied Polymer Science. 2009;114:3274-3291.

[5] Richeton J, Schlatter G, Vecchio KS, Rémond Y, Ahzi S. A unified model for stiffness modulus of amorphous polymers across transition temperatures and strain rates. Polymer. 2005;46:8194-8201.

[6] Wang K, Ahzi S, Matadi Boumbimba R, Bahlouli N, Addiego F, Rémond Y. Micromechanical modeling of the elastic behavior of polypropylene based organoclay nanocomposites under a wide range of temperatures and strain rates/frequencies. Mechanics of Materials. 2013.

[7] Tandon GP, Weng GJ. The effect of aspect ratio of inclusions on the elastic properties of unidirectionally aligned composites. Polymer Composites. 1984;5:327-333.

[8] Pukánszky Jr B, Bagdi K, Tóvölgyi Z, Varga J, Botz L, Hudak S, Dóczi T, Pukánszky B. Nanophase separation in segmented polyurethane elastomers: Effect of specific interactions on structure and properties. European Polymer Journal. 2008;44:2431-2438.

[9] Gueguen O, Richeton J, Ahzi S, Makradi A. Micromechanically based formulation of the cooperative model for the yield behavior of semi-crystalline polymers. Acta Materialia. 2008;56:1650-1655.

[10] Mori T, Tanaka K. Average stress in matrix and average elastic energy of materials with misfitting inclusions. Acta Metallurgica. 1973;21:571-574.

[11] Mortazavi B, Baniassadi M, Bardon J, Ahzi S. Modeling of Two-Phase Random Composite Materials by Finite Element, Mori-Tanaka and Strong Contrast Methods. Composites Part B Engineering. 2013;45:1117–1125.

[12] Dasari A, Yu ZZ, Mai YW, Kim JK. Orientation and the extent of exfoliation of clay on scratch damage in polyamide 6 nanocomposites. Nanotechnology. 2008;19.

[13] Fornes TD, Paul DR. Modeling properties of nylon 6/clay nanocomposites using composite theories. Polymer. 2003;44:4993-5013.

[14] Chow TS. Effect of particle shape at finite concentration on the elastic moduli of filled polymers. Journal of Polymer Science: Polymer Physics Edition. 1978;16:959-965.

[15] Chow TS. Effect of particle shape at finite concentration on thermal expansion of filled polymers. Journal of Polymer Science: Polymer Physics Edition. 1978;16:967-970.

[16] Spencer MW, Paul DR. Modeling the mechanical and thermal expansion behavior of TPO-based nanocomposites. Polymer. 2011;52:4910-4919.

[17] Yoo Y, Spencer MW, Paul DR. Morphology and mechanical properties of glass fiber reinforced Nylon 6 nanocomposites. Polymer. 2011;52:180-190.

[18] Mahieux CA, Reifsnider KL. Property modeling across transition temperatures in polymers: a robust stiffness-temperature model. Polymer. 2001;42:3281-3291.

[19] Mahieux CA, Reifsnider KL. Property modeling across transition temperatures in polymers: application to thermoplastic systems. Journal of Materials Science. 2002;37:911-920.

[20] Matadi Boumbimba R, Said A, Nadia B, David R, José G. Dynamic mechanical properties of PMMA/Organoclay Nanocomposite:Experiments and Modeling. Journal of Engineering Materials and Technology. 2011;133:030908

[21] Martinatti F, Ricco T. High-rate fracture toughness of polypropylene-based, hybrid, particulate composites. Journal of Materials Science. 1994;29:442-448.

[22] Velasco JI, De Saja JA, Martínez AB. Fracture behaviour of untreated and silane-treated talc-filled polypropylene composites. Fatigue & Fracture of Engineering Materials & Structures. 1997;20:659-670.

[23] Wang K, Addiego F, Bahlouli N, Ahzi S, Rémond Y, Toniazzo V, Muller R. Analysis of thermomechanical reprocessing effects on polypropylene/ethylene octene copolymer blends. Polymer Degradation and Stability. 2012;97:1475–1484.

[24] Wang K, Bahlouli N, Addiego F, Ahzi S, Rémond Y, Ruch D, Muller R. Effect of talc on the re-extruded polypropylene/talc composites. Polymer Degradation and Stability. 2013.

[25] Sperling LH. Introduction to Physical Polymer Science. 4 ed. New Jersey: John Wiley & Sons, Inc.; 2006.

[26] Xiao C, Jho JY, Yee AF. Correlation between the Shear Yielding Behavior and Secondary Relaxations of Bisphenol A Polycarbonate and Related Copolymers. Macromolecules. 1994;27:2761-2768.

[27] Brown EN, Rae PJ, Gray GT. The influence of temperature and strain rate on the tensile and compressive constitutive response of four fluoropolymers. J Phys IV France. 2006;134:935-940

[28] Richeton J, Ahzi S, Daridon L, Remond Y. A formulation of the cooperative model for the yield stress of amorphous polymers for a wide range of strain rates and temperatures. Polymer. 2005;46:6035-6043.

[29] Takayanagi M. Mem Fac Eng. Kyushu Univ. 1963;23:1.

[30] Ward IM, Sweeney J. An introduction to the mechanical properties of solid polymers. 2nd ed: Wiley; 2004.

[31] Matadi Boumbimba R, Wang K, Bahlouli N, Ahzi S, Rémond Y, Addiego F. Experimental investigation and micromechanical modeling of high strain rate compressive yield stress of a melt mixing polypropylene organoclay nanocomposite. Mechanics of Materials. 2012;52:58-68.

[32] Gueguen O, Richeton J, Ahzi S, Makradi A. Micromechanically based formulation of the cooperative model for the yield behavior of semi-crystalline polymers. Acta Materialia. 2008;56:1650-1655.

[33] Aït Hocine N, Médéric P, Aubry T. Mechanical properties of polyamide-12 layered silicate nanocomposites and their relations with structure. Polymer Testing. 2008;27:330-339.

Conclusions and future works

5. Conclusions and future works

There are three main objects of this study:

1. Identification the degradation mechanisms of polypropylene-based composites with the impact of the fillers' content.

2. Characterization the impact of the degradation mechanisms on the rheological, thermal, physical, and mechanical properties of the materials.

3. Prediction the elastic modulus and the yield stress of dynamic behavior of the recycled materials.

In this PhD thesis, commercial polypropylene (PP) was compounded with different concentration of talc and ethylene octene copolymer (EOC) filler (0 wt.%, 10 wt.% and 20 wt.%). Neat PP and PP-based composites were then subjected to up-to-six extrusion cycles for the purpose of studying the degradation mechanisms of PP-based composites and the effects of filler content on the latters.

We found that the molecular weight of the recycled materials slightly decreased after six reprocessing passes. The decrease of molecular weight of materials can be attributed to the chain scissions mechanism because the recycled materials were underwent high temperature and intensive shearing reprocessing condition. This decreased molecular weight resulted in a decreasing viscosity of materials. Therefore, a continuous increase of MFI with the recycling number was measured for all the materials. In the same time, the reduction of the length of PP chains may increase their mobility and hence, facilitate their rearrangement during the crystallization. This higher mobility caused a small increase of crystallinity with the reprocessing. Although the process induced material degradation, the change of decomposition

temperature was limited. It indicated that the recycled materials could be used in the same temperature range as well as the non-recycled ones. In addition, due to the presence of the anti-oxidant, no significant oxidation was observed.

For quasi static tensile properties, we found that the EOC inclusions stabilized the tensile elongation at break up to 3 recycling cycles due to a decrease of their size and a homogenization of their shape during the reprocessing. Otherwise, the talc fillers increased the tensile stiffness and the tensile strength of composite with the number of recycling cycle due to a decrease of their size and an increase of their aspect ratio.

Dynamic compressive behaviors of PP-based composites were investigated by using split Hopkinson pressure bars at five temperatures and under four strain rates. The results showed that the considered materials are strain-rate, temperature and recycling sensitive. With the increasing of recycling number, the dynamic behaviors (the yield stress and Young's modulus) of neat PP and PP/EOC composite decreased due to the chain scission mechanism. The dynamic responses (the yield stress and Young's modulus) of PP/talc increased with increasing of reprocessing cycle due to a more important self-reinforcement mechanism by talc particle size reduction. For PP/EOC/talc composites, the dynamic responses were not significantly modified by the reprocessing cycles, because of the equilibrium between the above two mechanisms.

For modeling the elastic and the yield behaviors of non-recycled and recycled PP-based composites, we proposed to extend the Richeton model and the Gueguen model. In these new approaches, the mechanical responses of PP-based composites depended on the strain rate and temperature as well as on the filler content and

reprocessing cycles. Good agreement between the model predictions and the experimental data were found for all non-recycled and recycled PP-based composites.

Since this study was conducted on lab-made materials, we did not consider the effects of pollutants and ageing which exist in the plastics from end-of-life car bumpers. The reprocessing effect on the materials properties was not significant. However, we characterized and modeled the thermomechanical behavior of polypropylene-based composites with recycling and filler content effects in this present work.

The perspectives of this thesis are many. From my point of view, it might include the following:

1. Performing the quasi static compressive test at different temperatures and under different strain rates for non-recycled and recycled materials to validate and optimize our proposed yield and stiffness models.

2. Studying in mode details the cavitation and more generally the damage of the materials after the dynamic compressive test by taking the temperature and strain rate in consideration.

3. Measuring the increase of temperature during the dynamic test for non-recycled and recycled materials.

4. Investigating the different morphology evolutions between the non-recycled and recycled materials by in-situ tensile testing.

5. Incorporating the proposed new approaches into the constitutive model to predict the true stress-strain curves for both non-recycled and recycled materials.

6. Integrating the models in the finite element simulation to predict the behavior of semi or finite structure such as car bumper.

7. Optimizing the micromechanical models with less parameter and studying the sensitivity of parameters with recycling effect.

Appendices

A. Appendices

A1. Evaluation of the shear stress of BUSS extruder and the critical shear stress to break talc particles

In order to verify whether the applied shear stress of extruder can break the talc particles during the processing, we need to check whether the shear stress in the extruder exceeds the critical shear stress to break talc particles. The detailed estimation is reported below:

(1) Shear stress in the BUSS extruder

We measured the complex viscosity of our material (PP/talc 80/20 (20 wt. % of talc)) by using the Physica MCR Rheometer at 200°C (our process temperature). The complex viscosity of the PP/talc 80/20 is reported in Figure A1-1:

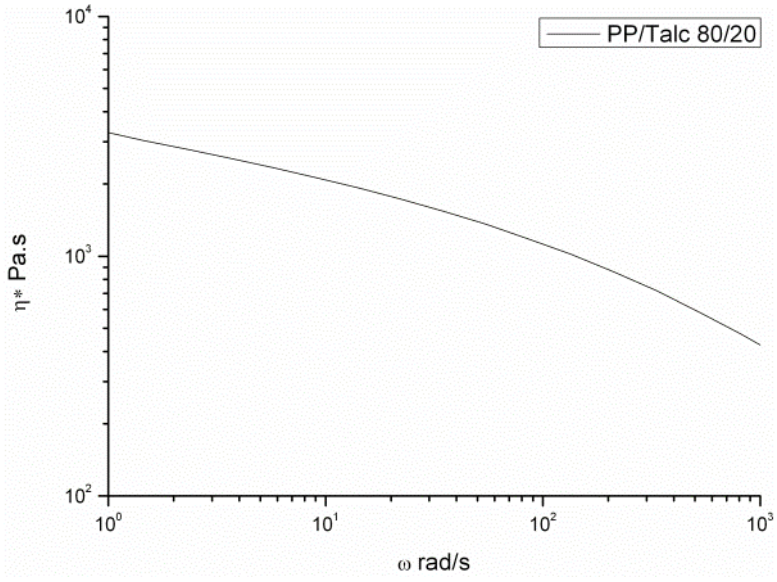

Figure A1-1: Complex viscosity of PP/talc 80/20 at 200 °C.

For ω=50rpm (screw speed of the extruder, 50 rmp = 5.23rad/s), the complex viscosity of PP/talc 80/20, $\eta^*_{pp/talc}$, is equal to 2413 Pa·s (Figure A1-1).

The shear rate for the Buss kneader, $\dot{\gamma}$, is about 200 s^{-1} with a screw speed of 50 rpm [1]. Therefore, the applied shear stress of the extruder is calculated by using the complex viscosity of the PP/talc 80/20 and the shear rate of the Buss kneader for a given screw speed:

$$\tau = \eta^*_{pp/talc} \times \dot{\gamma} \approx 2413 \times 200 = 482600 \text{ Pa} \quad \text{(A1-1)}$$

(2) Critical shear stress to break talc particles:

For talc particles, if the thickness of the platelet is δ and the interplatelet distance or gallery spacing is d, then the interaction energy, U, is given below [2]:

$$U = -\frac{A_{11}}{12\pi}\left(\frac{1}{d^2} + \frac{1}{(d+\delta)^2} - \frac{2}{(d+\delta)^2}\right) \quad \text{(A1-2)}$$

A_{11}: Hamaker constant (19.3×10^{-20} J for talc [3])

The exfoliation of talc particles can be schematically represented as shown in Figure A1-2.

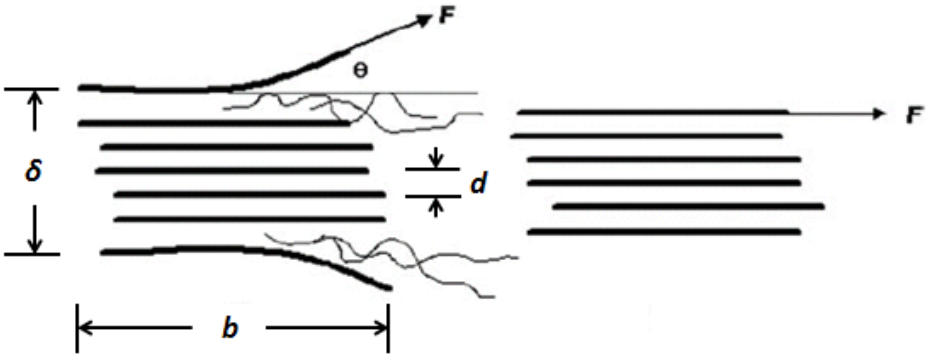

Figure A1-2: Exfoliation process (left) peeling (right) lap shearing [2].

By supposing that the exfoliation process occurred at θ°, the adhesive fracture energy was given by [2]:

$$G = \frac{F}{b}(1-\cos\theta) + \frac{F^2}{2E\delta b^2} \quad \text{(A1-3)}$$

F: Shear force required to break the talc particles

E: Young's modulus of talc (12000 MPa [4])

b: Platelet width of talc

If the adhesive facture energy is equal to the interaction energy of talc particles (using Equation (A1-2) and Equation (A1-3)), it is possible to estimate the required shear stress to break talc particles depending on the gallery spacing, d, of talc particles and on the peeling angle, θ.

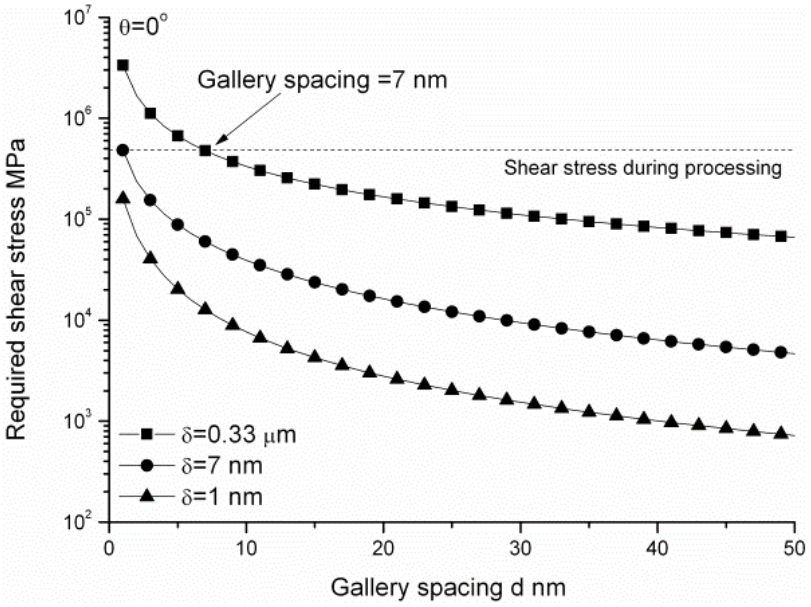

Figure A1-3: Required shear stress to break different thick talc particles with the peeling angle 0°.

Figure A1-3 shows the required shear stress to break different thick talc particle with peeling angle θ=0° (b=1.91 μm, measured by SEM, see section of morphology analysis of the paper). The required shear stress increases with increasing platelet thickness (see figure 3). For 0.66 μm thick talc particle (measured by SEM), the highest required shear stress was used to break talc particle into two halves (δ=0.33 μm). With δ=0.33 μm, the applied shear stress of extruder can break the talc particle with gallery spacing higher than 7nm. In addition, in Figure A1-3, we can see that the applied shear stress during processing can break the talc particle with talc particle thinner than 7 nm.

In Figure A1-4, we calculated the required shear stress to break 0.33 μm thick talc particle with different gallery spacing as function of the peeling angle, θ. For the gallery spacing d=1 nm, we can see that the shear stress during processing is enough to break the 0.33 μm thick talc particle with the peeling angle larger than 6 °.

Based on the above calculations, we believed that the applied shear stress in the extruder is possible to delaminate talc particles with peeling angle larger than 6 °.

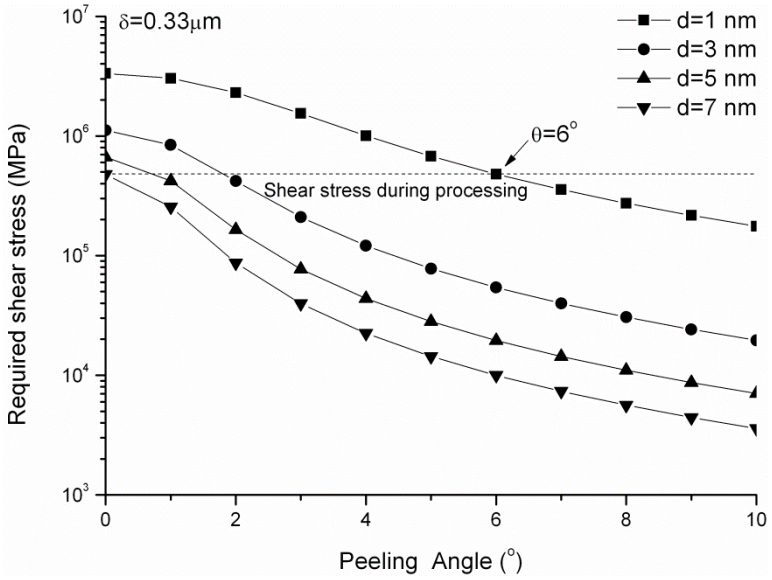

Figure A1-4: Required shear stress to break 0.33 um thick talc particles with different peeling angles.

A2. The Mori-Tanaka and Chow equations

Pertinent relationships used in the Mori-Tanaka and Chow models are [5]:

$$A_1 = D_1(B_4 + B_5) - 2B_2 \tag{A2-1}$$

$$A_2 = (1 + D_1)B_2 - (B_4 + B_5) \tag{A2-2}$$

$$A_3 = B_1 - D_1 B_3 \tag{A2-3}$$

$$A_4 = (1 + D_1)B_1 - 2B_2 \tag{A2-4}$$

$$A_5 = (1 - D_1)/(B_4 - B_5) \tag{A2-5}$$

$$A = 2B_2 B_3 - B_1(B_4 + B_5) \tag{A2-6}$$

and

$$B_1 = \phi D_1 + D_2 + (1-\phi)(D_1 S_{1111} + 2S_{2211}) \tag{A2-7}$$

$$B_2 = \phi + D_3 + (1-\phi)(D_1 S_{1122} + S_{2222} + S_{2233}) \tag{A2-8}$$

$$B_3 = \phi + D_3 + (1-\phi)[S_{1111} + (1 + D_1)S_{2211}] \tag{A2-9}$$

$$B_4 = \phi D_1 + D_2 + (1-\phi)(S_{1122} + D_1 S_{2222} + S_{2233}) \tag{A2-10}$$

$$B_5 = \phi + D_3 + (1-\phi)(S_{1122} + S_{2222} + D_1 S_{2233}) \tag{A2-11}$$

and

$$D_1 = 1 + 2(\mu_f - \mu_m)/(\lambda_f - \lambda_m) \tag{A2-12}$$

$$D_2 = (\lambda_m + 2\mu_m)/(\lambda_f - \lambda_m) \tag{A2-13}$$

$$D_3 = \lambda_m/(\lambda_f - \lambda_m) \tag{A2-14}$$

$$D_4 = -2(\mu_f - \mu_m)/(\lambda_f - \lambda_m) - 3 \tag{A2-15}$$

where λ_m and μ_m and λ_f and μ_f are the *Lamé* constants of the matrix and the filler, respectively, and S is Eshelby's tensor. The *Lamé* constants for isotropic materials are related to the Young's modulus and the Poisson's ratio by

$$\lambda = \frac{Ev}{(1+v)(1-2v)} \tag{A2-16}$$

$$\mu = \frac{E}{2(1+v)} \tag{A2-17}$$

The components of Eshelby's tensor, S_{ijkl}, are given below.

For spherical inclusions where $a = 1$,

$$S_{1111} = S_{2222} = S_{3333} = \frac{7 - 5v_m}{15(1 - v_m)} \tag{A2-18}$$

$$S_{1122} = S_{2233} = S_{3311} = \frac{5v_m - 1}{15(1 - v_m)} \tag{A2-19}$$

$$S_{1212} = S_{2323} = S_{3131} = \frac{4 - 5v_m}{15(1 - v_m)}. \tag{A2-20}$$

For ellipsoidal inclusions where $a \neq 1$,

$$S_{1111} = \frac{1}{2(1-\nu_m)}\left\{1-2\nu_m + \frac{3a^2-1}{a^2-1} - \left[1-2\nu_m + \frac{3a^2}{a^2-1}\right]g\right\} \quad \text{(A2-21)}$$

$$S_{2222} = S_{3333} = \frac{3}{8(1-\nu_m)}\frac{a^2}{a^2-1} + \frac{1}{4(1-\nu_m)}\left[1-2\nu_m - \frac{9}{4(a^2-1)}\right]g \quad \text{(A2-22)}$$

$$S_{2233} = S_{3322} = \frac{1}{4(1-\nu_m)}\left\{\frac{a^2}{2(a^2-1)} - \left[1-2\nu_m + \frac{3}{4(a^2-1)}\right]g\right\} \quad \text{(A2-23)}$$

$$S_{2211} = S_{3311} = -\frac{1}{2(1-\nu_m)}\frac{a^2}{a^2-1} + \frac{1}{4(1-\nu_m)}\left[\frac{3a^2}{a^2-1} - (1-2\nu_m)\right]g \quad \text{(A2-24)}$$

$$S_{1122} = S_{1133} = -\frac{1}{2(1-\nu_m)}\left[1-2\nu_m + \frac{1}{a^2-1}\right] + \frac{1}{2(1-\nu_m)}\left[1-2\nu_m + \frac{3}{2(a^2-1)}\right]g \quad \text{(A2-25)}$$

$$S_{2323} = S_{3232} = \frac{1}{4(1-\nu_m)}\left\{\frac{a^2}{2(a^2-1)} + \left[1-2\nu_m - \frac{3}{4(a^2-1)}\right]g\right\} \quad \text{(A2-26)}$$

$$S_{1212} = S_{1313} = \frac{1}{4(1-\nu_m)}\left\{1-2\nu_m - \frac{a^2+1}{a^2-1} - \frac{1}{2}\left[1-2\nu_m + \frac{3(a^2+1)}{a^2-1}\right]g\right\} \quad \text{(A2-27)}$$

where

$$g = \frac{a}{(1-a^2)^{3/2}}\left[\cos^{-1} a - a(1-a^2)^{1/2}\right] \quad \text{(A2-28)}$$

in the case of disks where $a < 1$ and

$$g = \frac{a}{(a^2-1)^{3/2}}\left[a(a^2-1)^{1/2} - \cosh^{-1} a\right] \quad \text{(A2-29)}$$

in the case of fibers where $a > 1$.

The bulk and shear moduli for isotropic materials are related to the Young's modulus and the Poisson's ratio by

$$k = \frac{E}{3(1-2v)} \tag{A2-30}$$

$$\mu = \frac{E}{2(1+v)} \tag{A2-31}$$

The pertinent parameters related to Eshelby's tensor used in the Chow model are

$$\xi = \frac{K_1}{1+2(\mu_f/\mu_m-1)(1-\phi)S_{2323}} \tag{A2-32}$$

$$\zeta = \frac{1+(\mu_f/\mu_m-1)(1-\phi)(S_{3333}-S_{1133})}{1+2(\mu_f/\mu_m-1)(1-\phi)S_{2323}} \tag{A2-33}$$

$$K_i = 1+(k_f/k_m-1)(1-\phi)b_i \tag{A2-34}$$

$$G_i = 1+(\mu_f/\mu_m-1)(1-\phi)c_i \tag{A2-35}$$

where

$$b_1 = 2Q/3-2(1-I)R \tag{A2-36}$$

$$b_3 = 2Q/3-2(2I-1)R \tag{A2-37}$$

$$c_1 = \left(\frac{2}{3}-\frac{2-3I}{1-a^2}\right)Q-4(I-1)R \tag{A2-38}$$

$$c_3 = \left(\frac{2}{3} - \frac{(2-3I)a^2}{1-a^2}\right)Q + (2-I)R \tag{A2-39}$$

$$2S_{2323} = \frac{2}{3}\left(\frac{1}{2} - \frac{(2-3I)}{4(1-a^2)}\right)Q + 2IR \tag{A2-40}$$

$$S_{3333} - S_{1133} = \left(\frac{1}{2} - \frac{7}{12}\frac{(2-3I)}{1-a^2}\right)Q + (2-I)R \tag{A2-41}$$

where

$$Q = \frac{3}{4}\frac{1}{1-\nu_m} \tag{A2-42}$$

$$R = \frac{1}{4}\frac{1-2\nu_m}{1-\nu_m} \tag{A2-43}$$

and

$$I = \frac{a}{(1-a^2)^{3/2}}\left[\cos^{-1} a - a(1-a^2)^{1/2}\right] \tag{A2-44}$$

for $a < 1$ and

$$I = \frac{a}{(a^2-1)^{3/2}}\left[a(a^2-1)^{1/2} - \cosh^{-1} a\right] \tag{A2-45}$$

for $a > 1$.

When $a \rightarrow 1$,

$$I = \frac{2}{3} \tag{A2-46}$$

$$\frac{2-3I}{1-a^2}=\frac{2}{5} \tag{A2-47}$$

we have

$$b_1=b_3=\frac{1}{3}\frac{1+\nu_m}{1-\nu_m} \tag{A2-48}$$

$$c_1=c_3=S_{2323}=S_{3333}-S_{1133}=\frac{2}{15}\frac{4-5\nu_m}{1-\nu_m}\,. \tag{A2-49}$$

References

[1] Knittel FL. Compounding Technologies, Advantages and Applications of Buss Kneaders. 2011.

[2] Borse NK, Kamal MR. Estimation of stresses required for exfoliation of clay particles in polymer nanocomposites. Polymer Engineering and Science. 2009;49:641-650.

[3] Médout-Marère V. A Simple Experimental Way of Measuring the Hamaker Constant A11 of Divided Solids by Immersion Calorimetry in Apolar Liquids. Journal of Colloid and Interface Science. 2000;228:434-437.

[4] Ma Q, Tibbenham PC, Lai X, Glogovsky T, Su X. Micromechanical modeling of the mechanical behavior of thermoplastic olefin. Polymer Engineering and Science. 2010;50:536-542.

[5] Spencer MW, Paul DR. Modeling the mechanical and thermal expansion behavior of TPO-based nanocomposites. Polymer. 2011;52:4910-4919.